UNIVERSIDADE FEDERAL DO RIO GRANDE DO SUL

INSTITUTO DE GEOCIÊNCIAS

PROGRAMA DE PÓS-GRADUAÇÃO EM GEOCIÊNCIAS

CORRELAÇÃO GEOLÓGICO-ESTRUTURAL E MODELO INTEGRADO DE EVOLUÇÃO PARA O CINTURÃO DOM FELICIANO SOB TRANSPRESSÃO INCLINADA NO NEOPROTEROZOICO DO SUL DO BRASIL

GIUSEPPE BETINO DE TONI

ORIENTADORA – Prof[a]. Dr[a]. Maria de Fátima Bitencourt

CO-ORIENTADOR – Prof. Dr. Jiří Konopásek

Porto Alegre – 2019

UNIVERSIDADE FEDERAL DO RIO GRANDE DO SUL

INSTITUTO DE GEOCIÊNCIAS

PROGRAMA DE PÓS-GRADUAÇÃO EM GEOCIÊNCIAS

CORRELAÇÃO GEOLÓGICO-ESTRUTURAL E MODELO INTEGRADO DE EVOLUÇÃO PARA O CINTURÃO DOM FELICIANO SOB TRANSPRESSÃO INCLINADA NO NEOPROTEROZOICO DO SUL DO BRASIL

GIUSEPPE BETINO DE TONI

ORIENTADORA – Prof[a]. Dr[a]. Maria de Fátima Bitencourt

CO-ORIENTADOR – Prof. Dr. Jiří Konopásek

BANCA EXAMINADORA:

Prof. Dr. Léo Afraneo Hartmann – Universidade Federal do Rio Grande do Sul (UFRGS)

Prof[a]. Dr[a]. Renata Da Silva Schmitt – Universidade Federal do Rio de Janeiro (UFRJ)

Prof. Dr. Sebastián Oriolo – Consejo Nacional de Investigaciones Científicas y Técnicas (CONICET) e Universidad de Buenos Aires (UBA)

Tese de doutorado apresentada como
Requisito parcial para a obtenção do Título
de Doutor em Ciências

Porto Alegre – 2019

UNIVERSIDADE FEDERAL DO RIO GRANDE DO SUL

Reitor: Rui Vicente Oppermann

Vice-Reitor: Jane Fraga Tutikian

INSTITUTO DE GEOCIÊNCIAS

Diretor: André Sampaio Mexias

Vice-Diretor: Nelson Luiz Sambaqui Gruber

CIP - Catalogação na Publicação

De Toni, Giuseppe Betino
Correlação geológico-estrutural e modelo integrado de evolução para o Cinturão Dom Feliciano sob transpressão inclinada no Neoproterozoico do sul do Brasil / Giuseppe Betino De Toni. -- 2019.
270 f.
Orientadora: Maria de Fátima Bitencourt.

Coorientador: Jiří Konopásek.

Tese (Doutorado) -- Universidade Federal do Rio Grande do Sul, Instituto de Geociências, Programa de Pós-Graduação em Geociências, Porto Alegre, BR-RS, 2019.

1. Ciclo orogênico. 2. Transpressão. 3. Cinturão Dom Feliciano. 4. Partição da deformação. I. Bitencourt, Maria de Fátima, orient. II. Konopásek, Jiří, coorient. III. Título.

Elaborada pelo Sistema de Geração Automática de Ficha Catalográfica da UFRGS com os dados fornecidos pelo(a) autor(a).

“O real é a rocha que o poeta lapida...”

Itamar Assumpção (1949 – 2003),

maldito, benedito, vulgo nego dito.

AGRADECIMENTOS

Ao professor e naturalista Irajá Damiani Pinto, fundador da nossa Escola de Geologia da UFRGS;

Ao professor e geólogo Rubens de Souza Picada, que precoce deixou a vida e a Geologia, e o melhor mapa de lineamentos do Escudo Sul-riograndense já feito;

Agradeço em especial à professora geóloga, doutora, exemplo de profissional e de pessoa, Maria de Fátima Bitencourt, minha madrinha e de mais vários queridos colegas e amigos de grupo de pesquisa. Obrigado por me proporcionar, ao longo de todos estes anos (pois é), um ambiente tão propício para o meu crescimento profissional e pessoal, onde encontrei liberdade pra formular minhas próprias perguntas. Obrigado por ouvir estas perguntas com atenção e me estimular a seguir perguntando, e por fim, por me incentivar a ir além deste ambiente de conforto. Obrigado pelo exemplo! Obrigado por acreditar em mim! És minha segunda mãe.

Aos professores que aceitaram o convite pra avaliar esta tese, Léo Hartmann, Renata Schmitt e Sebastián Oriolo, agradeço pela disposição, tempo dedicado, e também pela inspiração que já me trouxeram.

Aos professores da Geologia da UFRGS Milton L. Formoso, Nelson A. Lisboa, Léo A. Hartmann, Lauro V.S. Nardi, Luís A.D. Fernandes, Farid Chemale Jr., Maria do Carmo “Kaya” P. Gastal, Ruy P. Philipp, Carla Porcher, Márcia Boscatto Gomes, Edinei Koester, Rommulo V. Conceição, C.A. Sommer, Márcio M. Pimentel, André S. Mexias, Claiton Scherer, Karin Goldberg, Evandro “Chinês”, Ary Roisenberg, Luis F. De Ros, Carlos Schultz, Marina Bento Soares, N. Dani, R. Menegat, J.C. Frantz, J. Charão, e todos os demais professores que contribuíram para a minha formação e de tantos geólogos, que seguem contribuindo para a expansão e disseminação do conhecimento acerca das coisas da Terra. Muito obrigado!

Falando em UFRGS, agradeço também a todos os funcionários da universidade que possibilitaram este projeto se desenvolver, em especial o pessoal da laminação (Dedi e Lucas, e anteriormente Marcelo e Juliano), o pessoal da microssonda (Susan, Lucas, Rafael), os motoristas (Jarson, Armando, Adalto, Claudinho), o Paulo da tesouraria, e ao pessoal do PPGGEO (Roberto, Letícia, Gabriela).

Aos professores e geólogos Antônio Romalino S. Fragoso Cesar (gaúcho desgarrado que foi parar na USP) e Eberhard Wernick (UNESP - *in memorian*), com quem não por acaso tive o acaso de me encontrar em distintos momentos da trajetória acadêmica, obrigado pela inspiração.

Ao meu pai, professor e farmacêutico Celito De Toni Jr., que infelizmente nos deixou inesperadamente, e que eu acho que gostaria de estar aqui agora, vendo isso tudo que tem acontecido. Saudade do exemplo e inspiração.

À minha mãe, professora e farmacêutica Cláudia Hernandes Ogeda, que além de mãe, por um tempo também foi pai, e que além de professora é mestre cervejeira! Obrigado pelas oportunidades que me permitiram estar aqui.

Aos jovens amigos professores e colegas de profissão, irmãos e irmãs de pedra e de caminhada: Luana Moreira Florisbal, que de certa forma tem culpa de eu ter encontrado o caminho que me trouxe até aqui, e que em tantos momentos diferentes deste caminho teve sempre uma influência muito construtiva nessa trajetória, *muchas gracias*! Aos professores e amigos com quem tive oportunidade de aprender fora de sala de aula, Tiago Rafael Gregory, Eduardo Fontana, Felipe Guadagnin, Roberto S. de Campos. Todos vocês são fontes de inspiração.

Ao amigo e colega de aprender, Amós Martini “Pitch”, *rocky brother*, obrigado pela horizontalidade no fazer Geologia, desde lá atrás. Foi uma oportunidade incomparável aprender a aprender do teu lado. Viva a visada do cabrito!

Ao amigo e colega de ensinar, Rodrigo W. Lopes, parceiro de UNISINOS em Exploração e Avaliação de Depósitos Minerais “Projeto 3”, obrigado pela paciência, disposição e vontade de construir conjuntamente um projeto de aprender a ensinar.

Obrigado a todos os professores e inspirações. Ser professor é ser exemplo, é uma vocação, e é também uma sina. Em tempos em que ser professor virou uma afronta ao *status quo*, que por sinal vai de mal a pior, eu tenho orgulho de estar me tornando um nos últimos 8 meses (aproximadamente), forjado nos fornos da sala de aula e do trabalho de campo, visto que não recebemos treinamento formal pra isso no curso de Geologia. Obrigado a todos os estudantes com quem tive oportunidade de interagir até o momento, enquanto colegas e especialmente durante estes quase dois semestres lecionando na UNISINOS. É com vocês que eu tenho aprendido a ensinar a cada instante de interação e a todo o momento.

Obrigado a todos os colegas que também serviram de inspirações. Obrigado especialmente aos colegas de mapeamento (professores e estudantes) do Projeto Várzea do Capivarita (PVC-2011) da disciplina de Mapeamento Geológico Básico. Mais que especialmente meu agradecimento vai pros colegas de grupo da Faixa 7 (só os ossos!), Ezequiel “Zazá” Galvão de Souza, João Rodrigo “Joco” Vargas Pilla Dias e Marco Bincowski Rossoni (alemão couro de rato, o “tonteador”), e não menos especialmente aos colegas do grupo da faixa 5, Gustavo “Guga” Zvirtes, Samuel “Fera” Sbaraini, Heiny “Passarinho” P. Kloss e Maciel Gilmar Jacobs. Vocês são foda e aquela foi uma Encruzilhada da minha vida, da qual eu jamais vou me esquecer.

Aos colegas de grupo Magmatismo Sintectônico, atuais e novos, já tá virando covardia listar, visto a legião que se enfileira dentre os aprendizes de feiticeiros da profa. Dra. Maria de Fátima Bitencourt nos últimos (aproximadamente) doze anos (Lua, Cris, Greg, Mari, Duda Fontana, DaniBoy, Sargento, Moni, Anja, Amós, Fera, Evelyn, Sté, Camila Tomé, Fran, Diego, Pedro, Dioni, Érico, Felipe, Matheus, Duda, Elisa, Victor, João, Thayse, Pezzat, Camila,...). Foi e é um prazer ser colega de cada um de vocês, neste grupo tão diverso e potente. Desculpem se esqueci de alguém, e desculpas pela minha ausência ou falta de paciência nos últimos tempos. Peço, porém, licença pra agradecer aos colegas diretos de pesquisa, meus co-autores: Matheus Ariel Battisti, que teve a oportunidade de conhecer o pólo norte no verão, obrigado por dividir parte do nosso objeto de pesquisa, esse Super Complexo Porongos, tão múltiplo de si e certamente nos guardando ainda muitas surpresas; Elisa Oliveira da Costa, obrigado por também dividir durante teu TCC essas questões quentíssimas da Várzea do Capivarita; Pedro H. S. Andrade, obrigado pela força e astral em memoráveis trabalhos de campos no paraíso que é a península de Bombinhas, com direito a banhos voluntários e involuntários, e muito mais.

À tribo remanescente “CAEGang” do Centro Acadêmico de Estudantes de Geologia, meu fraterno abraço e entusiasmo a todos que seguem contribuindo a este espaço coletivo, autônomo e livre. Local onde aprendi Geologia tanto quanto em sala de aula, e muito mais sobre o ser humano do que jamais aprendi em lugar algum. Vida longa ao diretório! Espero que se renove sem perder o espírito coletivo que já foi força criadora de tanta coisa. Vale aqui a título de exemplo o resgate de que a “Hipótese da Deriva dos Continentes”, de Fernando Flávio Marques de Almeida, foi pela primeira vez apresentada e editada por ocasião da segunda Semana de Debates Geológicos, organizada até hoje anualmente pelo CAEG.

Agradeço aos amigos e mais que quase geólogos Gabriel Drago e Maximiliano “Max” Albers, parceiros alquimistas da arte de fazer cerveja (ou como chamamos, “Magma”), *grazzie tanto*! Saudades de uma boa brassagem.

Aos amigos de experimentação musical (“Sons do Pântano”) e colegas de longa data: Rafael Firmino Ballester, Rodrigo Moraes Alberto e Felipe Rosa, onde também se somou o meu amigo Max, obrigado por criarem um ambiente propício a abrigar tanta subjetividade. A música cura o espírito.

Agradeço ainda às minhas irmãs e irmão, Giovana, Daniela e Alessandro, pela hospitalidade e fraternidade irrestrita com que sempre me receberam nas oportunidades em que a Geologia me enviou até próximo de vocês. À Fabrizzia De Toni, meus agradecimentos incomensuráveis por ser teu irmão. Saudades.

À Mariah Xavier Rocha, geóloga e artista, a pessoa com quem espero passar décadas (ou séculos) podendo chamar de minha companheira. Obrigado pelo incentivo ao novo, à transcendência, e também pela paciência nos momentos de ausência, quando (um de nós dois) em trabalho de campo, ou como agora, isolado pra tentar escrever. Eu te amo e te admiro em múltiplos sentidos.

I would like to thank professors Jörn H. Kruhl, Roberto Weinberg, Rudolph Trouw and Holger Stünitz, by opportunities of discussion and learning in different moments.

To all my friends from UiT and Tromsø, I would like to express my deep gratitude for you which hosted me during that unforgettable time. That was a long and dark winter when I learned a lot about geology, pseudosections and myself.

To Jirka, thank you so much by your patience discussing tectonic scenarios or explaining me about petrological questions, as well as how to write properly a scientific paper, and specially during the last running-as-crazy weeks. I hope we will manage to keep working together in the next steps. “… the best ever! ... So far.”

Para todos com quem tive oportunidade de discutir, e pra você que está lendo, muito obrigado!

Ao povo brasileiro, que pagou isso com seu suor e sangue, minha eterna gratidão.

RESUMO

O estudo de duas áreas-chave, limítrofes dos domínios de ante-país e além-país do Cinturão Dom Feliciano, permitiu a sua correlação geológico-estrutural. Uma seção geológica entre Porto Belo e Balneário Camboriú (SC) levou à correlação cinemática entre os domínios. Um evento de colisão oblíqua com topo-para-NNW (650-645 Ma), após afetar a área como um todo, progrediu através da partição da deformação em domínios estruturais. A transpressão oblíqua no além-país é acompanhada de migmatização (700°C/4,3 Kbar) e progrediu para um regime tangencial (625-615 Ma) a francamente transcorrente destral (após 615 Ma). Enquanto isso, o componente contracional foi absorvido pelo ante-país, causando domeamento e exumação da sua infra-estrutura pré-brasiliana, que sofria processo de fusão parcial assistida por água (ca. 635 Ma, de >5 Kbar até 3,4). Uma zona de descolamento separa a infra- da supra-estrutura, que por consequência foi abatida, localmente aquecida até fácies anfibolito, e registra a inversão tectônica discreta de empurrão para extensão.

Na região de Encruzilhada do Sul (RS), ambos domínios registram o magmatismo cálcio-alcalino Toniano (ca. 800 Ma) pré-colisional, típico de arco-magmático, o qual é intercalado com sequências sedimentares semelhantes. Isto sugere que representem sequências vulcanossedimentares depositadas em bacias semelhantes, se não em uma mesma bacia. A correlação cinemática, com transpressão destral e empurrões para W/NW, juntamente com um contraste de trajetórias metamórficas, indica a exumação dos granulitos de baixa P do além-país como uma nappe empurrada sobre os xistos do ante-país, soterrados tectonicamente. A progressão da deformação transpressiva, reativações rúpteis das zonas de cisalhamento, assim como o magmatismo pós-colisional, obliteraram as relações originais entre os complexos e originaram o Bloco Encruzilhada.

A caracterização do magmatismo pré-colisional Toniano (ca. 800 Ma) do Complexo Porto Belo e sua correlação ao longo do além-país do Cinturão Dom Feliciano, e localmente em seu ante-país, sugere que estes domínios não representam dois paleo-continentes distintos. Sua correlação com outras rochas pré-colisionais, aflorantes na região de São Gabriel, permite traçar um modelo de evolução para o Sistema Orogênico Kaoko-Dom Feliciano-Gariep. Este modelo assume uma única subducção mergulhando para leste, cuja variação cíclica do ângulo de subducção é responsável pela migração lateral da atividade de arco magmático no cinturão antes de culminar na colisão oblíqua, através dos seguintes estágios: a)925-880 Ma

espalhamento oceânico e início da subducção; b) 820-770 Ma subducção em baixo ângulo, com migração do magmatismo para o retro-arco e gênese dos protólitos dos ortognaisses tonianos; c) 765-700 Ma verticalização da subducção e migração do arco magmático para o ante-arco, com gênese das rochas do Bloco São Gabriel, enquanto extensão afetava o retro-arco, desencadeando rifteamento; d) 700-660 Ma fim da subducção, colisão entre o Bloco São Gabriel e o Cráton Rio de la Plata; e) 660-630 Ma colisão oblíqua, inversão da bacia de retro-arco, transpressão bivergente, metamorfismo de alta-T/baixa-P e exumação do além-país; f) 630-580 Ma magmatismo pós-colisional e desenvolvimento de zonas de cisalhamento dominantemente transcorrentes; g) 580-550 Ma colisão secundária, deformação do ante-país e magmatismo pós-colisional tardio no Cinturão Dom Feliciano, e migração do fronte orogênico para os cinturões Kaoko e Gariep.

ABSTRACT

The study of two key-areas which are boundaries between Dom Feliciano Belt foreland and hinterland domains allow its geological and structural correlation. A cross section from Porto Belo to Balneário Camboriú (SC) led to the kinematic correlation between domains. A top-to-NNW oblique collisional event (650-645 Ma) affected the whole area and evolved through strain partitioning into structural domains. Oblique transpression in the hinterland occurs with migmatization (700 °C/4.3 Kbar) and progressed to a tangential regime (625-615 Ma) to dextral strike-slip tectonics (after 615 Ma). At the same time, the contractional component was absorbed by the foreland, which caused doming and exhumation of its pre-Brasiliano infrastructure, which was partial melting at water-saturated conditions (ca. 635 Ma; from >5 to 3.4 Kbar). A detatchment zone occurs between infra- and suprastructure, which unroofing caused local heating up to amphibolite-facies, as well as local, discrete tectonic inversion from thrusting towards extension.

At Encruzilhada do Sul area (RS), both tectonic domains record the Tonian (ca. 800 Ma) calc-alkaline, pre-collisional magmatism, typical of arc magmatism, which is interleaved with similar sedimentary sequences. This suggests that both volcanossedimentary sequences were deposited in a similar, if not the same, basin. A kinematic correlation, with dextral plus top-to-W/NW transpression, together with contrastant PT-paths, indicate low-P granulite exhumation as a nappe which came from the hinterland over the underthrusted foreland schists. Progressive transpressional deformation, with possible brittle reactivations and post-collisional magmatism caused blurred contacts between the complexes and originated the Encruzilhada Block.

The Tonian (ca. 800 Ma) pre-collisional magmatism of Porto Belo Complex characterization and its correlations along Dom Feliciano Belt hinterland, and locally in its foreland, suggests that both domains do not represent two distinct paleo-continents. Correlation with pre-collisional rocks from São Gabriel Block outline an evolution model to the Kaoko-Dom Feliciano-Gariep Orogenic System. This model assumes a single, eastwards subduction, which subduction angle cyclic changes is responsible for lateral migration of magmatic arc activity in the belt, before culminate in oblique collision, through the following stages: a) 925-880 Ma ocean floor spreading and beginning subduction; b) 820-770 Ma flat-slab subdiction, with back-arc magmatism generating Tonian protoliths; c) 765-700 Ma subduction steepening

and fore-arc magmatism generating São Gabriel Block rocks while extension affected back-arc, triggering rifting; d) 700-660 Ma subduction ends, with collision between São Gabriel Block and Rio de la Plata Craton; e) 660-630 Ma oblique collision, back-arc basin inversion, bivergent transpression, high-T/low-P metamorphism and hinterland exhumation; f) 630-580 Ma post-collisional magmatism and strike-slip shear zone development; g) 580-550 Ma secondary collision, foreland deformation and late post-collisional magmatism in Dom Feliciano Belt, while the orogenic front migrated towards Kaoko and Gariep belts.

SUMÁRIO

1. INTRODUÇÃO

O Cinturão Dom Feliciano é classicamente definido como “a faixa móvel adjacente ao Cráton Rio de la Plata”[1] (Fragoso Cesar, 1980). Diversos são os modelos evolutivos já propostos para este cinturão, os quais retratam o estado da arte de seu tempo, assim como a filosofia de pesquisa e inerente opinião dos seus autores (Fragoso Cesar, 1980; 1991; Fragoso Cesar et al., 1990; Fernandes et al., 1992; 1995a,b; Chemale Jr., 2000; Hartmann et al., 2007; Philipp et al., 2016; Hueck et al., 2018).

Cabe aqui um destaque para: os trabalhos de Rubens de Souza Picada, sintetizados em seu artigo póstumo (Picada, 1971), que definiu com precisão boa parte das estruturas regionais que compartimentam a porção central do Escudo Sul-riograndense; os trabalhos de Fragoso Cesar (1980, 1991) e Fragoso Cesar et al. (1986; 1991), que trouxeram os conceitos da então emergente tectônica de placas para a renovação do entendimento (na época, visionário) do contexto regional; e o trabalho de Fernandes et al. (1992), até hoje o único trabalho moderno de cunho regional baseado em Geologia Estrutural.

Apesar da diversidade de modelos, a subdivisão do Cinturão Dom Feliciano é relativamente consensual. Resguardadas as porções encobertas pelo Fanerozoico, tanto a chamada Faixa de Dobramentos Tijucas (Hasui et al., 1975, ou *schist belt* de Basei et al., 2008), e aqui também chamada *foreland fold and thrust belt* (cinturão de dobras e cavalgamentos de ante-país), ou simplesmente *foreland*, quanto a faixa constituída pelos batólitos, também chamada aqui de *hinterland* (além-país, ou *granite belt* de Basei et al., 2008) têm continuidade ao longo de todo o Cinturão Dom Feliciano, sendo consideradas seus domínios tectônicos principais. Ambos os domínios tectônicos mencionados ocorrem paralelos, delimitados por um conjunto de zonas de cisalhamentos (muitas reativadas enquanto falhas), desde Punta Ballena, na ponta extremo sul da Zona de Cisalhamento Sierra Ballena, na foz do

[1] A recente redelimitação do Cráton Rio de la Plata (Oyhantçabal et al., 2011), distinto do chamado Terreno Nico Perez (TNP), que é por sua vez correlato ao Cráton do Congo (Oriolo et al., 2016), mostra a fragilidade desta definição. O reconhecimento da continuidade deste terreno até a porção sudoeste do Escudo Sul-riograndense e sua ocorrência também como septos do embasamento dentro do Cinturão Dom Feliciano (Philipp et al., 2016) indica que o mesmo foi edificado na margem do TNP.

Rio de la Plata (extremo-sul do Uruguai), até a ponta aflorante da Zona de Cisalhamento Major Gercino, na península de Porto Belo, no litoral de Santa Catarina, totalizando cerca de 2.000 km em direção que varia de N-S (Uruguai) a N60°E (litoral catarinense).

A presente tese de doutorado tem como ponto de partida o reconhecimento de padrões semelhantes de evolução estrutural observados em duas áreas de estudo: nas cercanias de Encruzilhada do Sul, Rio Grande do Sul, e na península de Porto Belo/Bombinhas, Santa Catarina. Ambas as áreas de estudo compreendem estruturas regionais, limítrofes entre os dois principais domínios geotectônicos do Cinturão Dom Feliciano, e foram submetidas à transpressão durante o Neoproterozoico. As estruturas observadas em escala de afloramento, de forma simplificada, registram uma progressão de foliações de baixo ângulo, que dobradas assimetricamente, indicam empurrões para oeste/norte-noroeste, e por vezes desenvolvem zonas de cisalhamento de alto ângulo e cinemática dominantemente transcorrente destral em seus flancos curtos.

Se por um lado o “paralelismo das faixas” já enseja tentativas de correlações entre áreas distintas ao longo do orógeno, o seu caráter transpressivo sinaliza a impossibilidade de avaliar corretamente a arquitetura deste orógeno em seções bidimensionais isoladas. Justifica-se assim a proposta de correlação geológico-estrutural entre zonas transpressivas do Cinturão Dom Feliciano, nos Escudos Catarinense e Sul-riograndense, no sul do Brasil.

Como pano de fundo desta tese, é importante destacar que existe uma discussão sobre a natureza deste limite entre a faixa granítica e a faixa de xistos. Uma escola de pensamento, herdando a concepção original do Cinturão Dom Feliciano e do Batólito Pelotas (Fragoso Cesar, 1980; Fragoso Cesar et al., 1986) enxerga no *hinterland* batólitos do tipo andino, como um arco magmático alóctone, cujo limite com o *foreland* seria a chamada Zona de Sutura Sierra Ballena-Major Gercino (Basei et al., 2005; 2008; 2011; Passarelli et al., 2011; Hueck et al., 2018; entre outros). Esta hipótese presume a sutura de embasamentos não correlatos, a qual teria sido formada após o consumo do chamado Oceano Adamastor, cujas estimativas mais recentes para a colisão estão entre 615 e 585 Ma (Hueck et al., 2018).

De outro lado, diversos pesquisadores hoje corroboram a hipótese de que os granitos do *hinterland* representam o magmatismo pós-colisional do Cinturão Dom Feliciano (e.g. Bitencourt e Nardi, 2000; Philipp et al. 2005; Oyhantçabal et al., 2007;

Florisbal et al., 2012a,b; entre outros). Este volumoso magmatismo granítico sin- a pós-cinemático foi controlado por expressivas zonas de cisalhamento dominantemente transcorrentes, de orientação variável entre N-S e ENE-WSW, que são enfeixadas no Cinturão de Cisalhamento Sul-brasileiro (Bitencourt e Nardi, 2000). Florisbal et al. (2012b) compara o magmatismo granítico pós-colisional ao longo da Zona de Cisalhamento Major Gercino com granitos sincrônicos e composicionalmente semelhantes na Faixa de Dobramento Tijucas, e sugere que o limite não seja uma sutura, ou que a sutura seja anterior à entrada dos granitos. Bruno et al. (2018), baseado em geofísica, sugerem que a Zona de Cisalhamento Major Gercino têm caráter intracontinental, e que a sutura esteja mais à norte, no caso do Escudo Catarinense, limitando a Faixa de Dobramento Tijucas com o Cráton Luis Alves, coincidindo com a Zona de Cisalhamento Itajaí-Perimbó.

Trabalhos recentes de Konopásek (2016; 2017; 2018) principalmente desenvolvidos no Cinturão Kaoko (contra-parte africana da porção norte do Cinturão Dom Feliciano) questionam fortemente a existência do (paleo-) Oceano Adamastor, devido ao curto intervalo de tempo atribuído entre o fim do rifteamento do Cráton do Congo (durante a glaciação Sturtiana, entre 680 – 660 Ma) e a chegada dos sedimentos *flysch* provenientes do orógeno em edificação (pré-635 Ma). Segundo os autores, o período de cerca de 25 Ma seria insuficiente para a abertura e fechamento de um amplo domínio oceânico, motivo pelo qual lançam a hipótese de um Rift Adamastor.

Por outro lado, trabalhos recentes desenvolvidos na porção sul do *hinterland* do Cinturão Dom Feliciano demonstram a existência localizada de ofiolitos atribuídos ao Oceano Adamastor (Peel et al., 2018; Ramos et al., 2018; 2019).

Esta e outras controvérsias serão abordadas nesta tese, que está estruturada em torno de três artigos científicos submetidos a periódicos internacionais. Para além desta introdução, será apresentada, no capítulo 2, uma revisão conceitual, onde brevemente são abordados os conceitos de ciclo orogênico e transpressão. Por considerar que seria repetitivo, optou-se por abolir capítulos sobre o contexto geológico e materiais e métodos, que são descritos em cada artigo, sendo estes:

- ***Transpressive strain partitioning between the Major Gercino Shear Zone and the Tijucas Fold Belt, Dom Feliciano Belt, Santa Catarina, southern Brazil***, submetido ao *Journal of Structural Geology*;

- ***Origin and tectonic meaning of the Encruzilhada Block, Dom Feliciano Belt, south Brazil, based on aerogeophysics, image analysis and PT-paths***, submetido à revista *Tectonophysics*;
- ***Dom Feliciano Belt orogenic cycle tracked by its pre-collisional magmatism: the Tonian (ca. 800 Ma) Porto Belo Complex and its correlations in southern Brazil and Uruguay***, submetido à revista *Precambrian Research*.

Os manuscritos apresentados são idênticos aos submetidos, porém as figuras foram dispostas dentro do texto, para facilitar sua leitura. Tabelas são apresentadas ao fim de cada manuscrito/capítulo.

Um sexto e último capítulo de síntese enfeixa as considerações finais decorrentes da tese.

As referências bibliográficas de cada manuscrito são apresentadas nos seus respectivos finais, conforme no original, enquanto as referências dos capítulos 1, 2 e 6 são apresentadas conjuntamente ao fim da tese.

Por fim, o Anexo A contém o texto "***Why Cerro da Árvore Complex?*** *About the adopted Porongos (Super?) Complex subdivision*", escrito originalmente como um apêndice para uma versão inicial do manuscrito *Origin and tectonic meaning of the Encruzilhada Block*.

2. REVISÃO CONCEITUAL

2.1 Ciclo Orogênico

Orogênese (do grego oros, montanha; genna, nascimento) é um termo historicamente debatido, com diversas definições não consensuais. A palavra orógeno (orogen), na definição original de Kober (1921), era definida como uma faixa estreita de alta mobilidade (faixa móvel ou mobile belt), a qual circundaria um cráton (kratogen), por sua vez área de pouca ou nenhuma mobilidade. Sengör (1990), após uma profunda revisão histórica acerca do tema, define orogênese como o conjunto de processos atuantes em margens convergentes de placas. Vanderhaegue (2012), mais recentemente define orogênese como um período de acresção tectônica e magmática da crosta, acompanhado por espessamento, deformação, metamorfismo, soerguimento da superfície e erosão.

O movimento das placas litosféricas é principalmente uma consequência da subducção da litosfera oceânica (Miyashiro et al., 1982; Stern, 2002; Van der Pluijm e Marsak, 2004). Ao formar-se em uma dorsal mesoceânica, a jovem litosfera é basicamente formada pela crosta oceânica, quente e flutuante (buoyant) em comparação com a astenosfera subjacente, a qual é mais densa. Durante o espalhamento oceânico, a litosfera esfria e aumenta em espessura devido à progressiva acoplagem do manto litosférico por condução térmica. A densidade da litosfera oceânica é uma média das densidades da crosta oceânica e do manto litosférico ponderada pelas suas espessuras (Stern, 2002), e portanto aumenta com a idade. Quando a litosfera oceânica chega ao ponto de ser mais densa do que a astenosfera, torna-se instável e apta a subductar. Esta inversão de densidade leva, nas condições vigentes atualmente, entre 10 e 40 Ma, porém a idade média da litosfera oceânica atual é de 100 Ma (Stern, 2002). Segundo Van der Pluijm e Marsak (2004), a forma como inicia o processo de subducção ainda é assunto de debates, mas possivelmente ocorra aproveitando alguma anisotropia na placa prestes a ser subductada. As páginas que seguem são grandemente baseadas nestes autores.

2.1.1 Anatomia de orógenos convergentes não-colisionais

Junto com o princípio da subducção da litosfera oceânica inicia o processo de convergência de placas e a orogênese tipo andina ou não-colisional (Fig. 1),

caracterizada pela existência de uma fossa de subducção (*trench*), formação de um prisma acrescionário e de um arco vulcânico ou magmático, e de bacias adjacentes a este, em frente ao arco (*forearc basin*) e atrás do arco (*backarc basin*).

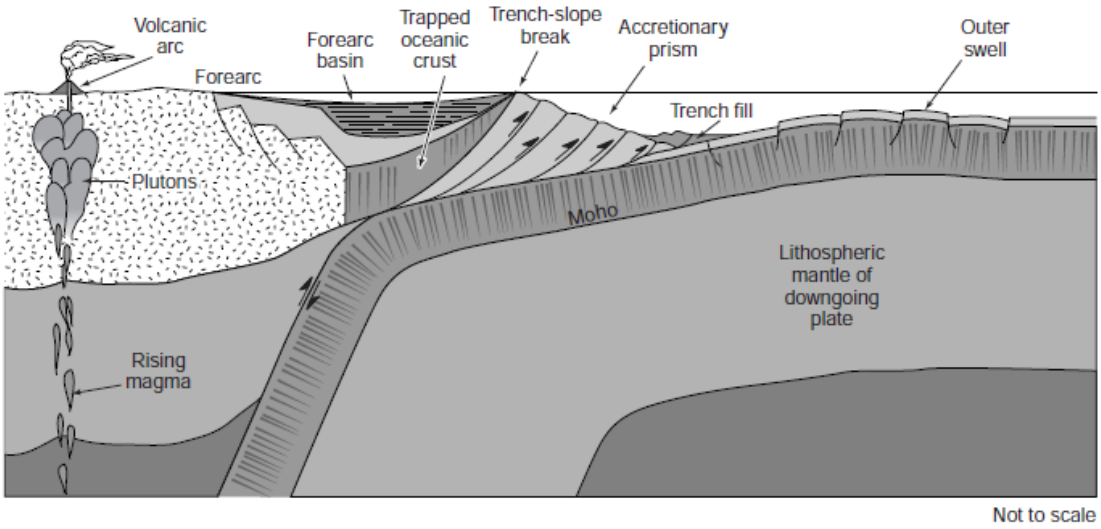

Figura 1 - Seção idealizada de uma margem continental convergente e termos relacionados. Neste caso observa-se o prisma acrescionário formado unicamente com vergência em direção ao oceano, devido ao efeito de uma lasca de crosta oceânica aprisionada (obstáculo). Extraída de Van der Pluijm e Marsak (2004).

A fossa existe devido ao puxão da placa subductada (*slab pull*), que rebaixa a porção próxima da subducção a uma profundidade maior do que se esta estivesse isostaticamente em equilíbrio. O puxão da placa descendente e a sucção causada pelo arraste do manto que descende juntamente, correspondem a cerca de 90% da força-motriz da tectônica de placas (Stern, 2002). O preenchimento da fossa é feito por turbiditos e fluxos de detritos que descem por cânions submarinos vindos do arco vulcânico ou do seu embasamento, da bacia de frente do arco, e de porções antigas do prisma acrescionário. O déficit de massa da fossa produz uma anomalia gravimétrica negativa, que é uma assinatura da zona de subducção (Van der Pluijm e Marsak, 2004).

O prisma acrescionário forma-se no contato entre as duas placas que convergem pelo cisalhamento causado entre a placa subductante e o limite da placa sobrejacente. É constituído por sedimentos pelágicos e basaltos oceânicos deformados, raspados da placa descendente, e de turbiditos deformados da fossa. A geometria do prisma acrescionário pode ser bivergente ou ter vergência assimétrica, com empurrões unicamente em direção ao oceano, caso haja um obstáculo (*backstop*), como um fragmento de crosta oceânica aprisionado entre a fossa e o arco. Rochas tipicamente formadas em prismas acrescionários são as associações

do tipo *mélanges*, misturas de fatias de rochas milonitizadas, incluindo sedimentos pelágicos e da fossa, porções da crosta oceânica e até lascas do manto serpentinizadas. O material pode ser transportado até a base do prisma, sendo metamorfizado em fácies xisto azul, e eventualmente trazido de volta à superfície pela ação de falhas inversas. O espessamento do prisma pode causar o colapso gravitacional das porções superiores, o que facilita a exumação das porções profundas (Van der Pluijm e Marsak, 2004).

A bacia de frente do arco recobre a área entre o alto topográfico característico do prisma acrescionário (*trench slope break*) e o arco vulcânico/magmático. Ela é preenchida por sedimentos provenientes do arco e do seu embasamento, cobrindo porções antigas do prisma acrescionário ou segmentos de crosta oceânica aprisionados no início da subducção, porções antigas do próprio arco ou o seu embasamento.

O arco vulcânico forma uma cadeia curva ao longo do limite da placa sobrejacente à zona de subducção, aproximadamente 100 – 150 Km acima da superfície da litosfera oceânica subductada. Grande parte do magmatismo é devido a liberação de voláteis da placa subductada, que promove fusão parcial da cunha astenosférica sobrejacente (Van der Pluijm e Marsak, 2004). O magmatismo característico de ambientes de arco é cálcio-alcalino em composição, podendo também incluir toleítos e/ou shoshonitos, a depender do grau e do tipo de interação com o embasamento do arco (Cawood *et al.*, 2013).

Arcos de ilha formam-se quando uma placa oceânica subducta sob outra litosfera oceânica, ou quando o arco cresce sobre uma lasca continental rifteada, separada do continente. Arcos continentais formam-se quando a litosfera sobrejacente é continental. Arcos de ilha têm predominância de magmatismo máfico a intermediário, enquanto arcos continentais também produzem rochas ácidas, incluindo batólitos graníticos, formados pela fusão da crosta aquecida pelo magmatismo mantélico e pela interação destes componentes.

A distância horizontal que separa a fossa do arco varia muito de orógeno para orógeno, e mesmo ao longo do comprimento de um mesmo orógeno. Os dois fatores principais que controlam esta variação são: o ângulo de mergulho da placa subductada, o qual é função, dentre outros fatores, da densidade desta; e a largura do prisma acrescionário, que por sua vez depende da taxa de sedimentação e do tempo transcorrido.

A região de trás do arco pode ser classificada em termos da dinâmica tectônica que apresenta, seja contracional, extensional ou estável. Esta dinâmica resulta de um balanço entre as direções e velocidades de migração da fossa, geralmente em direção ao oceano (*trench roll-back*) e da placa sobrejacente, a qual pode migrar tanto em direção à fossa quanto se distanciar dela (Fig. 2). Regiões de trás do arco caracterizadas por um balanço perfeito entre as velocidades são estáveis, visto que não acumulam deformação considerável.

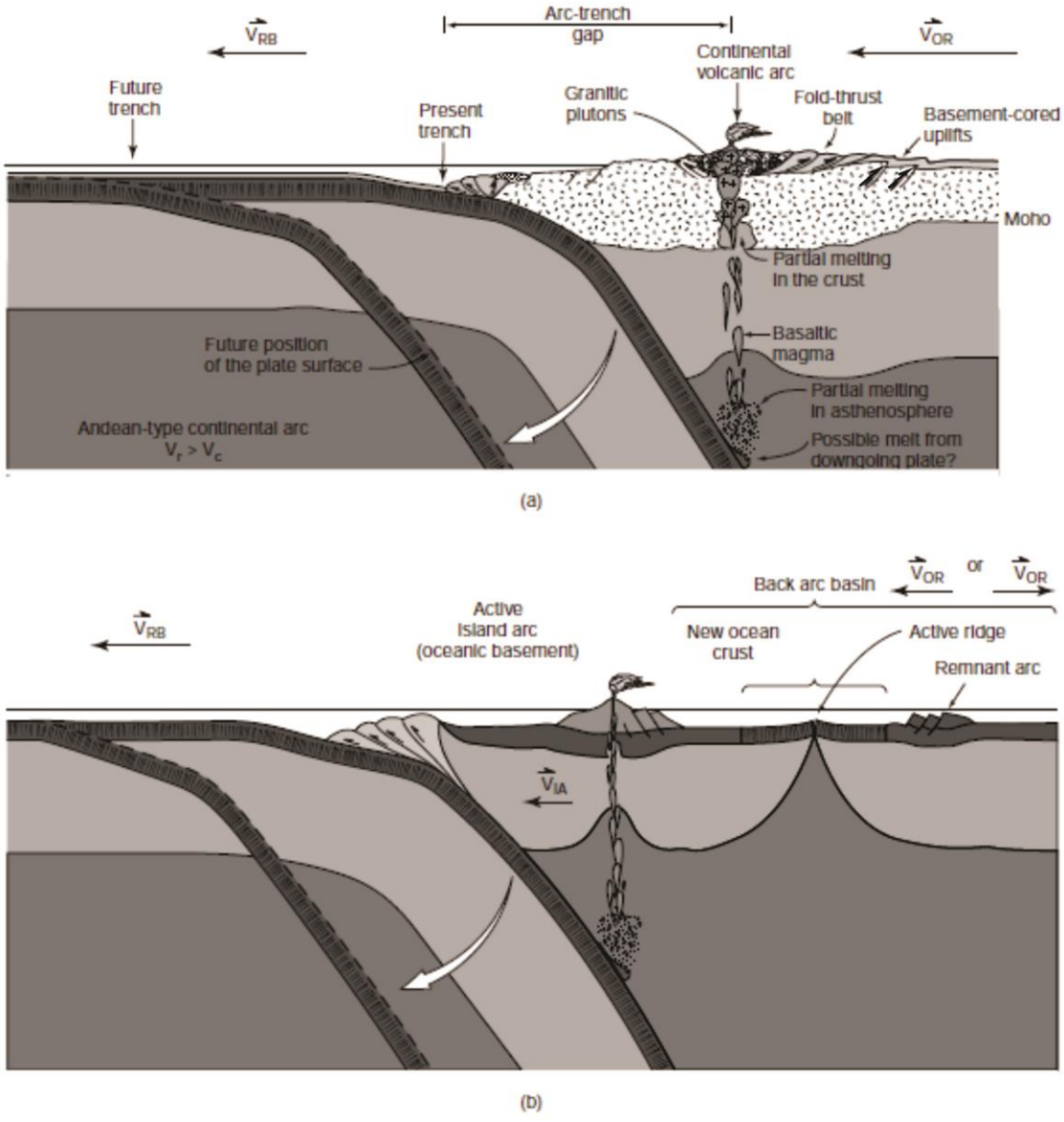

Figura 2 - Diferentes tipos de arcos e regiões de trás dos arcos. (a) Arco continental tipo-Andino, com região compressional de trás do arco, com a formação de um cinturão de dobras e cavalgamentos e soerguimento do embasamento. Plútons graníticos intrudem a base do arco. Esta situação se desenvolve quando a velocidade da placa sobrejacente excede a velocidade do recúo da fossa e possui mesmo sentido. (b) Arco de ilhas tipo-Mariana com região extensional de trás do arco. Neste caso o arco se desenvolve sobre crosta oceânica e a bacia de trás do arco desenvolve uma região de expansão de assoalho oceânico. Um arco remanescente foi rifteado e separado do arco vulcânico ativo. Esta situação se desenvolve quando o recuo da fossa excede a velocidade da placa sobrejacente ou quando esta se afasta da fossa. Extraída de Van der Pluijm e Marsak (2004).

Em *backarcs* contracionais, não forma-se uma bacia, mas sim um cinturão de dobras e cavalgamentos (*fold and thrust belt*; deformação tipo *thin-skin*) ou mesmo uma região de soerguimento do embasamento (deformação tipo *thick-skin*). Ambos exemplos de deformação são encontrados nas regiões de trás do arco andino, de forma que regiões de trás do arco com regime contracional são chamadas de *backarc* tipo Andino.

Em *backarcs* extensionais ocorre o estiramento da crosta, o qual pode resultar no rifteamento da crosta continental ou mesmo na expansão de nova crosta oceânica, à exemplo do Arco de Ilhas das Marianas (*backarc* tipo Marianas). Aparentemente estas bacias tendem a iniciar sobre a região do arco, resultando na fragmentação deste, de forma que uma porção do arco pode ser tornada inativa e separada do segmento ativo do arco pela expansão da nova crosta oceânica. Este é o processo de formação dos chamados arcos remanescentes.

Cabe aqui um destaque ao modelo proposto por Victor Ramos para o chamado Ciclo Orogênico Andino (vide figura 03 – Ramos, 2009). O seu modelo prevê a migração do *front* vulcânico de um arco magmático para a região de retro-arco em períodos de subducção *flat-slab*, devido a maior distância horizontal da fossa que a placa subductante percorre até que provoque a fusão da cunha do manto sobrejacente (figura 03 a, b e c). Simultaneamente cria-se uma tendência a compressão no retro-arco. Se a subducção for horizontal pode haver quiescência do arco (Fig. 3d). Subducção *flat-slab* pode ocorrer quando uma porção menos densa da crosta subductante chega à fossa, ou após *slab break-off*. Pelo outro lado, o *front* vulcânico migra para a região de ante-arco quando a subducção é verticalizada (Fig. 3e e f, provocando extensão atrás do arco, o que pode ser causado pela chegada de uma porção mais densa da placa na fossa, ou por incrementos no puxão da placa (*slab pull*) devido a eclogitização da crosta oceânica. Fatores adicionais, como a delaminação litosférica (Fig. 3f), podem atuar conjuntamente com o componente extensional, gerando soerguimento de platôs (Fig. 3g). Aparentemente estas variações são cíclicas. Diversos exemplos atuais, além dos Andes, são descritos na literatura (e.g. Cinturão Orogênico das Filipinas – Bachmann et al., 1983; Cinturão Orogênico de Myanmar – Zhang et al., 2018).

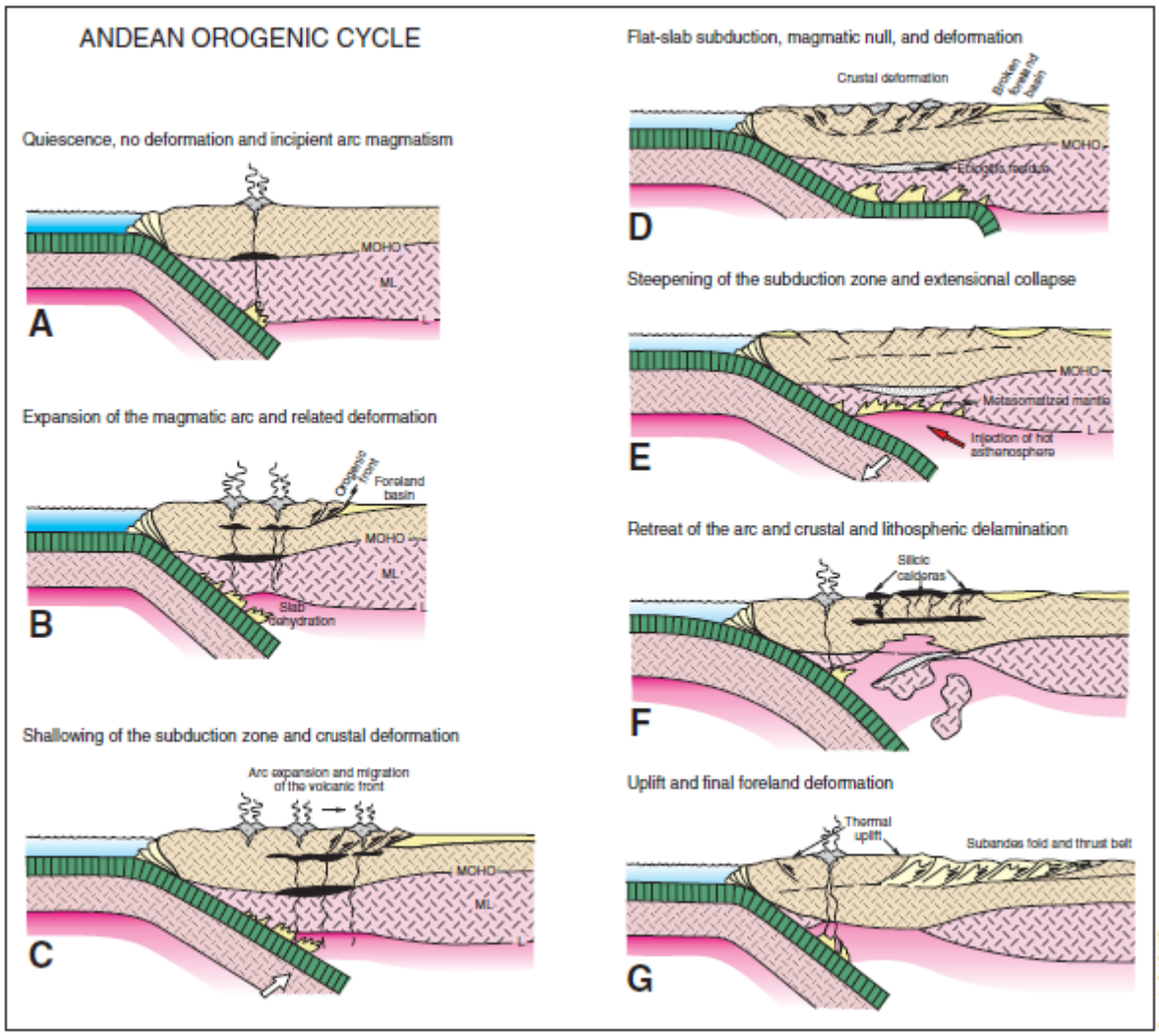

Figura 3 - Ciclo orogênico andino, idealizado por Ramos (2009), ilustrando a migração do *front* vulcânico em função de variações cíclicas do ângulo de subducção.

2.1.2 Estágios básicos da tectônica colisional

Com o consumo progressivo da litosfera oceânica, devido a sua flutuabilidade negativa com relação à astenosfera, porções da placa que eventualmente tenham flutuabilidade positiva se aproximam do limite convergente (Fig. 04a) e inevitavelmente transformam o ambiente do arco em uma zona de colisão. A litosfera continental, independente do seu tamanho, arcos de ilha, platôs oceânicos e dorsais mesoceânicas são exemplos de litosfera com flutuabilidade positiva que potencialmente envolvem-se em colisões. Independente do seu tipo, devido à flutuabilidade, estas porções da litosfera não podem ser completamente recicladas, ainda que hoje se saiba que ao menos a base da litosfera subcontinental tem condições de sofrer subducção (Mattauer, 1986).

A colisão em si é caracterizada pelo período principal de desenvolvimento de empurrões e máxima convergência, com o desenvolvimento de metamorfismo de alta pressão, sendo um período pouco favorável para a ascensão de magmas (Ligeois, 1998). Segundo Van der Pluijm e Marsak (2004), as rochas e estruturas formadas em orógenos colisionais dependem de variáveis como: i) o movimento relativo dos blocos, frontal ou oblíquo, o primeiro favorecendo movimentos perpendiculares ao limite dos blocos, este último favorecendo a partição da deformação entre zonas de empurrão e de transcorrência e colisões diacrônicas ao longo do comprimento do orógeno; ii) a forma dos blocos, com o efeito de promontórios ou recuos na linha de costa dos blocos, sendo que os primeiros penetram nas zonas de colisão causando alta concentração de deformação e o escape lateral de matéria, e ambos favorecem a formação de orógenos sinuosos; e iii) características físicas das placas colidentes, como temperatura, espessura e composição. Em geral, placas relativamente jovens, como as regiões de orógenos fanerozoicos, são quentes e menos rígidas, enquanto placas antigas, caracteristicamente cratônicas, são frias, espessas e rígidas. Cada cinturão orogênico apresenta características únicas, as quais são herdadas, retrabalhadas ou adquiridas através de sucessivas interações complexas entre múltiplos fatores. Tantas são as variáveis determinantes para a evolução de um orógeno, que dois orógenos nunca são exatamente iguais. Por outro lado, a comparação entre distintos orógenos é inevitável, e permite traçar em linhas gerais uma tendência evolutiva compreensível (Van der Pluijm e Marsak, 2004; Vanderhaegue, 2012).

Ainda que tratemos generalizadamente de orógenos colisionais que sucedem orógenos convergentes envolvendo subducção de litosfera oceânica, cabe ressalvar a possibilidade de que ocorram colisões independentemente da subducção de crosta oceânica, como no caso do fechamento ou inversão de riftes continentais, ou mesmo de *back-arc rifts* (Van der Pluijm e Marsak, 2004).

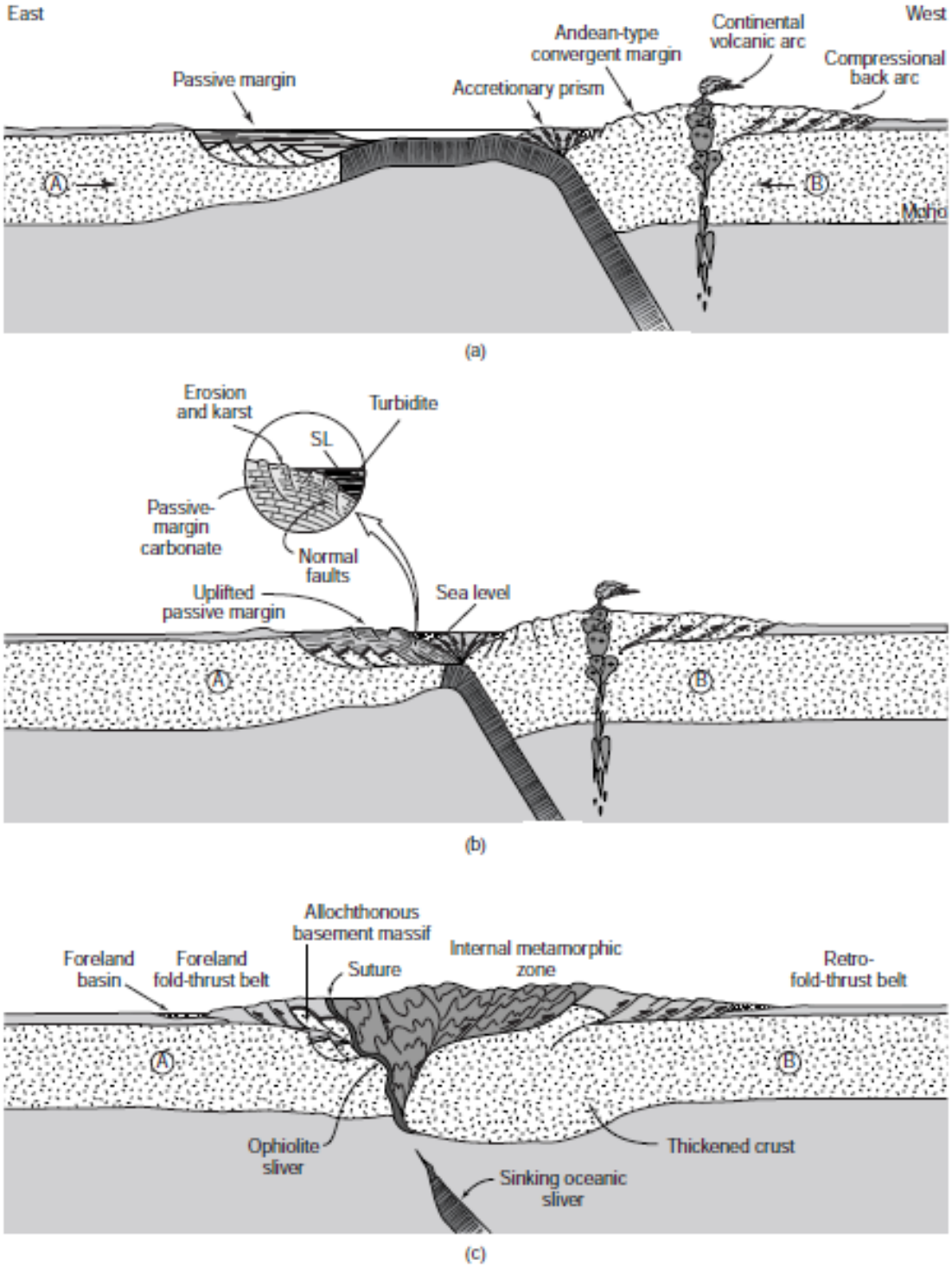

Figura 4 - Estágios idealizados de uma colisão continente-continente. (a) Pré-colisão, com o continente A possuindo uma margem passiva na sua costa leste e o continente B desenvolvendo uma margem ativa na sua costa oeste. (b) Estágio inicial de colisão, quando a margem passiva de A é soerguida e uma discordância é gerada. Turbiditos oriundos da margem ativa do continente B logo soterram a discordância (*zoom*). Falhas normais se desenvolvem devido ao estiramento da margem passiva, mas logo são reativadas como falhas inversas devido à propagação de empurrões do prisma acrescionário, provocando a inversão da bacia. (c) Orógeno colisional maduro, quando a placa subductada já quebrou, afundando no manto, a sutura já foi formada e rochas metamórficas encontram-se exumadas no interior do orógeno. Extraída de Van der Pluijm e Marsak (2004).

2.1.2.1 Estágios iniciais de uma colisão continental

Segundo Van der Pluijm e Marsak (2004), a aproximação hipotética de um continente de uma zona de subducção (Fig. 04b) se manifesta inicialmente por uma flexura e soerguimento da sua margem passiva, antes de ser puxado para a zona de subducção pelo segmento oceânico da placa, que já está sendo subductado. Os sedimentos plataformais são soerguidos acima do nível do mar e começam a ser erodidos, ao mesmo tempo que a borda do continente começa a ser estirada, e falhas normais tendem a se formar paralelas à fossa. Quando a superfície da plataforma continental torna-se o assoalho da fossa e turbiditos oriundos do sistema de arco vulcânico da margem ativa recobrem a plataforma erodida geram uma discordância. Este pacote de turbiditos sobre a discordância erosiva da plataforma marca o início da atividade orogênica no continente que vinha sendo puxado pela zona de subducção, e já foi historicamente chamado de *flysch*, contudo o uso deste termo é desencorajado (Van der Pluijm e Marsak, 2004).

2.1.2.2 Colisão e sutura

Com o princípio da colisão (Fig. 04c), os empurrões do prisma acrescionário tendem então a se propagar pelos espessos e contínuos estratos da margem passiva deste continente, formando um novo cinturão de dobras e cavalgamento, que com o tempo, cresce em direção ao seu antepaís (*foreland*, ou mais simplesmente o interior do continente, em direção ao cráton) e gera a inversão da bacia. O sobre-peso destes empurrões em direção ao *foreland* geram uma depressão por flexura, que forma uma nova bacia (*foreland basin*). Bacias de antepaís são geralmente assimétricas, sendo profundas na margem dos orógenos, e gradualmente menos profundas em direção ao cráton. Na porção do cinturão de dobras e cavalgamento mais próxima da além-país (*hinterland*, é a porção interna do orógeno), antigas falhas normais do embasamento, formadas quando da abertura da antiga margem passiva, são reativadas como empurrões e posicionam fatias do embasamento sobre os estratos plataformais, agora deformados.

Enquanto isto, o cinturão de dobras e cavalgamentos de *back*-arc (se este for compressivo) do outro continente segue ativo. Quando a placa subductada rompe-se, com a porção oceânica afundando no manto, a fonte de magmatismo para o arco cessa, e as rochas magmáticas características da subducção tendem a ser metamorfizadas na progressão da convergência. A deformação na placa

sobrejacente tende a seguir o mesmo estilo da outra, porém a vergência das estruturas é oposta. O orógeno colisional é, em geral, bivergente.

A zona de cisalhamento que marca o limite dos blocos outrora separados é denominada sutura (Fig. 04c). Eventualmente uma fatia da litosfera oceânica que separava os dois continentes pode ser empurrada sobre a margem passiva invertida do continente que vem colidindo, e define a sutura. Rochas de um lado da sutura eram parte de um continente, enquanto rochas do lado oposto, do outro. Segundo Klerey et al. (2009), outras características podem ser utilizadas para a delimitação de terrenos distintos, incluindo: i) proveniência, estratigrafia e história sedimentar; ii) afinidade petrogenética e trajetórias magmática e metamórfica; iii) a natureza, história e estilo deformacional; iv) paleoambientes e paleontologia; v) posição do paleopólo e paleodeclinação magnética.

2.1.2.3 Espessamento crustal e maturação do orógeno

Com a colisão dos dois continentes, a porção interna do orógeno sofre um enorme espessamento, com metamorfismo e deformação regionais ocorrendo em profundidade. Com a deformação progressiva, as rochas de alto grau tendem a mover-se para cima e em direção ao ante-país (Fig.04c; Van der Pluijm e Marsak, 2004). Rochas profundas podem ser expostas devido à exumação, que é a combinação dos processos de remoção das rochas da superfície e extrusão das rochas profundas. O transporte destas rochas por grandes distâncias (> 5 Km), sob a forma de grandes dobras recumbentes, caracteriza as *nappes*.

O espessamento causa sobrepeso da pilha e tende a promover maturação termal da base, com consequente enfraquecimento reológico, possivelmente acompanhado de fusão parcial da crosta. Vanderhaegue (2012) sugere que nesta fase da orogenia, se o espessamento é maior que a erosão, ocorre a transição entre orógenos em forma de cordilheira (*collisional range* de Van der Pluijm e Marsak, 2004; ou *wedge-shaped orogen* de Vanderhaegue, 2012) para platôs orogênicos. Se houver uma mudança nas condições de contorno, em termos de deslocamentos relativos das placas envolvidas na orogenia, estes mesmos fatores facilitam o colapso gravitacional do orógeno sobre o seu próprio peso, causando extensão/afinamento, descompressão e potencialmente mais fusão parcial. Adicionalmente, processos de delaminação da base da litosfera (que pode também ter sido espessada) podem promover ascensão da astenosfera e consequente magmatismo mantélico, provendo calor adicional para a fusão parcial da crosta.

2.1.2.4 O período pós-colisional

É importante distinguir o período colisional do período pós-colisional (*sensu* Ligeois, 1998), o qual não é menos tectonicamente ativo. O período pós-colisional é um longo período de convergência que sucede o fechamento do oceano e o impacto principal entre as duas porções litosféricas colidentes. É caracterizado pela movimentação horizontal de terrenos ao longo de zonas de cisalhamento de escala continental e amplo magmatismo associado. Este magmatismo geralmente contém uma componente juvenil importante, sendo predominantemente cálcio-alcalino alto-K, e em menor quantidade shoshonítico. Ocorrências de magmatismo peraluminoso e alcalino/peralcalino podem ser volumosas, mas são menos frequentes. As fontes do magmatismo pós-colisional, sejam crustais ou mantélicas, são geradas ou modificadas no período de subducção e colisão que o precedem.

As grandes zonas de cisalhamento características do período pós-colisional podem desenvolver-se em função da partição da deformação devido à convergência oblíqua durante a colisão ou devido ao escape tectônico lateral, causado pela sinuosidade do contorno dos terrenos colidentes (Van der Pluijm e Marsak, 2004). Estas zonas de cisalhamento podem tanto delimitar quanto cortar ou estruturar internamente os domínios do orógeno.

O fim do período pós-colisional é a transição para o período intraplaca, que inicia com o fim dos grandes movimentos laterais, quando o magmatismo tende a ser esparso. Este momento ocorre quando a área como um todo, incluindo crátons e orógeno adquirem um pólo único de rotação e constituem uma placa litosférica única (Ligeois, 1998).

2.1.3 Transpressão em diferentes ambientes geotectônicos

Zonas de deformação da litosfera tendem a se desenvolver preferencialmente ao longo e adjacente aos limites entre as placas que a compõem, onde a interação entre estas placas se dá em virtude dos seus deslocamentos relativos (Van der Pluijm e Marsak, 2004). Nestas regiões, vetores de deslocamento convergentes e divergentes oblíquos em relação aos limites de placas ou outras zonas de deformação adjacentes são uma consequência inevitável do movimento das placas na superfície (aproximadamente) esférica do planeta (Dewey *et al.*, 1998). Esta tendência ao deslocamento oblíquo é ainda acentuada pela forma naturalmente irregular dos limites das placas. Segundo Dewey *et al.* (1998), além de ser uma

característica comum em praticamente todos os segmentos de cinturões orogênicos colisionais (Fig. 04c), a transpressão pode ocorrer em margens com subducção ativa (Fig. 01 e 02), no prisma acrescionário, na bacia de ante-arco, no arco e no retro-arco contracional; em curvas de retenção (*restraining bends*) ao longo de zonas de cisalhamento transcorrentes, características do período orogênico pós-colisional; e de limites transformantes; e em cinturões de ardósia, onde também ocorre grande perda de volume. A deformação transpressiva pode provocar o deslocamento relativo e literalmente embaralhar os domínios geotectônicos de um orógeno natural, idealizadamente organizado em modelos como os apresentados acima.

2.2 Transpressão

2.2.1 Fundamentos conceituais e evolução dos modelos

O reconhecimento da convergência e divergência oblíquas entre placas litosféricas foi primeiramente reportado por Harland (1971). Este autor descreve estruturas de *thrust* e transcorrência sinistral em tilitos de Spitsbergen (Noruega) deformados na orogênese caledoniana, com estiramento de *boulders* da ordem de 5 a 10 vezes, paralelo ao eixo de dobras. Harland (1971) cunhou os termos transpressão (*transpression*) e transtração (*transtension*) para descrever os termos intermediários entre os movimentos relativos característicos dos três tipos de limites de placas consagrados: convergente (limite destrutivo), transcorrente (limite transformante) e divergente (limite construtivo).

Segundo Harland (1971), enquanto a transtração tende a acomodar-se pela formação de estruturas discretas, como falhas escalonadas entre zonas de extensão (comuns à riftes ou à zonas de expansão da litosfera oceânica), a transpressão, ao menos em seus estágios iniciais, apresenta um caráter mais penetrativo, tendendo a se distribuir como estruturas compressivas ao longo de zonas mais amplas (também de acordo com Egydio-silva *et al*., 2005). No modelo apresentado, a transpressão simples (*simple transpression*) tende inicialmente a formar um conjunto de dobras arranjadas *en echelon* (Fig. 5a), oblíquas em relação aos limites da zona transpressiva. Com a transpressão progressiva (Fig. 5b e c) os eixos das dobras tendem a paralelizar-se com os limites da zona, podendo ao fim ser confundidas como resultantes de compressão simples (Fig. 5d). O dobramento progressivo tende a formar dobras cada vez mais fechadas, concentrando camadas incompetentes e descontinuidades em posição subvertical, tendendo ao paralelismo com os limites da

zona transpressiva. Esta é uma posição propícia para o desenvolvimento de componentes de transcorrência. Assim a compressão em si desenvolve as condições para a o desenvolvimento de novas zonas de cisalhamento transcorrente, em uma espécie de retroalimentação. Um componente de elongação horizontal mais acentuado caracteriza o que este mesmo autor chamou de *shear transpression*, cuja deformação finita é uma combinação de: i) compressão normal; e ii) movimento paralelo a direção da zona. Harland (1971) já alertava de que esta combinação poderia ser tanto simultânea e diferencialmente distribuída no espaço, como em sequência, sobrepondo-se temporalmente.

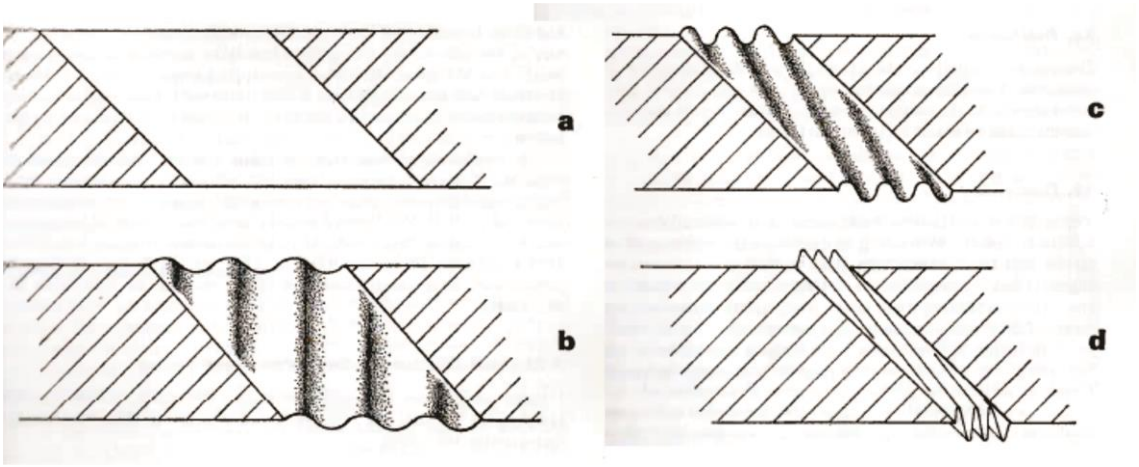

Figura 5 - Modelo esquemático de uma zona transpressiva evoluindo no tempo através da formação de uma sequencia de dobras com eixos oblíquos aos limites da zona. Os blocos rígidos (placas), que aproximam-se numa direção paralela à base da figura, estão caracterizados pelo traçado diagonal. Em (a) observa-se o estado indeformado. O dobramento em suas fases iniciais forma-se com os eixos perpendiculares à direção de encurtamento (b), e com a contração progressiva (c) tendem a paralelizar-se com os limites da zona (d). Extraído de Harland (1971).

Sanderson e Marchini (1984) deram o próximo passo na compreensão da deformação tridimensional ao propôr uma abordagem matemática do elipsoide de deformação finita, baseada em matrizes. Considerando a deformação homogênea de um volume constante dentro de uma zona de deformação, basal e lateralmente confinada (não há saída de matéria nas bordas da zona ou do modelo) e com a superfície superior livre, estes autores definem transpressão (Fig. 06a) como a deformação envolvendo encurtamento perpendicular a zona (α^{-1}), compensado por espessamento vertical (α) e acompanhado por cisalhamento transcorrente (γ). A matriz que descreve estes componentes pode ser fatorada como a seguir:

$$\begin{vmatrix} 1 & \gamma & 0 \\ 0 & 1 & 0 \\ 0 & 0 & 1 \end{vmatrix} \quad \begin{vmatrix} 1 & 0 & 0 \\ 0 & \alpha^{-1} & 0 \\ 0 & 0 & \alpha \end{vmatrix} \quad = \quad \begin{vmatrix} 1 & \alpha^{-1}\gamma & 0 \\ 0 & \alpha^{-1} & 0 \\ 0 & 0 & \alpha \end{vmatrix} \qquad (1)$$

Componente de cisalhamento simples (transcorrente) | **Componente de cisalhamento puro (contração)** | **Transpressão**

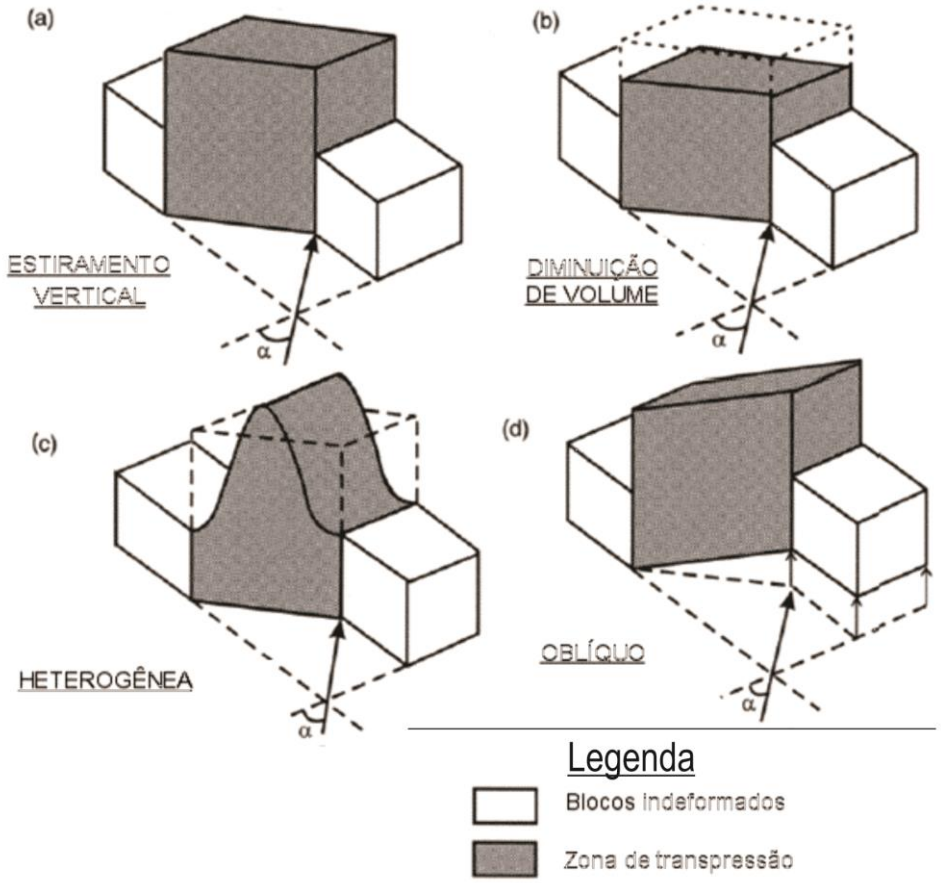

Figura 6 - Alguns exemplos de modelos de deformação por transpressão, ordenados aproximadamente em ordem cronológica do seu desenvolvimento, aumento de realismo e complexidade. (a) Modelo de transpressão de Sanderson e Marchini (1984), envolvendo volume constante e deformação homogênea em uma zona vertical, onde o encurtamento horizontal perpendicular à zona é acomodado por extensão vertical. (b) Modelo de transpressão de Fossen e Tikoff (1993), incluindo mudança de volume. (c) Modelo de transpressão de Robin e Cruden (1994), considerando a deformação heterogênea a partir de um gradiente de deformação desenvolvido a partir do deslocamento zero nas paredes da zona até extensão vertical máxima no centro da zona. (d) Modelo de transpressão oblíqua apresentado por Robin e Cruden (1994) e Jones e Holdsworth (1998), considerando um cisalhamento simples oblíquo. Modificada de Dewey *et al*. (1998).

A partir desta matriz, Sanderson e Marchini (1984) modelam uma série de elipsoides de deformação finita, em termos de comprimento relativo dos eixos e orientação, para diferentes valores de encurtamento e cisalhamento (Fig. 07). Eles

concluem que a forma do elipsoide de deformação varia de acordo com os valores de encurtamento, de forma que: para $\alpha^{-1} < 1$, que é o componente de encurtamento da transpressão, ocorrem elipsoides oblatos ($k < 1$; onde $k = (x/y - 1)/(y/z - 1)$, segundo Fossen, 2010); para $\alpha^{-1} = 0$, a deformação é plana ($k = 1$, Y é constante); enquanto para $\alpha^{-1} > 1$, que é o componente de extensão da transtração, os elipsoides são prolatos ($k > 1$). Para a transpressão, eles prevêm a formação de foliações verticais, com a possibilidade de inversão dos eixos X e Y, formando lineações (X) verticais ou horizontais. Dobras e falhas de empurrão são esperadas em baixo ângulo de obliquidade em relação à zona, enquanto estruturas extensionais ocorreriam em alto ângulo (Fig. 8). Os autores alertam para o fato de que, havendo um componente transcorrente ($\gamma \neq 0$), seções balanceadas perpendiculares à zona não podem ser utilizadas para a determinação direta do encurtamento total.

Uma das maiores críticas ao modelo de Sanderson e Marchini (1984) é o fato de não considerarem a possibilidade de cisalhamento simples ortogonal à direção do plano. Isto é traduzido nas estranhas propriedades físicas (friccionais) assumidas para as paredes da zona transpressiva (Schwerdtner, 1989), as quais não são reportadas em condições naturais. Estas propriedades de fricção anisotrópica permitem deslizamento vertical livre, sem transmissão de cisalhamento simples, ao passo que não admitem deslizamento horizontal livre, visto que transmitem a deformação nesta direção através de um componente de cisalhamento simples horizontal. Robin e Cruden (1994) traduzem estas características em um possível modelo físico, onde as paredes teriam corrugações verticais perfeitamente lubrificadas, permitindo deslizamento vertical livre (sem resistência) e promovendo a transmissão do cisalhamento horizontal via a resistência imposta pelas corrugações.

Ainda que o modelo apresentado por Sanderson e Marchini (1984) seja extremamente simplificado e contenha limitações, podemos considera-lo a pedra fundamental que alicerçou todos os trabalhos posteriores sobre o tema. Deste então a abordagem teórico-matemática passou a evoluir juntamente com os conceitos, modelos análogos (Pinet e Cobbold, 1992) e com a aplicabilidade dos modelos de transpressão em rochas naturalmente deformadas.

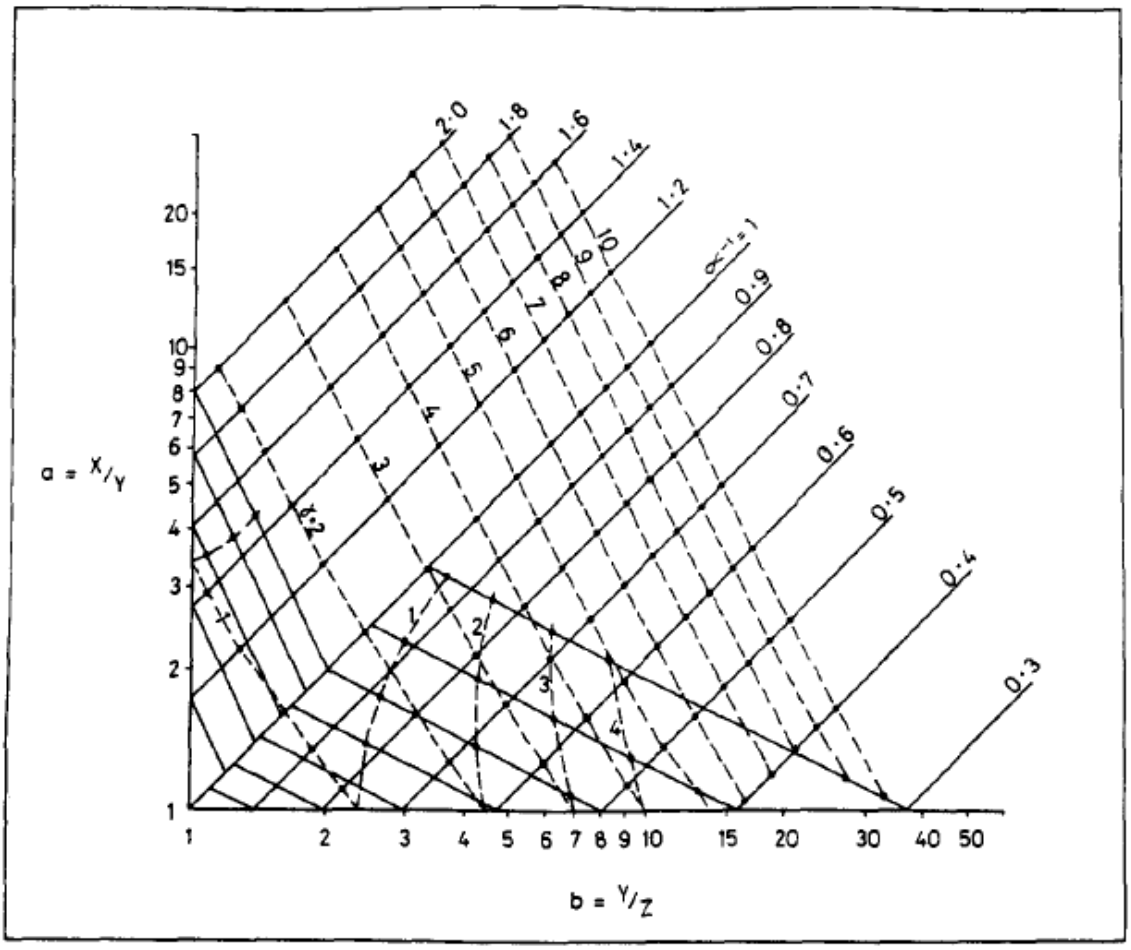

Figura 7 - Diagrama de Flinn, onde as razões do elipsoide finito de deformação produzido em distintas situações de transpressão, em termos de encurtamento (α^{-1} – linhas contínuas) e ângulo de convergência (γ – linha tracejada) são comparadas. A deformação plana ocorre sobre a diagonal $\alpha^{-1} = 1$, enquanto a transpressão é caracterizada por elipsoides oblatos, abaixo desta diagonal. Extraída de Sanderson e Marchini (1984).

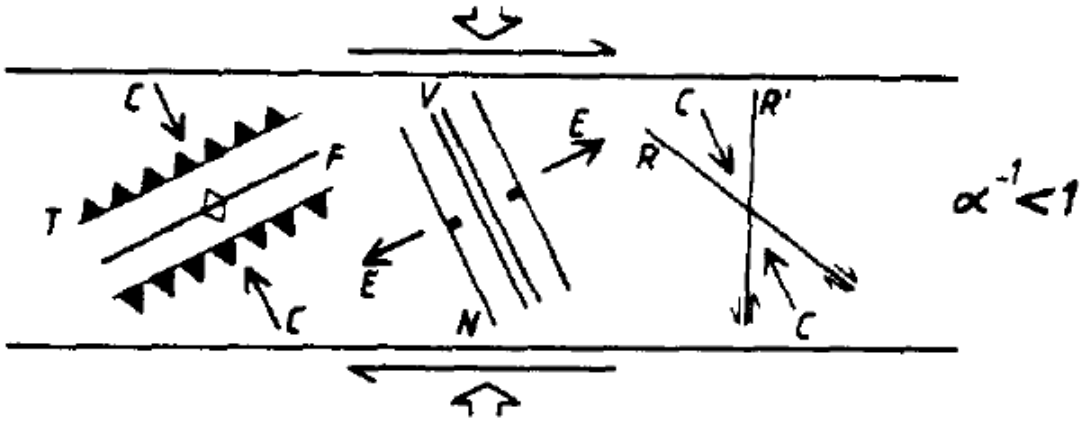

Figura 8 - Diagrama para ilustrar a orientação de estruturas no modelo de transpressão: C é o eixo de compressão (σ 1); E é o eixo de extensão (σ 3); N falhas normais; T falhas de empurrão; R, R' falhas cisalhantes de Riedel; V veios, diques ou fraturas extensionais; F eixo de dobras. Extraída de Sanderson e Marchini (1984).

Cabe aqui distinguir os modelos baseados na deformação finita (*e.g.* Sanderson e Marchini, 1984) dos que consideram os sucessivos incrementos infinitesimais da deformação instantânea (também chamada de deformação

incremental ou infinitesimal; Fossen e Tikoff, 1993; Robin e Cruden, 1994; Tikoff e Teyssier, 1994; Jones et al. 2004). A abordagem com base no elipsoide finito de deformação é puramente geométrica, tratando da soma total dos incrementos, portanto não considerando a trajetória de deformação. Já a consideração de incrementos sucessivos de fluxo tem o potencial de considerar a deformação nos seus diferentes estágios, sendo dependente do tempo e considerando a trajetória de deformação. Ao longo das últimas décadas, o modelo de transpressão originalmente proposto por Sanderson e Marchini (1984) sofreu sucessivas modificações, sendo aprimorado por diversos autores no que tange as suas condições de contorno (Fig. 6), o que permitiu considerar: variações de volume (Fossen e Tikoff, 1993), estiramento lateral (Dias e Ribeiro, 1994; Jones *et al.*, 1997), cisalhamento simples oblíquo (Robin e Cruden, 1994; Jones e Holdsworth, 1998), deformação heterogênea (Robin e Cruden, 1994), partição da deformação (Tikoff e Teyssier, 1994) e inclinação da zona (Dewey *et al.*, 1998; Jones *et al.*, 2004).

Fossen e Tikoff (1993) apresentam uma matriz unificada com base na mecânica do contínuo (aplicada à deformação de rochas primeiramente por Ramberg, 1975). Esta matriz de deformação tem o potencial de comportar cisalhamento simples em até três direções perpendiculares, cisalhamento puro (modifica a forma mas não distorce os ângulos internos, é coaxial) e mudança de volume simultâneos (Fig. 6b), e é capaz de analisar o elipsoide incremental e finito da deformação. Por considerar que a construção matemática da mesma vai além dos propósitos da presente revisão, optamos por omitir o seu desenvolvimento. Ao aplicar a matriz de deformação no estudo de situações de transpressão progressiva, utilizando os parâmetros e condições de contorno de Sanderson e Marchini (1984), Fossen e Tikoff (1993) discriminam sistemas transpressivos dominados por transcorrências, em que as lineações mudam (*switch*) de horizontal para vertical com a progressão da deformação, de sistemas altamente transpressionais, em que as lineações são sempre verticais. De forma geral, concluem que em sistemas transpressivos, a tendência das linhas é inicialmente rotacionar para a horizontal, e então tender à vertical com o acúmulo/progresso de deformação.

O significado de transpressão é discutido por Robin e Cruden (1994) ao contrapor dois sentidos vigentes, relacionados, porém sutilmente distintos. Segundo eles, transpressão do ponto de vista da tectônica regional, refere-se simplesmente ao deslocamento relativo entre duas regiões da litosfera adjacentes, combinando convergência e transcorrência (Harland, 1971). Em tom de crítica, eles ainda

completam: "*The tectonician is only accessorily concerned with the way in which rocks actually accommodate this imposed relative displacement of the two regions*". Um segundo sentido é encontrado do ponto de vista da geologia estrutural, no qual transpressão é definida como o que acontece a uma zona tabular submetida a cisalhamento ("*trans*") e achatamento ("*press*") simultâneos impostos pelas suas paredes. Segundo estes autores, daí advém um problema de espaço ("*room problem*"), causado pelo confinamento basal e lateral da zona de cisalhamento planar. Este problema só pode ser superado por perda de volume ou por extrusão vertical de matéria. Com isto, os autores chamam a atenção para a diferença entre a simples aplicação indiscriminada de um conceito ou modelo, e para a necessidade emergente de criticá-lo, reanalisando suas definições e parâmetros continuamente com o objetivo de aperfeiçoá-lo.

Estes autores propõem um modelo mais sofisticado, intitulado transpressão oblíqua (Fig. 6d). Este modelo contempla a possibilidade do componente de cisalhamento simples (distorce a forma, alterando os ângulos internos, deformação não-coaxial ou rotacional) ao longo do plano vertical ser oblíquo (*oblique-slip*). Este cisalhamento simples oblíquo pode ser fatorado em um componente transcorrente (*strike-slip*) e outro de empurrão (*dip-slip*), como na equação abaixo (proposta por Jones e Holdsworth, 1998).

$$\begin{vmatrix} 1 & \gamma_{xy} & 0 \\ 0 & 1 & 0 \\ 0 & 0 & 1 \end{vmatrix} \begin{vmatrix} 1 & 0 & 0 \\ 0 & 1 & 0 \\ 0 & \gamma_{zy} & 1 \end{vmatrix} \begin{vmatrix} 1 & 0 & 0 \\ 0 & \alpha^{-1} & 0 \\ 0 & 0 & \alpha \end{vmatrix} = \begin{vmatrix} 1 & \gamma_{xy}\alpha^{-1} & 0 \\ 0 & \alpha^{-1} & 0 \\ 0 & \gamma_{zy}\alpha^{-1} & \alpha \end{vmatrix} \qquad (2)$$

Cisalhamento Simples em XY (*strike-slip*)	Cisalhamento Simples em YZ (*dip-slip*)	Cisalhamento Puro em YZ (contração)	Transpressão Oblíqua

Outra característica importante da construção do modelo de Robin e Cruden (1994) é a heterogeneidade da deformação, derivada da base matemática da mecânica do contínuo, que considera que a rocha "transpressionada" tem uma reologia com variação linear de viscosidade, a qual diminui em direção ao centro da zona (Fig. 6c). Eles comparam este modelo com duas situações de zonas transpressivas observadas em campo: a Zona Milonítica Proterozoica do sudoeste da Suécia, que afeta granitos e gnaisses orto- e para-derivas, onde se observa a transição gradual entre indicadores de movimento de cavalgamento (foliações, lineações e indicadores cinemáticos) na margem abatida da zona ("muro") e transcorrentes sinistrais na margem soerguida ("teto"); e a Zona de Deformação

Arqueana Larder Lake-Cadillac, no Canadá, que afeta rochas supracrustais, onde indicadores cinemáticos destrais são vistos em planta, porém a lineação é frequentemente subvertical.

A modelagem numérica destes autores resulta em elipsoides de simetria triclínica, o que significa que o vetor de vorticidade (i.e. o eixo em torno do qual as partículas da rocha deformada rotacionam) não é necessariamente paralelo com nenhuma das direções principais do elipsoide de deformação. Traduzindo em termos práticos, duas consequências impactantes da simetria triclínica da deformação são a predição de variações sistemáticas na intensidade e orientação de lineações, e a possibilidade de que indicadores cinemáticos ocorrerão em outros planos além do XZ. Estas conclusões explicam satisfatoriamente os exemplos estudados pelos autores. Além disso, o caráter heterogêneo da deformação imposta no modelo de Robin e Cruden (1994) também trouxe à luz a possibilidade da partição cinemática desta deformação de simetria triclínica, a qual poderia se resolver distintamente em domínios, ora de simetria aparentemente monoclínica, ora triclínica.

Nos modelos de transpressão em que o cisalhamento simples é estritamente horizontal (*'transcurrent' transpression*), a distribuição da trama é simétrica com relação ao centro da zona, independente da profundidade (Fig. 09). Um domínio de achatamento ($k < 1$; é descrito no centro da zona, enquanto as suas bordas são invariavelmente caracterizadas por deformação plana ($k = 1$). Em um modelo considerando o cisalhamento oblíquo, a um ângulo de 75° com a direção do plano, os autores demonstram uma clara assimetria na distribuição das tramas, bem como uma grande dependência da sua geometria, intensidade e simetria (monoclínica/triclínica; relação do vetor de vorticidade com os eixos do elipsoide) para com a profundidade da zona que é observada, e em menor grau, para com a distância das margens da zona (Fig. 10).

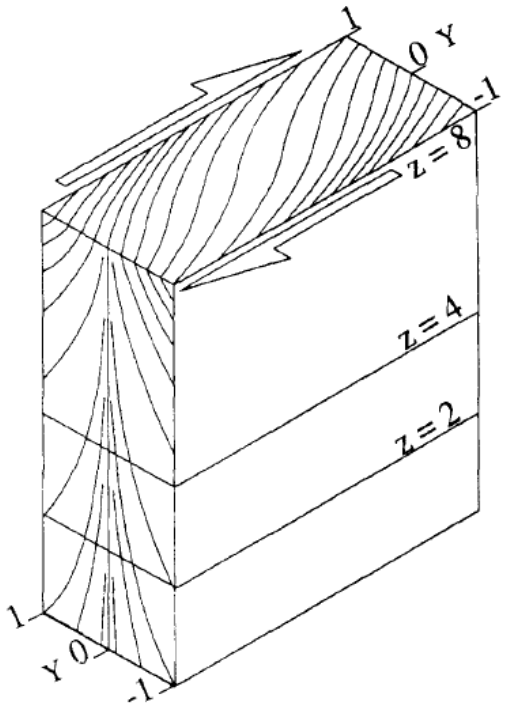

Figura 9 - O bloco diagrama resultante de um modelamento de transpressão dominada por transcorrência, feito com ângulo de convergência de 0° e uma razão "*press/trans*" = 0,1. Traços no bloco diagrama ilustram os traços de foliação em uma seção vertical e em planta. Z = altura relativa; Y = distância relativa do centro da zona. Extraída de Robin e Cruden (1994).

A partição da deformação em zonas transpressivas foi estudada por Tikoff e Teyssier (1994), ao modelar deformações homogêneas considerando um tensor com gradientes de velocidades em três dimensões para diferentes ângulos de convergência, o que permitiu a diferenciação entre casos de transpressão dominados por transcorrência e por cisalhamento puro. Neste modelo é ilustrada a relação existente entre o ângulo de convergência das placas com relação aos seus limites, os eixos do elipsoide de deformação instantânea e de deformação finita, demonstrando que os elipsoides instantâneo e finito não são coincidentes. Isto significa que não há uma relação geométrica necessariamente direta entre a deformação imposta num dado momento e as estruturas formadas durante períodos prolongados, as quais acumulam sucessivos incrementos de deformação (estruturas dúcteis, como foliações, lineações ou mesmo falhas e zonas de cisalhamento de escala crustal). Em outras palavras, nestes casos, os eixos de deformação finita X, Y e Z não são diretamente correlacionáveis aos respectivos eixos de tensão σ_3, σ_2 e σ_1. Eles ainda quantificaram a eficiência de falhas na partição cinemática da deformação em termos do campo de deslocamento (*displacement field*). Para a aplicação dos resultados do modelo numérico, os autores utilizaram os exemplos da Falha de San Andreas (Califórnia), a qual apresenta uma grande quantidade de

partição do campo de deslocamento, e a Grande Falha de Sumatra, a qual apresenta um rejeito pequeno, portanto, representando uma quantidade pequena de partição cinemática da deformação.

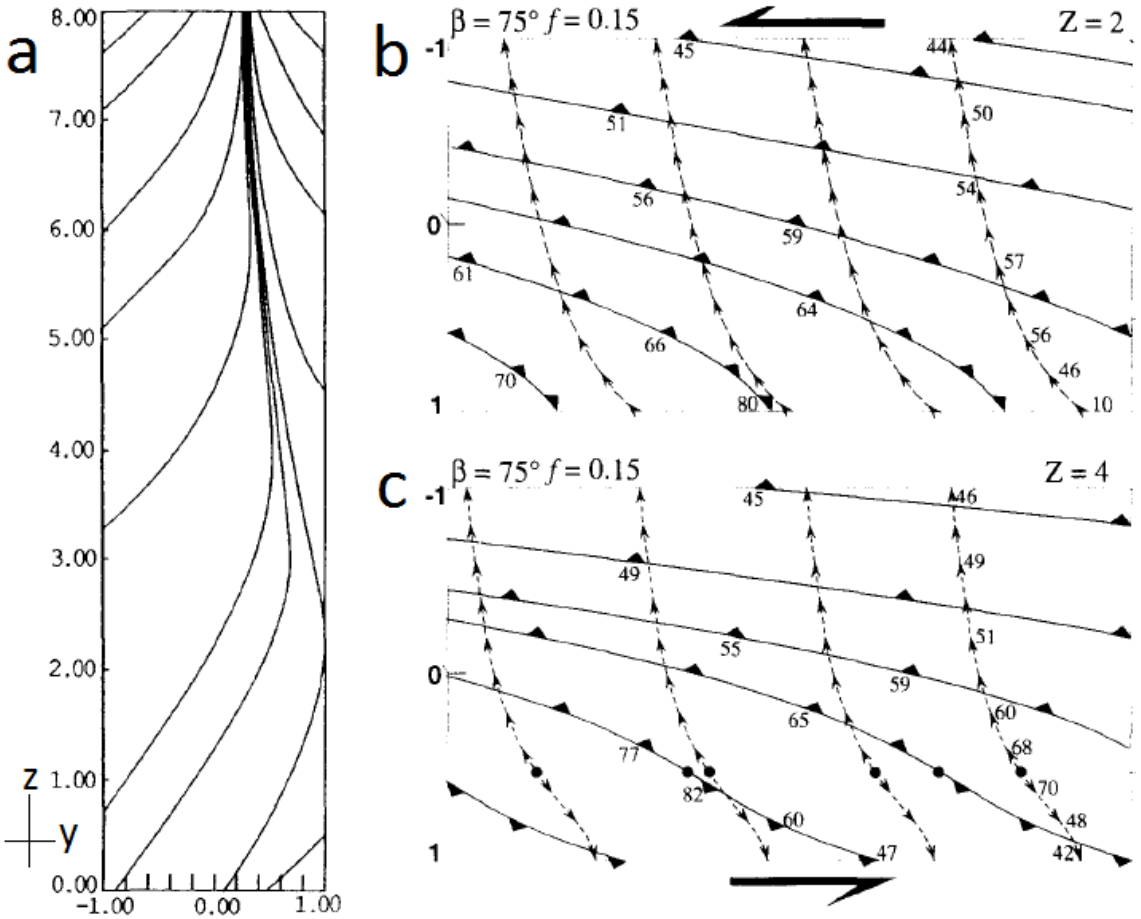

Figura 10 – Resultados do modelamento de uma zona transpressiva oblíqua com parâmetros de modelamento: razão “press/trans” = 0,15; e obliquidade de 75° para o componente de cisalhamento simples. (a) Traços de foliação visto em uma seção perpendicular à zona (plano YZ). O bloco abatido corresponde ao valor -1 no eixo Y. (b) e (c) Vistas em planta desta mesma zona, cortadas nas alturas relativas de Z = 2 (b) e Z = 4 (c). Linhas contínuas representam os traços da foliação, enquanto linhas pontilhadas representam lineações. Valores de mergulho e caimento são ilustrados. É notável a assimetria da distribuição e a variação de atitudes, que numa mesma seção passam de transcorrente para empurrão. Modificado de Robin e Cruden (1994).

Contrariando os seus contemporâneos, que argumentavam que a partição da deformação seria causada pela partição das tensões em regiões enfraquecidas (falhas) da crosta rígida (Zoback e Healy, 1992), Tikoff e Teyssier (1994) defendem que a partição da deformação em estruturas paralelas e perpendiculares aos orógenos é, em última instância, resultado do movimento relativo entre as placas e do ângulo com que este movimento se dá. Aprofundando os conceitos de transpressão dominada por transcorrência (*wrench dominated transpression*) e por cisalhamento puro (*pure-shear dominated transpression*), introduzidos por Fossen e

Tikoff (1993), os autores propõem o parâmetro θ, que é o ângulo entre o eixo horizontal máximo do elipsoide incremental de deformação e a margem das placas ou limite da zona. O parâmetro θ tem uma relação direta com o ângulo entre o movimento relativo e as margens das placas. Assim, postulam uma transição entre os regimes *wrench dominated* e *pure-shear dominated* com limiar no número de vorticidade W_k = 0,81 (Fossen e Tikoff, 1993) e θ = 35°, o qual corresponde ao ângulo de 20° para a convergência oblíqua entre as placas.

Segundo os autores, apoiados em modelos físicos análogos (Pinet e Cobbold, 1992), estruturas relacionadas à cinemática dominante se formariam em resposta a deformação instantânea (elipsoide infinitesimal), porém não estariam em posição favorável a acomodar a deformação finita transpressiva, imposta pelas condições de contorno (i.e. convergência oblíqua entre as placas). Por isso, em ambos tipos de transpressão, tanto falhas de empurrão quanto transcorrentes tendem a formar-se e a ser ativas simultaneamente. O efeito do componente de cisalhamento puro é registrado em deformação interna, espessamento e soerguimento topográfico. O efeito do componente de cisalhamento simples pode ser particionado entre deformação interna e deslizamento ao longo de falhas transcorrentes discretas. Para qualquer que seja o componente transcorrente particionado em falhas discretas, a vorticidade da zona transpressiva adjacente decresce (tornando-se mais contracional), visto que a formação de falhas transcorrentes discretas absorve parte do componente transcorrente do modelo de transpressão homogêneo (Tikoff e Teyssier, 1994). Desta forma é possível comparar quantitativamente de forma direta o ângulo de convergência das placas com relação aos seus limites e o parâmetro θ observado com a percentagem de deslocamento particionado em falhas transcorrentes (Fig. 11). Concluem que a partição da deformação é causa das falhas transcorrentes de sistemas transpressivos (independente da sua eficiência), e não o contrário.

Entretanto, o fator controlador do quanto do campo de deslocamento é particionado entre as falhas transcorrentes e os domínios transpressivos adjacentes é discutível. Na opinião dos autores isto pode também ser controlado pelo limiar (20°) entre a transpressão dominada por transcorrência e por cisalhamento puro. Esta hipótese abre a discussão sobre o grau de acoplagem mecânica entre os blocos adjacentes às falhas. Tikoff e Teyssier (1994) sustentam a opinião de que existe um grau de acoplagem importante, refletido na consistência da obliquidade das estruturas observadas a até 300 km de distância das falhas estudadas na

Califórnia e em Sumatra. Esta acoplagem pode ser devida à presença de um manto litosférico resistente, o qual sofre os efeitos do cisalhamento de forma penetrativa/bem distribuída (Molnar, 1992; Vauchez e Nicolas, 1991; Tikoff et al. 2002; Fig. 12).

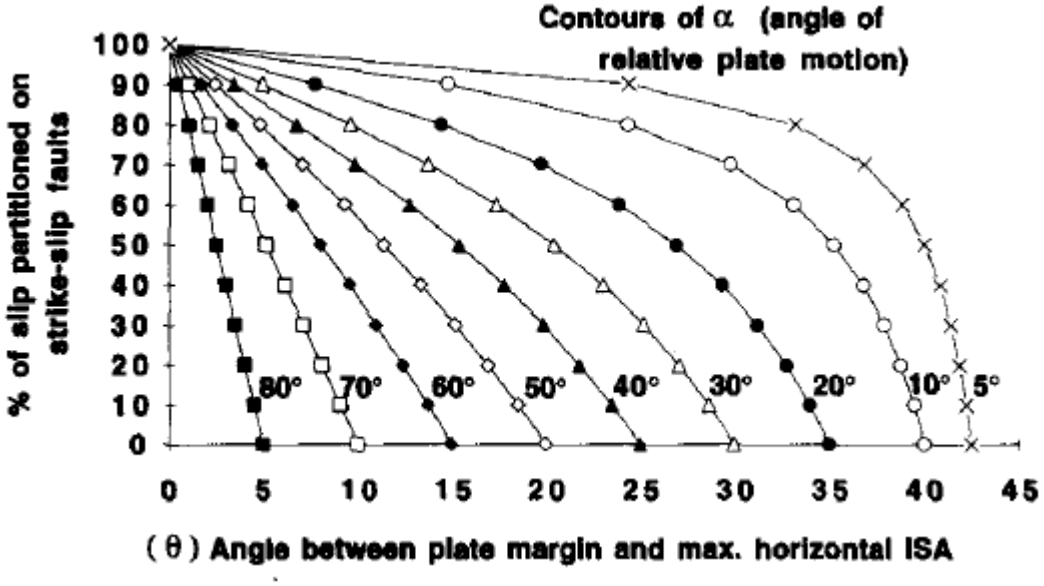

Figura 11 – Gráfico que relaciona o ângulo entre a orientação do eixo horizontal máximo do elipsoide de deformação instantânea (ISA) e a margem da placa com o ângulo do vetor movimento como uma função da partição da deformação em falhas transcorrentes. Extraída de Tikoff e Teyssier (1994).

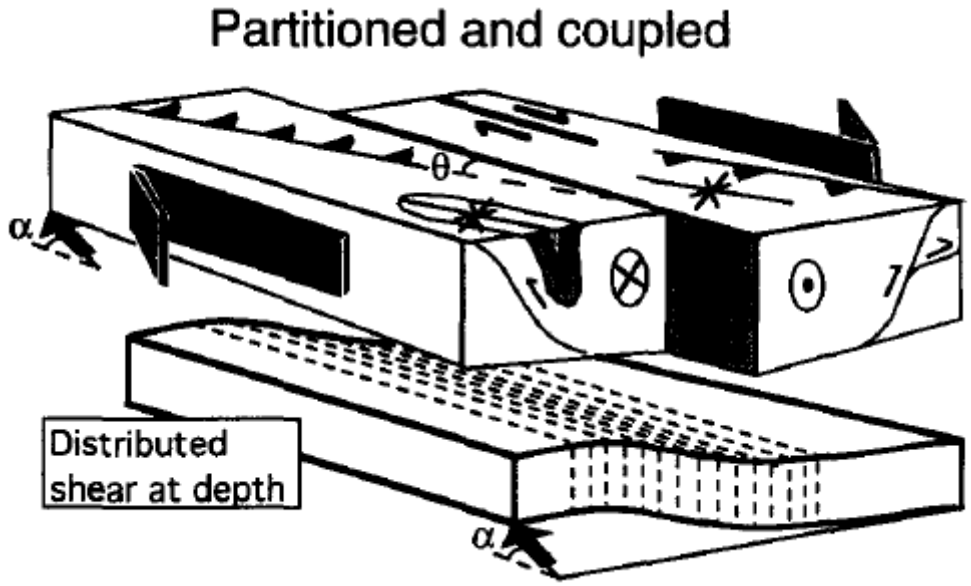

Figura 12 – Desenho esquemático ilustrando a partição cinemática da deformação em domínios contracionais separados por uma falha transcorrente discreta. A partição da deformação na crosta superior é controlada pela movimentação das placas em um sistema em que ambos blocos adjacentes à falha estão mecanicamente acoplados devido ao cisalhamento distribuído em profundidade. Extraído de Tikoff e Teyssier (1994).

Jones *et al.* (2004) apresenta o modelo de transpressão inclinada (Fig. 13). A transpressão inclinada, assim como a transpressão oblíqua, é definida em termos de contração, *strike-slip* e *dip-slip* simultâneos, porém, diferentemente desta, ocorre entre paredes paralelas não verticais. O modelo é desenvolvido a partir de modelagem numérica e é aplicado no estudo de uma zona de transpressão inclinada exposta em Eyemouth, SE da Escócia, a qual afeta uma sequência supracrustal e apresenta importante partição da deformação (descrita em detalhe por Holdsworth *et al.*, 2002). Todas as demais condições de contorno modeladas seguem as mesmas definidas por Sanderson e Marchini (1984): deformação homogênea, volume constante e confinamento lateral e basal. Em termos da matriz de deformação, a transpressão inclinada é expressa da mesma forma que a transpressão oblíqua. O autor fez uso da abordagem de Fossen e Tikoff (1993), a qual admite cisalhamento puro e simples simultâneos, e pode ser escrita da seguinte maneira:

$$\begin{vmatrix} 1 & \gamma_{XY}(1-\alpha_z^{-1})\ln(\alpha_z) & 0 \\ 0 & \alpha_z^{-1} & 0 \\ 0 & \gamma_{ZY}(1-\alpha_z^{-1})\ln(\alpha_z) & \alpha_z \end{vmatrix} \qquad (3)$$

Diferentes situações em termos de orientação do vetor movimento com relação à direção da zona (β, com valores de 10°, 20°, 40° e 70°) e ângulo de mergulho da zona (δ, variando entre 5° e 80°) são previstas. Para cada uma, diferentes quantidades de encurtamento (S) são avaliadas, marcando a progressão da deformação nos *strain paths* plotados nos diagramas de Flinn (Fig.14). A comparação entre as situações modeladas permite formular uma série de considerações sobre a transpressão inclinada. Para Jones *et al.* (2004), β tem um efeito marcante na forma do elipsoide finito, visto que para valores muito baixos ou muito altos do ângulo de convergência, as zonas adquirem características semelhantes à *strike-slip* e *overthrusting*, respectivamente. Já δ adquire maior influência quando os mergulhos são menores do que 30-40°. S marca a progressão de deformação.

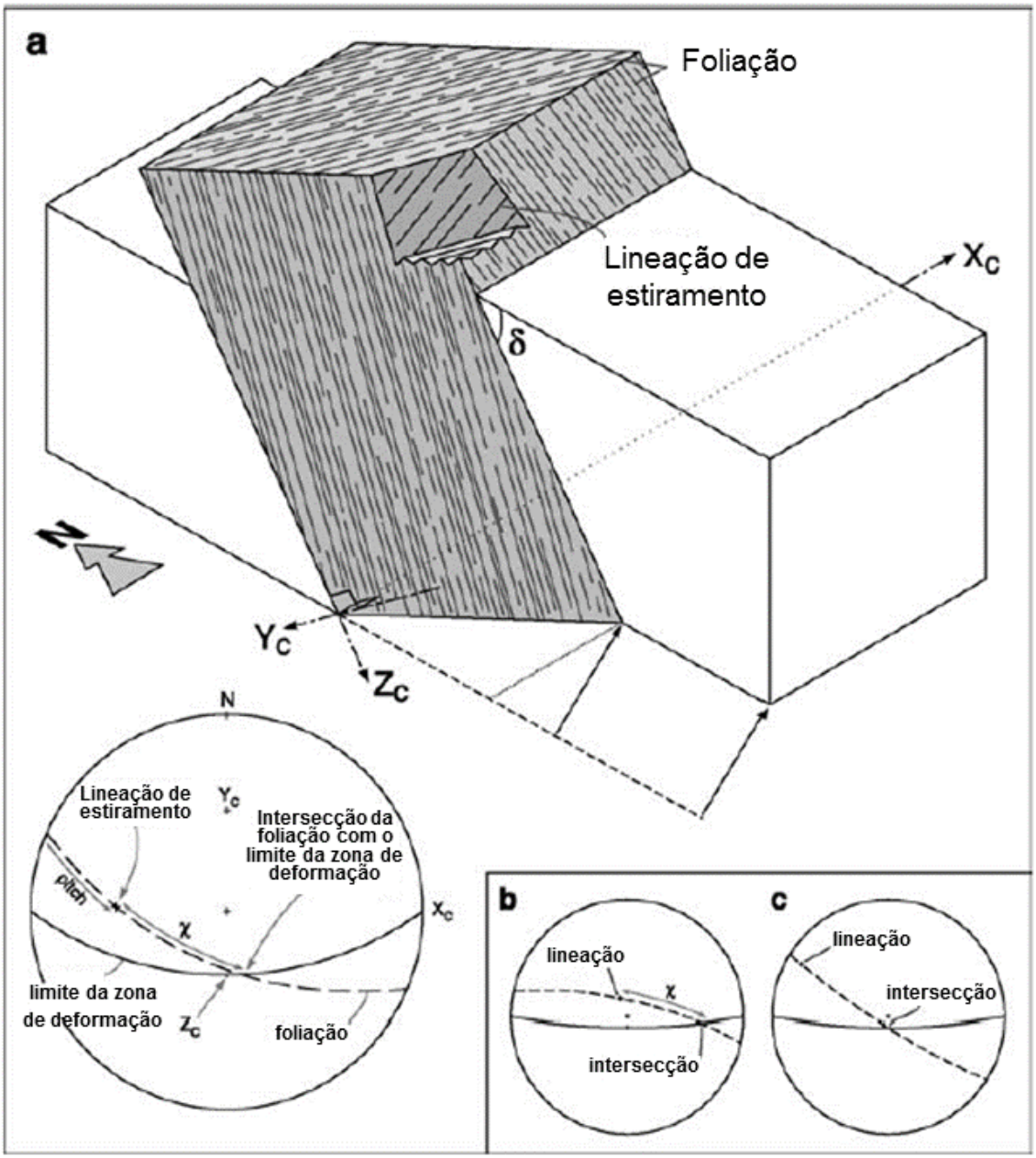

Figura 13 - Orientações típicas para foliação e lineação no modelo de transpressão inclinada. A direção da foliação é oblíqua em relação aos limites da zona, neste caso estando a direita, indica o componente sinistral da zona. O mergulho da foliação em geral é maior que o dos limites da zona, devido ao componente de cisalhamento simples no plano YZ (empurrão), que na figura (a) indica topo para o norte. O caimento da lineação pode ser alto (b), moderado (a) ou baixo (c), dependendo do estado da deformação finita. χ é o ângulo entre a lineação de intersecção dos planos de foliação e limite da zona e a lineação de estiramento medido no plano de foliação, que para deformações de simetria triclínica varia entre $0° < \chi < 90°$. Modificada de Jones *et al.* (2004).

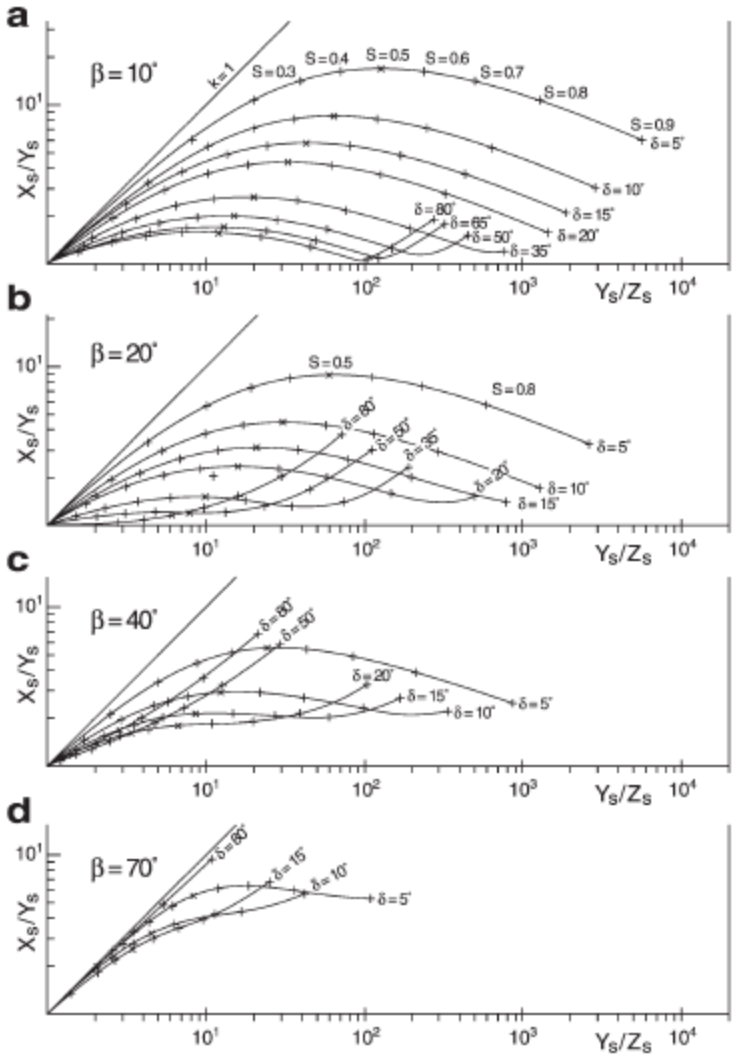

Figura 14 - Diagramas de Flinn mostrando trajetórias de deformação para transpressão simples inclinada modeladas para quatro diferentes ângulos de convergência (β), cada um mostrando quatro diferentes ângulos de mergulho da zona de deformação (δ). As trajetórias representam encurtamentos (S) de 0 a 90%. Os gráficos demonstram que a não ser que os mergulhos da zona sejam baixos (menor que 40°), a forma do elipsoide finito de deformação é pouco dependente de δ. Extraída de Jones *et al.* (2004).

Ao plotar em estereogramas a posição dos três eixos do elipsoide finito durante a progressão da deformação (Fig. 15), Jones *et al.* (2004) observa que estes são oblíquos aos limites da zona e que mudam de orientação com o encurtamento progressivo. Isto é atribuído a presença de um componente de vorticidade em torno dos 3 eixos, o qual caracteriza a deformação total resultante como de simetria triclínica. Daí resulta uma característica emergente do modelo de transpressão triclínica, que é a variação de orientação do eixo X (lineação) com a progressão da deformação (acúmulo de encurtamento). Para algumas trajetórias de deformação, o eixo X permanece praticamente paralelo à direção ou ao mergulho durante grandes quantidades de encurtamento progressivo, mas para a maioria das trajetórias previstas o ângulo de caimento de X muda significativamente durante a deformação

(Fig. 16). Esta característica é notável quando a deformação é caracteristicamente transpressional, (ambos componentes, “*trans*” e “*press*”, são significantes; Fig.16b e c). Por outro lado, quando β é muito baixo ou muito alto, a grometria da zona tende a um dos componentes extremos, transcorrência ou empurrão (Fig.16a e d, respectivamente). Nestes casos, o eixo intermediário do elipsoide finito de deformação (Y) é relativamente constante durante a deformação progressiva, resultando em uma deformação de simetria aparentemente monoclínica.

Segundo Jones *et al.* (2004), a não ser que a partição da deformação em domínios seja 100% efetiva, a foliação tectônica resultante da deformação transpressiva tende a apresentar uma direção e um mergulho não-paralelos aos limites da zona transpressiva (Fig. 13). A direção da foliação geralmente estará à esquerda da direção da zona quando esta tiver uma cinemática destral/horária, refletindo o componente transcorrente horário da deformação, com a tendência de rotacionar em direção ao paralelismo com a zona. Já o mergulho apresentado, geralmente será superior ao da zona, cuja tendência ao paralelismo reflete o componente não-coaxial de empurrão (*overthrusting*). O autor alerta para o fato de que em determinadas situações podem ocorrer mergulhos de foliação para o quadrante oposto do mergulho da zona.

Lineações de estiramento podem variar muito em orientação, com a possibilidade de obliquidade (*rake*) praticamente entre 0° e 90°. Lineações próximas destes extremos podem sugerir a partição da deformação em domínios monoclínicos, enquanto lineações de obliquidade intermediária são correlacionáveis com simetrias de deformação triclínica. De qualquer forma, interpretações realmente confiáveis do estado finito da deformação são obtidas quando é possível observar os limites bem definidos da zona transpressiva, e as estruturas documentadas podem ser comparadas com a sua orientação. A simetria triclínica da deformação é reconhecida quando o ângulo entre as lineações de estiramento e de intersecção (entre os planos de foliação e do limite da zona) é medido ao longo do plano de foliação, e não for nem 0°, nem 90° (Fig.13). Se os limites da zona podem ser delineados, esta é uma relação diagnóstica, mesmo que a zona como um todo tenha sofrido basculamento ou retrabalhamento.

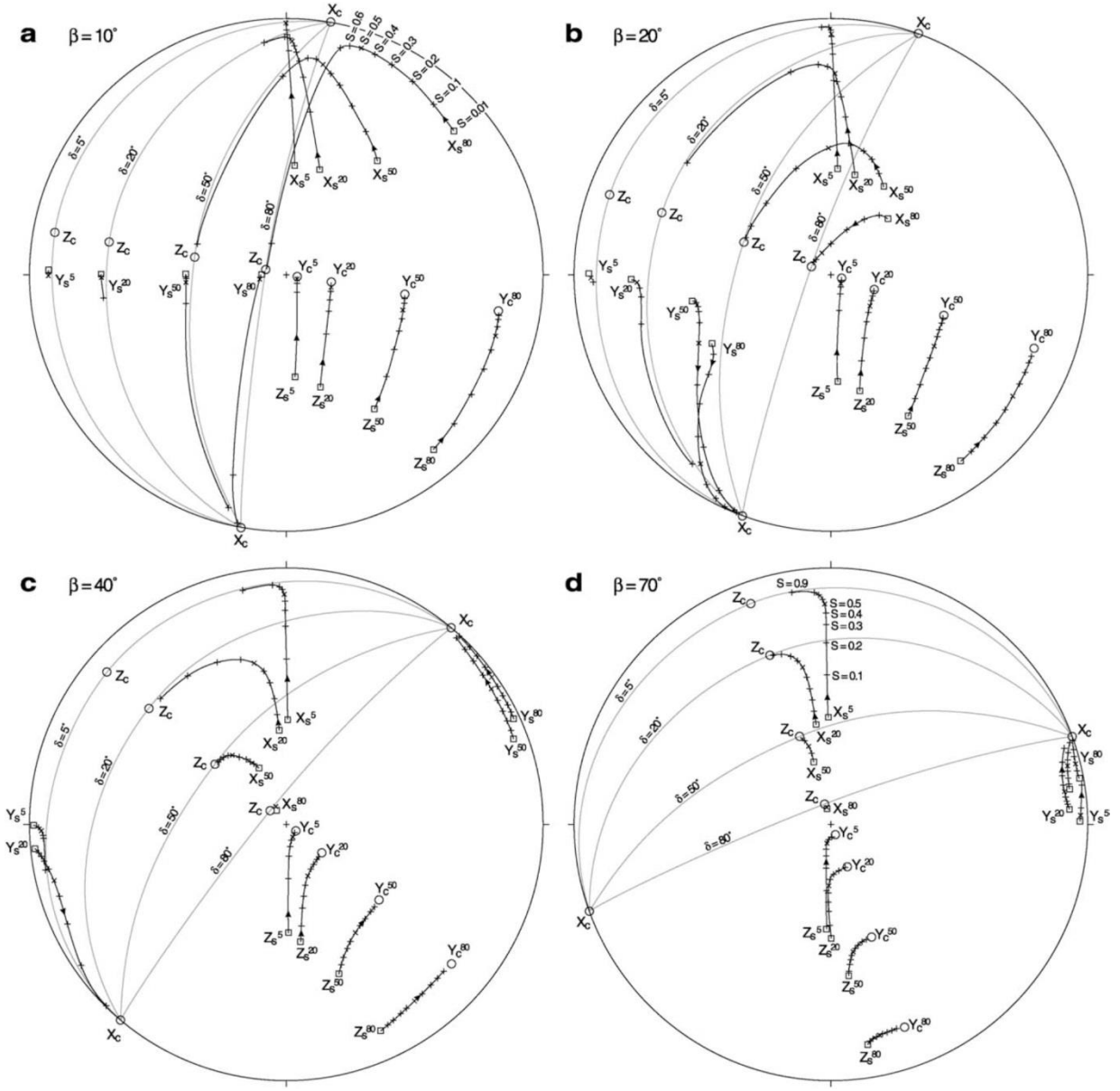

Figura 15 - Projeções estereográficas (hemisfério inferior, equiângulo) mostrando variações na orientação do elipsoide finito de deformação durante a progressão da transpressão simples inclinada e deformação homogênea. Os quatro diagramas representam modelos com diferentes ângulos de convergência (β). A geometria da zona é comparável com a exibida na figura 12. O vetor movimento é orientado N-S. A zona de cisalhamento é sinistral e mergulha para NW (WNW para baixos valores de β; NNW para valores altos), resultando em um componente de empurrão de topo para SE. Cada gráfico exibe orientações do elipsoide finito para diferentes mergulhos da zona (δ = 5°, 20°, 50° e 80°). Em todos os casos, o menor eixo do elipsoide (Z_S) é oblíquo aos três eixos cartesianos no princípio do encurtamento, mas tende a paralelizar com Y_C durante a progressão da deformação. De forma semelhante, o maior eixo do elipsoide (X_S) tende a rotacionar em direção ao mergulho da zona (Z_C), porém isso não seja uma regra. As trajetórias de X_S podem ser complexas. Para algumas trajetórias o eixo X_S atinge alto caimento enquanto a deformação se acumula, enquanto noutras acontece o oposto. Em alguns casos (e.g. β = 10°, δ = 50°), X_S inicia com alto caimento, progride para baixos caimentos, e então retorna a ser íngreme em direção ao Z_C. Extraída de Jones *et al.* (2004).

O autor chama a atenção para o fato de que na crosta média ou inferior, os fatores litológicos e ambientais (P, T, taxa de deformação, mineralogia, tamanho de grão, etc.) condicionam uma reologia que permite a reorientação progressiva da trama, a qual pode traduzir as predições do modelo (Figs. 14 - 16), ao menos para taxas de deformação moderadas. Com o aumento da deformação, é possível que a

foliação deixe de representar o plano XY do elipsoide finito de deformação, visto a possibilidade do desenvolvimento de tramas secundárias e o aumento da heterogeneidade/complexidade da deformação (Lister e Williams, 1983; Goodwin e Tikoff, 2002). Segundo Jones *et* al. (2004), neste contexto, podem surgir estruturas de campo enigmáticas. Ainda que evidências de tramas iniciais e sua rotação progressiva possam ser obliteradas pelo progresso da deformação, indicações da rotação tridimensional progressiva dos eixos do elipsoide de deformação podem ser buscadas em: relações de corte, crenulações, tramas secundárias, rotações de porfiroblastos e porfiroclastos, padrões de veios, diferenças nas orientações das lineações em zonas de alta e baixa deformação, evolução de dobras convolutas (rotação de eixos e desenvolvimento de dobras curvo-lineares), fraturamento polimodal, dados de estrias de falhas mostrando múltiplas fases de deslocamento, etc. (Dewey *et al.* 1998).

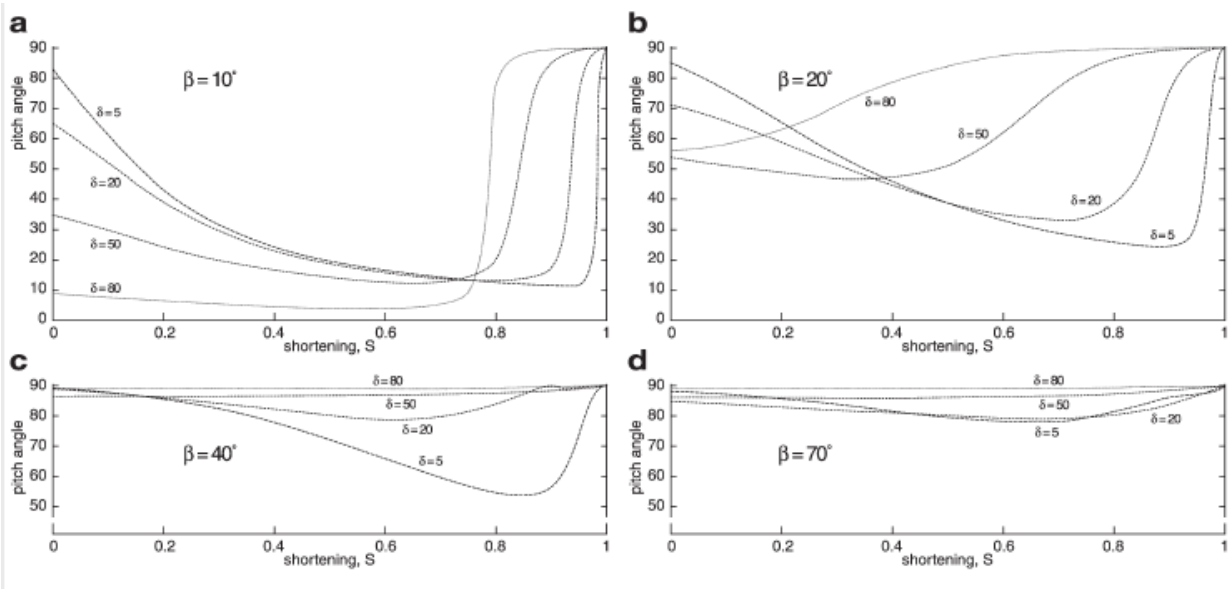

Figura 16 - Exemplos de trajetória da deformação na transpressão inclinada, mostrando a variação da obliquidade do eixo maior do elipsoide de deformação (medida no plano XY). Para algumas trajetórias X_S permanece próximo da direção ou do mergulho do plano durante grandes quantidades de encurtamento. Para a maioria das trajetórias a obliquidade de X_S varia consideravalmente, mesmo durante os primeiros 20 – 30% de encurtamento. Extraída de Jones *et al.* (2004).

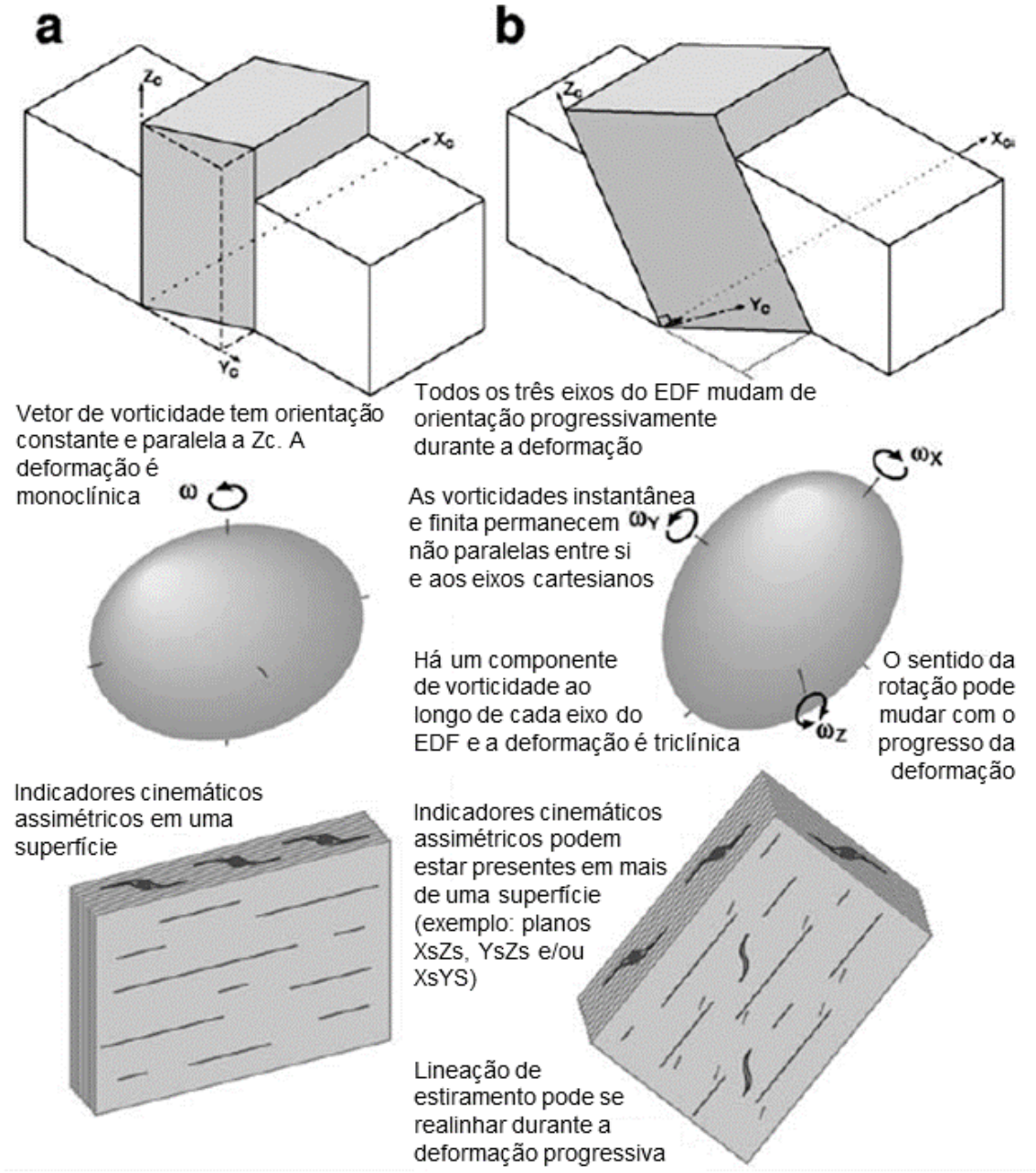

Figura 17 - Indicadores cinemáticos, vorticidade e simetria da deformação. (a) Transpressão vertical idealizada por Sanderson e Marchini (1984). A rotação ocorre em torno do eixo vertical, o que não causa mudanças de orientação com a progressão da deformação. O vetor de vorticidade instantânea é sempre paralelo ao eixo de vorticidade finita e a um dos eixos do elipsoide deformação de finito (EDF). A deformação tem simetria monoclínica e indicadores cinemáticos assimétricos são visíveis apenas em um plano. (b) Transpressão inclinada. Existe um componente de vorticidade atuante em torno dos três eixos do EDF. Portanto, os três eixos mudam de orientação durante a deformação progressiva, e os eixos de vorticidade instantânea e a rotação finita não estão alinhados. A deformação é triclínica, e para algumas trajetórias de deformação, indicadores cinemáticos assimétricos podem ser observáveis em seções paralelas ou perpendiculares ao eixo máximo do EDF e mesmo dentro do plano de foliação. Extraída de Jones *et al.* (2004).

Dentre as decorrências do modelo de transpressão inclinada, está o fato de que, devido a não coaxialidade dos componentes transcorrentes e de empurrão, tanto seções cortadas paralelas aos planos XZ quanto YZ apresentarão indicadores cinemáticos assimétricos. Mesmo dentro do plano de foliação (XY) poderão ocorrer evidências de não coaxialidade, desenvolvidas em função do realinhamento da

lineação (X) durante a deformação progressiva (Figs. 16 e 17). O quanto indicadores assimétricos se desenvolverão em superfícies de diferentes orientações depende da trajetória de deformação experienciada pela rocha, a qual pode provêr rotações relativamente simples ou complexas, com mudanças de orientação dos três eixos do elipsoide e mesmo mudanças no sentido da vorticidade ao longo da trajetória. O quanto a vorticidade estará registrada em indicadores cinemáticos assimétricos também depende da reologia da rocha e dos processos deformacionais atuantes. O constante realinhamento do vetor de vorticidade finita e do elipsoide finito de deformação, e o seu desalinhamento com o elipsoide instantâneo de deformação, podem favorecer a partição da deformação (Tikoff e Teyssier, 1994).

Outra decorrência importante do modelo de transpressão inclinada, apenas aparentemente contraditória, é o fato de que um componente de movimento normal é uma característica inerente. Enquanto um dos limites da zona (o “muro”) tem um robusto componente de empurrão, para dar conta da extrusão vertical de matéria devida à contração, o outro limite (“teto”) apresenta um componente de movimento normal. Desta forma, falhas ou zonas de cisalhamento normais podem estar intimamente relacionadas à processos de encurtamento e espessamento crustais. Portanto, a presença de falhas normais não implica contextos tectônicos extensionais, como indicam alguns *detatchments* de baixo ângulo e cinemática normal reportados nos Himalaias (Burchfiel et al., 1992).

Um último modelo é apresentado por Fernandez e Díaz-Azpiroz (2009), intitulado transpressão triclínica com extrusão inclinada, partindo de pressupostos muito semelhantes aos de trabalhos anteriores (e.g. Jones et al., 2004). A transpressão triclínica acontecerá quando nenhum dos eixos principais do elipsoide de deformação for estritamente paralelo ao vetor de vorticidade. Segundo os autores, o plano normal ao vetor de vorticidade (*vorticity normal section* – VNS) será aquele em que a rocha apresentará a máxima assimetria, geralmente concentrando a distribuição alinhada dos pólos de foliações, com desvio inferior a 5°. O ângulo (ζ) entre a direção de cisalhamento simples e a direção de extrusão é um dos principais parâmetros controlando a trama final, com elipsoides de deformação plana para $\zeta < 40°$ e tendência a elispoides oblatos com $\zeta > 40°$. Este modelo prevê diversos padrões de distribuição de lineações para diferentes situações envolvendo as direções de cisalhamento simples e extrusão e o ângulo entre elas, incluindo distribuições ao longo de guirlandas completas, quando a direção de extrusão desviar menos de 30° em relação à vertical. O modelo de Fernandez e Díaz-Azpiroz

(2009) também confirma a tendência de reorientação dos componentes da trama com a deformação progressiva já observada por Jones et al. (2004) e trabalhos anteriores. Um protocolo de estudos para situações de transpressão triclínica é proposto por Fernandez et al. (2013), testando o modelo de transpressão triclínica com extrusão oblíqua. Para tanto é necessário que se conheçam os limites da zona de cisalhamento (orientação), assim como a orientação da trama, e se possível dados quantitativos da deformação da rocha.

2.2.2 Heterogeneidade e partição da deformação

A deformação das rochas é geralmente heterogênea. Domínios homogêneos são encontrados quando delimitamos arbitrariamente uma escala e um volume de rocha a ser analisado. Gradientes de deformação em zonas de cisalhamento são comuns, com um aumento de intensidade em direção ao centro das zonas (Robin e Cruden, 1994), assim como a sua flutuação entre zonas de baixa deformação intercaladas com zonas anastomosadas de alta deformação (Ramsay, 1967; Girard, 1993).

Como grande parte dos mecanismos de deformação das rochas tende a transmitir ou propagar anisotropias, principalmente durante as fases iniciais de deformação, as heterogeneidades prévias ou adquiridas afetam a forma como a deformação incremental é resolvida (Goodwin e Tikoff, 2002). Potanto, mesmo que as condições de contorno sejam favoráveis à deformação inicialmente homogênea, é natural que a complexidade dos sistemas cisalhados aumente com a progressão da deformação, e em última instância, com o tempo.

A partição da deformação ocorre quando a deformação total (*bulk strain*) imposta em uma dada escala propaga-se através das escalas inferiores de forma a dissipar-se de forma compartimentada em domínios ou entre os constituintes do sistema deformado. A partição pode se dar em termos de intensidade, mecanismos e/ou cinemática. A deformação total em sistemas transpressivos geralmente tem seus constituintes cinemáticos particionados em domínios, onde estruturas de geometrias contrastantes são desenvolvidas.

A partição, assim como a transpressão, ocorre naturalmente em qualquer escala, como por exemplo: quando dois fenocristais ou porfiroblastos se aproximam e a matriz fina, espremida entre eles escapa absorvendo a deformação; ou quando uma unidade ou grupo de unidades litológicas incompetentes é comprimida entre duas unidades mais competentes; ou por fim quando observamos uma faixa

orogênica delimitando o contato entre duas entidades cratônicas, tendo absorvido e concentrado a deformação resultante do seu encontro. Em todos estes exemplos buscamos uma justificativa no contraste reológico para a partição da deformação, onde fica fácil entender o porquê ocorre partição. A partição da deformação ocorre em resposta a anisotropias estruturais, sejam elas iniciais ou induzidas pela deformação (Jones e Tanner, 1995). Desta forma, a reativação de estruturas facilita a partição. A progressão da deformação, a imposição de sucessivos incrementos deformacionais acompanhados da rotação dos eixos e o não paralelismo dos elipsoides finito e incremental são fatores que propiciarão a formação de estruturas distintas, orientadas de forma conveniente a resolver os distintos componentes da deformação total, mesmo em uma massa rochosa inicialmente homogênea (Tikoff e Teyssier, 1994). Tikoff e Teyssier (1994) sugerem que a partição é especialmente facilitada onde o ângulo de convergência/divergência é inferior a 20°, devido ao não paralelismo dos eixos dos elipsoides finito e incremental.

Um método gráfico de representação e análise da partição da deformação triclínica intitulado “triângulo de deformação” é apresentado por Jones *et al.* (1997) e Jones e Holdsworth (1998) (Fig. 18 e 19). As pontas do triângulo representam os componentes de movimento isolados, os quais compõem a matriz de deformação (contração, transcorrência e *dip-slip*). As arestas do triângulo são combinações entre dois destes três extremos, e a área dentro do triângulo representa uma transpressão/transtração oblíqua ou inclinada. Ainda que plotar a posição de estruturas ou domínios estruturais no triângulo de deformação (Fig. 19) seja uma abordagem qualitativa (em parte subjetiva), é uma forma eficiente de avaliação e demonstração da partição da deformação de regiões submetidas à transpressão/transtração (Holdsworth *et al.*, 2002; Zibra *et al.*, 2014). Jones *et al.* (2004) ainda chama a atenção para o fato de que há uma tendência natural da partição da deformação transpressiva ocorrer em domínios de transcorrência e contração não coaxial.

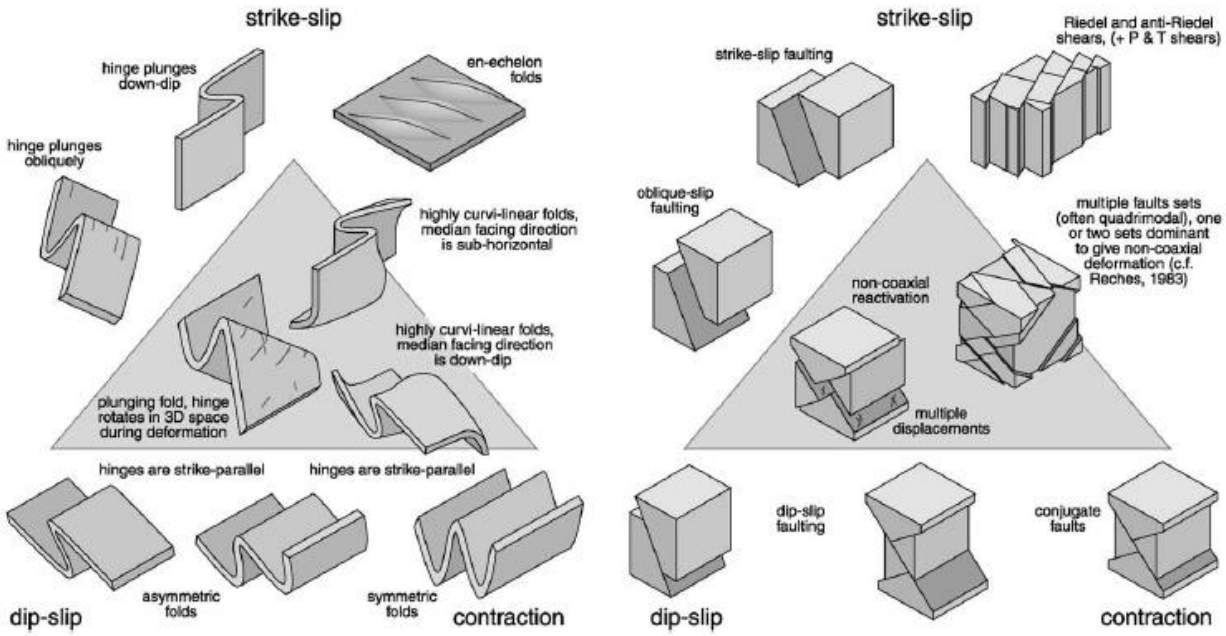

Figura 4 - O triângulo de deformação e o significado cinemático de estruturas individuais tipicamente encontradas em zonas de transpressão oblíqua ou inclinada. Extraída de Jones *et al.* (2004).

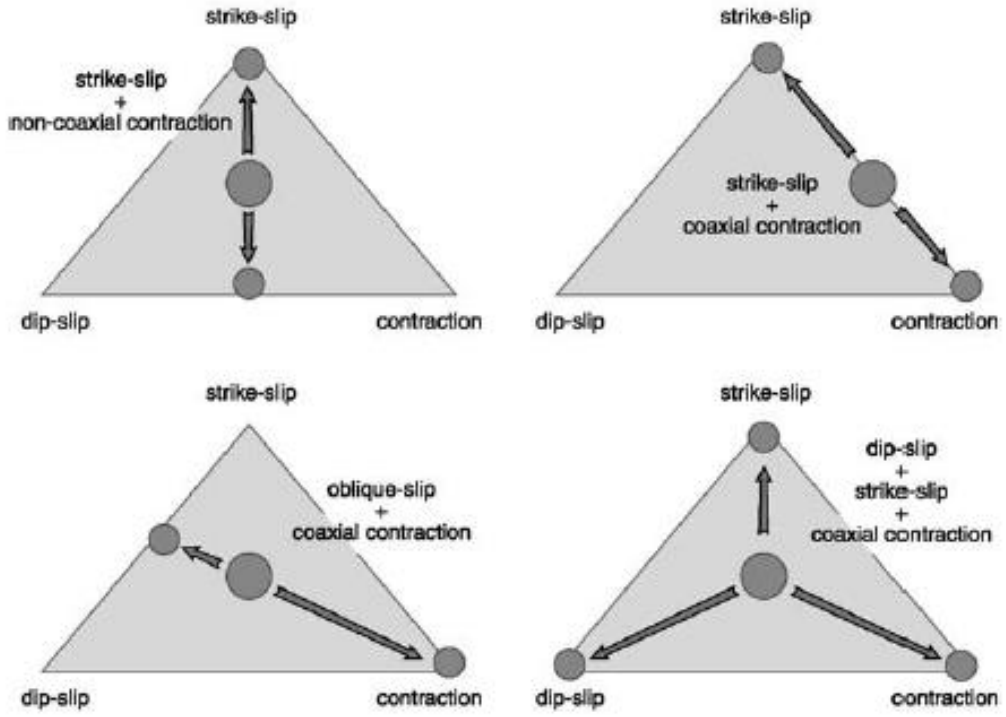

Figura 1**9** - Algumas formas de partição da deformação transpressiva total em domínios deformacionais. Aplicável a transpressão oblíqua e inclinada. A partição da transpressão inclinada total em transcorrência e contração não-coaxial é comum, e provavelmente mais favorável que a partição em cisalhamento simples oblíquo e contração coaxial (Molnar, 1992; Dewey *et al.*, 1999). Extraída de Jones *et al.* (2004).

2.2.3 Transpressão e magmatismo sintectônico

Em regiões onde ocorre amplo magmatismo sintectônico, como em contextos de arco magmático (Robin e Cruden, 1994) ou de magmatismo pós-colisional (Romeo *et al.*, 2006; Zibra *et al.*, 2014), é esperado que ocorra a facilitação da partição da deformação, devido ao contraste de viscosidade entre o magma e suas encaixantes.

A relação entre zonas de cisalhamento e magmatismo sintectônico é vastamente documentada e debatida na literatura (Paterson *et al*., 1989; Zibra *et al.*, 2012; entre outros). Relações de causa e efeito são argumentadas de ambos os lados, como a focalização da migração de magmas ao longo de zonas de cisalhamento (Brown, 1994) *vs.* a concentração de deformação sobre corpos magmáticos parcialmente cristalizados (Tommasi *et al.*, 1994; Neves *et al.*, 1996). Brown e Solar (1998) propõem de forma conciliadora que estes sejam pontos de vistas distintos, mas não excludentes, de um mesmo processo de retroalimentação.
Mais recentemente, De Saint Blaquat *et al.* (2011) defendem que existe uma correlação entre o tamanho/volume dos corpos magmáticos e o seu tempo de construção. Segundo estes autores, corpos magmáticos grandes, da ordem de 10.000 Km^3, podem registrar duração de até 10 Ma de atividade magmática, o que permite estabeler relações de *feedback* com processos tectônicos. Corpos magmáticos pequenos, com cerca de até 1.000 Km^3, não registram mais do que 1 Ma de atividade magmática, tendo limitado registro de processos geotectônicos de larga escala, e sendo condicionados pelas relações entre a dinâmica magmática e o contexto geológico local.

Zibra *et al.* (2014) descrevem a construção de um plúton sintectônico à uma zona de cisalhamento transpressiva inclinada de idade arqueana, a partir de pulsos sucessivamente mais diferenciados, que duraram um total 20 Ma. Os autores descrevem a partição cinemática da deformação entre encaixantes (tectonitos máficos) e intrusivas (tectonitos félsicos), tendo as encaixantes um predomínio de contração combinada com empurrão, enquanto as intrusivas absorveram a maior parte da transcorrência. As encaixantes apresentam geometria sinclinal em ambas margens do plúton, relacionada a um *detatchment* superior e a um empurrão inferior, o que permitiu a ascenção do plúton.

Brown e Solar (1998, 1999) avaliam o papel zonas de cisalhamento em orógenos e a suas relações de retroalimentação com o magmatismo de um ponto de

vista sistêmico. Os autores (Brown e Solar, 1998) consideram cinturões orogênicos como sistemas longe do equilíbrio, e cinturões e zonas de cisalhamento como estruturas dissipativas, que junto com o magmatismo, são expressões da auto-organização e do aumento de ordem e complexidade destes sistemas. Segundo eles, em cinturões orogênicos existem dois mecanismos eficientes para a migração de líquidos magmáticos, ambos guiados pela direção de elongação máxima do elipsoide finito de deformação ao longo de estruturas tectônicas. O fluxo percolativo (*percolative flow*) de líquido ocorre através do seu bombeamento por microestruturas e estruturas de meso-escala. Se a pressão do líquido aumenta suficientemente, ocorre a fragilização do sistema (*melt embrittlement*) e o fraturamento causa a transferência de líquido por fluxo canalizado.

Com base neste modelo, Brown e Solar (1998) propõem uma distinção no padrão estrutural desenvolvido em granitos sintectônicos a zonas de cisalhamento transcorrentes e de empurrão. Onde o eixo finito de elongação máxima é (sub)horizontal, o desenvolvimento de estruturas do tipo S-C é comum, atestando a ascensão concomitante a deformação. Em orógenos dominantemente contracionais, com deslocamentos inversos (empurrão), o eixo finito de elongação máxima tende ao ângulo de mergulho das zonas de cisalhamento. Isto facilita a migração vertical dos magmas, governada pela sua diferença de densidade com relação às encaixantes, e inibe o aumento excedente da pressão do líquido, o que permite a eficiência do fluxo percolativo.

Brown e Solar (1999) documentam a partição da deformação em migmatitos que intercalam domínios com tramas S > L e L > S. Os migmatitos S > L apresentam estruturas estromáticas (bandas concordantes de granitos intercalam-se com o bandamento metamórfico) sugestivas de fluxo percolativo, e são intrudidos por corpos tabulares métricos de granitos, concordantes a subconcordantes. Já os migmatitos L > S são heterogêneos, sugerindo transporte de massas fundidas (*en masse)* possivelmente por fluxo granular assistido por fusão. Estes migmatitos são intrudidos por corpos irregulares métricos de granitos, de forma aproximadamente circular em planta e elíptica em perfil, do tipo chaminés alongadas de acordo com o eixo máximo do elipsoide finito de deformação. Os autores defendem que este processo de migração de magmas esquenta regiões do orógeno, formando uma "antiforme termal", a qual amplifica a região onde mecanismos dúcteis de deformação são eficientes para níveis mais rasos. Isto causa uma retroalimentação, facilitando e permitindo a migração penetrativa de fusões até níveis mais rasos da

crosta orogênica, permitindo a construção de plútons e contribuindo para cenários de metamorfismo regional de alta T/baixa P.

2.2.4 Transpressão em diferentes níveis crustais

Os modelos de transpressão apresentados na sessão 2.2.1 tem geralmente como base observacional situações de tectônica recente (e.g. Tikoff e Teyssier, 1994) ou desenvolvidas sobre rochas supracrustais (e.g. Harland, 1971; Jones *et al.*, 2004). Robin e Cruden (1994), que por um lado utilizam como estudo de caso uma situação transpressiva afetando rochas graníticas e gnáissicas, por outro observam em seu modelo uma limitação na profundidade relativa das zonas transpressivas dúcteis, que teria uma relação de proporcionalidade com a sua largura. Eles sugerem que a deformação transpressiva seja geralmente restrita à crosta superior, com o seu movimento sendo transferido em profundidade para zonas não transpressivas, a não ser que “circunstâncias geológicas especiais” permitam que se estabeleçam zonas de baixa viscosidade com espessuras quilométricas. Situações de alto fluxo térmico e reologia dúctil são favorecidas em porções da crosta por onde ascendam magmas (e.g. antiforme termal de Brown e Solar, 1999).

Dewey *et al.* (1998) chamam a atenção para a falta de compreensão da variação em estilo e cinemática da deformação ao longo de estruturas transpressivas em diferentes profundidades. Segundo estes autores, zonas transpressivas de larga-escala, com mergulho de alto ângulo, devem desenvolver topografias superficiais expressivas. Estas topografias podem ser suficientes para gerar episódios deformacionais governados pela ação da gravidade, que por sua vez podem auxiliar no processo de exumação de rochas profundas. Esta é outra forma de raciocinar a chamada extrusão vertical, consequência implícita nos modelos de transpressão (Robin e Cruden, 1994; Jones *et al.*, 2002).

Situações de transpressão em terrenos de alto grau metamórfico têm sido documentadas na literatura principalmente na última década (Egydio-Silva *et al.*, 2005; Chetty e Bhaskar Rao, 2006; Martil, 2016). Egydio-silva *et al.* (2005) descrevem a variação estrutural de rochas granulíticas ao longo da curvatura do Cinturão Ribeira em torno do Cráton São Francisco, auxiliados por dados de anisotropia de susceptibilidade magnética. Esta curvatura é acompanhada pela transição entre tectônicas contracional e transcorrente. O domínio sul do cinturão apresenta cinemática dominantemente transcorrente e é associado à atuação da Zona de Cisalhamento Além-Paraíba (ZCAP), de direção E-W e cinemática

dominantemente destral. O domínio norte é dominantemente contracional, sendo subdividido em um subdomínio oeste, dominado por empurrão (foliação de baixo ângulo com lineação de alta obliquidade), o qual transiciona gradualmente para o subdomínio leste, de movimentação oblíqua (foliação de alto ângulo, com lineações de obliquidade média a baixa). Entre a porção norte e a sul ocorre um domínio transicional, com características mistas dos dois domínios e a ocorrência de zonas de cisalhamento discretas, marcando também a transição de uma deformação mais penetrativa no norte para a localização da deformação caracterizada pela atuação da ZCAP no domínio sul.

Os autores sugerem que a partição da deformação no domínio norte é bastante limitada, visto que transcorrência e empurrão coexistem em várias escalas, e mesmo na sua subcompartimentação, os dois subdomínios mantém o caráter transpressivo e apresentam transição gradual. Eles consideram que a trama metamórfica é relativamente homogênea na área como um todo, sendo a deformação então distribuída independente da geometria (orientação) da estrutura. Segundo os autores, a ausência de partição da deformação significativa é esperada, visto as condições de alta temperatura, favoráveis a uma deformação penetrativa e homogênea (amplamente distribuída). Por outro lado, a variação na partição da deformação de norte (domínio contracional, pouca partição) para sul (domínio transcorrente, partição efetiva) está de acordo com o previsto por Tikoff e Teyssier (1994).

2.2.5 Transpressão e exumação

Segundo Foster *et al.* (2009) a exumação de rochas da crosta profunda e a justaposição de domínios estruturais e metamórficos que representem distintos níveis crustais de um orógeno transpressional podem ocorrer: i) durante um estágio de progressão na evolução deste orógeno, devido a extrusão vertical decorrente da transpressão; ou ii) durante um estágio retrógrado, devido a extensão. Baseados na integração de dados de petrologia metamórfica, termocronologia e geologia estrutural, estes autores propõem um modelo envolvendo ambos estágios sucessivos para uma exumação rápida de rochas de alto grau e sua justaposição com terrenos de diferentes níveis crustais, no Cinturão Kaoko, Namíbia.

Xypolias *et al.* (2003) propõem um modelo de exumação para xistos azuis onde a transpressão sucede a extrusão tectônica das rochas de alta pressão aflorantes na ilha de Evia, Grécia. O modelo inclui a integração de dados estruturais

das rochas metamórficas e de um cinturão de rochas sedimentares deformadas (com metamorfismo incipiente). Os xistos azuis inicialmente retornam da zona de subducção devido à sua baixa densidade, na forma de uma *nappe*, quando então a tectônica transpressiva forma um domo que justapõem estas rochas com os níveis crustais mais rasos. Segundo os autores, a erosão também pode ter contribuído para o processo de exumação durante o processo.

Já Chatzaras *et al.* (2013), documentam um processo de exumação relacionada à transpressão em rochas de alta pressão na Zona Transversa da ilha de Creta, Grécia. Zonas transversas são porções de um cinturão de cavalgamentos onde as estruturas estão dispostas com alta obliquidade em relação às estruturas principais do cinturão. Geralmente conectam duas porções do cinturão com variações significativas ao longo da sua direção em termos de estilo, quantidade de encurtamento ou padrão cinemático. A rampa oblíqua estudada registra primeiramente uma cinemática dominantemente transcorrente, responsável pela exumação das rochas de 35 Km para 10 Km, seguida por falhas inversas e dobras contracionais que marcam a transição rúptil-dúctil e trouxeram as rochas até a superfície, onde novamente uma cinemática transcorrente é marcada, desta vez por falhas.

Uma estrutura de flor positiva de escala crustal, com cerca de 100 Km de largura, é descrevita por Chetty e Bhaskar Rao (2006) no Terreno Granulítico Sul, Índia. Este terreno neoarqueano experienciou tectônica transpressiva neoproterozoica, quando estruturas de escala crustal pré-existentes foram reativadas como zonas de cisalhamento de um sistema transpressivo. A movimentação foi responsável pela exumação das rochas, enquanto as zonas de cisalhamento serviram de condutos para magmas supostamente produzidos durante o espessamento relacionado à transpressão, os quais facilitaram a movimentação. Os autores aventam ainda, com base em dados sísmicos, que uma zona de cisalhamento enraizada no manto conecte-se com esta estrutura em flor.

Carosi e Palmeri (2002) descrevem a sobreposição da tectônica transpressiva dominada por transcorrência (D_2) sobre a de empurrão (D_1), e a subsequente exumação de rochas de fácies anfibolito no Cinturão Variscano, NE da Sardínia, Itália. O trabalho tem base na integração de dados de petrologia metamórfica e análise estrutural detalhada. Segundo estes autores, uma mudança na vergência do componente de empurrão (D_1) de sul para norte na fase de transpressão (D_2) foi acompanhada de um incremento significativo no transporte paralelo ao orógeno. Os

autores defendem que este é um processo eficiente na exumação e ao mesmo tempo tem o potencial de inibir a crosta previamente espessada de entrar em colapso gravitacional generalizado.

Diferentes cenários hipotéticos em orógenos transpressivos são examinados por Thompson *et al.* (1997), propondo uma correlação das trajetórias P-T-t de rochas exumadas com base em variações do de ângulo convergência entre placas (α). Eles sugerem que, em orógenos transpressivos dominados pelo componente transcorrente (α ~ 10°), as rochas podem ser transportadas horizontalmente por longas distâncias (centenas de Km), permanecendo em profundidade por longos períodos. Isso permite que as rochas sejam aquecidas até a fácies granulito, eventualmente atingindo temperaturas passíveis de fundir. Em orógenos verdadeiramente oblíquos (α ~ 30°) os autores esperam que ocorram sequências barrovianas, com taxas de exumação tipicamente esperadas para erosão constante e isostasia. Já em orógenos transpressivos dominados pelo componente de empurrão (α ~ 90°), as rochas são exumadas rapidamente sem aquecimento significativo, possibilitando a exumação de rochas metamórficas de alta P.

Goscombe e Gray (2009) alertam para o caso em lineações de estiramento não são coincidentes com o fluxo extrusivo das zonas que levam à exumação, como é o caso da Zona de Cisalhamento Kalinjala, no sul da Austrália. Estes autores afirmam a importância de estudos coordenados de Geologia Estrutural e Geotermobarometria para uma compreensão mais completa dos fenômenos da transpressão.

2.2.6 Considerações finais

Os modelos de transpressão propostos ao longo das últimas quatro décadas têm evoluído juntamente com o conceito de transpressão e um acúmulo cada vez maior de dados geológicos. Condições de contorno e variáveis mais realistas resultam em predições mais confiáveis, as quais podem e devem ser testadas através de comparações com situações naturais. Ao mesmo tempo o aprofundamento do conhecimento geológico de cada região, com diferentes abordagens e níveis de detalhe, propicia um quadro passível da integração das múltiplas escalas envolvidas nos processos geodinâmicos da orogênese. Os novos quadros delineados em cada situação geológica particular por sua vez realimentam os novos modelos.

A transpressão, sendo uma consequência inevitável da deriva dos continentes, é uma realidade esperada em contextos como o das faixas móveis neoproterozoicas. Do ponto de vista mais amplo e sistêmico, a transpressão não é somente um produto da interação das placas litosféricas, mas sim um processo que retroalimenta a dinâmica do sistema, pois é também capaz de causar mudanças marcantes na configuração dos orógenos. Exumação e soerguimento são uma consequência esperada da transpressão, expondo níveis profundos da crosta e promovendo evoluções topográficas, com erosão em potencial e consequente sedimentação em bacias orogênicas.

Para pensarmos em maior detalhe, faz-se necessário considerar a progressão da deformação e a sua heterogeneidade. O modelo de transpressão triclínica (Jones et al., 2004; Fernandez e Díaz-Azpiroz, 2009; Figs. 15 e 16) prevê a sobreposição temporal de tramas planares de baixo e alto ângulo, e vice-versa, com lineações muito variáveis, de alta até baixa obliquidade. Por outro lado, considerando a possibilidade da deformação heterogênea (Robin e Cruden, 1994; Fig. 10), a qual é muito mais uma regra do que uma excessão na natureza, estas mesmas tramas distintas podem coexistir lateralmente em um determinado tempo. Neste sentido, ecoam as palavras de Harland (1971), que já antevia em seu trabalho pioneiro que “uma sequencia temporal complexa de uma distribuição complexa de formas” era uma expectativa razoável quando se estudasse um contexto transpressivo. A predominância de uma configuração estrutural sobre a outra vai depender primeiramente do ângulo de convergência entre os blocos/placas envolvidos (Robin e Cruden, 1994), assim como da geometria da zona (mergulho e curvilinearidade) e das suas heterogeneidades ou anisotropias pré-existentes, que determinarão uma tendência ou não de partição da deformação em domínios estruturais. É imprescindível, portanto, que se realizem de forma coordenada estudos de detalhe e de integração das várias escalas de espaço e tempo envolvidas, a partir de uma abordagem multi-técnicas (e.g. Goscombe e Gray, 2009).

3. *Transpressive strain partitioning between the Major Gercino Shear Zone and the Tijucas Fold Belt, Dom Feliciano Belt, Santa Catarina, southern Brazil*

CHASQUE WEBMAIL
Universidade Federal do Rio Grande do Sul

Assunto **Successfully received: submission Transpressive strain partitioning between the Major Gercino Shear Zone and the Tijucas Fold Belt, Dom Feliciano Belt, Santa Catarina, southern Brazil for Journal of Structural Geology**

Remetente Journal of Structural Geology <EviseSupport@elsevier.com>

Para <gdetoni@ufrgs.br>

Responder para <jsg@elsevier.com>

Data 2019-10-13 22:03

This message was sent automatically.

Ref: SG_2019_344
Title: Transpressive strain partitioning between the Major Gercino Shear Zone and the Tijucas Fold Belt, Dom Feliciano Belt, Santa Catarina, southern Brazil
Journal: Journal of Structural Geology

Dear Dr. De Toni,

Thank you for submitting your manuscript for consideration for publication in Journal of Structural Geology. Your submission was received in good order.

To track the status of your manuscript, please log into EVISE® at: http://www.evise.com/evise/faces/pages/navigation/NavController.jspx?JRNL_ACR=SG and locate your submission under the header 'My Submissions with Journal' on your 'My Author Tasks' view.

Thank you for submitting your work to this journal.

Kind regards,

Journal of Structural Geology

Have questions or need assistance?
For further assistance, please visit our Customer Support site. Here you can search for solutions on a range of topics, find answers to frequently asked questions, and learn more about EVISE® via interactive tutorials. You can also talk 24/5 to our customer support team by phone and 24/7 by live chat and email.

Transpressive strain partitioning between the Major Gercino Shear Zone and the Tijucas Fold Belt, Dom Feliciano Belt, Santa Catarina, southern Brazil

De Toni, GB[1]; Bitencourt, MF[2]; Konopásek, J[3,4]; Martini, A[1]; Andrade, PHS[1]; Florisbal, LM[5]; de Campos, RS[5].

[1] Programa de Pós Graduação em Geociências, Universidade Federal do Rio Grande do Sul, Brazil

[2] Departamento de Geologia, Universidade Federal do Rio Grande do Sul, Brazil

[3] Department of Geosciences, UiT – The Arctic University of Norway in Tromsø, Norway

[4] Czech Geological Survey, Czech Republic

[5] Departamento de Geologia, Universidade Federal de Santa Catarina, Brazil

ABSTRACT

A composite cross-section from the Florianópolis Batolith towards the Tijucas Fold Belt in the northern Dom Feliciano Belt (southern Brazil) is divided in three structural domains: the Major Gercino Shear Zone, the suprastructural Brusque Complex and the infrastructural Camboriú Complex. A kinematic correlation among the structural domains is based on structural and petrological data integrated with geochronology. An oblique collisional event at 650-645 Ma affected all structural domains and is best recorded in the Porto Belo Complex, which shows migmatization (700°C/4.3 Kbar) and top-to-the-NNW+dextral shear along the Major Gercino Shear Zone. Subsequent strain partitioning led to progressive tangential movement recorded in the Quatro Ilhas Granitoids (625-615 Ma) followed by later granitic intrusions (after 615 Ma) controlled by dextral strike-slip. Meanwhile, the contractional component was absorbed by the Tijucas Fold Belt infrastructure, causing exhumation of the Camboriú Complex migmatites (from 5 to 3.4 Kbar) and unroofing of the suprastructural Brusque Complex (around 635 Ma). Tectonic juxtaposition occurred along a dextral+normal detatchment zone between the complexes. As a consequence, heating of the Brusque Complex locally reached amphibolite-facies conditions and suprastructure thrusting inverted to extension, which is recorded in discrete shear structures with normal kinematics. The sequence of events and their age suggest that the hinterland Porto Belo Complex and the foreland Tijucas Fold Belt were juxtaposed already at ca. 650–645 Ma, which questions the validity of the subduction-related tectonic models in the northern Dom Feliciano Belt.

1. Introduction

Most of the present-day plate tectonic boundaries are activated obliquely (Philippon and Corti, 2016). Convergent or divergent oblique displacement vectors are the inevitable consequence of irregular plates moving over the approximately spherical surface of the planet. Obliquely moving plate boundaries are common in almost any segment of every collisional orogenic belt, along active subduction margins, and in restraining bends of faults, shear zones and transform boundaries (Dewey et al., 1998).

Obliquity of the convergence vector with respect to a plate boundary or high-strain zone is the main reason for transpressional deformation (Harland, 1971; Sanderson and Marchini, 1984). Transpression is defined as “what happens to a tabular zone submitted to both compression and (simple) shear simultaneously imposed by its walls” (Robin and Cruden, 1994). The understanding of transpressional deformation evolved through the coupled development of more accurate and increasingly complex mathematical models (Fossen and Tikoff, 1993; Tikoff and Teyssier, 1994; Robin and Cruden, 1994; Jones et al., 2004; Fernandez and Diaz-Azpiroz, 2009) and the description of natural occurrences (Holdsworth et al., 2002; Czeck and Huddleston, 2003; Egydio-Silva et al., 2005; Zibra et al., 2014; Martil, 2016; Oriolo et al., 2016a).

The distinction of wrench-dominated transpression and pure-shear dominated transpression was introduced by Fossen and Tikoff (1993) and Tikoff and Teyssier (1994). These authors also discussed the importance of coupling between both sides of the colliding zone in depth, given by the consistency of the obliquity of the structures observed until 300 km away from California and Sumatra faults (Tikoff and Teyssier, 1994). Strain partitioning can distribute transpressional deformation in relatively homogeneous structural domains which may coexist laterally (e.g. Holdsworth et al., 2002) or vertically (e.g. Vanderhaeghe et al., 1999), and is dependent of convergence obliquity (Tikoff and Teyssier, 1994; Robin and Cruden, 1994).

Jones et al. (2004) introduced the concept of inclined transpression, considering non-vertical shear zone walls in a mathematical model based on structures exposed in Eyemouth, SE Scotland (described in detail by Holdsworth et al., 2002). Jones et al. (2004) pointed out the non-coaxiality of thrust and transcurrence components and changes in orientation of the instantaneous strain ellipsoid axis. The presence of kinematic indicators in both XZ and YZ sections, the possibility of non-coaxial

structures inside the XY plane due to X reorientation, and the change of vorticity sense during the rock deformation history are consequences predicted in their model. Another feature is the presence of a relative normal-sense of movement in the hanging wall due to the vertical extrusion of matter from the inner portion of the shear zone (Jones et al., 2004), somehow similar to the relative movements of the Main Central Thrust and the South Tibet Detatchment in the Himalaya (Burchfiel et al., 1992). Fernandez and Diaz-Azpiroz (2009) presented an improved model called triclinic transpression with inclined extrusion. They predicted many of observed natural features of transpressional shear zones, as distribution of lineations along girdles or their double plunge. The non-coincidence of the vorticity vector with any of the finite strain axis is characteristic of oblique, triclinic transpression (Fernandez and Diaz-Azpiroz, 2009).

This paper presents a structural research integrated with petrological and previously published geochronological data from the northernmost segment of the Dom Feliciano Belt (DFB – Fig. 1a), Santa Catarina state (SC), southern Brazil. The DFB is a mobile belt adjacent to the Rio de la Plata Craton and represents the South American portion of the Dom Feliciano-Kaoko-Gariep Orogenic System active during the western Gondwana assembly (Konopásek et al., 2016, 2018). The study investigates and proposes a kinematic correlation between the two major tectonic domains of DFB in SC (figures 1b and 2), separated hereby in three structural domains: (i) the northernmost portion of the Florianópolis Batolith (defined by Jost and Hartmann, 1984), which is affected by the Major Gercino Shear Zone (MGSZ – Bitencourt and Nardi, 1993, 2000; Bitencourt, 1996; Florisbal et al., 2012a; Hueck et al., 2018) that separates the batholith from the Tijucas Fold Belt (TFB – as defined by Hasui et al., 1975). The TFB in the northern Dom Feliciano Belt is represented by (ii) the supracrustal Brusque Complex (Silva, 1991; Philipp et al., 2004; Basei et al., 2011; de Campos et al., 2012; Fischer et al., 2019) and (iii) the infracrustal Camboriú Complex (Basei et al, 2013; Martini et al., 2019a,b). The correlation is proposed by evaluating and comparing the structural record in terms of geometry and kinematics, strain progression and partitioning, timing and deformation conditions in each structural domain. The data are then interpreted and compared with previous models of tectonic evolution of the area, suggesting possible alternative interpretation of the Western Gondwana assembly registered in the northernmost DFB.

2. Geological Setting

2.1 Dom Feliciano Belt Geology

The tectonic evolution and significance of the Dom Feliciano Belt is still a matter of intense debate, illustrated by various models proposed in the past decades (Fernandes et al., 1992, 1995a, 1995b; Chemale Jr., et al 2012; Philipp et al., 2016). Apart from many differences among these models, the DFB is consensually subdivided in four major tectonic domains (Fig. 1) limited by major geological and geophysical lineaments or discontinuities (e.g. Fernandes et al., 1995a,b). The São Gabriel Block, which is exposed exclusively in the western portion of Rio Grande do Sul state shield area, represents a Neoproterozoic active margin with relicts of an early (oceanic?) arc phase (948 to 850 Ma – Leite et al., 1998; Arena et al., 2016) and a well recognized continental arc (786 – 700 Ma – Salmaan et al., 2011; Arena et al., 2016; Philipp et al., 2018). The Tijucas Fold Belt (Hasui et al., 1975) is a foreland fold-and-thrust belt. It presents at least two diachronous volcano-sedimentary sequences, metamorphosed and deformed at *ca.* 650 Ma and shortly after 580 Ma (e.g. Jost and Bitencourt, 1980; Höfig et al., 2017; Battisti et al., 2018), with Paleoproterozoic basement outcroping in inner portions of regional antiforms (Encantadas Complex – Saalmann et al., 2006; Camboriú Complex –Martini et al., 2019a,b). The foreland is covered by late-orogenic sedimentary rocks representing infill of narrow grabens (Camaquã Basin – Paim et al., 2014; Itajaí Basin – Guadagnin et al., 2010). Farther to the south-east, the inner portion of DFB is represented by batholiths made of polyphase and multi-intrusive, dominantly post-collisional granitic bodies with associated mafic magmatism, the intrusion of which was structurally controlled by the Sul-Brasileiro Shear Belt (SBSB – Bitencourt and Nardi, 1993, 2000; Bitencourt, 1996; Florisbal et al., 2012a). Paleoproterozoic (e.g. Gregory et al., 2015), minor Mesoproterozoic (Chemale Jr. et al., 2011) and early-Neoproterozoic rocks (Lenz et al., 2011; Koester et al., 2016; Martil et al., 2017) occur as basement inliers or as regional scale roof pendants (e.g. Encruzilhada Block of Jost and Hartmann, 1984; De Toni, 2019; and the Punta del Este Terrane – Oyhantçabal et al., 2009). Finally, the late Neoproterozoic flysch-type sedimentary rocks of the Rocha Group represent an eastermmost part of the DFB exposed exclusively along the eastern coast of Uruguay (Betucci and Burgueno, 1993).

Both the TFB and the batoliths outcrop from southern Uruguay up to the Santa Catarina coast (southern Brazil – Fig. 1a) as a N–S to NE–SW–trending, *ca.* 2000 Km long units limited by some of the major shear zones representing the SBSB.

Basei et al. (2005; 2008) interpreted the batoliths as a magmatic arc accreted to the TFB during the Neoproterozoic and proposed that the boundary between these tectonic domains is a suture zone active during collision at *ca.* 600 Ma (Basei et al., 2008). On the other hand, Florisbal et al. (2012a,b,c) demonstrated that synchronous 630 – 610 Ma magmatic intrusions along the MGSZ and within the TFB correlate in terms of their geochemical affinity. Additionally, recent studies in Uruguay (Oriolo et al., 2016a) and Rio Grande do Sul (Martil, 2016; Martil et al., 2017; Battisti et al., 2018; De Toni, 2019) demonstrate that both domains record coherent structural evolution.

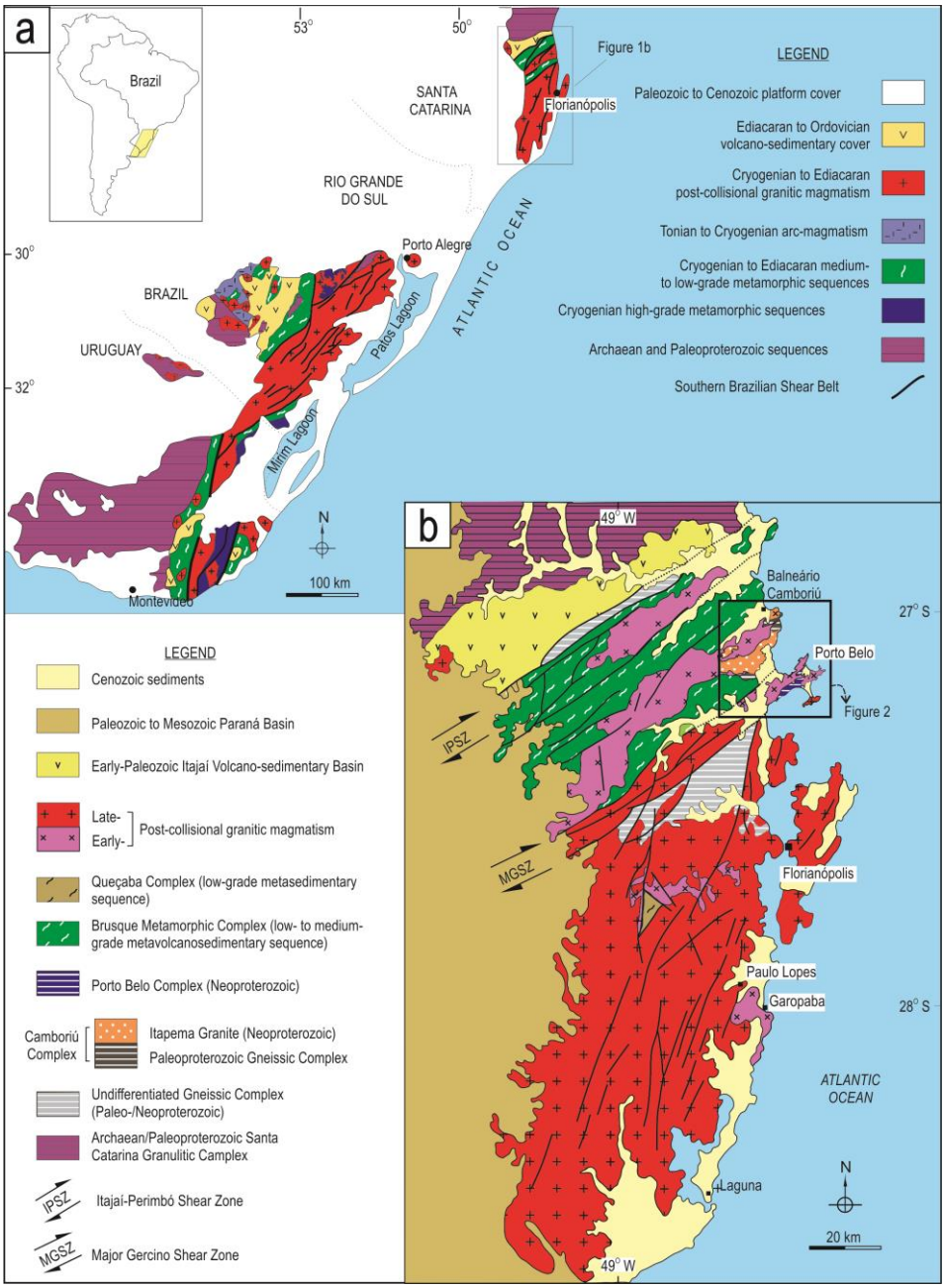

Fig. 1 – (a)Tectonic sketch of southern Brazil and Uruguay showing the Dom Feliciano Belt and cratonic adjacent areas (modified from Bitencourt and Nardi, 2000, Ramos et al., 2018; Will et al., 2019). (b) Santa Catarina shield area geological map (modified from Bitencourt and Nardi, 2004) with location of studied area shown in figure 2.

2.2. The Santa Catarina Shield and the study area

The northern portion of the Santa Catarina Shield (Fig. 1b) represents Archean to Paleoproterozoic basement called the Santa Catarina Granulitic Complex or Luis Alves Craton (Hartmann et al., 2000 and references therein), partially covered by the foreland Itajaí Basin (e.g. Guadagnin et al., 2010) in its southern part. The central portion of the shield area is represented by the TFB, which is limited against the northern cratonic block and its cover by the dextral Itajaí-Perimbó Shear Zone (IPSZ – Silva, 1991), and separated from the southern Florianópolis Batolith by the dextral Major Gercino Shear Zone (MGSZ). The later shear zone controlled syntectonic granitic magmatism of the Florianópolis Batholith along its northern boundary (Bitencourt and Nardi, 1993, 2000; Bitencourt, 1996; Passarelli et al., 2010, 2011; Florisbal et al., 2012a) in a post-collisional setting (sensu Ligeois, 1998). The studied area covers the boundary between the TFB and the Florianópolis Batolith, including the coastal portion of the MGSZ (Fig. 2 and 3).

2.2.1 The Tijucas Fold Belt

The geology of the northern TFB can be simplified into three major tectonic units. The Brusque Complex is the supracrustal unit, with metavolcanosedimentary successions interpreted as rift-related deposits metamorphosed under mid- to upper greenschist facies conditions, between chlorite and garnet zones, and locally reaching amphibolite facies conditions (Silva, 1991; Philipp et al., 2004; Basei et al., 2011; de Campos et al., 2012). Its lower succession, named Rio do Oliveira Sequence by Silva (1991) (the Rio do Oliveira Formation of Basei et al., 2011), includes an important phase of dominantly mafic, tholeiitic magmatism, interpreted by de Campos et al. (2012) as related to the rifting stage of the precursor basin. The authors estimated the local amphipolite-facies conditions at 650 to 660°C, and recognized an early greenschist-facies phase at *ca.* 550°C, both at an arbitrarily fixed pressure of 5 Kbar. Recently estimated PT conditions in the garnet-bearing succession (Botuverá Formation of Basei et al., 2011) of the Brusque Complex by Asvald (2018) point to early garnet growth at 510°C and 4.8 Kbar, with peak conditions at 560-570°C and 6-7 Kbar.

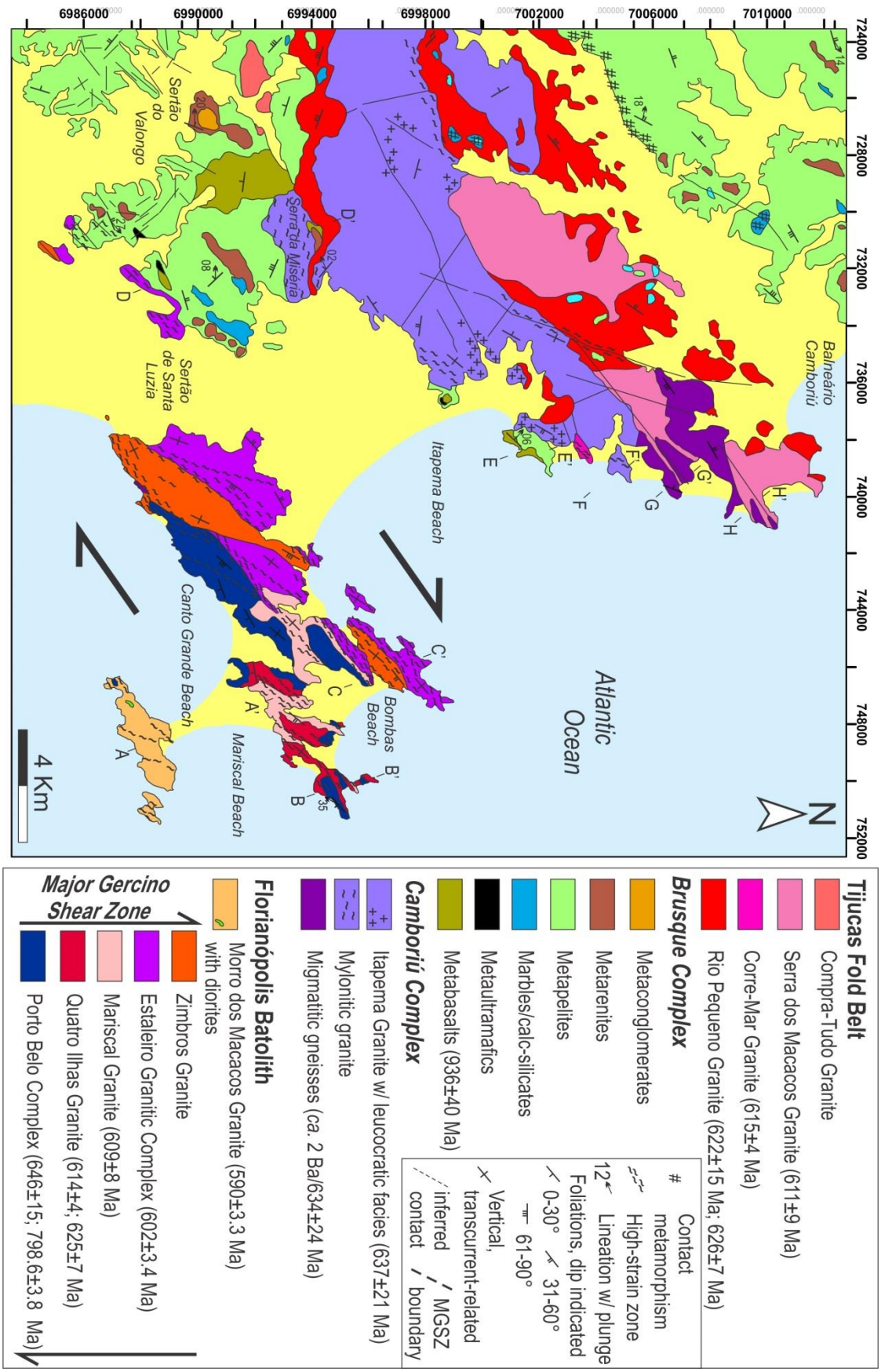

Fig. 2 – Porto Belo – Camboriú geological map (modified from Florisbal et al., 2012a, after Bitencourt, 1996; UFRGS, 2000; Philipp et al., 2004). The location of individual sections described in the paper and integrated in the composite section of figure 3 is shown.

An early deformation phase of thrusting towards NW is recognized in these rocks (Silva, 1991; Philipp et al., 2004; Fischer et al., 2019). Syntectonic peraluminous granites are intrusive along the low-angle fabric during the main deformation episode (Philipp and de Campos, 2010) and are collectively named the São João Batista Suite (Hueck et al., 2016). These structures are reworked by high-angle, NE-strike, and later NW-strike, brittle-ductile structures (e.g. Philipp et al., 2004).

The TFB basement is represented by the Camboriú Complex (CC), which includes ortho- and minor paragneisses of dominantly Archean to Paleoproterozoic protolith ages with minor Mesoproterozoic mafic intrusions and abundant Neoproterozoic melting features, and the Itapema Granite, interpreted as product of the CC anatexis during Neoproterozoic water-fluxed melting (Hartmann et al., 2003; Rivera et al., 2004; Bitencourt and Nardi, 2004; Basei et al., 2013, Martini et al., 2019a,b). Basei et al. (2013) presented SHRIMP U-Pb ages of 634 ± 24 Ma for a deformed leucosome in the CC, and of 637 ± 21 Ma for the Itapema Granite (so-called Ponta do Cabeço Diatexite).

Late-tectonic granitic intrusions are abundant in both complexes and mostly obliterate contacts between them. The most voluminous intrusions are the biotite ± hornblend, porphyritic Rio Pequeno Granite (622±15 Ma; 626±7 Ma – U-Pb zircon LA-ICP-MS – Florisbal et al., 2012b), and the younger biotite ± muscovite Serra dos Macacos Granite (611±9 MA – U-Pb zircon LA-ICP-MS; Florisbal, 2012b). The Rio Pequeno intrusion is responsible for development of contact metamorphism in the Brusque Complex metasedimentary rocks (Philipp et al., 2004; Fischer et al., 2019) and over the Caboriú Complex xenoliths (Peternell et al., 2010). The deformation of these granites is relatively weak and therefore they are considered to intrude a low-strain zone in relation to the Major Gercino Shear Zone (Peternell et al., 2010; Florisbal et al., 2012b). Local evidences of discrete high-strain zones with NNE-strike and sinistral displacement were reported by Martini et al. (2015), who studied the syntectonic Corre-Mar Granite (615±4 Ma – U-Pb zircon LA-ICP-MS; Martini et al., 2015), instrusive in the Camboriú Complex along some of these later structures.

2.2.2 The Major Gercino Shear Zone and the Florianópolis Batolith

The Major Gercino Shear Zone is a major structure with dextral, transpressive to transcurrent movement, which conditioned the syntectonic emplacement of the northernmost granitic and associated mafic intrusions that build the Florianópolis Batolith along its limit with the Tijucas Fold Belt (Bitencourt and Nardi, 1993; Florisbal

et al., 2012a; Hueck et al., 2018 among others). The basement of the Florianópolis Batolith in the area is the Porto Belo Complex, mostly composed of granitic, granodioritic and tonalitic orthogneisses and foliated tonalites (Bitencourt, 1996; Florisbal et al., 2012a,b). De Toni (2019) presents crystallization age of 798 ± 3.8 Ma (zircon, U-Pb, LA-ICP-MS) for an orthogneiss protolith, whereas Chemale Jr. et al. (2012) presented 649 ± 7 Ma (zircon, U-Pb, LA-ICP-MS) and 646 ± 15 Ma (zircon, U-Pb, ID-TIMS) magmatic ages for the foliated tonalites. The low-angle fabric in the Porto Belo Complex was briefly described by Bitencourt and Nardi (1993) and attributed to an unspecified, older tectono-metamorphic event. These authors, however, mentioned that the coincident low-rake lineations of both gently-dipping and subvertical fabrics along MGSZ suggest tangential movement compatible with the early stages of transcurrence.

The earlier intrusions along the Major Gercino Shear Zone are the coarse- to very coarse-grained, porphyritic Quatro Ilhas Granitoids. These rocks present a flat-lying magmatic foliation, sub-parallel to the basement structure (Bitencourt and Nardi, 1993, 2000). Asymmetric folds show top-to-NNW shear sense (Bitencourt, 1996; Florisbal et al., 2012b). Florisbal et al. (2012b) presented magmatic ages of 625 ± 6.5 Ma and 614 ± 4 Ma (zircon, U-Pb, LA-ICP-MS) for the granodioritic and monzogranitic varieties, respectively.

The Quatro Ilhas Granitoids are intruded by the Mariscal Granite (Bitencourt and Nardi, 1993; Bitencourt, 1996) at 609 ± 8 Ma (zircon, U-Pb, LA-ICP-MS – Florisbal et al., 2012a), which is then intruded by the Estaleiro Granitic Complex, consisting mainly of a heterogeneously deformed, porphyritic granodiorite, synplutonic dikes, and a network of granitic veins, specially developed in the mylonitic portions (Bitencourt, 1996). Peruchi (2016) presented ages of 611.9 ± 1.7 Ma and 611.2 ± 2.7 Ma for the undeformed and mylonitic varieties of the granodiorite, respectively (zircon, U-Pb, LA-ICP-MS), while Chemale Jr. et al. (2012) reported an age of 602 ± 4.2 Ma (zircon, U-Pb, ID-TIMS). Both igneous and mylonitic fabrics of the Mariscal and Estaleiro Granitic Complex are transcurrent, with predominantly dextral kinematics (Bitencourt and Nardi, 1993; 2000; Florisbal et al., 2012a).

The Zimbros Intrusive Suite includes the late-transcurrent Zimbros Granite and hypabissal rocks along the Major Gercino Shear Zone, and the Morro dos Macacos Granite, emplaced outside, south of the high-strain zone (Bitencourt, 1996). The ages of the Zimbros Intrusive Suite presented by Chemale Jr. et al. (2012) are 587 ± 7.5 Ma (zircon, U-Pb, LA-ICP-MS) for the Zimbros Granite, 587 ± 8.7 (zircon, U-Pb,

SHRIMP) for an acid dike, and 588 ± 3.3 for the Morros dos Macacos Granite (zircon, U-Pb, ID-TIMS). Both the Zimbros Granite and the Estaleiro Granodiorite are intrusive in the southeastern portion of the Brusque Complex, where supracrustal rocks present thermal and shearing effects related to the Major Gercino Shear Zone later magmatism (Bitencourt and Nardi, 1993; Philipp et al., 2004).

3. Materials and methods

This study is based mostly on field observations and structural data from key outcrops selected after geological mapping (1:25.000 scale – Bitencourt, 1996; UFRGS, 2000). These data were integrated with petrography, microstructural observations, new and published geothermobarometric and geochronological data, and represent a robust dataset for the three studied structural domains. Eight cross sections were made orthogonal to the main structural trend and tectonic boundaries of the area (NE to ENE) and they are integrated in the composite cross section presented in figure 3.

One pseudosection was constructed with the Perple_X 6.7.0 software (Connoly, 2005) and the thermodynamic database of Holland and Powell (1998, revised 2002), based on whole-rock geochemistry obtained using a Rigaku RIX 2000 X-Ray Fluorescence (XRF), in the X-ray Fluorescence Laboratory of the Petrology and Geochemistry Research Center (CPGq), Geosciences Institute (IGEO), at the Federal University of Rio Grande do Sul (UFRGS), Brazil. Microprobe analysis was carried in the Microprobe Laboratory, CPGq, UFRGS, using a Cameca SXFive electron microprobe. The analytical conditions were 14.8 keV, 15 nA current, and beam size of 20 μm.

Microprobe data are also used for conventional plagioclase-hornblend geothermobarometry (Schmidt, 1992; Holland and Blundy, 1994).

Additionaly, quartz c-axis fabric from one key sample is also evaluated to complement the kinematic array. EBSD mapping was carried using a 9.5 μm step-size with a Scanning Electron Microscope (SEM) Zeiss Merlin VP Compact from the SEM Laboratory at the Faculty of Health Sciences of the Arctic University of Norway in Tromsø. The mapped area was 2 cm^2 (1 cm perpendicular to S_{mil} by 2 cm along it). Post-processing of SEM data was made with AzTEC software. All thin-sections analysed in SEM, both with microprobe or EBSD, were carbon coated.

4. The Porto Belo – Camboriú cross section

The data from each individual cross-section which compose figure 3 will be presented separately, from southeast towards northwest, with a special focus on: a) the Major Gercino Shear Zone basement and early intrusive rocks (B-B' – see figure 2 for localization of the cross-section on the map); b) the coastal section of the southern Brusque Complex (E-E'); c) detailed observation of the contact relationships along the Brusque–Camboriú Complex boundary (second half of D-D') and d) the Camboriú Complex internal structure (F to H').

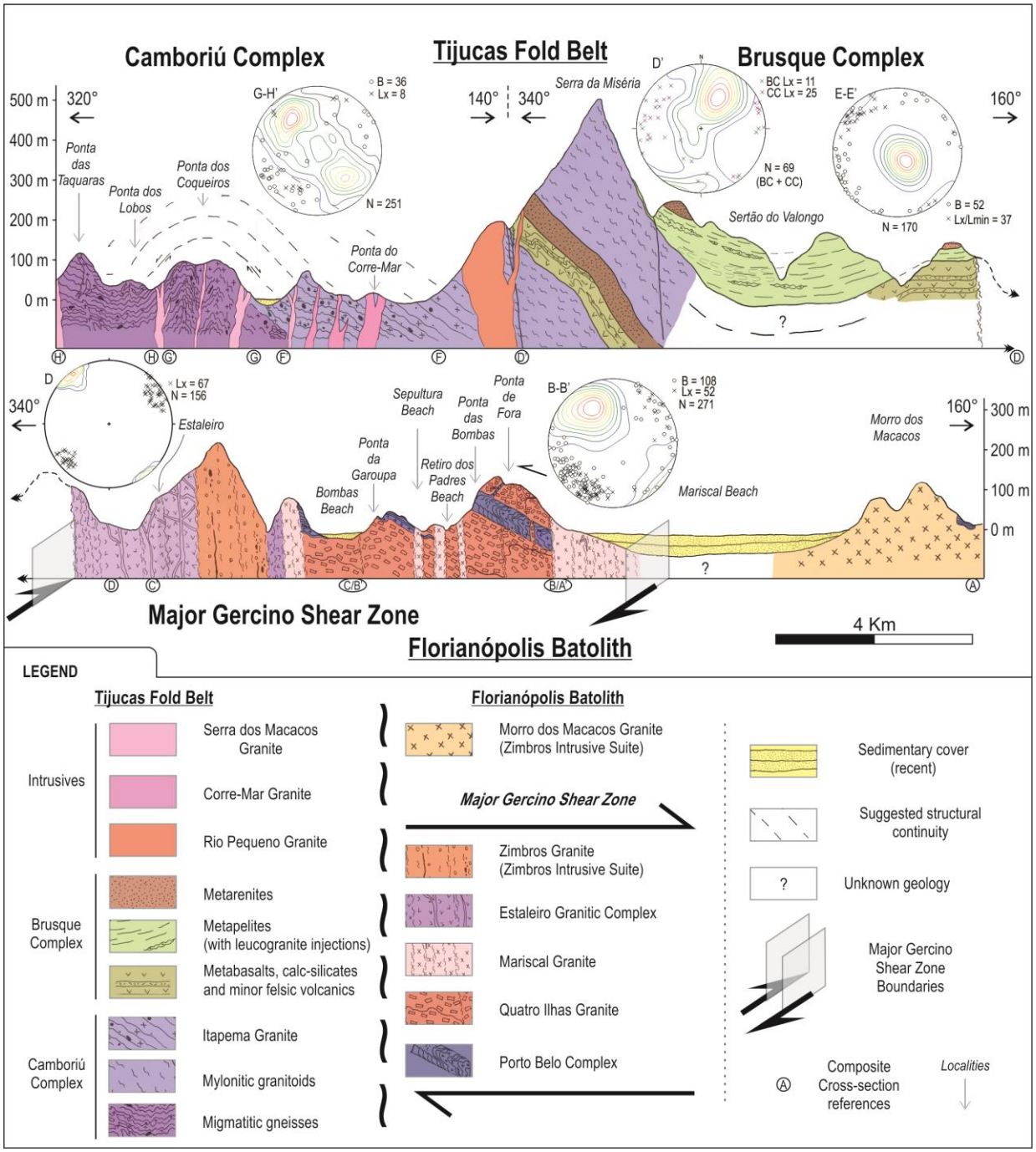

Fig. 3 – Porto Belo – Camboriú composite cross-section. Notice that 340°- 160° is the cross-section orientation for Major Gercino Shear Zone and Brusque Complex structural domains, while it is changed for 320° - 140° in the Camboriú Complex. Location of the individual sections is presented, as well as stereonets representative of the main subdomains presented in the text.

4.1 Morro dos Macacos Granite and the Major Gercino Shear Zone southeastern boundary

The profile A–A' (fig. 2) starts in the Morro dos Macacos Granite, which is described by Bitencourt and Nardi (1993) as an isolated intrusion without observable contact relationships. The granite is dominantly isotropic, altough magmatic foliation and discrete shear zones are locally developed. Xenoliths or roof pendants of the Porto Belo Complex are exposed in its southwestern portion. Northern limit of the profile is placed in the Mariscal Granite, which represents the inferred southeastern boundary of the Major Gercino Shear Zone. The Mariscal Granite is commonly found as small intrusions in the Quatro Ilhas Granite (Bitencourt and Nardi, 1993, as depicted in section B – B', fig. 3) and comprises fine- to medium-grained rock recording dextral transcurrence both during earlier high-T and later low-T deformation, along mostly subvertical shear zones (Bitencourt and Nardi, 1993, 2000; Bitencourt, 1996; Florisbal et al., 2012a).

4.2 Quatro Ilhas Granitoids at Ponta de Fora

The cross section from Ponta de Fora to Ponta da Garoupa (B – B' section in fig. 2 and 3) exposes interleaving of the Quatro Ilhas Granitoids with the Porto Belo Complex along its original flat-lying foliation at map and outcrop scale. The Quatro Ilhas Granitoids represent the earlier intrusions along the Major Gercino Shear Zone (Bitencourt and Nardi, 1993; 2000; Bitencourt, 1996; Florisbal et al., 2012a). This porphyritic granite presents leucocratic and mafic-rich varieties interleaved along the main magmatic foliation (Fig. 4a and b), mostly defined by the alignment of subhedral K-feldspar phenocrysts (ranging 0.5 to 5 cm) and matrix minerals, mainly biotite. A mylonitic foliation is heterogeneously developed parallel to it (fig. 4a). The foliation mostly dips to SE at low to high-angles due to its asymmetric folding. The folding brings the foliation to subvertical attitudes, where strike-slip high-strain zones may develop. The asymmetric folding leads to a half-girdle pattern of the pole to foliation distribution in the stereonet (Fig. 4c). A mineral lineation is defined by the phenocryst orientations along the XY plane, and a stretching lineation is developed parallel to it due to recrystallization of both K-feldspar phenocrysts and quartz-feldspathic matrix. Both mineral and stretching lineations present low rake and they are also parallel to the fold axes (Fig. 4c).

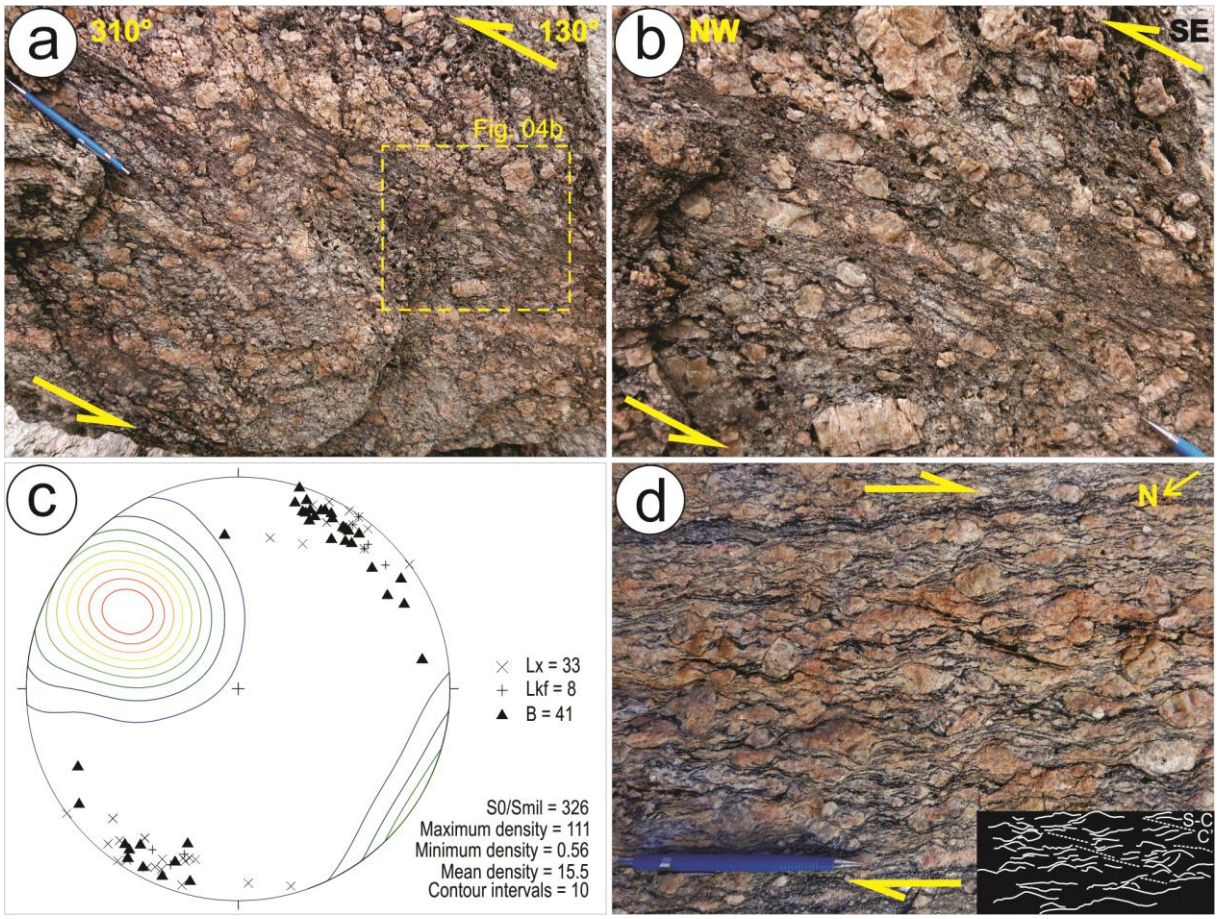

Fig. 4 – Quatro Ilhas Granitoids general features at Ponta de Fora outcrop. (a) Quatro Ilhas Granitoids typical aspect at NW-SE subvertical section approximately perpendicular to the lineation and to fold axis (fold profile). The asymmetry of the fold indicate top-to-the-NW. (b) Detail of figure 4a, where it is possible to observe the heterogeneity of deformation along originally textural/compositional distinct layers. Central layer present a stronger foliation and K-feldspar porphyroclasts with well-developed recrystallization tails indicating top-to-the-NW sense of shear. (c) Stereonet presenting contoured pole-to-foliation of Quatro Ilhas Granitoids and linear fabrics (mineral and stretching lineation plus fold axis). (d) Horizontal section, approximately XZ-parallel, showing highly asymmetric structures such as S-C-C' (see sketch) and dextral, asymmetrical porphyroclasts, which recrystallization tails define a discontinuous banding along the S-C mylonitic foliation. C' are discrete planes mostly developed in the central portion of the picture (see sketch).

Fold profiles (YZ section of the finite strain ellipsoid, approximately NW – SE) present folded zones of aligned K-feldspar phenocrysts with well-preserved subhedral igneous shape. These sections were ideal to observe the shortening and top-to-NW thrusting components of the transpressional deformation recorded in these rocks (Fig. 4a and b). On the other hand, subhorizontal surfaces (near XZ section, subparallel to lineation) record the dextral transcurrent component of it with well developed S-C-C' structures and mostly asymmetric porphyroclasts (Fig. 4d).

4.3 Porto Belo Complex at Ponta das Bombas

The Porto Belo Complex main outcrop in this section is at Ponta das Bombas (Fig. 5a and b) representing the inner portion of a major antiformal structure build up by the Porto Belo Complex rocks and flanked by the Quatro Ilhas Granitoids (see Fig. 3). Most of the rocks in the area are granites to tonalities in composition and texture, with gneiss lenses or tabular bodies (maximum 1.5 m width and up to 10 m long) (see fig. 5c, d and e). Igneous rocks present medium- to fine-grained hypidiomorphic texture, although that with different degrees of deformation. They apparently represent a continuous variation between foliated leucocratic syenogranites with sparse biotite aggregates and schlieren (fig. 6a and b), through foliated or banded biotite±muscovite-bearing monzogranites (Fig. 6c) to biotite±(hornblend+epidote) granodiorites and tonalites (Fig. 5e and Fig. 6d), with either irregular, abrupt, gradual or diffuse contacts among them (Fig. 5d and e). The banded varieties present a discontinuous banding with irregular width, characterized by biotite-rich, mm-wide bands or lenses, and by variations of grain-size (medium to fine, locally pegmatitic) and mafic content. Elongated gneissic lenses enhance the banding (Fig. 5d) and contribute to its development by mechanical disaggregation of its margins by magmatic flow, the disruption of which eventually grades into schlieren along the foliation of granitic rocks (e.g. lower portion/first plane of Fig. 5b and fig. 6a and b). The gneisses are predominantly biotite (± hornblend) orthogneisses with quartz-dioritic, tonalitic and granodioritic compositions (Fig. 6e and f). Calc-silicate paragneisses made up of *ca.* 90% diopside are subordinate to one specific level where they are boudinaged into dm-diameter, rounded, greenish fragments (fig. 7a). They occur in the southern portion of the Ponta das Bombas outcrop, which represents the upper structural level of the Porto Belo Complex sequence, dipping to SE.

Igneous and metamorphic rocks are interpreted as intimately related in a migmatitic association. Some of the orthogneiss fragments present cm-size melt patches with euhedral titanites (up to 3 mm long) immersed in alotriomorphic quartz-feldsphatic matrix coarser than the surrounding gneissic matrix. These structures are very similar to those described by Martini et al. (2019a,b), being suggestive of in situ partial melt in presence of water (according to Weinberg and Hasalova, 2014 – see Fig 7b with inset and fig. 6e). The mobility of melt was efficient along the main banding of metatexites (since they preserve the main structure of the migmatitic system), leading

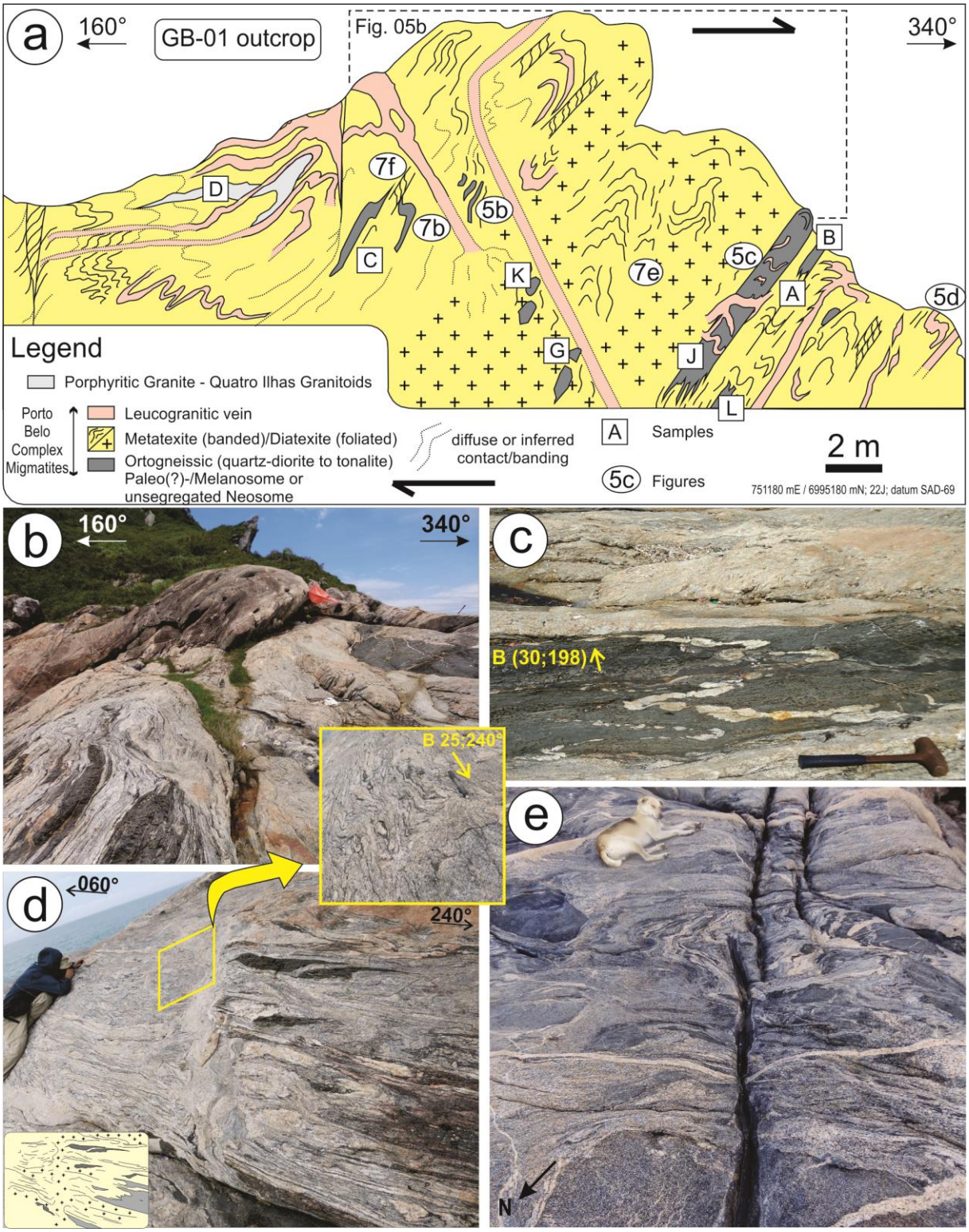

Fig. 5 – Porto Belo Complex general features at Ponta das Bombas area. (a) Ponta das Bombas main outcrop, 340° - 160° cross-section, presenting the lithology distribution and main structural features. Samples sites and references to pictures are indicated. (b) Overview of the central portion of the same outcrop. The main antiformal structure of the outcrop is expressed by its morphology, with both limbs and the axial plane dipping towards SSE. In the far-right portion of the picture the bigger tabular gneissic body (fig. 5c) can be observed. (c) Orthogneiss (melanosome) tabular body along the main foliation of the leucocratic granite. The granite intrudes the orthogneiss as cm-size veins which are folded and boudinaged, probably due to high-obliquity original (cont.)

contacts. Fold axis is indicated. (d) Typical aspect of a metatexitic migmatite along an oblique exposition, with interleaving of igneous and metamorphic rocks along the main banding, crossed by a leucogranitic vein. The vein presents very irregular and diffuse contacts with the migmatite, interfingering with some bands with textural continuity (inset). A simplified sketch is presented in the lower-left portion of the figure. (e) Typical aspect of a diatexitic migmatite in an approximately horizontal exposition. The dog for scale is 75 cm long. Outcrop located *ca.* 100 m south of the portion represented in figure 5a.

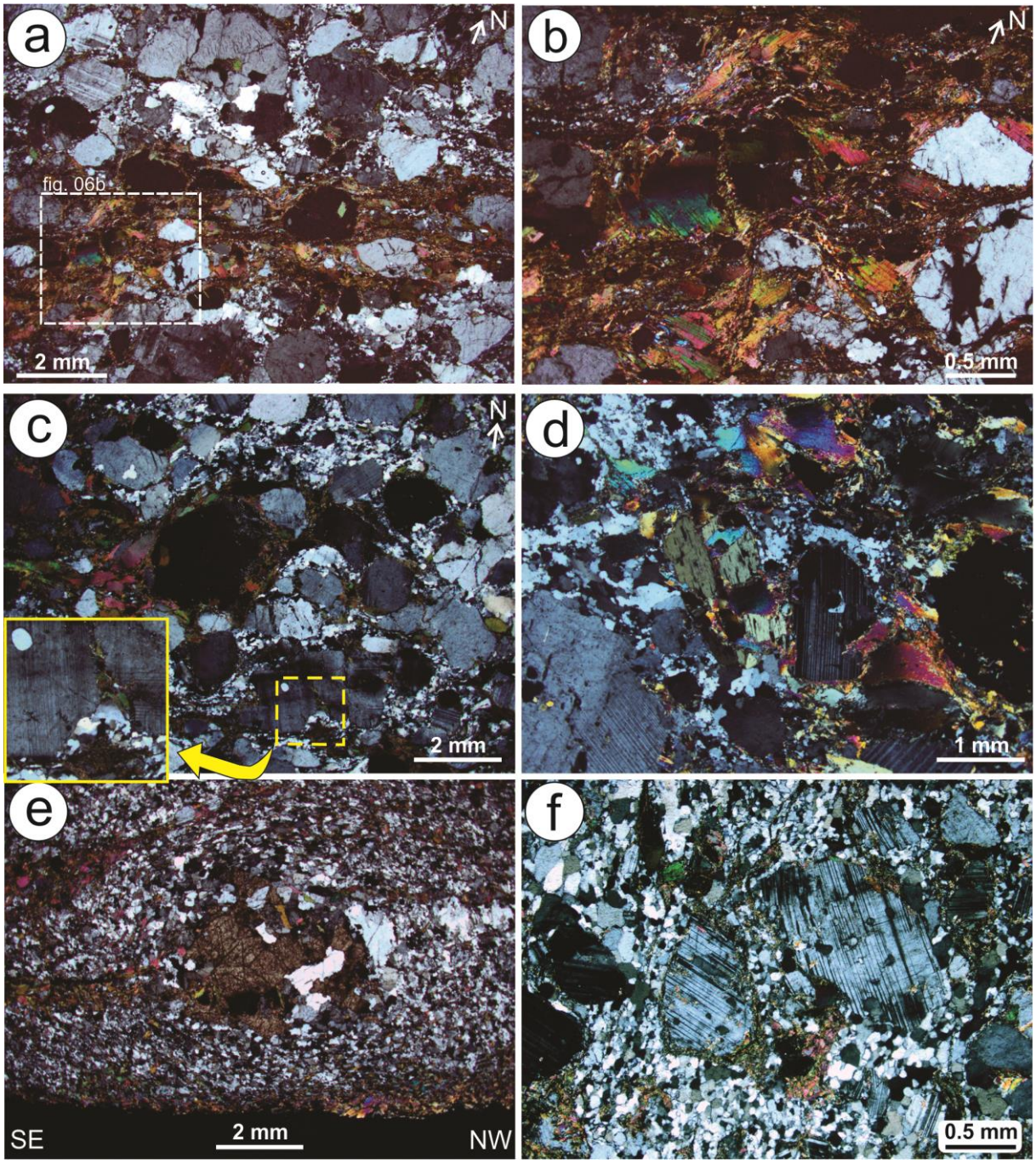

Figure 6 – Petrographic aspects and microstructures from Porto Belo Complex rocks. (a) Foliated leucogranite with biotite schlieren (sample GB-01A). Notice the presence of fine-grained, quartz-feldsphatic, recrystallized matrix. Dextral porphyroclasts are observed in the central portion. The section is subhorizontal, XZ plane. (b) Detail of the schlieren from figure 6a. Notice the hinge zone marked by a coarse-grained, kinked biotite grain, in the center of the picture. Very fine-grained mica occur due to low-temperature recrystallization. (c) Banded biotite monzogranite (metatexite – GB-01C) general view, with recrystalizated matrix between igneous relicts (upper portion). Asymmetric porphyroclasts indicate dextral shear sense. (cont.)

The lower porphyroclast show an incomplete boudinage (see inset). The section is subhorizontal, XZ plane. (d) Foliated biotite hornblend tonalite with epidote (GB-01E). Notice the pair of subhedral hornblend and plagioclase at the center, the first partially replaced by biotite. Recrystallized quartz grains present polygonal granoblastic texture. (e) General view of the tonalitic biotite orthogneiss (GB-01B), presenting a fine-grained granoblastic fabric and the contrastant texture of a titanite-bearing pocket leucosome, which asymmetry points the top-to-the-NW sense of shear. The section is subvertical, XZ plane. (f) Aspect of a tonalitic biotite orthogneiss (sample PB-57G, from Mariscal Beach) from a dextral, strike-slip high-strain zone, with fine-grained, quartz-feldspathic, granoblastic matrix.

to coalescence along mm- to cm-wide veins that crosscut obliquely the main banding in certain places (Fig. 5c, 5e, 7b). The melt network along the main banding and oblique veins also coalesce in wider leucogranitic injections, rooted in the banded rock (Fig. 5d and inset), or even in certain wider bands which do not preserve the main banding, but are structurally independent diatexitic levels which may carry fragments of its source rocks (fig. 5e and 7a). Because of magmatic flux, some cumulates of mafic minerals (e.g. hornblendites) are found locally.

The structural framework of the Porto Belo Complex migmatites at Ponta das Bombas is presented in Fig. 7c. The poles to foliation are arranged in a half-girdle, which represents the closed to isoclinal folds (Fig. 7d-f) with a subhorizontal to subvertical NE to ENE striking foliation, and the single-maximum representing foliation dipping at medium angle to SE. The mineral and stretching lineations are displayed at a half-girdle in the SW quadrant, ranging mainly from low- to medium-angle plunge towards SW (240°) to south (180°). Orientation of axial planes is very similar to the foliation distribution, while fold axes orientation is similar to lineation distribution, but more spread. This spreading of fold axes is probably due to the high melt mobility, with local development of convolute (fig. 7e) and disharmonic folds (Fig. 7f).

Contact relationships between the Porto Belo Complex migmatites and the Quatro Ilhas Granitoids are best observed in the southern portion of the Ponta das Bombas. In this area, the Quatro Ilhas granite overlies the migmatitic rocks (Fig. 8a) and mutual crosscuting relationships are observed. Leucogranitic injections rooted in the metatexite melt-rich bands cross the units contact and the magmatic foliation of the Quatro Ilhas granite (Fig. 8b and c). The Quatro Ilhas granite surrounds slices of the metatexites in the contact vicinity, with parallel foliation disrupting and probably assimilating it during magmatic flow (Fig. 8d).

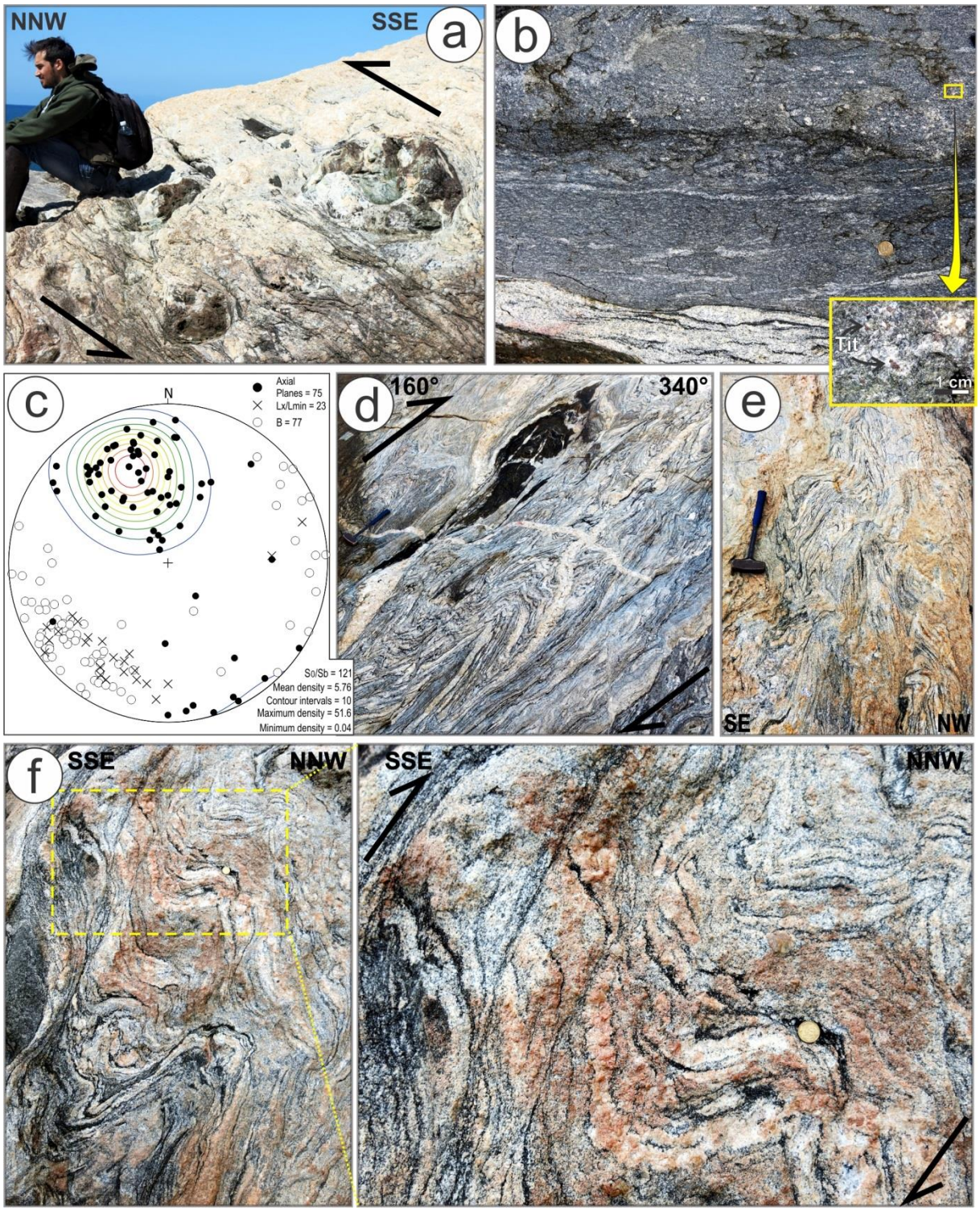

Fig 7 – Structures from Porto Belo Complex at Ponta das Bombas area. (a) Diatexite with calc-silicate fragments and other enclaves showing top-to-NNW apparent movement. Same area of figure 5e. (b) Migmatitic orthogneiss heterogeneous deformation. Small patches with titanite-bearing leucogranitic material are interpreted as in situ pocket melts (see inset). The central, darker area presents diffuse and elongated patches, indicative of higher strain. The lower portion presents the surrounding leucogranite with schlieren. (c) Stereonet from Porto Belo Complex at Ponta das Bombas, presenting contoured pole to foliation, lineations, poles to axial planes and fold axis. Equal area, lower hemisphere projection. (d) Vertical section, fold profile showing asymmetric, isoclinal folded metatexite with an orthogneissic melanosome presenting a sigmoid shape indicative of top-to-NNW (cont.) thrust component. Location is *ca.* 50 m south of the portion represented in figure 5a. (e) Convolutely folded metatexite presenting subvertical axial planes truncated by discrete subhorizontal structures. (f) Disarmonic fold

developed in metatexite. The central portion presents the coincidence of an antiform and a sinform hinge zone, culminating with a dilatant site filled with milky quartz. The upper portion of the picture (inset) present top-to-NNW shear sense marked by transposition shear zones, with a duplex structure at outcrop scale.

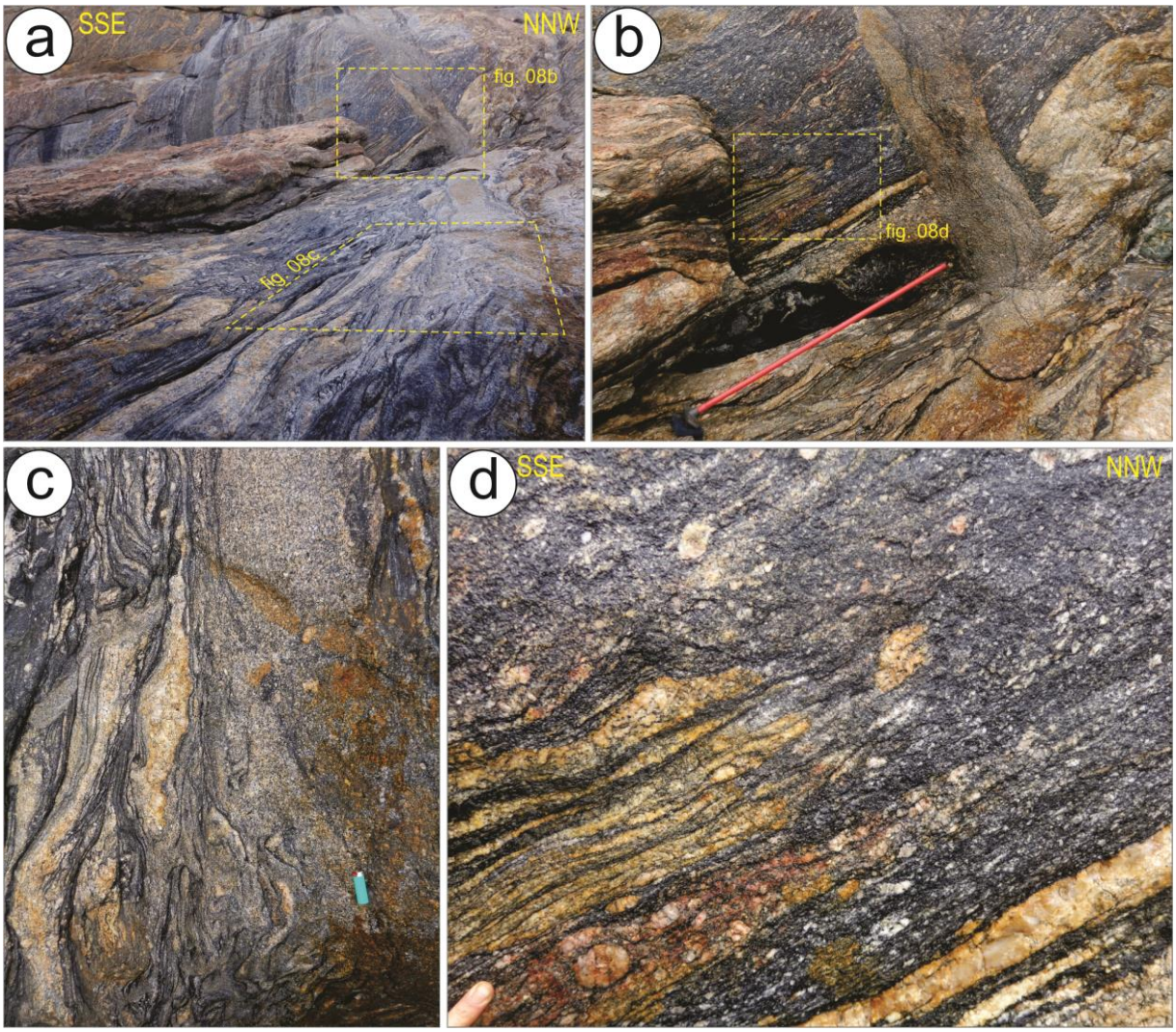

Fig. 8 –Porto Belo Complex and Quatro Ilhas Granitoids contact relationships. (a) General overview with Porto Belo Complex migmatites at lower-right half of the picture, and Quatro Ilhas Granitoids at upper-left. Notice the metatexite at first plan (lower portion of the picture), grading to the granitic injection which crosscuts the contact between the units and the Quatro Ilhas Granitoids foliation in the upper portion of the outcrop. (b) Detail of the intrusive contact of the leucogranitic injection crosscutting both the contact and the igneous foliation of the Quatro Ilhas Granitoids. Note that to the left of the injection there is a fragment of migmatite surrounded by the porphyritic Quatro Ilhas Granite. (c) Horizontal view of the lower portion from figure 08a, with the gradual to diffuse contact between the metatexite and the leucogranitic injection rooted in its main banding. (d) Vertical view, detail from figure 8b, with the porphyritic Quatro Ilhas Granite partially assimilating and disrupting the Porto Belo Complex metatexite. Notice the Quatro Ilhas Granite cm-size porphyroclasts.

It is worth to note that NNW – SSE (most 340° - 160°) sections represent fold profiles that are oblique to perpendicular to lineations, and expose the best kinematic indicators seen at the outcrop, including abundant gneissic fragments as asymmetric “sigma clasts” (Fig. 7a and 7d) and high-strain zones where the axial planes evolved

into a transposition foliation, developing duplex structures (Fig. 7f and its inset) at outcrop scale. All observed kinematic indicators along NNW – SSE subvertical exposures express an apparent top-to-NNW thrusting component, while kinematic indicators exposed along subhorizontal planes indicate a dextral component. The evidences point to a coherent kinematic framework of oblique, top-to-NNW dextral transpression, very similar to the one observed within the Quatro Ilhas Granitoids.

Microstructures like asymmetric porphyroclasts of both deformed granitoids (fig. 6d and 8d) and orthogneisses (fig. 6f), and sheared melt pockets found in the later (fig. 6e) are consistent with this kinematics. Microstructures in the granitoids show widespread quartz recrystallization. However, feldspar porphyroclasts are mostly rounded or lenticular relict crystals with mica or quartz shaping the asymmetric recrystallization tails (e.g. Fig. 6a, b and c), which is indicative of minor feldspar recrystallization processes. The feldspar porphyroclasts are very often fractured, with some of these fractures filled by subhedral to anhedral crystals, which is suggestive of deformation in presence of liquid (as for example in the Fig. 6c inset). Subhedral phenocrysts are also common as a preserved igneous texture (Fig. 6c and d). On the other hand, orthogneisses present both high temperature and lower temperature deformation features, as for example recrystallized plagioclase in the granoblastic matrix and kinked plagioclase porphyroclasts, marginally replaced by fine-grained mica (fig. 6f).

The outcrops at Retiro dos Padres and Sepultura beaches (Fig. 3) represent lower structural levels in relation to the Ponta das Bombas outcrop. The observed features in these places are very similar to those described above, apart from discrete dextral transcurrent shear zones that become more important, some of them assisting the emplacement of the Mariscal Granite intrusions.

4.4 Major Gercino Shear Zone strike-slip syntectonic magmatism

Both the Estaleiro Granitic Complex (EGC) and the Zimbros Granite present NE-striking dextral strike-slip tectonics (see stereonet “D” in figure 03) recorded by both magmatic and mylonitic fabrics (Bitencourt and Nardi, 1993; Bitencourt, 1996) and are best observed in the northern portion of the peninsula. Bitencourt (1996) discussed the relative stratigraphic position of the EGC in relation to the Mariscal Granite in terms of indirect observations, since there are no good exposures of it. The author preferred the hypothesis of the EGC being intrusive in the Mariscal Granite due to: contact geometry at map-scale (Fig. 2); the presence of some

preserved subhorizontal structures in the Mariscal Granite and its virtual absence in the EGC, pointing to the earlier character of the first; the absence of xenoliths of the shoshonitic EGC in the peraluminous Mariscal Granite, which is supposed to be a colder magmatic body, and vice-versa, being the first a hotter magmatic body and theoretically able to assimilate the Mariscal Granite composition. This relationship was confirmed by further geochronological studies (Chemale Jr. et al, 2012; Florisbal et al., 2012a; Peruchi, 2016).

Bitencourt (1996) described the Zimbros Granite as a late-transcurrent magmatic body. It crosscuts the Estaleiro Complex at the map scale (Fig. 2), while presenting mostly sheared contacts at outcrop scale, with intrusive contacts locally preserved. The stratigraphic position of this unit was also further confirmed by the geochronological study of Chemale Jr. et al (2012).

4.5 Brusque Complex and the Major Gercino Shear Zone northern boundary

The contact between the granodiorites of the EGC and metapelitic schists of the Brusque Complex was first observed by Silva (1991) in the Sertão de Santa Luzia region (see fig. 2). Bitencourt (1996) described the progression from the undeformed facies of the Estaleiro granodiorite to foliated and mylonitic rocks, while Brusque Complex rocks in the NW present a strong mylonitic foliation oriented (060°/65°NW), transposing older subhorizontal contacts between quartzites and garnet-muscovite schists. Bitencourt (1996) attributed these rocks to the Rio do Oliveira Sequence and interpreted them as the Estaleiro Granitic Complex country rocks at the NW boundary of the Major Gercino Shear Zone. To the author, the supracrustal rocks were intruded by the synkinematic Estaleiro Granitic Complex after Brusque Complex main metamorphic and deformation event.

4.6 Brusque Complex southern coastal section

The approximately 4 km long E – E’ section along the 340° - 160° trend crosses the metavolcanosedimentary pile of the Rio do Oliveira Sequence (Fig. 9a; see also de Campos et al., 2012). From the whole section, one outcrop was chosen for detailed observations due to its convenient orientation perpendicular to the structural trend and continuous exposure (Fig. 9b). The exposed sequence comprises metabasalts, calc-silicate rocks of variable mineralogy, qtz+bt schists, minor ultramafic rocks and syn-kinematic leucogranite injections, mostly as cm- to m-thick bodies at low-angle or along the main foliation, but also as bigger bodies crossing the fabric at high-angle

(Philipp and de Campos, 2010; fig. 9). The main foliation (S_x) is defined at the outcrop-scale by interleaving of the above-mentioned lithologies. At the hand-sample scale, it is characterized by the alignment of metamorphic minerals such as amphibole and feldspar (metabasalts and calc-silicates) or interleaving of biotite-rich and quartz-rich bands (schists). The schists present intrafolial folds with partially transposed earlier foliation (S_{x-1} parallel to S_x – not shown) marked mainly by trails of opaque minerals along biotite aggregates. The main foliation presents generally NE-SW strike and gentle dip to NW (Fig. 9c), with poles to foliation forming an incomplete girdle due to asymmetric to recumbent folding (see fig. 9d). The folds observed in the cross-section, independent of scale, present a strong asymmetry suggestive of top-to-NNW sense of shear. Axial planes are mostly coincident with the pole to foliation distribution due to the closed character of the folds. Fold axes spread in the SW quadrant and subordinately in the NE, mostly near the strike of foliation and axial planes. Mineral and stretching lineations are consistently concentrated near the dip direction, plunging at shallow angle towards NW. The rotation of fold axes in the SW and NE quadrants observed in the stereonet (fig. 9c), between the fold axes maximum and the stretching direction, also points to fold shearing during progressive deformation. Apart from fold asymmetry, kinematic indicators are virtually lacking, which is attributed to the absence of good markers.

The deformation of the heterogeneous rock pile, with a high rheology contrast between the layers, is exemplified by disharmonic folding of different compositional layers, commonly showing thickened fold hinges and thinned or boudinaged limbs (e.g. figs. 9d and 10a). Fold asymmetry along this section consistently shows top-to-NW vergence (Fig. 10b and 10c). A lower carbonate-rich calc-silicate layer presents apparent softer rheology than the central, boudinaged epidote-rich layer (Fig. 10c), and shows a very asymmetric fold pattern given by the SE long-limb and the NW short- or inverted-limb. It is also possible to observe that there is a relation between wave-length and amplitude of the fold, which is not constant along the same axial plane. This feature is interpreted as a local strain gradient and suggests the fold propagation towards NW, by amplification of an irregularity, somehow restricted to that layer, since it does not affect the layer above. It is also noteworthy that the layer directly below the boudinaged one presents completely different fold shapes, interpreted as driven by bending mechanisms linked to the boudinaged of the overlying layer. The contact of the layers represents a rheological boundary, acting as a detatchment at the outcrop scale.

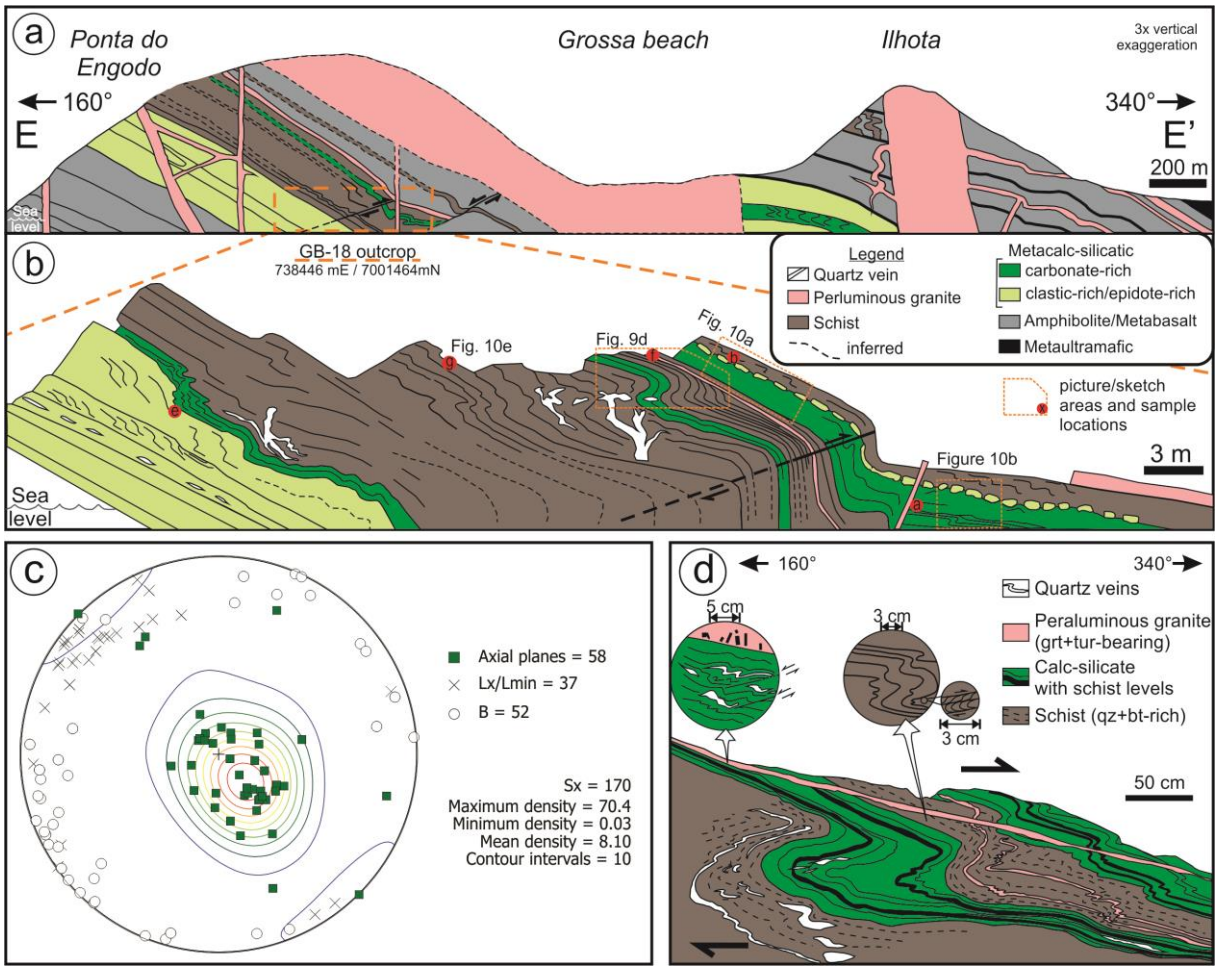

Figure 9 – Rio do Oliveira Formation, Brusque Complex general aspects along E – E' section. (a) E – E' cross-section presenting the recognized lithotypes and major structural elements. (b) Cross-section (160° - 340°) at Grossa beach with the main structural features and localization of samples, detailed sketches and pictures. (c) Stereonet for contoured pole to foliation (S_x), pole to axial planes, lineation and fold axis. Equal area, lower hemisphere projection. (d) Sketch from the central portion of the outcrop from figure 9b, presenting asymmetric to recumbent folds developed over calc-silicate and schist layers, as well as slightly oblique cm-wide leucogranitic earlier injections. Later leucogranitic injections crosscuts the folded layers. Intrafolial folds are locally preserved along schistosity and represent a pre-S_x structure (right-side inset). Antithetic, top-to-SE shear bands are locally observed shearing quartz veins or quartz-rich layers (left-side inset).

Discrete, antithetic shear bands are locally present in the quartz-biotite schists (Fig. 10b) and epidote-rich calc-silicate rocks in the southern portion of the outcrop (Fig.10d). The quartz-biotite schists present cm-spaced planar structures, which develop stretching preferentially subparallel or along the long limbs of cm-size asymmetric folds. These structures are marked mainly by the thinned or disrupted quartz-rich layers, but also by obliquely oriented, discontinuous flanking structures (see fig. 10b inset), which segmented the rock into asymmetric foliation boudins. Some of these structures are filled with quartz-feldspathic material (upper-left portion of fig. 10b), which suggests their extensional character.

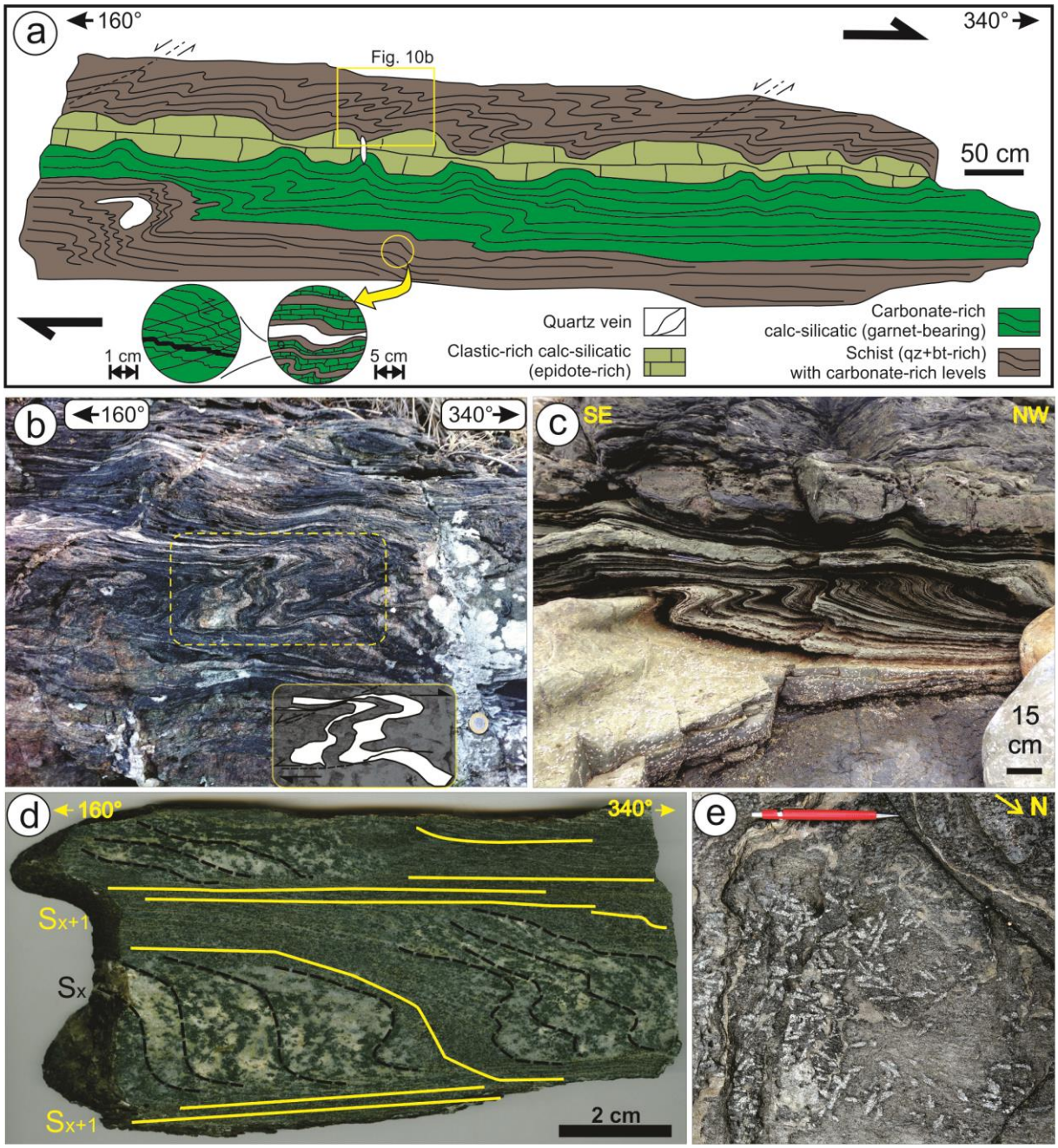

Figure 10 – Structural features Rio do Oliveira Formation, Brusque Complex, at Grossa beach. (a) Sketch from the uppermost layers from figure 9b. Asymmetric folds are developed over a carbonate-rich calc-silicatic layer and the schist, while boudinage affected the central epidote-rich calc-silicatic layer. (b) Detail from the central-upper portion of the figure 10a. The schist presents a banding given by biotite-rich (dark) and quartz-rich layers (light). Asymmetric folds given a top-to-the-NNW shear sense. The light bands are good markers to identify the antithetic, discrete shear bands which affected the rocks later, with an opposite top-to-the-SSE shear sense (see inset). (c) Photograph from the NW extreme of the same uppermost sequence from figure 10a, showing the less competent, asymmetricaly folded carbonate-rich calc-silicatic rock in the lower portion, and the boudinaged, epidote-rich calc-silicatic rock in the center, with the schist admixed with calc-silicatic thinner layers on the top. The very asymmetric shape of the folds in the lowermost strata changes wave-length and amplitude while it propagated upwards. The discontinuity between the layers acted as a rheological boundary, and the layer below the boudinaged one presents gently open folds bending in the boudin necks.. (d) Hand-specimen slab of a calc-silicatic, plagioclase-epidote-actinolite schist, presenting an asymmetricaly folded $S_{x,}$ which is interpreted as top-to-NNW shear sense. This fabric is reworked by a mylonitic foliation S_{x+1} defined by neocrystallization of (cont.)

biotite which anostomosed along the previous foliation and axial planes/long limbs, defining sigma-shaped pods of S_x with top-to-the-SSE shear sense. (e) Ramdomly growth porphyroblasts pseudomorphosed by white mica along certain schistosity levels (see figure 9b for location), indicative of static thermal metamorphism.

The epidote-rich calc-silicate rocks also present the same asymmetric fold pattern recorded in a relatively coarse-grained (cm-size) fabric made up by epidote, amphibole, plagioclase and quartz (S_x in fig. 10d), while a later, fine-grained (sub-mm), biotite-rich mylonitic fabric (S_{x+1} in fig. 10d) reworks it in an anastomosed array following the previous structure, but mostly along a transposition foliation sub-parallel to the axial planes. These hinge zones are domains of preserved S_x, which acted like pods surrounded by high-strain zones of antithetic S_{x+1}. An apparent strain gradient is observed towards the center of these structures, where grain-size is minimum and elongation is maximum. Together with the pods asymmetry, the deflection of the folded metamorphic foliation towards high-strain S_{x+1} indicates a top-to-SE movement along the later structure. These structures suggest reactivation of low-angle planar structures at disctinct PT-fluid and/or higher-strain conditions. Its kinematics may be interpreted in terms of a local antithetic component or backthrust during, or shortly after, main top-to-NNW movement, or alternatively, as a non-progressive, later deformation phase with opposite shear-sense.

The development of randomly-oriented, post-kinematic porphyroblasts, (andalusite?) pseudomorphically replaced by white mica, is locally observed at a few quartz-biotite schist layers along the profile (fig. 10e). Thermal effects like this are in agreement with observations made by Philipp et al. (2004) along the contacts of the Brusque Complex with Camboriú Complex.

4.7 Brusque Complex and Camboriú Complex contact relationships at Serra da Miséria

The direct contact between the supra- and infracrustal units of the Tijucas Belt is exposed in the area behind the Serra da Miséria ridge, which is made up of a mylonitic leucogranite considered as a part of the Camboriú Complex (Hartmann et al., 2003; Bitencourt and Nardi, 2004; Rivera et al., 2004). This mylonite, in contrast to the rest of the Camboriú Complex, presents a strongly linear fabric, including some L ≥ S tectonites. Behind this ridge there is a *ca.* 1 km long, approximately east-west oriented lens of metabasalt and siliciclastic metasediments of the Brusque Complex occurring as an enclave along the mylonites at the boundary of the Camboriú

Complex (see Fig. 2). Along the valley north of Serra da Miséria, it is possible to observe the boundary between the complexes at outcrop scale (Fig. 11a), where they present concordant foliation parallel to the contact (Fig. 11b).

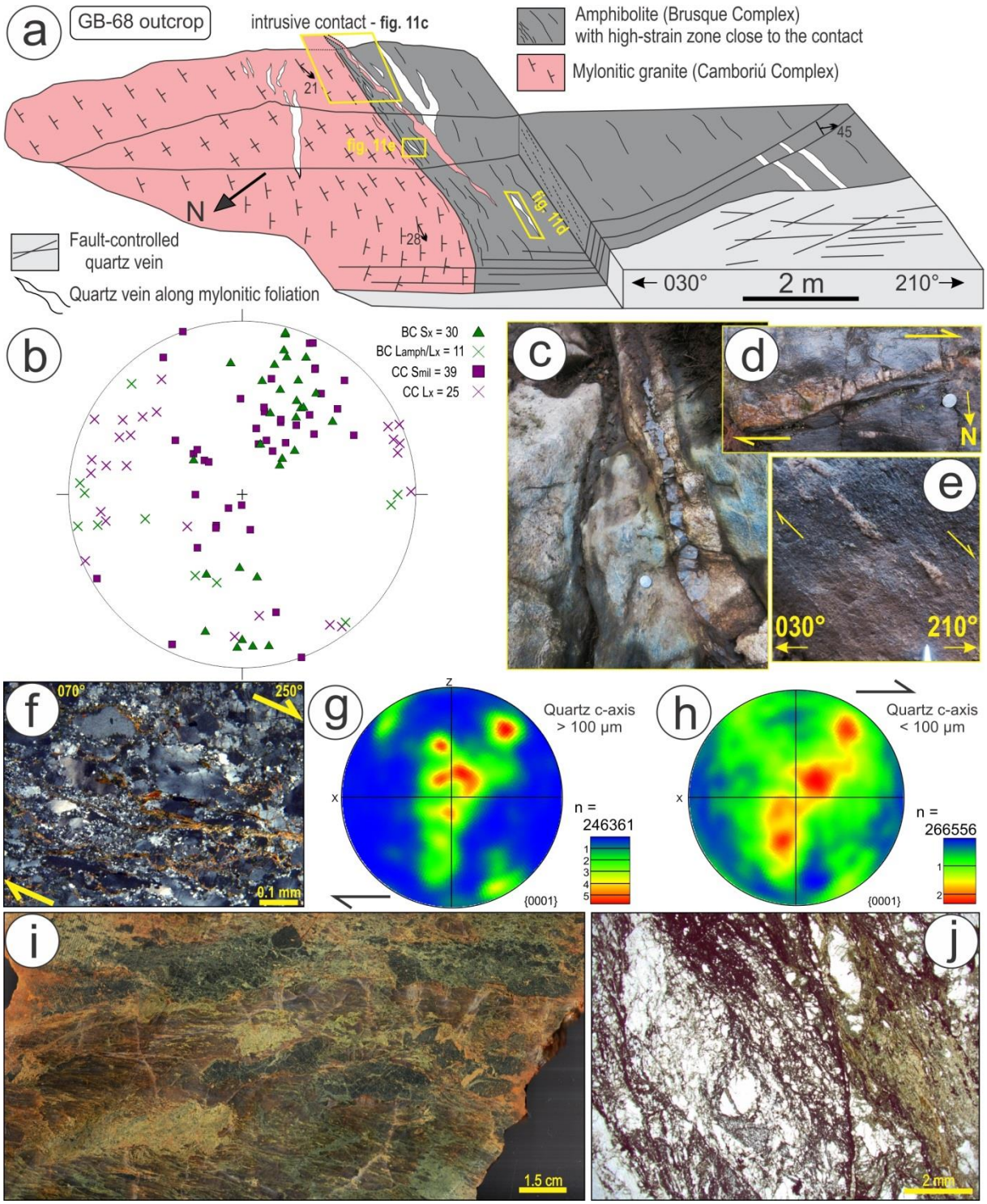

Fig. 11 – Contact between Brusque Complex amphibolites and Camboriú Complex mylonitic leucogranite in the Serra da Miséria. (a) Outcrop sketch (block-diagram) where both units present concordant mylonitic structures parallel to the contact. The mylonitic granite is locally intrusive in the amphibolites. Faults and fractures crosscut the contact at high-angle and a later-quartz vein is emplaced along these planes. (b) Stereonet presenting pole to foliation and lineation from both units, showing the concordance of attitudes. Lower hemisphere, equal area projection. (c) Horizontal view of the contact shown in the central upper portion of figure 11a. (cont.)

The left-side of the picture is the Camboriú Complex mylonitic leucogranite, which is lighter and coarse-grained if compared with Brusque Complex amphibolites, finer and darker. The concordant contact is observed and highlighted by erosional effects. A discordant vein of leucogranite with milky quartz crosscuts the amphibolite and merges with the mylonitic leucogranite in the upper portion of the picture. (d) Detail from a sheared quartz vein in horizontal view, showing dextral apparent sense of shear. (e) Detail from a sheared quartz vein in vertical view, showing normal, or top-to-210° apparent sense of shear. (f) Photomicrograph from a mylonitic leucogranite showing quartz and feldspar porphyroclasts surrounded by biotite + opaque and fine-grained quartz-rich recrystallized matrix (< 100 μm) showing apparent dextral asymmetry (top-to-250°). (g) Stereonet for mylonitic leucogranite quartz c-axis representing the population bigger than 100 μm. A girdle with clear apparent dextral asymmetry confirms the sense of shear identified at thin-section. (h) Stereonet for mylonitic leucogranite quartz c-axis representing the population smaller than 100 μm. The asymmetry is very similar to the first stereonet, but the distribution is more widespread, with a smaller maximum. (i) Slab from a fault-related rock handsample collected close to the detailed outcrop. It presents angular (cm-size) and rounded (mm-size) amphibolite fragments as block-in-matrix immerse in mylonitic quartz with different proportions of fine-grained, epidote-bearing, greenish material. (j) Fault-related rock photomicrograph presenting both the mylonitic leucogranite (left-side) and the amphibolite (righ-side), juxtaposed after cataclasis.Distribution of foliations from both units (Fig. 11b) suggests a coherent girdle. The girdle presents a single maximum, which dips at medium angle towards SSW, parallel to the observed contact (fig. 11a).

CC mylonite lineation (n = 25) presents spread of orientations, mostly with low-rake, with a main cluster bearing 245° to 325°, a second cluster between E and 065°. This orientation is therefore close to the expected fold axis. Additionally, some measurements present orientation plunging to the south. From the Brusque Complex amphibolites, only small number of lineation measurements are presented (n = 11), but their spread is very similar to the lineations in the Camboriú Complex mylonitic rocks, ranging from a small number of near dip-direction lineations, to a major subparallel-to-strike distribution, roughly E – W. The presented distribution suggests a lineation girdle approximately coincident with the average foliation of both complexes and the observed contact plane, typical of triclinic transpressional deformation (Fernandez and Días-Aspiroz, 2009, and references therein). Additional spread of lineations is interpreted as a consequence of regional, open folding.

The contact of both complexes is mostly abrupt and parallel to foliation. There is an apparent strain gradient in the Brusque Complex amphibolites with increasing strain towards the contact with the Camboriú Complex, observed as a development of more pervasive mylonitic foliation. A composite, deformed vein of leucogranite and milky quartz crosscuts the amphibolite foliation at low-angle, very close to the boundary with the Camboriú Complex mylonitic granite, apparently merging with it below the soil and vegetation cover (Fig. 11c). This feature is interpreted as suggestive of: i) the intrusive relationship of the mylonitic granite into the Brusque Complex amphibolite

during the main deformational episode which was responsible for the juxtaposition of the complexes; and ii) that the mylonitic granite of the Camboriú Complex may be representative of migmatitic melts of this complex, similarly to the Itapema Granite leucocratic facies. Smaller, disrupted milky-quartz single veins are found in both units nearby the contact. Some of them, observed transposed along the mylonitic foliation of the amphibolites, are indicative of oblique shearing with dextral (fig. 11d) and normal (top-to-SE – fig. 11e) components.

A CC mylonitic granite presenting L > S was evaluated in terms of observed deformation mechanisms and kinematics through petrography and EBSD. The rock presents up to 50% of quartz, which occurs as porphyroclasts (up to 3 mm long) with undulose extinction and oblique subgrain boundaries, and dynamically recrystallized fine-grained matrix (< 100 μm). K-feldspar porphyroclasts (*ca.* 2 mm) present extensional fractures filled by quartz. Micas are very rare. The obliquity of porphyroclasts long-axis, asymmetry of lens-like fine-grained quartz aggregates or mica lenses contouring porophyroclasts, and more rarely seen mica fishes, are indicative of an oblique, dextral, top-to-ESE movement along the mylonitic fabric (fig. 11f).

Quartz c-axis orientation data were processed in two different grain-size groups with arbitrary threshold at 100 μm, according to a change in histogram of grain-size distribution (not shown). C-axis distribution from quartz crystals larger than 100 μm form an asymmetric, well-defined single girdle, or an ill-defined crossed girdle (fig. 11g). Quartz crystals smaller than 100 μm present c-axis distributed in a very similar shape when compared with the main segment of it better defined crossed-girdle (fig. 11h). The general orientation is much more random when compared with the fabric of the larger grains, as shown by the density of the maximum in contoured diagram. The dextral asymmetry, however, is still coherent and clear. This is interpreted in terms of progressive deformation under retrograde conditions and relatively constant strain ellipsoid orientation, corresponding to an oblique, dextral-normal, top-to-250° sense of shear.

The contact of the two units is reworked by a NE – SW fault system, possibly related to a late reactivation of the Major Gercino Shear Zone (Hueck et al., 2018). The effects of later movements were observed at the outcrop as fault-controlled quartz veins and fracture zones (fig. 11b). Fault-related rocks are observed as breccia of amphibolite fragments occurring as “blocks-in-matrix” along with mylonitic quartz (fig. 11i – collected not in situ) or cataclastic juxtaposition of both units along microfaults

(fig. 11j). This is in agreement with the hypothesis of progressive deformation under retrograde conditions affecting the early-formed high-T contact of both units.

4.8 Itapema Granite

The Itapema Granite was described in detail by Rivera et al. (2004) and Bitencourt and Nardi (2004), as a hornblend-biotite granodiorite to monzogranite with a high proportion of xenoliths (ca. 20 fragments/m^2) organized along a strongly developed, subhorizontal magmatic flow banding (fig. 12a). The banding is given by different proportion of oriented mafic minerals, disrupted xenoliths, schlieren and pegmatites injected parallel to the main foliation (fig. 12c). However, no lineation is found. Apparent kinematic indicators, as asymmetric xenoliths, are observed along NW – SE sections, but they are not conclusive in terms of a coherent movement, which is interpreted as due to flattening and/or chaotic magmatic flow.

4.9 Camboriú Complex migmatites

The Camboriú Complex main petrological and structural features were recently described by Martini et al. (2019 a,b) and the main results and interpretations are summarized as follows. The metamorphic rocks are mostly orthogneisses and amphibolites, with minor paragneisses of pelitic and calc-silicatic composition. The main structure is a metamorphic banding enhanced by partial melting (fig. 12d). Its original attitude was subhorizontal and lineations are rarely found (fig. 12b). A possibly older folding phase was recognized locally as transposed, intrafolial folds, which significance remains unknown. The main banding is then folded into folds with a NE – SW to N-S, double-plunging subhorizontal axes and subvertical axial planes (e.g. fig. 12d). There are open to close, upright folds developed during partial melting, as suggested by syn-magmatic shear bands along limbs and axial planes (fig. 12e). These structures were used as channels for melt migration from the folded main banding upwards. Opposite limbs of the same antiform may act as conjugated shear bands with opposite shear sense, causing collapse of limbs and synforms, while antiforms are extruded (fig. 12f). These channels occasionally coalesce to generate melt extraction dikes, which are interpreted as feeders of the Itapema Granite magmatic chamber (Martini et al., 2019a,b). These features are interpreted in terms of an important pure shear component active during or just after peak metamorphism associated with the partial melting. The structural control of the melting process and

magma migration is registered as the symmetrical folding and transposition by syn-magmatic shear zones and dykes, and probably assisted the CC exhumation.

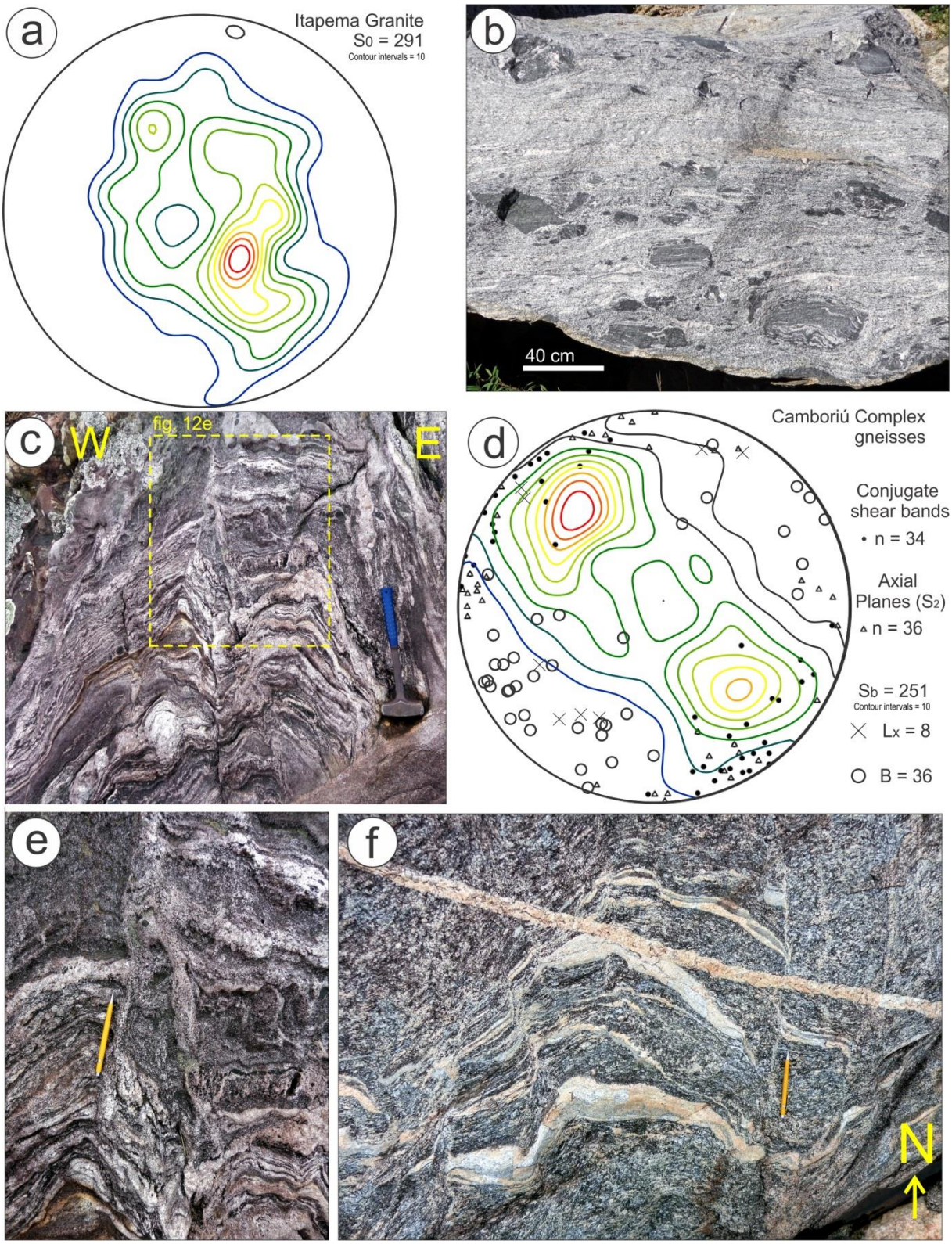

Fig. 12 – Camboriú Complex structures. (a) Stereonet for Itapema Granite contoured pole to foliation distribution. Lower hemisphere, equal area projetction. (b) Itapema Granite general aspect, with magmatic banding given by different proportion of mafic minerals and gneissic xenoliths, enhanced by foliation-parallel leucocratic injections and pegmatites. (c) Migmatitic orthogneisses from Camboriú Complex presenting disharmonic folding. Notice that while some layers are boudinaged, others present high-mobility due to magmatic flow. (cont.)

(d) Stereonet for Camboriú Complex gneisses with contoured pole to foliation, stretching lineation, fold axis, axial plane (S2) and conjugate shear zone attitudes. Lower hemisphere, equal area projection. (e) Detail from the center of figure 12c, where it is observed the mobility of leucosomes along fold limbs and sin-magmatic transposition shear bands along axial planes. (f) Folded granitoids among migmatitic gneisses from Camboriú Complex. The foliation is enhanced by layer-parallel injections of fine-grained leucosomes which are folded together. Note that opposite limbs act as sin-magmatic shear bands of opposite shear sense, with the eastern limb acting as east-side down, while the western limb acted as west-side down, with vertical extrusion of the antiform hinge zone.

4.3 Geothermobarometry

4.3.1 Porto Belo Complex crystallization conditions

One sample from a diatexitic hornblend-biotite tonalite with epidote and titanite was selected for geotermobarometry. The rock is foliated and presents well-preserved igneous textures, as exemplified by subhedral plagioclase and hornblend crystals (e.g. fig. 6d).

Nine representative hornblend – plagioclase pairs were selected based on apparent equilibrium conditions (table 1 and 2), as exemplified by direct contact relationships and preserved igneous shapes. The analysed spots were preferentially positioned close to the shared boundaries. The results from each pair are presented in the table 3. The estimated conditions range from 676 to 722 °C, and from 3.7 to 4.8 Kbar. The average conditions are 707 °C and 4.3 Kbar.

4.3.2 Camboriú Complex metamorphism and melting conditions

A migmatitic sillimanite-garnet-biotite gneiss (fig. 13a) was selected for pseudosection modelling. The rock presents *ca.* 5% of garnet porphyroblasts (up to 1.5 cm in diameter) embedded in a sillimanite-bearing, biotite-rich matrix, which also contains ilmenite as an accessory phase. The rock also presents irregular pockets and lenses of granitic leucosome along the banding. Subhedral garnet is present in the leucosome, which suggests its equilibrium during partial melting at peak metamorphic conditions (fig. 13b). The metapelite presents rare relics of kyanite, partially replaced by sillimanite (fig. 13c), which suggests prograde metamorphic history and/or exhumation from deeper to shallower levels.

The pseudosection for this rock (fig. 14) presents the observed assemblage biotite + garnet + sillimanite + plagioclase + quartz + ilmenite ± melt ± water in its central portion. The fields are limited from the lower pressure fields by the cordierite-out curve and from the higher pressure fields by the kyanite – sillimanite reaction boundary. The melt-in curve position should be taken with care and is not considered

a boundary to the estimated conditions. Since it is visible from the hand-sample that the melt was somehow mobile, the system composition may be impoverished from the melt loss, and the melt-in curve will be shifted to higher temperatures.

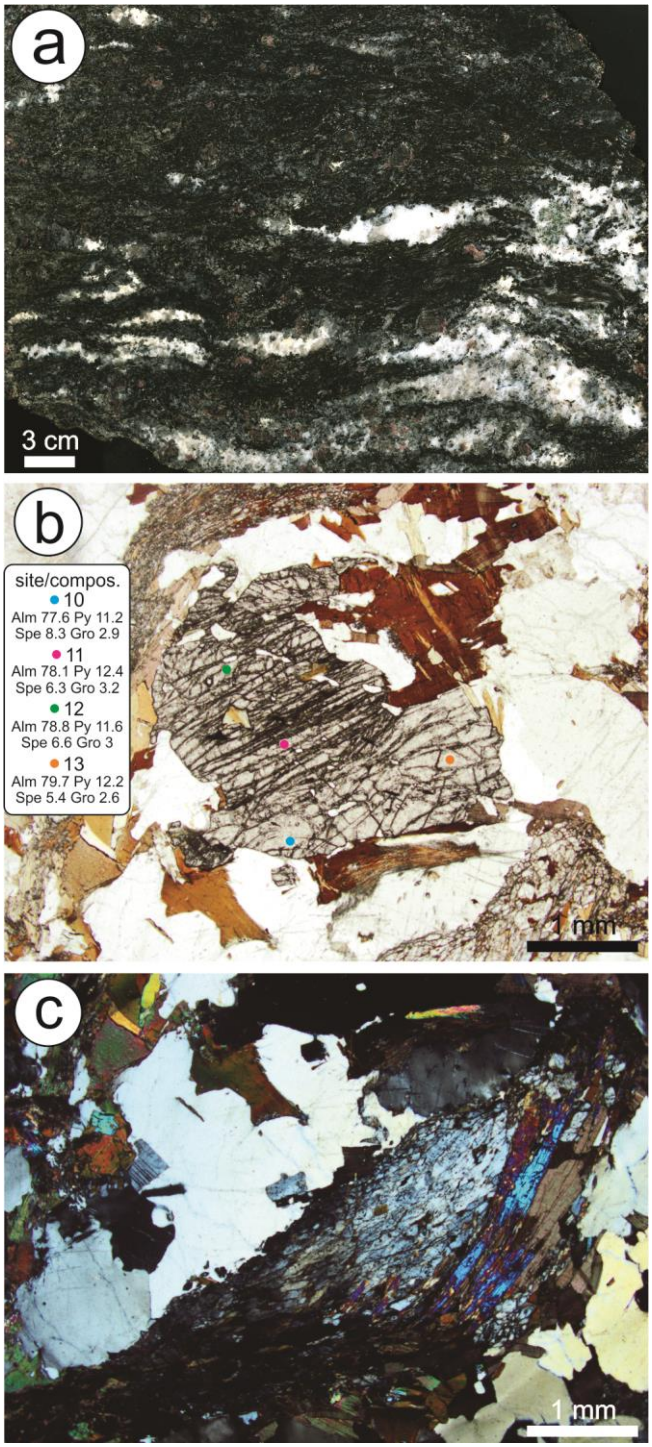

Figure 13 – Camboriú Complex metapelitic migmatite (CA-20Q) main petrographic characteristics. (a) Rock slab showing the relation and contrast between melanosome (mostly fine-grained, dark area, garnet-bearing, mafic-rich) and leucosome (coarser-grained, lens-like, light areas). (b) Photomicrograph of a garnet porphyroblast surrounded by both metamorphic and igneous minerals, as biotite and silimanite, and feldspar and quartz, repestively. Points of garnet chemical analysis are labeled. (c) Kyanite relict (dark gray at the center) partially replaced by silimanite (pink and blue to the right) and surrounded by quartz and biotite.

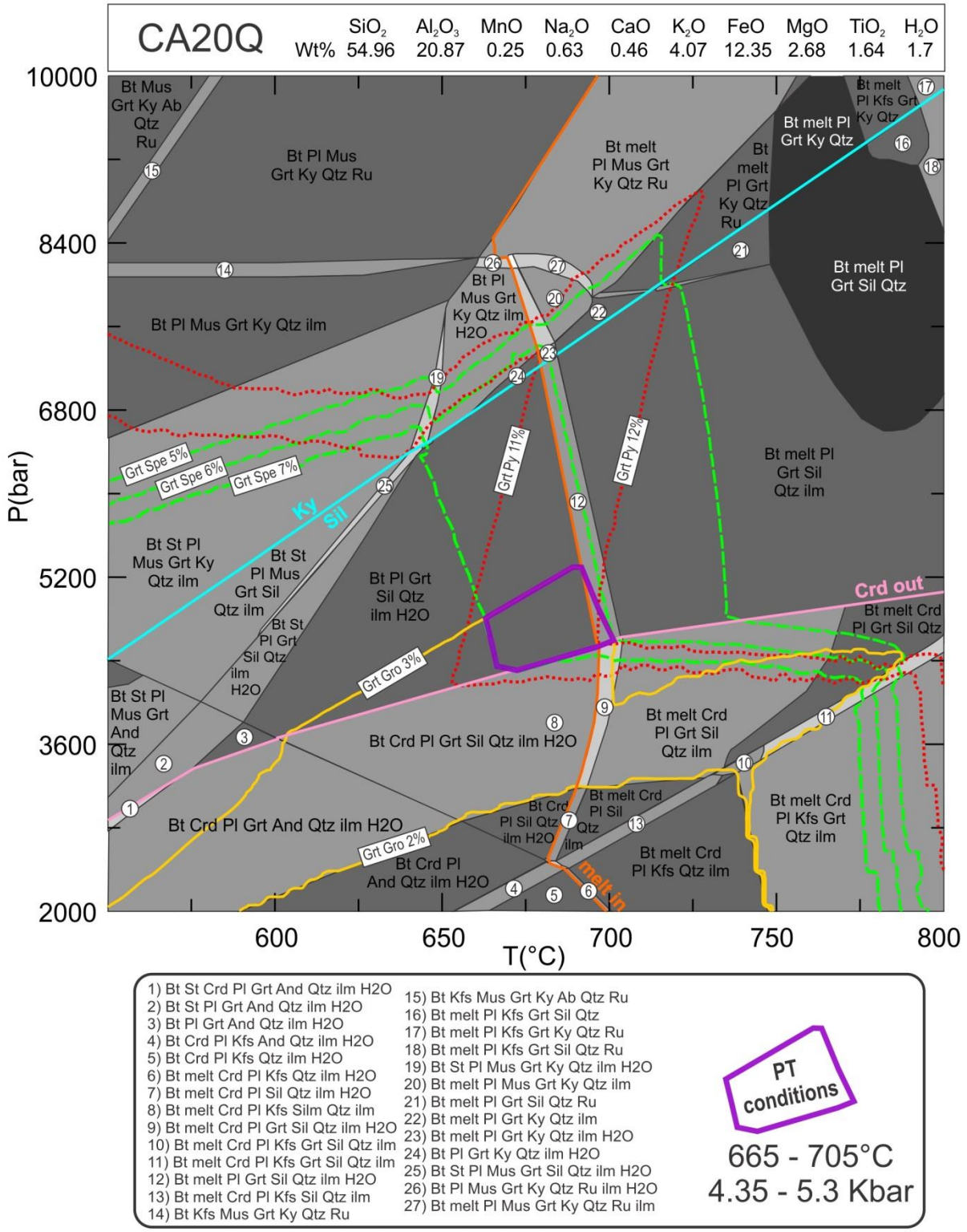

Fig. 14 – Pseudosection modeled for Camboriú Complex metapelitic migmatite (CA-20Q, system composition is presented in the heading). The curves for kyanite – sillimanite, cordierite-out and melt-in are shown. The isopleths for garnet pyrope (11 – 12%), grossular (2 – 3%) and spessartine (5 – 7%) are presented and constrain the range of 665 – 705°C and 4.35 – 5.3 Kbar as equilibrium conditions.

Representative mineral chemistry of biotite and garnet is presented in table 4. Thirteen biotite grains were analysed in the metamorphic matrix. The compositional range is expressed by XMg (Mg/[Mg+Fe]) values from 0.31 to 0.37, with a median and average of 0.34. The isopleths for the observed range of XMg values for biotite are widely spaced and cover most of the stability fields representing the observed assemblage. Since these isopleths do not help to constrain the PT conditions, they were not plotted in the figure 14.

From three analysed garnet porphyroblasts, just one of them presented core – rim zonation, while the other two presented nearly constant composition independent of position. In the weakly zoned garnet crystal, core presents slightly higher content of grossular and lower almandine component ($Alm_{74-75}Py_{12}Sp_{7}Gro_{7-8}$) if compared with rim ($Alm_{78}Py_{11}Sp_{8}Gro_{3}$ – see fig. 13b).

Isopleths for grossular (up to 3%), pyrope (11 – 12%) and spessartine (6 – 7%) define a narrow area overlapping the stability fields of the observed mineral assemblage, which is above the cordierite-out limit and crosses the melt-in curve. This area is equivalent to 665 – 705°C and 4.4 to 5.3 Kbar, which is interpreted as the conditions of residual melanosome reequilibration after some melt loss (fig. 14). Almandine isopleths were not plotted because they are widely-spaced and do not help to constrain the PT conditions. The upper limit of temperature and the pressure range are compatible with the solidus conditions of the Itapema Granite estimated by Rivera et al. (2004) at 700 °C and 4–4.5 Kbar, and within the range of the in situ leucosome crystallization conditions of 700 – 750° and 3.4 – 4.2 Kbar by Martini (2019). Additionally, the estimated conditions for Camboriú Complex migmatitization are also comparable with crystallization conditions of the Porto Belo Complex diatexite.

5. Discussion

5.1 Oblique transpression recorded in the Major Gercino Shear Zone progressive deformation

The Porto Belo Complex presents structural features indicating a transpressive shear with dextral plus thrust-to-NNW components. Such features are best seen in the Ponta das Bombas outcrop, and include close to isoclinal asymmetric folds from dm-scale to microfolds (Figs. 5a to c, 6b and 7d), syn-magmatic shear zones occurring along transposed axial planes (Fig. 7f), porphyroclasts and sigma-shaped enclaves (Fig. 7d) and melt patches (Fig. 6e). Additionally, a lineation half-girdle showing

orientations from close to dip-direction to double-plunging, near strike-parallel attitude also suggests an oblique, triclinic character of the transpressional deformation (Fernandez and Díaz-Azpiroz, 2009). According to Fernandez and Díaz-Azpiroz (2009), the triclinic character may be a consequence of non-vertical shear zone or due to the existence of an angle between extrusion (ε_1) and shearing (γ) directions (named ξ by the authors).

Partial melt features are conditioned by these structures, which apart from asymmetry resemble the same partial melt processes described by Martini et al. (2019a,b) in the Camboriú Complex. The presence of titanite and hornblend as perithetic phases (as argumented by Weinberg and Hasalova, 2014), and locally of magnetite (Sawyer, 2010) suggests water-fluxed melting processes (see the review by Weinberg and Hasalova, 2014). The estimate of crystallization conditions from a diatexitic tonalite is ca. 710°C and 4.5 Kbar.

The age recently reported by De Toni (2019) suggests Tonian (798±4 Ma – zircon, U-Pb, LA-ICP-MS) protolith of the Porto Belo orthogneiss. Crystallization ages of ca. 650 Ma for foliated tonalites in the same unit (Chemale Jr. et al., 2012) may be taken as a good approximation of the partial melt event coeval with the main thrusting towards NNW (as also argumented by Hueck et al., 2018).

Subhorizontal structures attributed to an early deformational phase are also observed within the Quatro Ilhas Granitoids. They present a low-angle magmatic/mylonitic foliation dipping to SE, which is asymmetrically folded indicating a top-to-NNW thrust component (fig. 4a and b). The asymmetrical folding presents more open geometry if compared with the one observed in the Porto Belo Complex rocks. Mineral and stretching lineations show exclusively low-rake attitude, which is together with low-angle foliation characteristic of a tangential regime. These observations are taken together as an evidence of the later character of deformation of the Quatro Ilhas Granitoids following the climax of the thrust-dominated transpressional phase recorded by the Porto Belo Complex. The development of folds with steep axial planes together with the exclusive low-rake lineations points to the transitional character of the transpressional deformation between a thrust-dominated phase to a transcurrent-dominated one in time (e.g. Jones et al., 2004; Fernandez and Díaz-Azpiroz, 2009), during emplacement and cooling of the Quatro Ilhas Granitoids from ca. 624 to 615 Ma (Florisbal et al., 2012a), the gently-dipping foliation of which acted as a lateral-ramp during tangential regime.

Observed mutual crosscuting relationships between the Quatro Ilhas Granitoids and extraction dikes from the Porto Belo Complex migmatites (see fig. 8) also contribute to the understanding of the progressive deformational history recorded by the above-mentioned units.

The dextral strike-slip tectonics along the Major Gercino Shear Zone is well recorded by the Mariscal Granite (614 ± 27 Ma, Florisbal et al., 2012a) and definitely stablished during emplacement of the Estaleiro Granitic Complex (between 611.9 ± 1.7 Ma and 602 ± 4.2 Ma, Peruchi et al., 2016; Chemale Jr. et al., 2012). Bitencourt (1996) argumented that granitic veins which crosscut the Estaleiro Granodiorite sum up to ca. 20% in volume, suggesting that a descompression episode at the end of the Estaleiro Granodiorite crystallization would have opened the space needed for the later intrusions, ascending the magmatic system and making possible the intrusion of the Zimbros Intrusive Suite at shallower levels.

As the later intrusions along the Major Gercino Shear Zone, the rocks of the Zimbros Intrusive Suite present transcurrent magmatic fabric and minor solid-state deformation along discrete, dextral shear bands (Bitencourt, 1996). The late-tectonic Zimbros Granite presents chilled margins, which together with the hypabissal rock association (which includes a dike swarm) indicate the shallow character of the intrusions (Bitencourt, 1996). Bitencourt (1996) pointed out that the oblique character of the Major Gercino Shear Zone dextral transcurrence is increasingly important in its later structures, given by stretching lineations with plunges of 20 to 25° SW recorded in the Zimbros Intrusive Suite (crystallization at *ca.* 587 Ma; Chemale Jr. et al., 2012). This later, oblique component, together with the dextral shear sense, is responsible for an uplift of the NW block (TFB) in relation to the SE one (Florianópolis Batolith, according to Bitencourt, 1996).

5.2 Camboriú Complex symmetrical folding and exhumation path: from partial melting to emplacement and crystallization

The main banding of the Camboriú Complex (S_b) contains early-formed, transposed, intrafolial folds of uncertain origin. The banding, which rarely presents any linear structure or consistent (apparent) asymmetry, was originally subhorizontal or gently inclined, and is now symmetrically folded by generally NW-SE oriented compression, resulting in upright folds with NE – SW striking, double-plunging axes and subvertical axial planes. The axial planes locally evolve into a discrete transposition cleavage marked by syn-magmatic shear bands, which served as migration paths for partial

melt. The syn-magmatic shear bands with opposite shear sense along limbs of outcrop-scale folds suggest apparent extrusion of Camboriú Complex hinge zones (fig. 12f – Martini et al. 2019a,b) and are similar to situations found in various migmatitic terranes (e.g. Sawyer, 2008; Weinberg et al., 2013). These features, together with a general absence of lineation, are interpreted as an indication of important pure shear component during the progressive deformation of the Camboriú Complex (Martini et al., 2019b). The structural control of the melt migration along syn-magmatic shear zones and dikes related to symmetrical folding points to interplay of melting and deformational processes which assisted the exhumation of the complex.

The exhumation path of the Camboriú Complex can be traced from the integrated PT estimates for its various lithologies, from 4.5 – 5.5 Kbar to 3.5 Kbar. This is illustrated in figure 15, where the PT estimates from the other structural domains are also shown for comparison. Additionally, CC metapelite presents a kyanite relict, which is considered as a marker for PT conditions pre-dating the modeled equilibrium of the metapelite stable assemblage. As previously pointed out, these conditions are not precisely determined, but may be either of higher pressure or lower temperature, or a combination of both, as shown in the figure 15 as a hatched area.

Crystallization ages of 637 ± 21 Ma and 634 ± 24 Ma were presented by Basei et al. (2013) for the Itapema Granite and for a neosome of the Camboriú Complex, respectively. Despite the large errors, CC ages are in agreement with field relationships and ages of the intrusives Rio Pequeno Granite (622±15 Ma; 626±7 Ma) and Serra dos Macacos Granite (611±9 Ma –U-Pb zircon LA-ICP-MS, according to Florisbal, 2012b), both emplaced along the contacts of the Camboriú and Brusque complexes. The Camboriú Complex exhumation, tracked by PT data, is considered to reflect tectonic juxtaposition of it side-by-side to the Brusque Complex suprastructure.

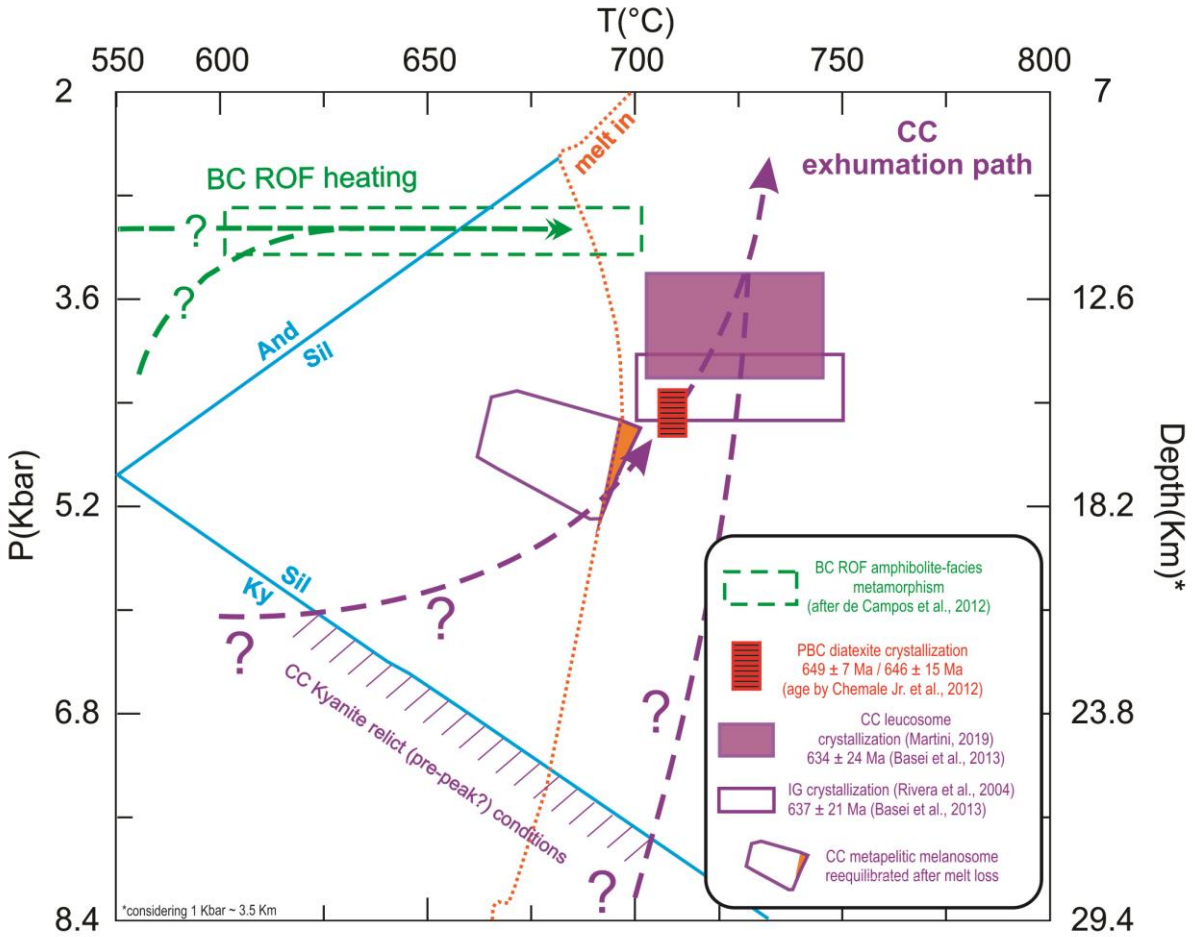

Fig. 15 – PT diagram summarizing the estimatives for the three structural domains, with exhumation and heating paths correlated with previous published ages. Kyanite-sillimanite-andalusite and melt-in curves are from figure 14.

5.3 Brusque Complex as the Foreland Fold and Thrust Belt: thrust followed by extension?

In the Brusque Complex, the gently dipping foliation towards NNW at the coastal section (E-E') is interpreted as possibly tilted, and its original attitude is interpreted as sub-horizontal. Sub-horizontal foliation (S_x) contains a near-dip mineral/stretching lineation (L_x) towards NNW (NNW-SSE if restored). It is noteworthy that S_x is systematically affected by asymmetric to recumbent folds ranging from micro to cross-section scale, with predominantly NE-SW subhorizontal axes (fig.9c and d), suggestive of an important thrust event verging NNW. NW vergence of a gently-dipping, early deformation phase is consistently argumented by numerous authors in different portions of Brusque Complex (e.g. Silva, 1991; Philipp et al., 2004; Basei et al., 2011; Fischer et al., 2019).

Discrete, antithetic shear bands (S_{x+1}) developed along certain fold long limbs along the coastal section (fig. 10). S_{x+1} shear bands indicate extensional reactivation along flanking structures, with relative collapse of the SE block in relation to the NW one (fig. 10b and d). This interpretation is in agreement with the oblique dextral plus normal shear observed at the contact with Camboriú Complex in the Serra da Miséria area, as well as with the later increments of the low-obliquity dextral strike-slip of the Major Gercino Shear Zone. An extensional reactivation of thrust nappe stacks is well recognized e.g. in the Caledonian nappes of Norway, where it is considered as intimately related to exhumation process during the post-collisional period (Fossen and Rykkelid, 1992; Andersen, 1998).

An alternative interpretation of such structures may consider the folding as a direct result of extension, with asymmetry developed during back-rotation between two high-strain zones of normal movement (e.g. fig 10b and d), as argumented by Harris et al. (2002). The consistency of asymmetry presented by all observed folds along the profile (e.g. fig. 09), in multiple scales, mostly not limited by antithetic-looking shear bands do not favour this hypothesis. Additionally, the observed fold propagation pattern (Fig. 10c) agrees with top-to-NNW vergence. However, it does not exclude possible effects of back-rotation (e.g. Harris et al., 2002), which potentially reinforced the apparent vergence of top-to-NW asymmetric folds.

Local effects of contact metamorphism along the same cross-section are observed (fig. 10e) and also reported in the literature nearby the contacts with the Camboriú Complex (Philipp et al., 2004) and also with later intrusions (Philipp et al., 2004; Peternell et al., 2010; Fischer et al., 2019). Actually, it is noteworthy that amphibolite-facies conditions of Brusque Complex are restricted to the Itapema area, where it occurs exclusively in contact with the Camboriú Complex (Philipp et al., 2004; de Campos et al., 2012), despite the regional greenchist facies observed elsewhere in the eastern part of the Brusque Complex (Silva, 1991; Philipp et al., 2004; Basei et al., 2011; de Campos et al., 2012; Asvald, 2018; Fischer et al., 2019).

Altogether, the evidence suggests that the regional greenschist facies, top-to-NW thrust event which affected the Brusque Complex also affected the studied coastal section (as argued by de Campos et al., 2012) but that the rocks locally reached amphibolite facies conditions by progressive exhumation of the underlying Camboriú Complex migmatites due to regional transpression. It progressively led to Brusque Complex unroofing, with discrete (cm- to m-spaced) development of antithetic shear bands (fig. 10d) simultaneous to static neocrystallization of low-pressure

metamorphic minerals along relatively undeformed bands (fig. 10e) observed at the coastal section. On the other hand, structures and contact relationship between both complexes observed inland (fig. 11) suggest that Brusque Complex amphibolite facies fabric locally developed coaxially in respect to the mylonitic fabric of Camboriú Complex, with increasing amount of finite strain towards the contact. Tectonic juxtaposition of the complexes is interpreted as due to dextral-normal shear along their boundary, which acted as a detatchment zone.

The depth of such event should be equal or shallower than CC migmatite emplacement at 4 – 5 Kbar (see previous section). The depth is tentatively estimated by calculation proposed by Molina et al. (2015) with hornblend – plagioclase microprobe data of de Campos et al. (2012), which points to pressures of 3 to 3.2 Kbar (see electronic appendix). Considering the thermal effect of the Camboriú Complex migmatites over the Brusque Complex and the intrusive relationship observed in the contact outcrop (fig. 11a and c), the juxtaposition of them may have taken place approximately during the crystallization age of the neosomes and of the Itapema Granite (ca. 635 Ma – Basei et al., 2013), and must be older than Rio Pequeno Granite (ca. 625 Ma – Florisbal et al., 2012b), since the later presents thermal effects over both complexes (Peternell et al., 2010).

5.4 Kinematic correlation and contrasting PT paths

5.4.1 Oblique collision

Each of the three studied domains record the thrusting event at a different crustal level and corresponding PT conditions, as summarized in the figure 15 and schematically depicted in figure 16a. Based on the available geochronological data, this event is considered to have occurred around 650 – 645 Ma (fig. 16a), as recorded by metamorphism and associated partial melting in the Porto Belo Complex (Chemale Jr. et al., 2012). However, a slightly diachronous evolution during strain propagation through the different domains and structural levels cannot be discarded.

A characteristic triclinic transpressional pattern (as defined by Jones et al., 2004; Fernandez and Diaz-Azpiroz, 2009; Fernandez et al., 2013; and references therein) is recorded in the structures of the Porto Belo Complex, with a combination of thrust-to-NNW and dextral kinematics. Hornblend – plagioclase geothermobarometry of a tonalitic diatexite point to crystallization conditions of 705 – 710°C and 4.5 Kbar.

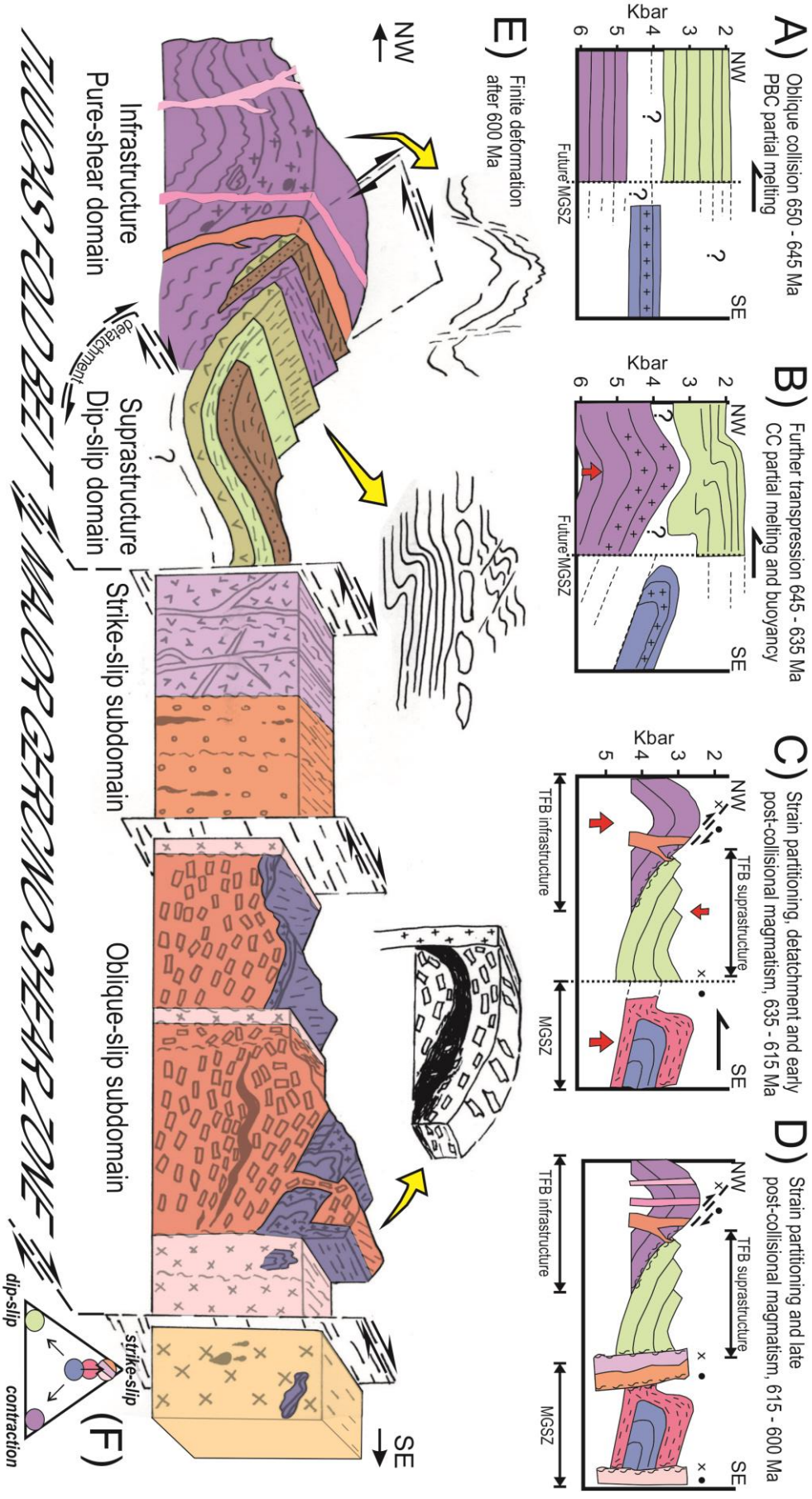
A) Oblique collision 650 - 645 Ma
PBC partial melting
Kbar
NW
SE
Future MGSZ
B) Further transpression 645 - 635 Ma
CC partial melting and buoyancy
C) Strain partitioning, detatchment and early
post-collisional magmatism, 635 - 615 Ma
TFB suprastructure
TFB infrastructure
MGSZ
D) Strain partitioning and late
post-collisional magmatism, 615 - 600 Ma
E) Finite deformation
after 600 Ma
Infrastructure
Pure-shear domain
detachment
Suprastructure
Dip-slip domain
Strike-slip subdomain
Oblique-slip subdomain
TWIN-STACKED BELT OF MAJOR GERCINO SHEAR ZONE
(F)
dip-slip
strike-slip
contraction

Fig. 16 (previous page) – Tectonic evolution cartoon (not in scale). (a) Oblique collision early configuration (650 – 645 Ma). (b) Further transpression and infrastructure partial melting (645 – 635 Ma). (c) Strain partitioning and early post-collisional magmatism (636 – 615 Ma), with nucleation of Major Gercino Shear Zone. Strain partitioning leds exhumation of the Camboriú Complex and consequently extension of Brusque Complex through the development of a dextral-normal detatchment, prior to Rio Pequeno Granite emplacement. (d) Strain partitioning and late post-collisional magmatism (615 – 600 Ma). (e) Finite deformation, after 600 Ma, which illustrates the actual configuration (based on figure 03). Zoom-in insets (yellow arrows) show examples of characteristic subhorizontal S_1 preserved in the three structural domains. Horizontal and vertical scale are loosely mantained. (f) Deformation triangle (proposed by Jones et al., 2004) illustrating the kinematic partitioning of the area. Collors in this figure are the same as in figure 2 and 3.

The Camboriú Complex rocks present a subhorizontal banding almost without any lineation. Even with lineation lacking, the highest degree of asymmetry of individual CC structures is still observed along 340° - 160° to 320° - 140° subvertical sections. Both top-to-NW and top-to-SE apparent shear senses are observed in sigma-looking gneissic enclaves along the Itapema Granite main banding. The uncertain vergence suggests flattening, and also may be attributed to the “chaotic” magmatic flow absorbing deformation. On the other hand, the presence of partially transposed, intrafolial fold relicts observed along the migmatitic gneisses the Camboriú Complex main banding suggest shortening of a pre-existing foliation. Peak conditions are estimated at 700 – 750°C and 4.5 – 5.5 Kbar, although a kyanite relict points to an even deeper origin for the Camboriú Complex. The age of CC main tectono-thermal event is recorded at ca. 635 Ma (Basei et al., 2013 – see fig. 16b).

The ages “younging” from 650-645 Ma melting in the Porto Belo Complex to ca. 635 Ma in the Camboriú Complex suggest strain propagation (fig. 16b), starting from hinterland (SE) towards the foreland (NW), which is in agreement with top-to-NNW vergence of the oblique collision.

The Itapema coastal outcrops of the Brusque Complex also present a top-to-NNW thrust, mainly recorded in asymmetrical folds (Fig. 10), similarly to what is recognized by many authors in other parts of the complex (Silva, 1991; Philipp et al., 2004; de Campos et al., 2012; Fischer et al., 2019). The main thrust and contractional movements in the BC are kinematically coherent with other studied units and interpreted as related in time and cause to the low-angle fabrics observed in the other structural domains. Additionally, the ca. 645 Ma oblique collision hereby described for the northern Dom Feliciano Belt is correlated with similar tectonic evolution recognized by many authors in the central and southern Dom Feliciano Belt (e.g. Lenz et al., 2011, Chemale Jr. et al., 2011, Battisti et al., 2018, among others).

5.4.2 Post-collisional strain partitioning

Strain partitioning during progressive deformation is interpreted as responsible for tectonic juxtaposition of different crustal levels (fig. 16c and d) and the contrasting finite deformation which is characteristic of the different structural domains (fig. 16e). It is noteworthy that strike-slip structures prevail in the Major Gercino Shear Zone domain, while they are discrete along the whole Tijucas Fold Belt, which is considered a low-strain zone relative to the Major Gercino Shear Zone strike-slip tectonics (e.g. Florisbal et al., 2012c; Martini et al., 2015). A deformation triangle (fig. 16f; Jones et al., 2004) qualitatively illustrates the kinematic partitioning of the overall oblique transpression, of which the Porto Belo Complex structures are considered the best representant, into components which were localized in each of the distinct structural domains.

At the Major Gercino Shear Zone, oblique transpression progressively evolved into strike-slip by rotation of foliation towards subvertical attitudes due to asymmetric folding and progressive development of the transposition foliation. The transitional phase is marked by the Quatro Ilhas Granitoids (crystallization at 625 – 615 Ma, according to Florisbal et al., 2012a) structures, which present both open folded, gently-dipping and subvertical foliation, with exclusively low-rake, magmatic and stretching lineations (fig. 16c). The Porto Belo Complex and Quatro Ilhas Granitoids are considered part of an inner oblique-slip subdomain of MGSZ (see fig. 16). Strike-slip is recorded by magmatic and high-T solid-state fabrics of sucessive intrusions, which are younger than 615 Ma (fig. 16d; Bitencourt, 1996; Chemale Jr. et al., 2012; Florisbal et al., 2012a).

In the Tijucas Fold Belt, strain partitioning led to the decoupling between the infrastructure and suprastructure. Exhumation of the CC migmatite was driven by partitioning of the contraction component of overall transpression and the buoyancy of the magma-rich system at around 635 Ma. At the same time, the Rio do Oliveira Formation amphibolites (southern Brusque Complex) present: i) a local high thermal gradient recorded as amphibolite-facies metamorphism in contrast to the BC regional greenschist-facies; ii) discrete structures, with an antithetic, extensional character, reworking the thrust-related main foliation (fig. 10b and d); iii) which in turns separates domains locally overprinted by static metamorphism (fig. 10e); and iv) presents a local strain gradient increasing towards the contact with the CC mylonites, where both complexes present a concordant deformation observed at its contact,

with a low-obliquity, dextral plus normal (top-to-WSW) movement. (fig. 11). The local amphibolite facies in relation to the regional greenschist facies metamorphism of the Brusque Complex (Philipp et al., 2004; de Campos et al., 2012; among others) is attributed to the effects of the elevated geothermal gradient during exhumation of the magma-rich, migmatitic Camboriú Complex (fig. 16c).

The timing of this event in the BC is constrained indirectly. The NW-verging, thrust-related fabric in the Brusque Complex must be older than 635 Ma, as this is the age of the Itapema Granite (Basei et a., 2013), and it is likely that the fabric originated at ca. 650 – 645 Ma, coeval with the PBC main thrust. The extension is interpreted to have affected the Brusque Complex concomitantly with the Camboriú Complex exhumation, which should be bracketed by the CC neosome and Itapema Granite crystallization, and the Rio Pequeno Granite emplacement, i.e. between ca. 635 – 625 Ma. Tectonic inversion is inferred to have occurred at ca. 635 Ma. The extensional ductile structures of the southern coastal Brusque Complex are considered to represent the ductile thinning of the suprastructure, related to the Camboriú Complex doming during the post-collisional period (e.g. Vanderhaeghe et al., 1999 – fig. 16c).

The exhumation of the infrastructure took place while extension affected the suprastructure, culminating by the juxtaposition of Camboriú Complex and the Brusque Complex (fig. 16a-c) as it is observed today. The first is the core complex in the inner portion of a major antiformal structure, while the later occur at its limbs (fig. 16d). Similar situation of migmatitic core exhumation due to orogen collapse during regional convergence is reported by Vanderhaeghe et al. (1999 and references therein) for French Variscides and the Canadian Cordillera and supported by rheological modeling of the lithosphere (Brun et al., 1994).

The detatchment of middle and upper crust in the studied case is recorded at a narrow, discrete, high-strain shear zone, where L-tectonites locally developped over leucogranites of the Camboriú Complex along its southern boundary (Miséria Mylonites from Hartmann et al., 2003) , whereas amphibolites of the Brusque Complex were coaxially deformed (see fig. 11). Constrictional strain occurred localized along the rheological interface, which attributed to a combination of the regional NW-SE shortening vector and the vertical shortening due to ductile thinning during exhumation. Constrictional fabric is common in rocks exhumed during oblique transtension (Krabbendam and Dewey, 1998), and in our case it represents a local feature in the regional transpressive scenario. Along the contact, the leucogranites

are locally intrusive in the Brusque Complex amphibolites (see Fig. 11a and c), and both units presents parallel mylonitic structures (Fig. 11b). The contact kinematics presents dextral plus normal components, giving a top-to-WSW general vergence (Fig.11f to h), although lineations are spread due to late open folds. This contact is later reworked by faulting, suggesting that the whole system reached the brittle-ductile transition during exhumation (Fig. 11i and j).

The Rio Pequeno Granite (ca. 625 Ma – Florisbal et al., 2012b) crosscuts the above-mentioned structure, being a time marker for the low-strain phase of the Tijucas Fold Belt, when most of the deformation was foccused along the Major Gercino Shear Zone. Later intrusions (after 615 Ma) are attributed to partial melting of sources similar to CC and are also mostly hosted inside it (Florisbal et al., 2012b,c and Martini et al., 2015).

5.5 Tectonic implications for the Dom Feliciano Belt evolution

The understanding of Major Gercino Shear Zone nature is central in the debate regarding the evolution of the Dom Feliciano Belt. The presented model challenges some hypotheses from the literature, concerning the tectonic meaning of the Major Gercino Shear Zone as a suture and the allochtonous or exotic character of the Florianópolis Batolith in relation to the Tijucas Fold Belt (Basei et al., 2005; 2008; Hueck et al., 2018). This may be exemplified by evidence of similar metamorphic and partial melt conditions of both Camboriú and Porto Belo complexes at upper amphibolite facies (roughly 4 – 5 Kbar and 700 – 750°C). It means that at 650 – 635 Ma (Fig. 16a and b), both complexes were already juxtaposed. This time-span was previously considered as an “early convergence” period which preceded a supposed oblique collision at 615 – 585 Ma (e.g. Hueck et al., 2018). Our, as well as published data do not support such late crustal thickenning, since this period corresponds to the age of the post-collisional granites, which are syntectonic with respect to the dextral strike-slip tectonics sensu stricto (Chemale Jr. et al., 2012; Florisbal et al., 2012; Peruchi, 2016), later relatively to the ductile thinning of the Tijucas Fold Belt suprastructure in the study area.

Although the presence of a former suture zone (pre-645 Ma) cannot be excluded yet, no direct evidence of oceanic crust consumption (i.e. ophiolitic association) is recognized in the Santa Catarina Shield area. Additionally, based mostly on regional aerogeophysical data, Bruno et al. (2018) considers that the boundary between unrelated basement domains is the Itajaí-Perimbó Shear Zone, instead of the Major

Gercino Shear Zone, which is understood as an intracontinental shear zone, confirming the hypothesis of Florisbal et al. (2012c).

6. Conclusions

Evaluation of geology, structures, avaliable PT conditions and ages were integrated along a geological cross-section in the northern Dom Feliciano Belt, crossing from the Florianópolis Batolith (hinterland) boundary towards the Tijucas Fold Belt (foreland). The results can be summarized as follows:

i) The structural pattern of the whole area presents a NE-to-ENE trend, with S_1 preserved as a fabric gently dipping mostly towards SE, or refolded into open to closed folds. This pattern was recognized in all structural domains, and together with variably plunging lineation is interpreted as a record of a NNW-verging oblique collision which affected the whole area at, or before, aproximately 650 – 635 Ma.

ii) The oblique collision is recorded as a transpressional progressive deformation, which led to strain partitioning into three structural domains that absorbed different kinematic components, in agreement with theoretical and analogue models. Both lateral co-existence and temporal progression of tectonic regimes, usually from subhorizontal to subvertical foliations, and from high- to low-obliquity lineations, are characteristic of triclinic, transpressional deformation and exemplified by the geology of the studied cross-section.

iii) A progression from oblique transpression with inclined extrusion (Porto Belo Complex, 650 Ma – 645, at ca. 707 °C/3.7 – 4.8 Kbar), through tangential regime (Quatro Ilhas Granitoids, 625 – 615 Ma) towards strike-slip tectonics (Mariscal Granite and younger intrusions, after ca. 615 Ma), is recorded along the Major Gercino Shear Zone.

iv) The Camboriú Complex absorbed the contractional component as a pure shear-dominated domain, as documented by ambiguous asymmetric objects, lack of lineation, upright, double-plunging, symmetric folding and a conjugated, axial planar shear cleavage. The complex records regional doming and exhumation from at least 5 Kbar (possibly deeper than 6 Kbar) up to 3.4 Kbar, assisted by the positive buoyancy of high proportions of melt (at 635 Ma or shortly after).

v) Slightly delayed ages point to a possible diachronic evolution with partial melting and oblique collisional deformation starting some million years earlier in the hinterland (MGSZ) and propagating towards the foreland infrastructure.

vi) Meanwhile, pervasive greenschist-facies NNW-verging thrust of the Brusque Complex (Rio do Oliveira Formation) is followed by discrete amphibolite-facies fabric, which affected the rocks around 635 Ma during the CC upwelling. The thermal effect of the exhuming CC over the BC is documented as localized transposition zones close to the contact with the CC migmatites and along static, contact metamorphic domains separated by opposite sense reactivations of their gently-dipping early fabric. Both higher geothermal gradient and local tectonic inversion are interpreted as a result of the Camboriú Complex doming related to the transpressional strain partitioning.

The Major Gercino Shear Zone is understood as an intracontinental shear zone, which focused intrusion of post-collisional magmas and absorbed the dextral strike-slip component of the overall oblique transpression. This oblique collision affected both infra- and suprastructure of Tijucas Fold Belt and Florianópolis Batolith which were contiguous blocks at least since 650 – 645 Ma.

7. Acknowledgements

GB De Toni thanks the Conselho Nacional de Pesquisa (CNPq) and the Coordenação de Aperfeiçoamento do Pessoal do Ensino Superior (CAPES) for the PhD scholarship. He also appreciates financial support of his stay at the UiT - The Arctic University of Norway in Tromsø, organized within the framework of a CAPES (Brazil) – SIU (Norway) cooperation program. J Konopásek appreciates financial support of the Czech Science Foundation (grant no. 18-24281S). Kai Neufeld is acknowledged for his help with SEM-EBSD at UiT. We are also grateful to Susan Drago for her kind help during microprobe analysis at UFRGS.

References

Andersen, T.B., 1998. Extensional tectonics in the Caledonides of southern Norway, an overview. Tectonophysics, 285, 333-351.

Arena, K.R., Hartmann, L.A., Lana, C., 2016. Evolution of neoproterozoic ophiolites from the southern Brasiliano Orogen revealed by zircon U-Pb-Hf isotopes and geochemistry. Precambrian Research, 285, 299–314.

Asvald, C. Metamorphic evolution in external zones of the Dom Feliciano-Kaoko orogenic system. Unpublished Master Thesis. The Arctic University of Norway. 82p. Avaliable at: https://munin.uit.no/handle/10037/12816

Basei, M.A.S., Frimmel, H.E., Nutman, A.P., Preciozzi, F., Jacob, J., 2005. The connection between the Neoproterozoic Dom Feliciano (Brazil/Uruguay) and Gariep (Namibia/South Africa) orogenic belts. Precambrian Research, 139, 139–221.

Basei, M.A.S., Frimmel, H.E., Nutman, A.P., Preciozzi, F., 2008. West Gondwana amalgamation based on detrital zircon ages from Neoproterozoic Ribeira and Dom Feliciano belts of South America and comparison with coeval sequences from SW Africa. In: Pankhurst, R.J., Trouw, R.A.J., de Brito Neves, B.B., de Wit, M.J. (eds) West Gondwana: Pre-Cenozoic Correlations Across the South Atlantic Region, London. Geological Society London, Special Publication 294, pp 239–256.

Basei, M.A.S., Campos Neto, M.C., Castro, N.A., Nutman, A.P., Wemmer, K., Yamamoto, M.T., Hueck, M., Osako, L., Siga, O., Passarelli, C.R., 2011. Tectonic evolution of the Brusque group, Dom Feliciano belt, Santa Catarina, Southern Brazil. Journal of South American Earth Sciences, 32(4), 324–350.

Basei, M.A.S., Campos Neto, M.C., Lopes, A.P., Nutman, A.P., Liu, D., Sato, K., 2013. Polycyclic evolution of Camboriú Complex migmatites, Santa Catarina, Southern Brazil: integrated Hf isotopic and U-Pb age zircon evidence of episodic reworking of a Mesoarchean juvenile crust. Brazilian Journal Geology, 43, 427–443.

Battisti, M.A., Bitencourt, M.F., De Toni, G.B., Nardi, L.V.S, Konopásek, J., 2018. Metavolcanic rocks and orthogneisses from Porongos and Várzea do Capivarita complexes: A case for identification of tectonic interleaving at different crustal levels from structural and geochemical data in southernmost Brazil. Journal of South American Earth Sciences, 88, 253-274.

Bettucci, L.S., Burgueño, A.M., 1993. Análisis sedimentológico y faciológico de la Formación Rocha (ex Grupo Rocha). Revista Brasileira de Geociências, 23, 323-329.

Bitencourt, M.F., Nardi, L.V.S. 1993. Late- to Post-collisional Brasiliano Magmatism in Southernmost Brazil. Anais da Academia Brasileira de Ciências, 65, 3-16.

Bitencourt, M.F., Nardi, L.V.S., 2000. Tectonic setting and sources of magmatism related to the Southern Brazilian Shear Belt. Revista Brasileira de Geociências 30, 186–189.

Bitencourt, M.F., Nardi, L.V.S., 2004. The role of xenoliths and flow segregation in the genesis and evolution of the Paleoproterozoic Itapema Granite: a crustally-derived magma of shoshonitic affinity from Southern Brazil. Lithos 73, 01–19.

Bitencourt, M.F., 1996. Granitóides sintectônicos da região de Porto Belo, SC: uma aboradagem petrológica e estrutural do magmatismo em zonas de cisalhamento.

Tese de Doutorado, Instituto de Geociências, Universidade Federal do Rio Grande do Sul, 310 pp.

Blundy, J. D. & Holland, T.J.B. 1990. Calcic amphibole equilibria and a new amphiboleplagioclase geothermometer. Contrib. Mineral. Petrol., 104, 208-224.

Bruno, H., Almeida, J., Heilbron, M., Salomão, M., Cury, L., 2018. Architecture of major precambrian tectonic boundaries in the northern part of the Dom Feliciano Orogen, southern Brazil: Implications for the West Gondwana amalgamation. Journal of South American Earth Sciences, 86, 301-317.

Burchfiel, B.C., Z. Chen, Hodges, K.V., Y. Liu, Royden, L.H., C. Deng, J. Xu, 1992. The South Tibetan Detatchment System, Himalayan Orogen: Extension Contemporaneous with and Parallel to Shortening in a Collisional Mountain Belt. Geological Society of America Special Paper, 269.

de Campos RS, Philipp RP, Massonne HJ, Chemale F Jr, Theye T, 2012. Petrology and isotope geology of mafic to ultramafic metavolcanic rocks of the Brusque Metamorphic Complex, southern Brazil. International Geology Reviews, 54(6), 686–713

Chemale Jr., F., Philipp, R.P., Dussin, I.A., Formoso, M.L.L., Kawashita, K., Berttotti, A.L., 2011. Lu-Hf and U-Pb age determination of Capivarita anorthosite in the Dom Feliciano Belt, Brazil. Precambrian Res. 186, 117-126

Chemale Jr., F., Mallmann, G., Bitencourt, M.F., Kawashita, K., 2012. Time constraints on magmatism along the Major Gercino Shear Zone, southern Brazil: implications for West Gondwana reconstruction. Gondwana Research 22 (1), 184–199.

Connolly, J.A.D., 2005. Computation of phase equilibria by linear programming: a tool for geodynamic modeling and its application to subduction zone decarbonation. Earth and Planetary Science Letters, 236(1–2), 524–541

Czeck, D.M., Hudleston, P.J., 2003. Testing models for obliquely plunging lineations in transpression: a natural example and theoretical discussion. Journal of Structural Geology 25, 959-982.

Dewey, J.F., Holdsworth, R.E., Strachan, R.A., 1998. Transpression and transtension zones. In: Holdsworth, R.E., Strachan, R.A., Dewey, J.F. (Eds.), Continental Transpressional and Transtensional Tectonics. Special Publication of the Geological Society, London 135, pp. 1–14.

De Toni, 2019. Correlação geológico-estrutural e modelo integrado de evolução para o Cinturão Dom Feliciano sob transpressão inclinada no Neoproterozoico do sul do Brasil. Unpublished PhD thesis. Universidade Federal do Rio Grande do Sul.

Egydio-Silva, M., Vauchez, A., Raposo, M.I.B., Bascouc, J., Uhleind, A., 2005. Deformation regime variations in an arcuate transpressional orogeny (Ribeira belt, SE Brazil) imaged by anisotropy of magnetic susceptibility in granulites. Journal of Structural Geology, 27, 1750-1764.

Fernandes, L.A.D., Tommasi, A., Porcher, C.C., 1992. Deformation patterns in the southern Brazilian branch of the Dom Feliciano Belt: a reappraisal. Journal of South American Earth Sciences, 5, 77-96.

Fernandes, L.A.D., Menegat, R., Costa, A.F.U., Koester, E., Kramer, G., Tommasi, A., Porcher, C.C., Ramgrab, G.E., Camozzato, E., 1995a. Evolução tectônica do Cinturão Dom Feliciano no Escudo Sul-rio-grandense: Parte I – uma contribuição a partir do registro geológico. Revista Brasileira Geociências 25, 351-374.

Fernandes, L.A.D., Menegat, R., Costa, A.F.U., Koester, E., Kramer, G., Tommasi, A., Porcher, C.C., Ramgrab, G.E., Camozzato, E., 1995b. Evolução tectônica do Cinturão Dom Feliciano no Escudo Sul-rio-grandense: Parte II – uma contribuição a partir das assinaturas geofísicas. Revista Brasileira Geociências 25, 375-384.

Fernández, C., Díaz-Azpiroz, M., 2009. Triclinic transpression zones with inclined extrusion. Journal of Structural Geology 31, 1255-1269.

Fischer, G., Fassbinder, E., Barros, C.E.M., Fossen, H., 2019. The evolution of quartz veins during the tectonometamorphic development of the Brusque Metamorphic Complex, Brazil. Journal of South American Earth Sciences 93, 174–182.

Florisbal, L.M., Bitencourt, M.F., Janasi, V.A., Nardi, L.V.S., Heaman, L.M., 2012a. Petrogenesis of syntectonic granites emplaced at the transition from thrusting to transcurrent tectonics in post-collisional setting: whole-rock and Sr–Nd–Pb isotope geochemistry in the Neoproterozoic Quatro Ilhas and Mariscal granites, southern Brazil. Lithos 153, 53–71.

Florisbal, L.M., Janasi, V.A., Bitencourt, M.F., Heaman, L.M., 2012b. Space–time relation of post-collisional granitic magmatism in Santa Catarina, southern Brazil: U–Pb LA-MC-ICP-MS zircon geochronology of coeval mafic-felsic magmatism related to the Major Gercino Shear Zone. Precambrian Research, 216, 132–151.

Florisbal, L.M., Janasi, V.A., Bitencourt, M.F., Nardi, L.V.S., Heaman, L.M., 2012c. Contrasted crustal sources as defined by whole-rock and Sr–Nd–Pb isotope

geochemistry of Neoproterozoic early post-collisional granitic magmatism within the Southern Brazilian Shear Belt, Camboriú, Brazil. Journal of South American Earth Sciences, 39, 24–43.

Fossen, H. & Rykkelid, E. 1992. Post-collisional extension of the Caledonide orogen in Scandinavia: structural expressions and tectonic significance. Geology, 20, 737-740.

Fossen, H., Tikoff, B., 1993. The deformation matrix for simultaneous simple shearing, pure shearing and volume change, and its application to transpression–transtension tectonics. Journal of Structural Geology, 15, 413–422.

Gregory, T.R., M.F., Bitencourt, Nardi, L. V., Florisbal, L. M, Chemale, F. Jr. 2015. Geochronological data from TTG-type rock associations of the Arroio dos Ratos Complex and implications for crustal evolution of southernmost Brazil in Paleoproterozoic times. Journal of South American Earth Science. 57, 49–60.

Guadagnin, F., Chemale Jr., F., Dussin, I.A., Jelinek, A.R., Santos, M.N., Borba, M.L., Justino, D., Bertotti, A.L., Alessandretti, L., 2010. Depositional age and provenance of the Itajaí Basin, Santa Catarina State, Brazil: implications for SW Gondwana correlation. Precambrian Research, 180, 156–182.

Harland, W.B., 1971. Tectonic transpression in Caledonian Spitzbergen. Geological Magazine 108, 27–42.

Harris, L.B., Koyi, H.A., Fossen, H., 2002. Mechanisms for folding of high-grade rocks in extensional tectonic settings. Earth-Science Reviews, 59, 163-210.

Hartmann, L. A., Santos, J. O. S., Mcnaughton, N. J., Vasconcellos, M.A.Z., Silva, L.C., 2000. Ion microprobe (SHRIMP) dates complex granulite from Santa Catarina, southern Brazil. Anais da Academia Brasileira de Ciências, Rio de Janeiro, 72(4), 560-572,.

Hartmann, L.A., Bitencourt, M.F., Santos, J.O., McNaughton, N.J., Rivera, C.B., Betiollo, L., 2003. Prolonged Paleoproterozoic magmatic participation in the Neoproterozoic Dom Feliciano belt, Santa Catarina, Brazil, based on zircon U–Pb SHRIMP geochronology. Journal of South American Earth Science 16, 477–492.

Hasui, Y., Carneiro, C.D.R. And Coimbra, A.W., 1975. The Ribeira folded belt. Revista Brasileira de Geociências, 5, 257–266.

Höfig, D.F., Marques, J.C., Basei, M.A.S., Giusti, R.O., Kohlrausch, C., Frantz, J.C., 2017. Detrital zircon geochronology (U-Pb LA-ICP-MS) of syn-orogenic basins in SW Gondwana: new insights into the cryogenian-ediacaran of Porongos complex, Dom Feliciano belt, southern Brazil. Precambrian Research, 306, 189-208.

Holdsworth, R.E., Tavarnelli, E., Clegg, P., Pinheiro, R.V.L., Jones, R.R., McCaffrey, K.J.W., 2002. Domainal deformation patterns and strain partitioning during transpression: an example from the Southern Uplands terrane, Scotland. Journal of the Geological Society of London 159, 401–415.

Holland, T.J.B., and Blundy, J.D., 1994, Non-ideal interactions in calcic amphiboles and their bearing on amphibole-plagioclase thermometry: Contributions to Mineralogy and Petrology, v. 116, p. 433–447.

Holland, T.J.B., Powell, R., 1998. An internally consistent thermodynamic data set for phases of petrological interest. Journal of Metamorphic Geology, 16, 309–343.

Hueck, M., Basei, M.A.S., de Castro, N.A., 2016. Origin and evolution of the granitic intrusions in the Brusque Group of the Dom Feliciano Belt, south Brazil: Petrostructural analysis and whole-rock/isotope geochemistry. Journal of South American Earth Sciences, 69, 131–151.

Hueck, M., Basei, M.A.S., Wemmer, K., Oriolo, S., Heidelbach, F., Siegesmund, S., 2018. Evolution of the Major Gercino Shear Zone in the Dom Feliciano Belt, South Brazil, and implications for the assembly of southwestern Gondwana. International Journal of Earth Sciences, 108(2), 403-425.

Jones, R.R., Holdsworth, R.E., Clegg, P., McCaffrey, K., Tavarnelli, E., 2004. Inclined transpression. Journal of Structural Geology 26, 1531–1548.

Jost, H., Bitencourt, M.F., 1980. Estratigrafia e tectônica de uma fração da Faixa de Dobramentos Tijucas no Rio Grande do Sul. Acta Geológica Leopoldensia, 4(7), 27-60.

Jost, H., Hartmann, L.A., 1984. Província Mantiqueira – Setor Meridional. in: Pré-Cambriano do Brasil. Coord.: Almeida, F.F.M., Hasui, Y. p. 345-368. Editora Edgard Blucher, São Paulo.

Koester, E, Porcher, C.C., Pimentel, M.M., Fernandes, L.A.D., Vignol-Lelarge, M.L., Oliveira, L.D., Ramos, R.C., 2016. Further evidence of 777 Ma subduction-related continental arc magmatism in Eastern Dom Feliciano Belt, southern Brazil: The Chácara das Pedras Orthogneiss. Journal of South American Earth Sciences, 68, 155-166.

Konopásek, J., Sláma, J., Košler, J., 2016. Linking the basement geology along the Africa–South America coasts in the South Atlantic. Precambr Res 280, 221–230.

Konopásek, J., Janoušek, V., Oyhantçabal, P., Sláma J ., Ulrich, S., 2018. Did the circum-Rodinia subduction trigger the Neoproterozoic rifting along the Congo–

Kalahari Craton margin? International Journal of Earth Sciences. https://doi.org/10.1007/s00531-017-1576-4

Krabbendam, M., Dewey, J.F., 1998. Exhumation of UHP rocks by transtension in the Western Gneiss Region, Scandinavian Caledonides. Geological Society, London, Special Publications, 135:159-181

Leite, J.A.D., Hartman, L.A., Mcnaughton, N.J., Chemale Jr., F., 1998. SHRIMP U/Pb Zircon Geochronology of Neoproterozoic Juvenile and Crustal-Reworked Terranes in Southernmost Brazil, International Geology Review, 40(8), 688-705.

Lenz C., Fernandes, L.A.D., McNaughton, N.J., Porcher, C.C., Masquelin, H., 2011. U–Pb SHRIMP ages for the Cerro Bori orthogneisses, Dom Feliciano Belt in Uruguay: evidences of a ~ 800 Ma magmatic and ~ 650 Ma metamorphic event. Precambrian Research 185, 149–163.

Liégeois, J.P., 1998. Some words on the post-collisional magmatism. Preface to Special Edition on Post-Collisional Magmatism. Lithos 45, xv–xvii.

Martil, M.M.D., 2016. O magmatismo de arco continental pré-colisional (790 ma) e a reconstituição espaço-temporal do regime transpressivo (650 Ma) no Complexo Várzea do Capivarita, sul da Província Mantiqueira. PhD thesis. Universidade Federal do Rio Grande do Sul. Avaliable at: https://lume.ufrgs.br/handle/10183/149194

Martil, M.M.D., Bitencourt, M.F., Nardi, L.V.S., Koester, E., Pimentel, M.M., 2017. Pre-collisional, Neoproterozoic (ca. 790 Ma) continental arc magmatism in southern Mantiqueira Province, Brazil: geochemical and isotopic constraints from the Várzea do Capivarita Complex. Lithos 274–275, 39–52.

Martini, A., Bitencourt, M.F., Nardi, L.V.S., Florisbal, L.M., 2015. An integrated approach to the late stages of Neoproterozoic post-collisional magmatism from Southern Brazil: Structural geology, geochemistry and geochronology of the Corre-mar Granite. Precambrian Research, 261, 25-39.

Martini, 2019. Migmatitos e a geração de granitos no Complexo Camboriú, SC: controle estrutural, condições de fusão da crosta e gênese do Granito Itapema. PhD thesis. Universidade Federal do Rio Grande do Sul. Porto Alegre, Brazil. 210 pp. Avaliable at: https://lume.ufrgs.br/handle/10183/189058

Martini, A., Bitencourt, M.F., Weinberg, R., De Toni, G.B. Nardi, L.V.S., 2019a. From migmatite to magmas - crustal melting and generation of granite in the Camboriu Complex, south Brazil. Lithos, 340–341:270–286.

Martini, A., Bitencourt, M.F., Weinberg, R., De Toni, G.B, 2019b. Melt-collecting structures and the formation of extraction dykes during syntectonic anatexis of the Camboriú Complex, south Brazil. Journal of Structural Geology, 127:103866.

Molina, J.F., Moreno, J.A., Castro, A., Rodríguez, C., Fershtater, G.B., 2015. Calcic amphibole thermobarometry in metamorphic and igneous rocks: New calibrations based on plagioclase/amphibole Al-Si partitioning and amphibole/liquid Mg partitioning. Lithos, 232, 286-305.

Oriolo, S., Oyhantçabal, P., Wemmer, K., Heidelbach, F., Pfänder, J., Basei, M.,A.,S., Hueck, M., Hannich, F., Sperner, B., Siegesmund, S., 2016a. Shear zone evolution and timing of deformation in the Neoproterozoic transpressional Dom Feliciano Belt, Uruguay. Journal of Structural Geology, 92, 59–78.

Oriolo, S., Oyhantçabal, P., Basei, M.A.S.,Wemmer, K., Siegesmund, S., 2016b. The Nico Pérez Terrane (Uruguay): from Archean crustal growth and connections with the Congo Craton to late Neoproterozoic accretion to the Río de la Plata Craton. Precambrian Research, 280, 147–160.

Oyhantçabal, P., Siegesmund, S., Wemmer, K., Presnyakov, S., Layer, P., 2009. Geochronological constraints on the evolution of the southern Dom Feliciano Belt (Uruguay). Journal of the Geological Society of London, 166, 1075–1084.

Oyhantçabal, P., Siegesmund, S., Wemmer, K., 2011. The Río de la Plata Craton: a review of units, boundaries, ages and isotopic signature. International Journal of Earth Sciences. 100, 201–220.

Paim, P.S.G., Chemale Jr., F., Wildner, W., 2014. Estágios evolutivos da Bacia do Camaquã (RS). Ciência e Natura, Santa Maria, v. 36 p. 183–193.

Peruchi, F.M., 2016. Evolução espaço-tempo do Granodiorito Estaleiro, região de Porto Belo, SC. Unpublished graduation thesis. Universidade Federal de Santa Catarina, Brazil. 81 pp. Avaliable at: https://repositorio.ufsc.br/handle/123456789/173323

Peternell, M., Bitencourt, M.F., Kruhl, J.H., Stab, C., 2010. Macro- and microstructures as indicators of developmentof syntectonic granitoids and host rocks in the Camboriú region, Santa Catarina, Brazil. Journal of South American Earth Sciences 29:738-750.

Philipp, R.P., Mallmann, G., Bitencourt, M.F., Souza, E.R., Liz, J.D., Wild, F., Arend, S., Oliveira, A.S., Duarte, L.C., Rivera, C.B., and Prado, M., 2004. Caracterização Litológica e Evolução Metamórfica da Porção Leste do Complexo Metamórfico Brusque, Santa Catarina: Revista Brasileira de Geociências, v. 34(1), 21–34.

Philipp, R.P., and Campos, R.S., 2010, Granitos peraluminosos intrusivos no Complexo Metamórfico Brusque: Registro do magmatismo relacionado a colisão Neoproterozóica no Terreno Tijucas, Itapema, SC: Revista Brasileira de Geociências, 40(3), 301–318.

Philipp, R.P., Pimentel, M.M., Chemale Jr., F., 2016. Tectonic evolution of the Dom Feliciano Belt in Southern Brazil: Geological relationships and U-Pb geochronology. Brazilian Journal of Geology, 46(1), 83–104

Philipp, R.P., Pimentel, M.M., Basei, M.A.S., 2018. The Tectonic Evolution of the São Gabriel Terrane, Dom Feliciano Belt, Southern Brazil: The Closure of the Charrua Ocean. In: S. Siegesmund, S., Basei, M.A.S., Oyhantçabal, P., Oriolo, S. (eds.). Geology of southwest gondwana, Regional geology reviews, Springer, Heidelberg, pp 243–265

Philippon, M., Corti, G., 2016. Obliquity along plate boundaries. Tectonophysics, 693, 171-182.

Ramos, R.C., Koester, E., Triboli, D.V., Porcher, C.C., Gezatt, J.N., Silveira, R.L., 2018. Insights on the evolution of the Arroio Grande Ophiolite (Dom Feliciano Belt, Brazil) from Rb-Sr and SHRIMP U-Pb isotopic geochemistry. Journal of South American Earth Sciences, 86, 38-53.

Rivera, C.B., Bitencourt, M.F., Nardi, L.V.S., 2004. Integração de parâmetros físicos do magma e composição química dos minerais na petrogênese do Granito Itapema, SC. Revista Brasileira de Geociências, 34, 361-372.

Robin, P.-Y.F., Cruden, A.R., 1994. Strain and vorticity patterns in ideally ductile transpression zones. Journal of Structural Geology 16, 447–466.

Saalmann, K., Remus, M.V.D., Hartmann, L.A., 2006b. Structural evolution and tectonic setting of the Porongos Belt, southern Brazil. Geological Magazine, 143(1), 59-88.

Saalmann K, Gerdes A, Lahaye Y, Hartmann LA, Remus MVD, Läufer A, 2011. Multiple accretion at the eastern margin of the Rio de la Plata craton: the prolonged Brasiliano orogeny in southernmost Brazil. International Journal of Earth Sciences, 100, 355–378.

Sanderson, D.J., Marchini, W.R.D., 1984. Transpression. Journal of Structural Geology 6, 449–458.

Sawyer, E.W., 2008. Atlas of migmatites. Canadian Mineralogist, Special Publication 9. Mineralogical

Association of Canada, 386 pp.

Schmidt, M. W. 1992. Amphibole composition in tonalite as a function of pressure: an experimental calibration of the Al-in-hornblende barometer. Contributions to Mineralogy and Petrology, 110, 304-10.

Silva, L.C., 1991. O cinturão metavulcanossedimentar Brusque e a evolução policíclica das faixas dobradas proterozóicas no sul do Brasil: uma revisão. Revista Brasileira de Geociências, 21, 60–73.

Tikoff, B., Teyssier, C., 1994. Strain modeling of displacement field partitioning in transpressional orogens. Journal of Structural Geology, 11, 1575-1588.

UFRGS, 2000. Mapeamento Geológico 1:25 000: Projeto Camboriú, 6 vol. Trabalho de Graduação do Curso de Geologia, Instituto de Geociências, Universidade Federal do Rio Grande do Sul.

Weinberg, R.F., Hasalová, P., 2015. Water-fluxed melting of the continental crust: A review. Lithos 212-215, 158-188.

Will, T.M., Gaucher, C., Ling, X.-H., Li, X.-H., Li, Q.-L., Frimmel, H.E. Neoproterozoic magmatic and metamorphic events in the Cuchilla Dionisio Terrane, Uruguay, and possible correlations across the South Atlantic. Precambrian Research, 320, 303-322.

Vanderhaeghe, O, Burc, J.-R, & Teyssier, C. 1999. Exhumation of migmatites in two collapsed orogens: Canadian Cordillera and French Variscides. In: Ring, U., Brandon, M. T., Lister, G. S. & Wilett, S. D. (eds) Exhumation Processes: Normal Faulting, Ductile Flow and Erosion. Geological Society, London, Special Publications, 154, 181-204.

Zibra, I., Smithies, R.H., Wingate, M.T.D, Kirkland, C.L., 2014. Incremental pluton emplacement during inclined transpression. Tectonophysics, 623, 100-122.

TABLES

Table 01 - Porto Belo Complex Plagioclase Compositions						
Unit	Porto Belo Complex					
Rock	Hb-bt tonalite					
Sample	GB-01E					
Mineral	3	10	15	16	25	30
SiO2	57.96	62.26	58.98	59.43	58.01	100.11
Al2O3	26.59	25.15	25.75	25.69	26.93	0.02
CaO	8.18	6.18	7.45	7.37	8.43	0.02
Na2O	6.97	8.61	7.39	7.38	6.75	0.02
K2O	0.06	0.06	0.08	0.16	0.07	0.00
MgO	0.00	0.00	0.00	0.00	0.00	0.01
TiO2	0.00	0.00	0.00	0.00	0.00	0.00
FeO	0.01	0.09	0.04	0.13	0.11	0.06
Total	99.77	102.35	99.73	100.15	100.30	100.23
End-member Calculations						
Or	0.342405	0.327228	0.455365	0.910853	0.402097	0
Anorthite	39.20618	28.30742	35.61546	35.2378	40.6699	35.59279
Albite	60.45141	71.36535	63.92918	63.85135	58.928	64.40721

Table 3 - Plagioclase-Hornblende Thermobarometry			
Unit		Porto Belo Complex	
Rock		Hb-bt tonalite	
Sample		GB-01E	
Pairs		Conditions	
Hb	Pl	T	P
1	3	714.8	3.9
2	3	712.0	3.8
11	10	676.5	4.6
12	10	711.4	4.7
13	10	684.7	4.8
14	15	712.6	4.7
17	16	717.7	4.1
24	25	722.0	3.7
31	30	709.9	4.6
Average Conditions		706.9	4.3
T by Holland and Blundy, 1994; Blundy and Holland, 1990 P by Schmidt, 1992 and Anderson and Smith, 1995			

Table 02 - Porto Belo Complex hornblend compositions									
Unit	Porto Belo Complex								
Rock	Hb-bt tonalite								
Sample	GB-01E								
Mineral	1 / 1 .	2 / 1 .	11 / 1 .	12 / 1 .	13 / 1 .	14 / 1 .	17 / 1 .	24 / 1 .	31 / 1 .
SiO2	45.49	45.86	45.47	44.13	44.69	43.50	45.01	45.67	43.95
FeO	14.81	15.16	15.29	15.57	15.57	15.87	14.91	14.82	15.66
MgO	12.47	12.32	12.75	12.17	11.81	11.11	12.50	12.56	11.55
Al2O3	8.83	8.71	9.13	9.81	9.54	9.58	9.16	8.85	9.62
CaO	11.69	11.76	10.46	11.74	11.78	11.44	11.78	11.86	11.85
Na2O	1.14	1.06	1.00	1.21	1.15	1.22	1.14	1.16	1.17
K2O	1.12	1.10	1.36	1.28	1.20	1.16	1.16	1.11	1.20
TiO2	0.45	0.60	0.58	0.63	0.66	0.59	0.61	0.58	0.64
MnO	0.52	0.56	0.54	0.49	0.56	0.56	0.54	0.54	0.56
Cr2O3	0.07	0.07	0.05	0.06	0.07	0.09	0.07	0.07	0.08
Total	96.59	97.21	96.61	97.09	97.04	95.13	96.89	97.22	96.29
Cations in Formula basis of 23 O									
Si	6.753341	6.773536	6.747329	6.543112	6.639811	6.61584	6.666399	6.740683	6.596044
Al (iv)	1.246659	1.226464	1.252671	1.456888	1.360189	1.38416	1.333601	1.259317	1.403956
Al (vi)	0.298777	0.290193	0.344551	0.257887	0.310829	0.333546	0.26583	0.280622	0.298153
Ti	0.050242	0.066648	0.064728	0.07025	0.073747	0.067484	0.067947	0.064381	0.072237
Fe (iii)	0.563584	0.546914	0.518435	0.71908	0.58286	0.582257	0.631277	0.548391	0.598751
Mg	2.758995	2.711901	2.819673	2.689197	2.615032	2.518207	2.759142	2.762767	2.58338
Mn	0.065391	0.070062	0.067875	0.06154	0.070477	0.072143	0.067747	0.067511	0.071191
Fe (ii)	1.26301	1.314282	1.184738	1.202046	1.347055	1.426363	1.208059	1.276328	1.366834
Ca	1.859565	1.861157	1.663155	1.865146	1.875361	1.864301	1.869484	1.87565	1.896171
Na	0.328151	0.303567	0.287722	0.347858	0.331291	0.359768	0.327381	0.331969	0.340469
K	0.21213	0.207279	0.25747	0.242126	0.227461	0.225079	0.21919	0.209015	0.229767
OH	2.000	2.000	2.000	2.000	2.000	2.000	2.000	2.000	2.000

Table 4 - Mineral chemistry from Camboriú Complex migmatitic metapelitic gneiss (CA20Q)									
Biotite									
site	s01	s01	s01	s01	s01	s02	s02	s02	s02
DataSet/Point	4 / 1 .	5 / 1 .	7 / 1 .	8 / 1 .	9 / 1 .	14 / 1 .	15 / 1 .	16 / 1 .	17 / 1 .
Na2O	0.14	0.13	0.25	0.12	0.16	0.14	0.15	0.16	0.15
SiO2	33.81	34.44	34.27	34.58	34.23	34.43	34.2	34.45	34.34
MgO	6.42	6.35	6.54	6.72	5.94	6.46	6.68	6.64	6.77
Al2O3	19.38	19.42	19.7	20.36	19.82	19.87	19.03	19.81	18.98
K2O	9.2	9.26	9.07	9.47	9.3	9.12	9.29	9.34	9.28
CaO	0	0	0	0.03	0	0.01	0	0	0
TiO2	3.02	3.5	3.53	3.51	3.82	3.42	3.3	3.59	3.18
FeO	23.43	22.49	22.01	20.56	22.57	22.57	23.12	21.85	23.17
MnO	0.17	0.19	0.08	0.14	0.12	0.17	0.13	0.09	0.12
Total	95.56	95.78	95.46	95.49	95.96	96.18	95.89	95.93	95.98
No. Cations in Formula									
Si	5.248	5.301	5.275	5.279	5.260	5.270	5.281	5.275	5.296
Al	3.546	3.523	3.574	3.664	3.590	3.585	3.464	3.575	3.450
Fe	3.041	2.894	2.833	2.625	2.900	2.889	2.985	2.798	2.988
Mg	1.485	1.457	1.500	1.529	1.360	1.474	1.537	1.515	1.556
Na	0.042	0.039	0.075	0.036	0.048	0.042	0.045	0.047	0.045
K	1.822	1.818	1.781	1.844	1.823	1.781	1.830	1.824	1.826
Ti	0.352	0.405	0.409	0.403	0.441	0.394	0.383	0.413	0.369
Mn	0.022	0.025	0.010	0.018	0.016	0.022	0.017	0.012	0.016
TOTAL	15.559	15.461	15.457	15.426	15.439	15.455	15.542	15.460	15.545
XMg	0.33	0.33	0.35	0.37	0.32	0.34	0.34	0.35	0.34

Table 4 - (cont.)			
Biotite			
site	s02-1	s03	s03
DataSet/Point	24 / 1 .	27 / 1 .	28 / 1 .
Na2O	0.18	0.09	0.18
SiO2	34.04	34.91	34.45
MgO	6.17	6.25	6.71
Al2O3	19.55	20.56	19.43
K2O	9.08	9.16	9.07
CaO	0	0	0
TiO2	3.2	3.27	2.93
FeO	23.24	21.02	22.53
MnO	0.12	0.13	0.13
Total	95.58	95.39	95.45
No. Cations in Formula			
Si	5.268	5.333	5.316
Al	3.566	3.702	3.534
Fe	3.007	2.685	2.907
Mg	1.423	1.423	1.543
Na	0.054	0.027	0.054
K	1.792	1.785	1.785
Ti	0.372	0.376	0.340
Mn	0.016	0.017	0.017
TOTAL	15.500	15.346	15.497
XMg	0.32	0.35	0.35

Table 4 – (cont.)									
Garnet									
site	s01	s01	s01	s02	s02	s02	s02	s03	s03
obs.	core	core	rim	rim	core	rim	rim	core	core
DataSet/Point	1 / 1 .	2 / 1 .	3 / 1 .	10 / 1 .	11 / 1 .	12 / 1 .	13 / 1 .	25 / 1 .	26 / 1 .
SiO2	37.3	37.45	37.19	37.47	37.44	37.45	37.39	37.54	37.23
MgO	2.86	2.82	2.74	2.76	3.05	2.86	3.04	3.08	3.1
Al2O3	21.19	20.93	21.06	21.07	21.21	21.21	21.18	21.14	21.35
CaO	2.25	2.61	1.01	0.99	1.09	1.02	0.91	0.94	1.24
TiO2	0	0.02	0	0	0.03	0.02	0	0.01	0.06
FeO	32.7	32.05	33.8	34.15	34.27	34.54	35.24	36.14	35.58
MnO	3.11	2.87	3.56	3.62	2.71	2.86	2.35	2.64	2.84
Cr2O3	0.02	0.02	0.02	0.02	0.02	0.03	0	0.02	0.03
Na2O	0.03	0.06	0	0	0	0	0.03	0.03	0
Total	99.46	98.82	99.39	100.08	99.83	99.99	100.14	101.54	101.42
No. Cations in Formula									
Si	6.020	6.066	6.028	6.036	6.027	6.029	6.015	5.985	5.941
Mg	0.688	0.681	0.662	0.663	0.732	0.686	0.729	0.732	0.737
Al	4.031	3.996	4.024	4.001	4.025	4.025	4.016	3.973	4.016
Ca	0.389	0.453	0.175	0.171	0.188	0.176	0.157	0.161	0.212
Ti	0.000	0.002	0.000	0.000	0.004	0.002	0.000	0.001	0.007
Fe	4.413	4.341	4.581	4.600	4.613	4.649	4.740	4.818	4.747
Mn	0.425	0.394	0.489	0.494	0.369	0.390	0.320	0.357	0.384
TOTAL	15.965	15.933	15.960	15.964	15.957	15.957	15.977	16.027	16.044
End-member calculations									
PY	12	12	11	11	12	12	12	12	12
ALM	75	74	78	78	78	79	80	79	78
GRO	7	8	3	3	3	3	3	3	3
SP	7	7	8	8	6	7	5	6	6
XMg	0.13	0.14	0.13	0.13	0.14	0.13	0.13	0.13	0.13

4. *Origin and tectonic meaning of the Encruzilhada Block, Dom Feliciano Belt, south Brazil, based on aerogeophysics, image analysis and PT-paths*

Assunto	**TECTO: Your new submission received**
Remetente	Tectonophysics <eesserver@eesmail.elsevier.com>
Para	<gdetoni@ufrgs.br>, <jepetostoned@gmail.com>
Cópia	<fatimab@ufrgs.br>, <matheus.ariel.battisti@gmail.com>, <elisa.oliveira@ufrgs.br>, <jairosavian@gmail.com>
Responder para	Tectonophysics <tecto-eo@elsevier.com>
Data	2019-10-14 17:22

CHASQUE WEBMAIL
Universidade Federal do Rio Grande do Sul

*** Automated email sent by the system ***

Dear Mr. De Toni,

Your submission entitled "Origin and tectonic meaning of the Encruzilhada Block, Dom Feliciano Belt, south Brazil, based on aerogeophysics, image analysis and PT-paths" has been received by Tectonophysics for the article type Research Paper.

Please note that submission of an article is understood to imply that the article is original and is not being considered for publication elsewhere. Submission also implies that all authors have approved the paper for release and are in agreement with its content.

You will be able to check on the progress of your paper by logging on to https://ees.elsevier.com/tecto/ as Author.

Your manuscript will be given a reference number in due course.

Thank you for submitting your work to this journal.

Kind regards,

Journal Management
Tectonophysics

Origin and tectonic meaning of the Encruzilhada Block, Dom Feliciano Belt, south Brazil, based on aerogeophysics, image analysis and PT-paths

Giuseppe Betino De Toni[1]*, Maria de Fátima Bitencourt[1], Matheus Ariel Battisti[1], Elisa Oliveira da Costa[1], Jairo Savian[1]

[1] Programa de Pós-graduação em Geociências, Instituto de Geociências, Universidade Federal do Rio Grande do Sul, Av. Bento Gonçalves, 9500, Porto Alegre, 91500-000, RS, Brazil.

*Corresponding author: gdetoni@ufrgs.br

ABSTRACT

Encruzilhada Block (EB) of Dom Feliciano Belt (southern Brazil) aerogeophysical characteristics presents low-magnetism, as the Tijucas Fold Belt (TFB), because of similar thick supracrustal sequences, while it is gammaspectrometrically part of the Pelotas Batolith, due to abundant post-collisional magmatism. Satellite image lineament analysis points the tectonic similarity between the EB and TFB, both with predominant NNW and NNE directions, while PB is mostly controlled by NE structures. The connection between EB and TFB is confirmed by a correlation between Várzea do Capivarita and Cerro da Árvore complexes in terms of igneous protolith geochemistry and age (800 – 780 Ma), sedimentary provenance, progressive top-to-the-W transpressive deformation and peak metamorphic age (660 – 640 Ma). Contrastant PT-paths suggest exhumation of Várzea do Capivarita Complex from 790 – 820 °C/4.4 – 4.8 Kbar high-T/low-P peak conditions to 660 – 720 °C/2.5 – 3.4 Kbar at ca. 630 Ma. On the other hand, Cerro da Árvore Complex rocks were submitted to progressive metamorphism from 555 – 565 °C/5.4 – 5.7 Kbar to 560 – 580°C/5.8 – 6.3 Kbar, which is interpreted as underthrusting. The evidence suggests that both complexes were originated in a similar, if not a single basin, over an attenuated lithosphere with high geothermic gradient. Oblique collision caused basin inversion and thrusting of the lower portions of the sequence over its margins. Subsequent transpressional deformation, reactivation of major lineaments and post-collisional magmatism blurred the original boundaries between the complexes, creating the Encruzilhada Block.

Keywords: Aerogeophysics; Pseudosection; High-T/Low-P; Nappe; Block

1. Introduction

The tectonic setting where high-T/low-P granulites (De Yoreo et al., 1991) are formed is still a matter of debate. Some authors assume collision and tickening of a previously extended crust to account for the combination of high geothermal gradients and gently-dipping contractional structures, as reported in many high-T/low-P regions (Harris and Holland, 1984; Clark et al., 2011; Fowler et al., 2015). As pointed out by Kelsey and Hand (2011), such geothermal conditions are not expected for a duplicated, overthickened, lithosphere. The sequence of tectonic pull and push during orogeny is expected when collision follows the opening of a rift or back-arc rift (Lister and Foster, 2009; Fowler et al., 2015), and is characteristic of hot orogens, as described by Fossen et al. (2017).

The processes which guide exhumation of high-grade metamorphic rocks are also under discussion (Stüwe and Barr, 1998; Ring et al. 1999; and references therein). Among the main factors acting on exhumation, Ring et al. (1999) considers erosion, normal faulting and ductile thinning of the lithosphere, which may act individually or interplay to bring high-grade rocks to the surface, especially in the case of convergent/transpressive tectonic settings. Additional questions arise concerning the necessary time for thermal maturation of the lithosphere, as discussed by Thompson et al. (1997). Fast exhumation is suggested by near isothermal decompression (ITD) recorded in metamorphic peak and exhumation-related assemblages of such high-T/low-P rocks. Cordierite + spinel is a characteristic assemblage of high-T/low-P metapelitic granulites worldwide, as exemplified by the Archean gneisses from the Limpopo Belt (Harris and Holland, 1984), the metapelitic granulites from Jetty Penninsula, eastern Antarctica (Hand et al., 1994), the Neoproterozoic Indian khondalites (Bindu, 1997; Cenki et al., 2002), the Austrian Variscan paragneisses (Tropper et al., 2006), and the metapelites from the Mesozoic accretionary Coastal Belt, Yukon Terrane, western Canada (Mezger et al., 2008).

In this study we present new PT data on two supracrustal units of the Neoproterozoic, Dom Feliciano Belt in southernmost Brazil. The Várzea do Capivarita Complex (VCC) represents high-T/low-P granulites (Gross et al., 2006; Martil et al., 2017) from the Encruzilhada Block (EB - defined by Jost and Hartmann, 198) of Dom Feliciano Belt hinterland (Fig. 1). The EB tectonic significance is briefly debated by Hartmann et al. (2016) based on aerogeophysical data. The author correlated the EB

to the Pelotas Batolith based in aerogammaspectrometry, apart of aeromagnetometric stronger similarity with the Tijucas Fold Belt. PT data on the VCC is used for comparison with PT data from the supracrustal rocks of the Cerro da Árvore Complex (CAC) as defined by Jost and Bitencourt (1980), which are part of the Tijucas Fold Belt (TFB). The proposed comparison between VCC and CAC takes into account previously published structural, geochemical and geochronological data from both. The geological comparison is accompanied by exhamination of large-scale geophysical and tectonic data on both units and on the limits of the Encruzilhada Block. The integration of geological, petrological and geophysical data is intended to open the discussion on the origin and tectonic significance of the Encruzilhada Block, a key piece to discuss tectonic boundaries, domains and evolution models for the Dom Feliciano Belt.

2. Materials and methods

Metamorphic conditions were estimated based on a representative set of three VCC samples and one additional sample from the neighbouring Cerro da Árvore Complex for comparison. The modelling was done with Perple_X 6.7.0 software (Connoly, 2005) and the thermodynamic database of Holland and Powell (1998, revised 2002). Pseudosections are constructed based on whole-rock geochemistry of major elements, whilst mineral chemical data are used for isopleth calculations. Whole-rock compositions were obtained from rock powder tablets in representative samples using a Rigaku RIX 2000 X-Ray Fluorescence (XRF), in the X-ray Fluorescence Laboratory from Centro de Estudos em Petrologia e Geoquímica (CPGq), Instituto de Geociências (IGEO), from Universidade Federal do Rio Grande do Sul (UFRGS), Brazil (methods detailed in Brown et al., 1973). Subdomains recognized in one sample (MN12C) were assumed to be closed systems, and their composition was obtained by compositional mapping, using a Scanning Electron Microscope (SEM) Zeiss Merlin VP Compact from the SEM Laboratory of the Health Sciences Faculty, Arctic University of Norway, Tromsø. The approach follows the methods described in Tajcmanova et al. (2007). Thin sections were carbon-coated and analytical conditions were 20 kV acceleration voltage and 120 µm aperture. Mineral compositions were determined at the Microprobe Laboratory, CPGq, UFRGS, using a Cameca SXFive microprobe at analytical conditions of 14.8 keV, 15 nA current, and beam size of 20 µm.

Geophysical data used in this paper result from airborne magnetic and gamma-ray spectrometric survey done by the Brazilian Geological Survey (CPRM, 2010) in southernmost Brazil, with line spacing of 500 m and control lines spaced of 10.000 m (NS and EW). Two adjacent ASTER images were used to build a digital elevation model of the area using ERDAS Imagine (2014), where lineament tracing at regional scale (0.25x zoom – 1:200.000 scale) resulted in 391 line segments.

3. Geological Setting

3.1 Regional Geology

The Precambrian geology of southern Brazil and Uruguay (Fig. 1) can be envisaged in terms of two main cratonic blocks and a mobile belt. To the north is situated the Luis Alves Craton (Hartmann et al., 2000), and to the south, the Rio de la Plata Craton and the Nico Perez Terrane (Oyhantçabal et al., 2011). The Dom Feliciano Belt (DFB) is the mobile belt adjacent to the Rio de la Plata Craton and its evolution has been subject of many different models (e.g. Fernandes et al., 1992, 1995a, 1995b; Chemale Jr., 2000; Hartmann et al., 2007; Philipp et al., 2016a). It is the South American portion of the Dom Feliciano-Kaoko-Gariep orogenic system, formed during Western Gondwana assembly (Konopásek et al., 2016; 2018 and references therein).

The DFB comprises four main tectonic domains limited by major lineaments (Fernandes et al., 1995a, 1995b; Chemale Jr., 2000; Hartmann et al., 2007; Philipp et al., 2016a). The western São Gabriel Block represents an early-Neoproterozoic magmatic arc with remnants of *ca.* 930 to 900 Ma ophiolites, ca. 890 and 860 Ma arc fragmentary record and a well preserved continental magmatic arc active from *ca.* 770 to 720 Ma (Arena et al., 2016; Philipp et al., 2018).

To the east, the Tijucas Fold Belt (Hasui et al., 1975) is represented by the Porongos Complex (PC), interpreted as a multi-phase, foreland (meta)volcano-sedimentary basin (Gruber et al., 2016b; Pertille et al., 2015; Höfig et al., 2017). Volcanic activity in the basin is dated at ca. 780 Ma (Saalman et al., 2011; Martil, 2016) and between ca. 600 Ma and 580 (Höfig et al., 2017), whereas recurrent, collision-related metamorphism/deformation events took place at *ca.* 650 (Lenz, 2006) and shortly after 570 Ma (Höfig et al., 2017; Battisti et al., 2018). The seminal work by Jost and Bitencourt (1980) recognized that the Tijucas Fold Belt in this area were build up by two distinct sequences, tectonically imbricated by a westward vergent thrust, with the Cerro da Árvore Complex (Porongos I of Höfig et al., 2017; Battisti et al., 2018)

thrusted over the Cerro dos Madeiras Group (Porongos II of Höfig et al., 2017; Battisti et al., 2018). Paleoproterozoic basement inliers outcrop in the core of regional antiforms (e.g. Encantadas Complex – Saalmann et al., 2006), whilst non-metamorphosed Ediacaran to Cambrian volcano-sedimentary successions fill NS-trending narrow grabens in the space between antiforms (Borba et al 2007; Paim et al 2014; de Oliveira et al, 2014; Fambrini et al., 2018).

Farther east, the Pelotas Batolith (PB) is interpreted as a post-collisional batholith formed between *ca.* 640 and 580 Ma (Bitencourt and Nardi, 1993; Philipp et al. 2002) in which magmatic pulses were controlled by the Southern Brazilian Shear Belt (SBSB) (Bitencourt and Nardi, 2000). The SBSB is an anastomosing array of shear zones which have acted as channels for both crustal and mantle-derived magmas. Recent studies suggest that this transpressive shear belt affected both the Pelotas Batholith and the supracrustals of the Tijucas Fold Belt (Oriolo et al., 2016; Battisti et al., 2018; De Toni, 2019).

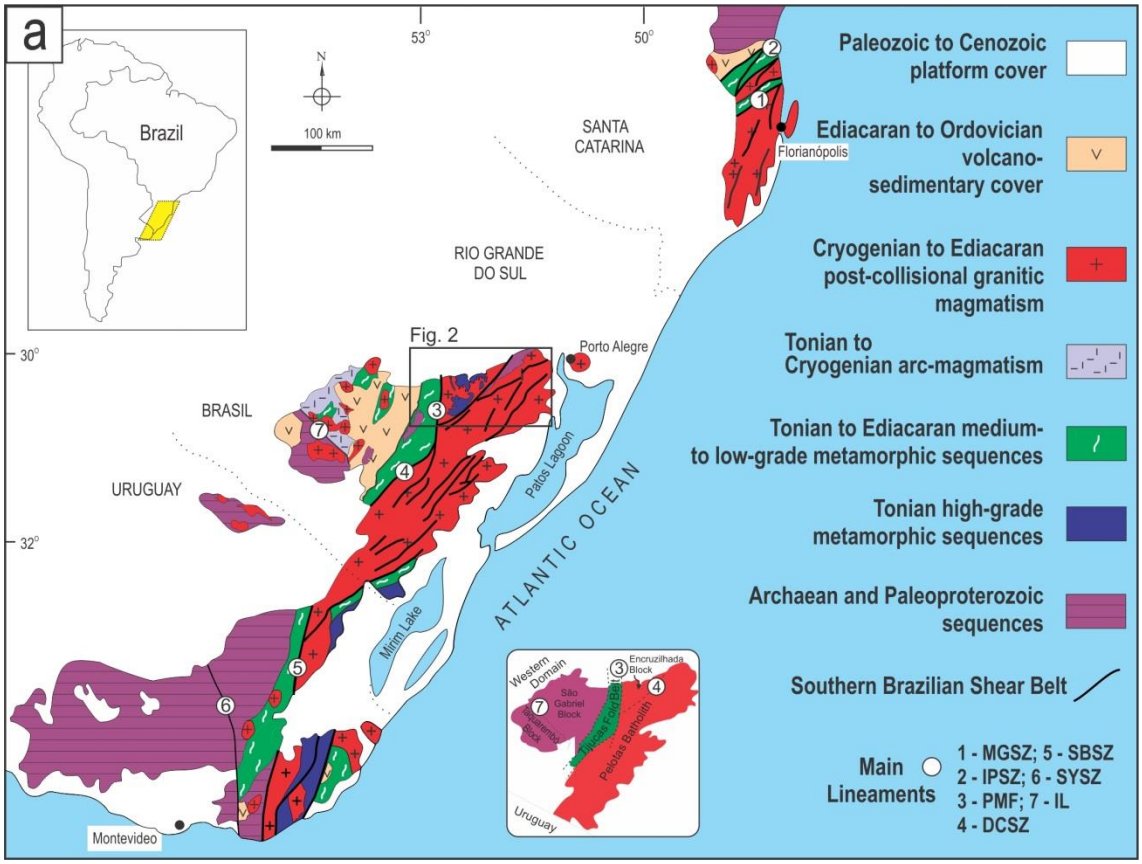

Figure 01 – Geotectonic sketch of Dom Feliciano Belt and surrounding cratonic (modified from Bitencourt and Nardi, 2000, Ramos et al., 2018; Will et al., 2019). The lower inset illustrates a simplified subdivision of the Sul-rio-grandense Shield, including the main lineaments which subdivided it. The rectangle in the center of the figure show the area of the geological map presented in figure 02.

Several roof pendants are reported on the PB granitoids (Fig. 2a), as (i) Paleoproterozoic TTG gneisses of the Arroio dos Ratos Complex (Gregory et al., 2015) between the Dorsal do Canguçu (DCSZ – Picada, 1971; Fernandes et al., 1992) and Quitéria-Serra do Erval shear zones (QSESZ – Gregory et al., 2015; Knijnik, 2018); (ii) Mesoproterozoic Capivarita Anorthosite (CA – Chemale Jr. et al, 2011) in the Encruzilhada Block, surrounded by the Neoproterozoic ortho- and paragneisses of the Várzea do Capivarita Complex (Gross et al., 2006; Bom et al., 2014; Philipp et al., 2016b; Martil et al., 2011, 2017; Martil, 2016). Additionally, km-sized blocks and xenoliths of early Neoproterozoic orthogneisses (Silva et al., 1999; Koester et al., 2016) are spread along the batholith. Based on the similar protolith ages and geochemical signatures, these early Neoproterozoic roof pendants and xenoliths are correlated with the basement of the Punta del Este Terrane in Uruguay, which is described in the southeast portion of the DFB (Fig. 1; Oyhantçabal et al., 2009; Lenz et al., 2011; 2013; Masquelin et al., 2012; Ramos et al., 2018). Dating of the orthogneiss protolith in Brazil and Uruguay gave a similar range of ages between ca. 800 and 777 Ma (Silva et al., 1999; Koester et al., 2016; Martil, 2016; Martil et al., 2017; Lenz et al., 2011). Based on geochemical and petrological evidence, these rocks were interpreted to have been formed within a ca. 800 Ma magmatic arc environment of the Dom Feliciano Belt (Lenz et al., 2013; Koester et al., 2016; Martil, 2016; Martil et al., 2017). The same 800 – 780 Ma arc-like magmatism was recently described (Saalmann et al., 2006; Martil, 2016; Martil et al., 2017; and Battisti et al., 2018) in metavolcanic rocks from the Cerro da Árvore Complex. These metavolcanic rocks are correlated with the VCC orthogneisses, which is taken as additional evidence that the Pelotas Batholith and Tijucas Fold Belt have been part of the same orogenic system since pre-collisional times. This is opposed to accretionary models proposed by Fernandes et al. (1992), Basei et al. (2005, 2008) and Chemale Jr. (2000). An alternative interpretation about the tectonic setting of the early Neoproterozoic rocks in the Dom Feliciano Belt is given by Konopasek et al. (2018), who consider them as deeper counterparts of rift-related volcano-sedimentary sequences recognized in the Kaoko Belt.

The extreme southeastern portion of the Dom Feliciano Belt is exposed exclusively in Uruguay. The Rocha Group (Betucci and Burgueno, 1993) is a supracrustal unit correlated with rocks from the Gariep Belt.

3.2 Geology of the Encruzilhada Block

The EB (Jost and Hartmann, 1984; Fig. 2a) is the northwestern portion of the Pelotas Batholith. It contains unique stratigraphic units like the Mesoproterozoic Capivarita Anorthosite (Chemale Jr., 2011) and a sequence of syn- to post-collisional syenitic intrusions (*ca.* 640 Ma Arroio das Palmas Syenite – De Toni et al., 2016; Bitencourt et al., 2016; 610 - 580 Ma Piquiri Syenite Massif – Nardi et al., 2008; Rivera, 2019; ca. 578 Ma Arroio do Silva Pluton – Padilha et al., 2019) without correlated rocks in the restant of PB.

The limit between the EB and the PB is the sinistral transcurrent Dorsal de Canguçu Shear Zone, where post-collisional, syntectonic, high-K calc-alkaline and peraluminous granites were emplaced between ca. 635 and 605 Ma (Fernandes and Koester, 1999, Knijnik, 2018). The boundary between the EB and the TFB is the Passo do Marinheiro Fault (PMF - Picada, 1971; Fig. 2a). This fault was interpreted by Jost (1981) as an originally dextral ductile structure. On the other hand, the PMF is usually interpreted as a sinistral, brittle structure, due to apparent displacement of the southwesternmost portion of the Encruzilhada Granite (see Fig. 2a – Picada, 1971, Jacobs et al., 2018).

3.2.1 Várzea do Capivarita Complex

The Várzea do Capivarita Complex comprises igneous and metamorphic rocks within two large roof pendants (Fig. 2a). The VCC main rock types are high-temperature, tectonically interleaved tonalitic–granitic orthogneisses of Tonian age protolith, and paragneisses (metapelites, calc-silicate rocks, marbles and rare quartzites) (Martil et al., 2011; Martil, 2016; Gruber *et al.*, 2016a; Battisti et al., 2018), with subordinate volume of syntectonic Arroio das Palmas Syenite (De Toni et al., 2016).

In the eastern portion of the northern roof pendant, VCC gneisses surround the Capivarita Anorthosite which forms the core of a regional antiform. Both rock associations were metamorphosed and deformed under granulite facies conditions at *ca.* 650 – 640 Ma (Chemale Jr., 2011; Martil, 2016), contemporaneous to the intrusion of the Arroio das Palmas Syenite (De Toni et al., 2016; Bitencourt et al. 2016).

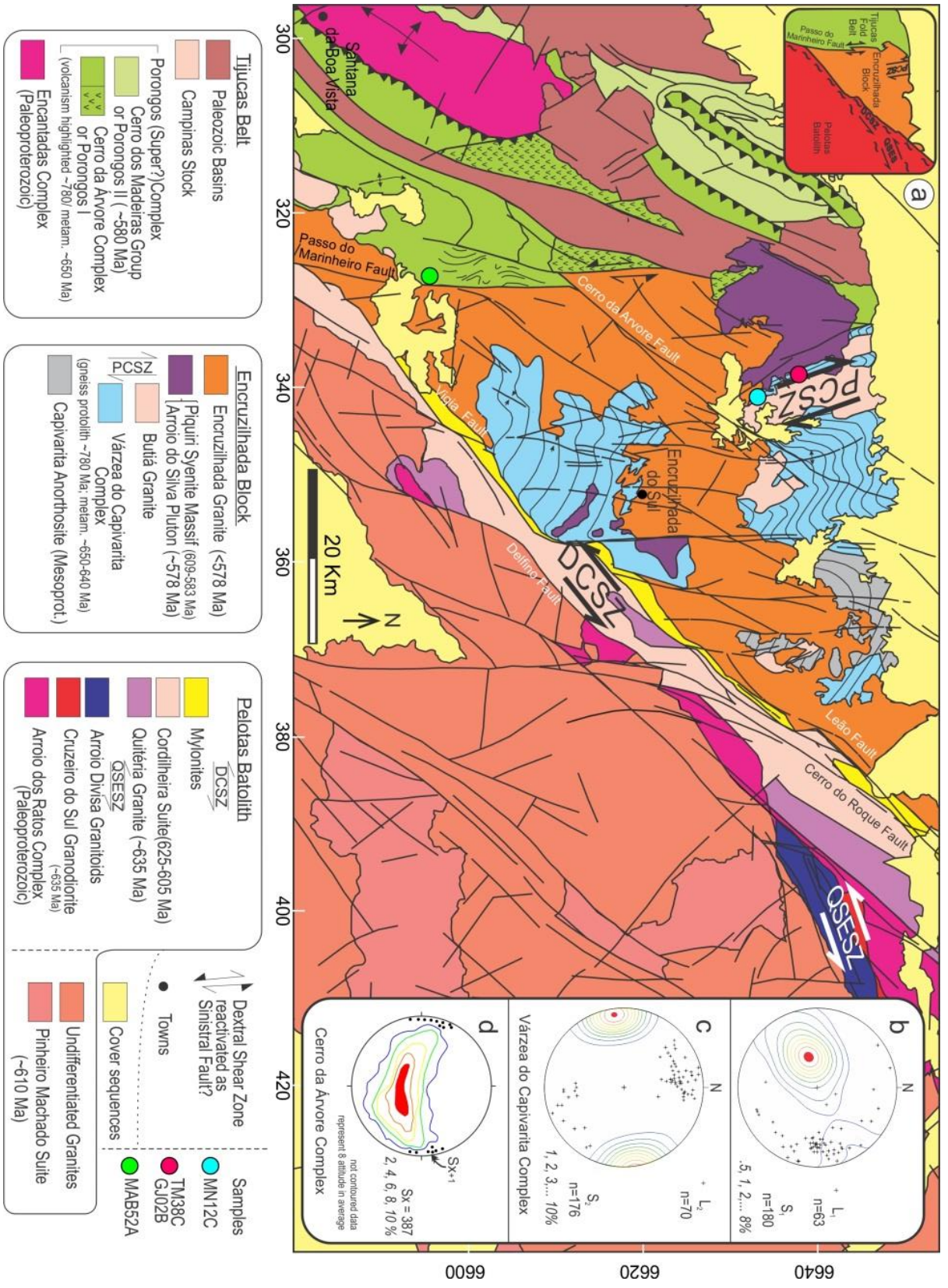

Figure 02 – (a) Geological map of the Encruzilhada Block and neighbor regions (compiled after Picada, 1971; Jost and Bitencourt, 1980; Ramgrab et al., 1996; Porcher and Lopes, 2000; UFRGS, 2008, 2009, 2010, 2011; Gregory et al., 2015; Martil, 2016; Höfig, 2017). The major faults and shear zones are labeled. The upper-left inset presents the Encruzilhada Block and the main tectonic domains subdivision as discussed in the text. The inset in the right-hand side presents structural data with contoured main foliation and lineation from Várzea do Capivarita Complex D_1 (b) and D_2 (c – both from Martil et al., 2017) and contoured main foliation Sx (cont.)

and transposition foliation Sx+1 from Cerro da Árvore Complex (d – from Jost and Bitencourt, 1980). Sample sites are indicated.

The structural characterization of the VCC gneisses progressive transpressional deformation is given by Martil (2016), and may be summarized as follows. Ortho- and parametamorphic rocks of the complex record an early foliation (S_1 – Fig. 2b) which strikes about 340° and dips at shallow angles to the east. A highly oblique stretching lineation (L_1) lies in the S_1 foliation plane, and its top-to-the-W kinematics is registered by outcrop-scale asymmetric folds, asymmetric deformed porphyroclasts, and S-C fabrics. The verticalization of S_1 towards the fold short limbs is accompanied by the rotation of the lineation L_1 towards subhorizontal position within dextral strike-slip domains (S_2 - L_2 – Fig. 2c). D_1 and D_2 are interpreted to be progressive under granulite-facies conditions, as recorded by orthopyroxene in tonalitic orthogneisses stable in both fabrics with similar age for the granulite-facies metamorphism (Martil et al., 2011, 2017) and syenite synyectonic emplacement along both fabrics (De Toni et al., 2016; Bitencourt et al., 2016). A D_2 high-strain zone was recognized at the northwestern portion of the VCC (UFRGS, 2008; Martil, 2016; Martil et al., 2011, 2017). It is called Passo das Canas Shear Zone (Fig. 2a) and controls syntectonic intrusions as the Arroio das Palmas Syenite (De Toni et al., 2016) and the sillianite-bearing Butiá Granite (Lyra et al., 2018). High-T/Low-P metamorphic conditions were estimated by Gross et al. (2006), in the range of 730 – 800°C and 3 to 4 kbar. In contrast, Philipp et al. (2013, 2016b) argue for medium-P/high-T conditions.

Martil (2016) reports protolith ages of 790-770 Ma for the orthogneisses, and age of high-grade metamorphism between 650-640 Ma (U-Pb zircon LA-ICP-MS and SHRIMP, several samples dated). A collision-related metamorphic age of 651.5 ± 8.8 Ma (U-Pb titanite LA-ICP-MS) from the Capivarita Anorthosite was reported by Chemale Jr. et al. (2011). On the other hand, Gross et al. (2006) reported a 626–604 Ma metamorphic age for the VCC metapelitic granulites (Sm-Nd garnet and whole-rock isochron). Similar ages of 620 ± 6.3 and 619 ± 4.3 Ma (U-Pb zircon SHRIMP) were reported by Philipp et al. (2016b) from a leucogranite vein and migmatitic metapelite, respectively. These age values are interpreted to result from synchronous migmatitization and leucosome crystallization which occurred right after metamorphic peak, as exemplified by Himalayan anatexis, which characteristically occurred 30 Ma after the main collision episode (Weinberg, 2016).

Despite the diferences in estimated timing and PT conditions of the high-grade metamorphism reported by different authors, the granulite-facies deformation fabric of the VCC rocks is taken as evidence of an important late-Cryogenian collisional episode in the central part of the DFB (Gross et al., 2006; Philipp et al., 2013, 2015; Martil, 2016; Martil et al., 2011, 2017).

3.2.2 Younger intrusive rocks

The VCC rocks are intruded by several granite and syenite units. The oldest intrusion is the sillimanite-bearing Butiá Granite (Niessing, 2008), syntectonic to the Passo das Canas Shear Zone (Fig. 2a) at 629.2 ± 6.8 Ma (U-Pb monazite ID-TIMS – Bitencourt et al., 2015). The emplacement conditions were determined by Niessing (2008) as 700 – 750 °C and 3 – 4.2 kbar. The Butiá Granite is correlated with other peraluminous syntectonic granites of similar age emplaced along active shear zones of the Pelotas Batolith, as the Cordilheira Suite from the DCSZ (Philipp et al., 2013 and references therein) and minor leucogranitic intrusions related to partial melting of the VCC rocks (Bom et al., 2014; Philipp et al., 2016b).

The Piquiri Syenite Massif (PSM) is a landmark in the Encruzilhada Block due to its unambiguous horse-shoe shape in map view, km-size (10 – 15 km diameter) and pronounced positive relief. It is important to note that the PSM intrusion crosscuts the Passo do Marinheiro Fault (Fig. 2a). The PSM is described as an ultrapotassic-shoshonitic association of syenites, granites and lamprophyres (Stabel et al., 2001; Nardi et al., 2008), which built the massif in pulses from 609 ± 2 Ma to 584 ± 2 Ma (Sbaraini, 2019; Rivera, 2019). Plá Cid et al. (2003) have shown that crystallization of the magma started between 4 and 6 GPa and that magma mingling started at lithospheric mantle pressures. Martil (2007) argued that the PSM caused localized contact metamorphism in VCC xenoliths and m-scale roof pendants, and that it erases the foliation in the CAC metavolcanic roof pendant (Martil, 2007; Battisti et al. 2018). From these observations one can conclude that the PSM was emplaced after the VCC and CAC were side-by-side. Other syenitic intrusions of similar age, as the Arroio do Silva Pluton (578 ± 4 Ma – LA-ICP-MS U-Pb zircon - Padilha et al., 2019) are found in the southern VCC roof pendant (Fig. 2).

The Encruzilhada Granite (EG, Fig. 2) is so far the youngest known intrusion in the EB. It develops important mixing and mingling features with a coeval mafic magma of tholeiitic affinity (Jacobs et al., 2018 and references therein). Contact metamorphism on the CAC metapelites west of Passo do Marinheiro Fault is attributed to the thermal effect of the EG (Lenz, 2006) and is taken as indicative of its shallow

emplacement. Babinski et al. (1997) presented a crystallization age of 594 ± 5 Ma for the EG. However, field relations indicate that the EG has assimilated blocks of the Arroio do Silva Pluton (Padilha et al., 2019), and therefore must be younger than 578 Ma.

4. Results

4.1. Characteristics and boundaries of the Encruzilhada Block

4.1.1. Satellite image analysis and tectonic framework

Two adjacent ASTER images were used to build a digital elevation model (DEM) with the combined visible and near infrared (VNIR) band 3 nadir and backwards. Tracing of 391 lineaments over the DEM is presented in terms of a lineament (Fig. 3a) map and rose diagrams for the whole dataset (Fig. 3b) and for each considered domain (Fig. 3c to e). The domain limits are the geological boundaries of the Encruzilhada Block, i.e. the Passo do Marinheiro Fault and the Dorsal de Canguçu Shear Zone.

The most frequent lineaments strike approximately north-south. The general diagram presents two maxima (22 lineaments each), at 350-360° and 010-020°, and additional secondary concentrations between 340° and 030°. Rose diagrams for each domain show similar patterns. The Encruzilhada Block domain (Fig. 3c) presents maximum lineament concentration at 340°-350°, with secondary maxima at 000-010° and 020-030°. NE-striking lineaments are virtually absent. On the other hand, the Dorsal de Canguçu Shear Zone domain (Fig. 3d) presents a maximum at 050-060° and two secondary concentrations at 040-050° and 080-090°. In the Tijucas Fold Belt domain (Fig. 3e), only two maxima are found, at 350-360° and 010-020°.

The EB lineament pattern is therefore similar to that of the TFB, but contrasts with that of the DCSZ domain. The similarity of EB and TFB structural styles was already mentioned by Battisti et al. (2018) for VCC and CAC metavolcanics. Similar lineament orientation patterns suggest a common tectonic framework for the TFB and EB, possibly related to a common structural evolution, and points to a different origin of, or an important structural overprint in, the DCSZ domain.

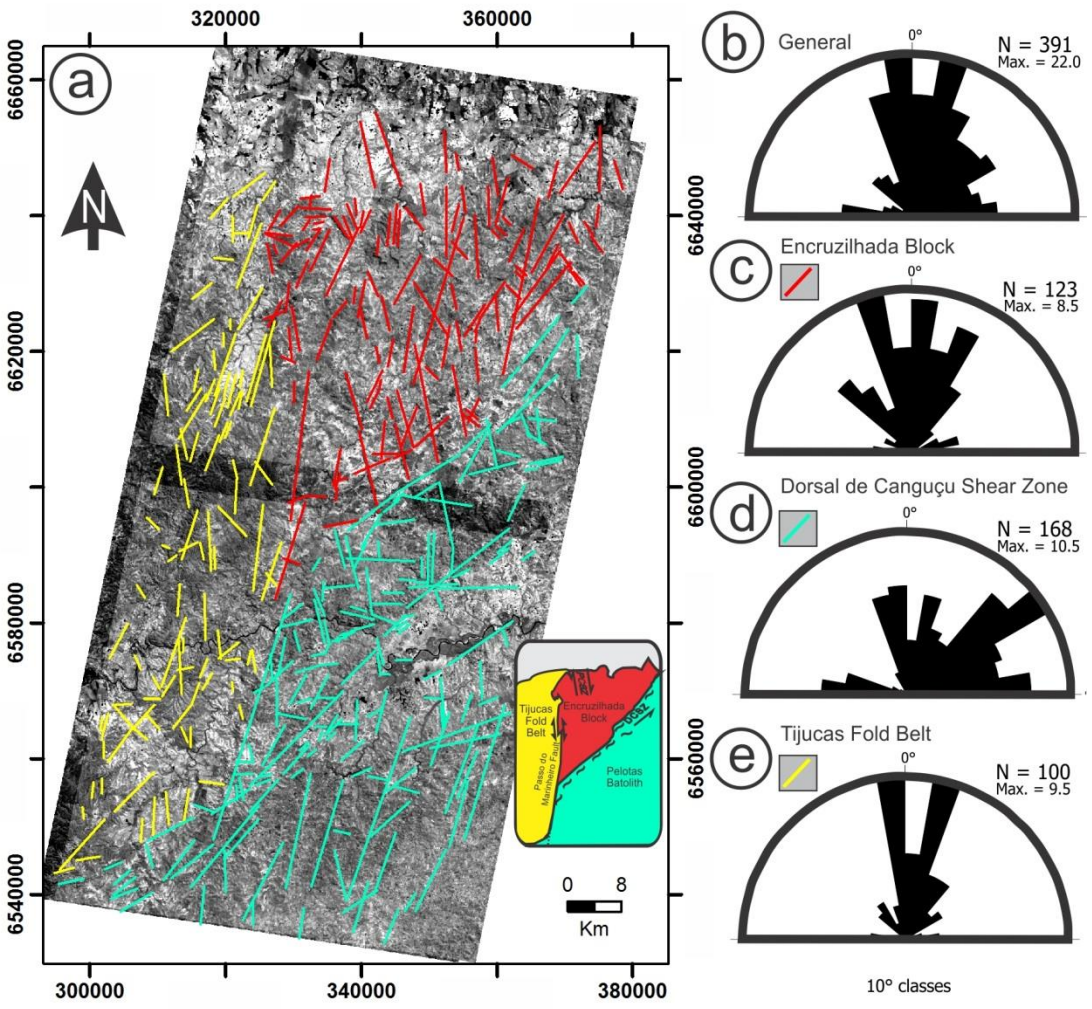

Figure 03 – Satellite image analysis. (a) ASTER images used for creation of digital elevation model and lineament tracing. Lower-right inset shows the tectonic domains subdivision as discussed in the text. (b) Rose diagrams representative of the general map and for (c) Encruzilhada Block, (d) Major Gercino Shear Zone and (e) Tijucas Fold Belt domains are presented. It is noteworthy the similarity of the dominantly NNW- to NNE-striking EB and TFD rose diagrams and the DCSZ NE to ENE contrastant pattern.

4.1.2. Aerogeophysical signatures

The aeromagnetometric analytical signal of the total magnetic field (Fig. 4a), aerogammaspectrometry (aerogamma hereafter) total counts (Fig. 4b) and ternary composition (Fig. 4c) maps covering the Encruzilhada Block geological map (Fig. 2a) are presented in figure 4. An interpretative sketch from the three geophysical maps is presented in figure 4d.

The aeromagnetometric map (Fig. 4a) shows contrasting patterns for the EB relative to its neighbouring areas. The map may be divided in three main magnetic domains named, from west to east, magnetic domains 1, 2 and 3 (Md1, Md2, and Md3, the later being further subdivided in Md3a and Md3b – Fig. 4d). The EB shows a

dominantly low magnetic signal (center of Fig. 4a; Md2 in fig. 4d). According to Shroder (2014), sedimentary rocks are less magnetic than igneous rocks, and negative magnetic anomalies are typical of sedimentary basins or troughs. The EB low sign is probably due to the pronounced thickness of metasedimentary rocks as the main source of the negative anomaly, with no significant magnetic rock bodies in depth. Higher isolated aeromagnetic signals in the EB are related to the PSM (near circular, positive anomaly in Fig. 4a; also shown in Fig. 4d as PSM) and other syenitic intrusions (smaller patches with positive anomaly at the center of Fig. 4a).

The Tijucas Fold Belt (Md1) is characterized by dominantly medium to high magnetic signal due to lithological heterogeneities. The contact between Md1 and Md2 is marked by an abrupt boundary between dominantly medium and low magnetic signal, and coincides with the Passo do Marinheiro Fault. The limit between Md2 and Md3 is given by an even better marked discontinuity, separating the low-signal Md2 (EB) and the medium- to high-signal Md3 (Pelotas Batholith). This important structure is named the Porto Alegre Lineament (after Fernandes et al., 1995b), and coincides with the southern boundary of the Quitéria-Serrra do Erval Shear Zone (Gregory et al., 2015 and references therein). In the Pelotas Batholith Domain (Md3), a high-signal area Md3b is separated from Md3a by an irregular boundary, probably marking intrusive contacts among distinct granitoids. Several high sign lineaments are oriented roughly E-W to WNW-ESE and may be observed mainly in the southern half of the map. These lineaments crosscut the main structures described so far, and are interpreted by Hartmann et al. (2016) to represent Mesozoic feeder dikes.

The aerogammaspectrometric total count map (Fig. 4b) shows the difference between the TFB, with low count values in the western portion (Gd1a and Gd1b), and the higher count values in the EB (Gd2) and the rest of the PB (Gd3). In the EB, the higher values, apart from the PSM, represent the Encruzilhada Granite. The very low count spot at the upper-center of figure 4b represents the Capivarita Anorthosite. The surrounding area, with relatively low count values, is the northern VCC roof pendant. It is noteworthy that similar low counts are found in the Cerro da Árvore region (greenish Gd1b). The medium-to-high values of the southern VCC roof pendant may indicate the effects of pervasive EG injections in its country rocks (UFRGS, 2010; Jacobs et al., 2018).

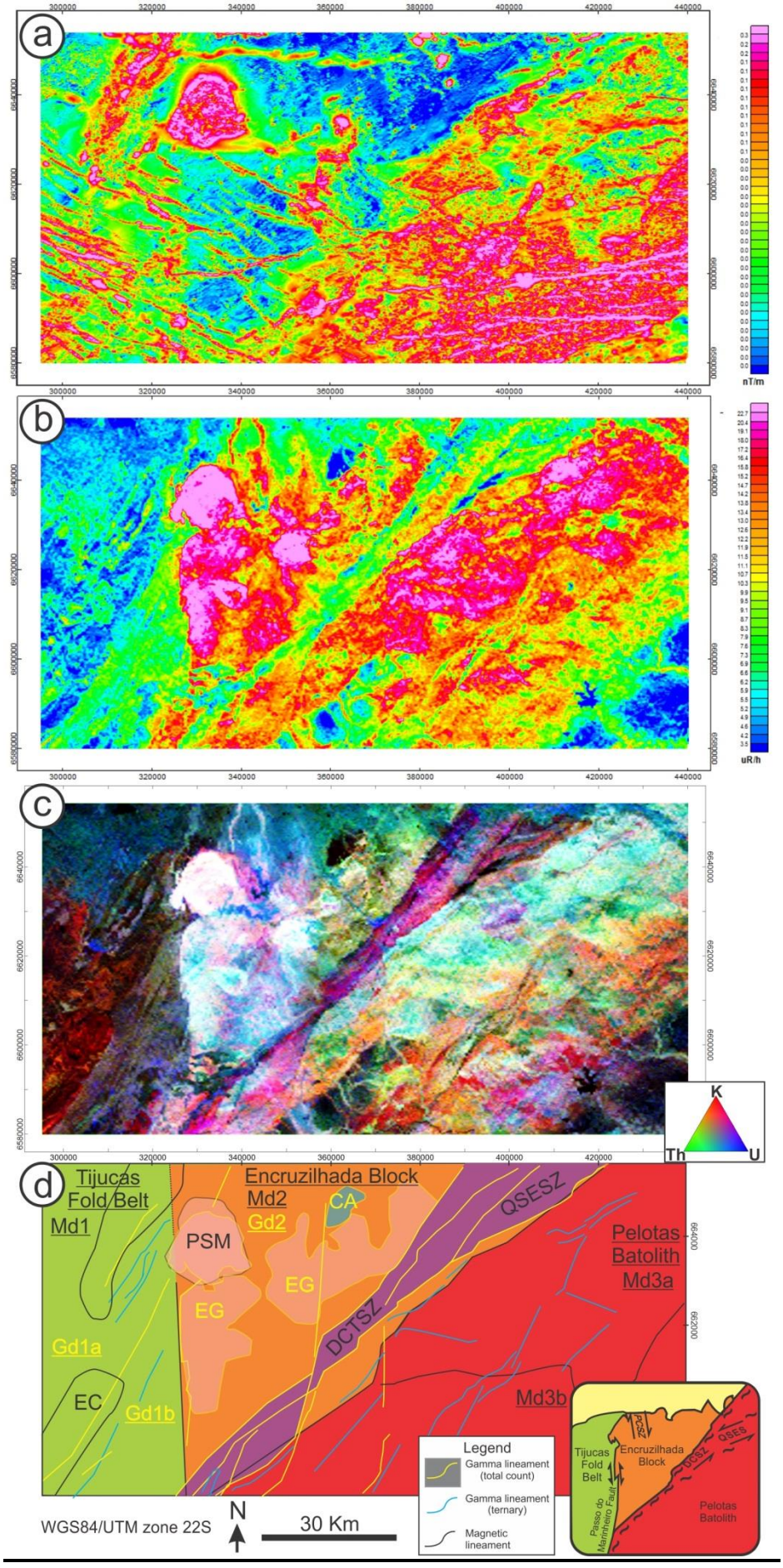
a
nT/m
b
uR/h
c
K
Th
U
d
Tijucas
Fold Belt
Md1
Gd1a
EC
Gd1b
PSM
Encruzilhada Block
Md2
Gd2
CA
EG
EG
DCTSZ
QSESZ
Pelotas
Batolith
Md3a
Md3b
Legend
Gamma lineament (total count)
Gamma lineament (ternary)
Magnetic lineament
WGS84/UTM zone 22S
N
30 Km
PCSZ
QSES
DCSZ
Passo do Marinheiro Fault

Figure 04 (previous page) – Aerogeophysical maps for the Encruzilhada Block and surrounding areas. All the maps cover the same area from geological map of the figure 02. (a) Aeromagnetometric analytical sign map; (b) Aerogammaspectrometric total counts map; (c) Aerogammaspectrometric ternary composition map; (d) Interpretative sketch containing geophysical lineaments and boundaries of key-units made from the three previous maps. The lower-right inset presents the Encruzilhada Block and surrounding tectonic domains subdivision as discussed in the text.

The contact between the EB and PB, marked by mylonites and DCSZ syntectonic granites, is a relatively low-count, NE-striking area, which in its northern portion widens and splits into the ENE-striking QSESZ (Fig. 4b). In the rest of the PB (east of DCSZ and QSESZ) it is possible to observe different shades of hot colours. Among them, it is possible to distinguish several NNE- to NE-trending structures of sigmoid pattern, best observed in the bottom-half of the DCSZ and Pelotas Batolith area (Fig. 4b). The NNE-trending structures are interpreted to be late structures which displace the main NE-trending, continuous and longer lineaments of synthetic sinistral movement.

The Aerogammaspectrometric ternary representation (Fig. 4c) shows the difference between the TFB, with low count values (darker) in the western portion, and the higher count values from the EB and the rest of the PB (dominantly light colours). Disconsidering the very low signals (black) that represent the recent sedimentary cover in the south portion of the PB, the abovementioned heterogeneities of the PB are clear. These subdivisions are more diffuse than in the other maps, but may be simplified in terms of: (i) a reddish, K-rich area in the south, mostly attributed to the Pinheiro Machado Suite (Ramgrab et al., 1996; Philipp and Machado, 2005); (ii) a light-green, Th-rich area in the north (undifferentiated granites in figure 2a); and (iii) a deep-magenta stripe corresponding to the DCSZ and QSESZ. This subdivision is in good agreement with the observed contact between Md3a and Md3b in the aeromagnetometric map (Fig. 4a and 4d). Again, it is possible to observe several NNE-trending structures along the PB which displace and/or drag the NE-trending main structures and are interpreted to be late sinistral structures at map scale.

A black spot marks the Capivarita Anorthosite at the EB northeastern portion, surrounded by bluish/greenish VCC gneisses. A very light pink spot marks the PSM at the northwestern corner of the EB. At the northeastern side of the EB, the VCC gneisses are represented by bluish and greenish hues, mainly in its northernmost portion surrounding the Capivarita Anortosite. On the western side of the EB, the gneisses are the dominantly blue area in the central portion of the block, where the

northern and southern roof pendants contrast with the brighter areas of younger magmatic rocks.

West of the PMF, the TFB may be subdivided in three domains of different aerogammaspetrometric responses: (i) the dark red and pale green area to the northwest (Gd1a), which represents the so-called Piquiri Basin (Borba et al., 2007); (ii) the Cerro da Árvore Complex, of dark-purple colour (Gd1b); and (iii) the slightly lighter red in the very southwest limit of the map, which represents the Encantadas Complex. To the north, it is possible to observe the subdivision of the Porongos unit in the Capané Antiform area, highlighted by the mixed light-purple, deep-red and pale-green NE-trending stripes that represent the CAC and the so-called Porongos II (sensu Höfig et al., 2017) tectonic interleaving. The dark-blue, northwest portion of the map represents younger sedimentary cover.

4.2 Sample descriptions and microprobe results

A representative set of VCC samples used for estimates of metamorphic conditions consists of a weakly migmatitic spinel-cordierite-garnet-biotite paragneiss collected from D_1 flat-lying fabric; an orthopyroxene-biotite tonalitic orthogneiss and a sample of mylonitic clinopyroxene-biotite syenite (dry high-strain zone mylonitic syenite of De Toni et al., 2016), both from the steeply-dipping D_2 fabric. The staurolite-garnet mica schist from the Cerro da Árvore Complex was studied for comparison purposes, and a second sample from the same outcrop was additionally described since it presents apparent contact metamorphism effects.

4.2.1 VCC spinel-cordierite-garnet-biotite paragneiss

The pelitic paragneiss (sample MN12C, see location in Fig. 2a) shows discontinuous banding marked by mm-thick bands and lenses of quartz + feldspar (± garnet), which alternate with cm-thick garnet-bearing, biotite-rich bands (indicated as S in Fig. 5a). A discrete, cm-spaced, second foliation (indicated as C in the same figure) locally drags the main banding. The second foliation is often marked by igneous-texture quartz-feldspathic material interpreted as leucosome. The leucosome transits between the two foliations which suggests synkinematic melt mobility. The contemporaneity of the two foliations characterizes them as an S-C pair indicative of top-to-the-NW kinematics, in agreement with other kinematic indicators reported to D_1 (Martil et al., 2011, 2017; Martil, 2016; De Toni et al., 2016).

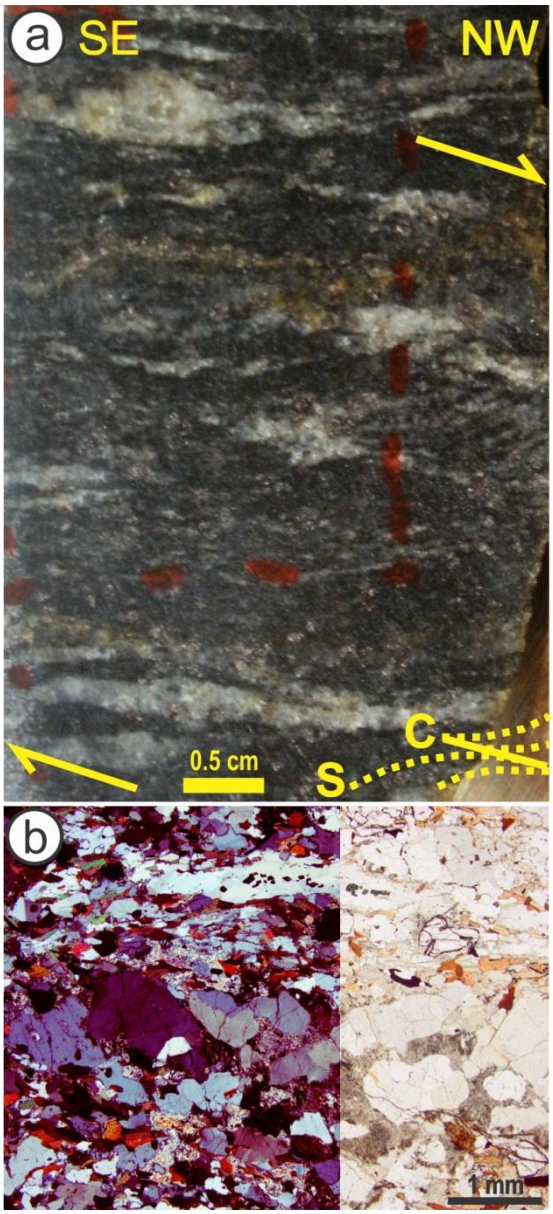

Figure 05 – VCC metapelite (MN12C) petrographic features. (a) Handsample overview. Metamorphic fabric is enhanced by leucocratic bands with igneous texture, interpreted as leucosome. Leucosome is distributed into a S-C fabric, indicating top-to-the-NW movement, as shown in the sketch. (b) Microscopic overview with crossed (left) and plane polarizers (right). Textural and compositional heterogeneity of the main banding may be observed.

The compositional banding of pelitic gneiss is spaced by less than 1 mm and given by alternating leucosome and melanosome bands (Fig. 5b), the latter showing different proportions of mafic minerals (biotite, cordierite and garnet). Mineral chemistry results are presented in table 1.

Lepidoblastic biotite flakes are less than 250 µm in size, aligned in the main banding and defining the main folation (Fig. 6a). Round biotite crystals form inclusions in garnet and cordierite. Accessory ilmenite is found in close spatial association with biotite. Biotite compositional parameters range from Al = 3.15 to 3.27 a.p.f.u. and X_{Mg}

(Mg/Mg+Fe) = 0.33 – 0.37. Composition of biotite as inclusions or in the main fabric does not vary.

Garnet porphyroblasts (up to 1.5 mm in size – Fig. 6a) are widespread, and their boundaries are either irregular or straight against the melanosome matrix minerals (Fig. 6a and 6b). Some melanosome garnets show embayed contacts with cordierite (Fig. 6b). Mineral inclusions in garnet are aligned with the matrix main foliation (Fig. 6a). Garnet composition (Table 1) recalculated to end-members is in the range of almandine 0.82 – 0.84, pyrope 0.10 – 0.13, grossular 0.03, and spessartine 0.02 – 0.03, independent of crystal size or position in the sample. No significant compositional zoning was observed in the analysed crystals.

Cordierite porphyroblasts up to 2 mm large are found in some melanosome bands as elongate grains and aggregates (Fig. 6a to c) or as more equant grains along leucosome bands (Fig. 5b). Cordierite crystals from leucosome are strongly pinitized, whilst melanosome cordierite is usually not. Marginal recrystallization is locally observed. Cordierite in melanosome contains 30 – 100 µm large inclusions of green spinel (Fig. 6b and c). Spinel forms well-aligned, elongate (Fig. 6a and b) or equant, randomly oriented crystals (Fig. 6c, both interpreted as intergrowths. The cordierite also encloses aligned biotite inclusions, which is interpreted to result from growth over pre-existing biotite-rich matrix (Fig. 6a and b). In the studied sample, sillimanite was only observed as relict aggregates included in cordierite (Fig. 6c inset), whereas other metasedimentary samples from VCC exhibit sillimanite as a main constituent (Gross. et al., 2006; Bom et al., 2014; Philipp et al., 2016b).

Spinel is found only as inclusions in cordierite and never as independent phase in the matrix. This feature is not specific of the studied sample, but is rather common and referred by many authors for the VCC metasedimentary rocks (e.g. Gross et al., 2006; Philipp et al., 2016b). The observed intergrowth is similar to the silica-defficient spinel-bearing ocellae described by Harris and Holland (1984), taken by the authors as indicative of metamorphic conditions of 750 ± 50 °C and pressures up to 4.5 Kbar. Such SiO_2-subsaturated domains were therefore considered as closed system (restricted in scale by the slow chemical diffusion of elements – see Fig. 6b) and analysed by means of compositional mapping (similar to the approach adopted by Tajcmanová et al., 2007) in order to obtain system compositions suitable for modelling of stabilization of the cordierite + spinel assemblage. Cordierite X_{Mg} values are between 0.53 and 0.57, whereas spinel shows constant X_{Mg} of 0.12.

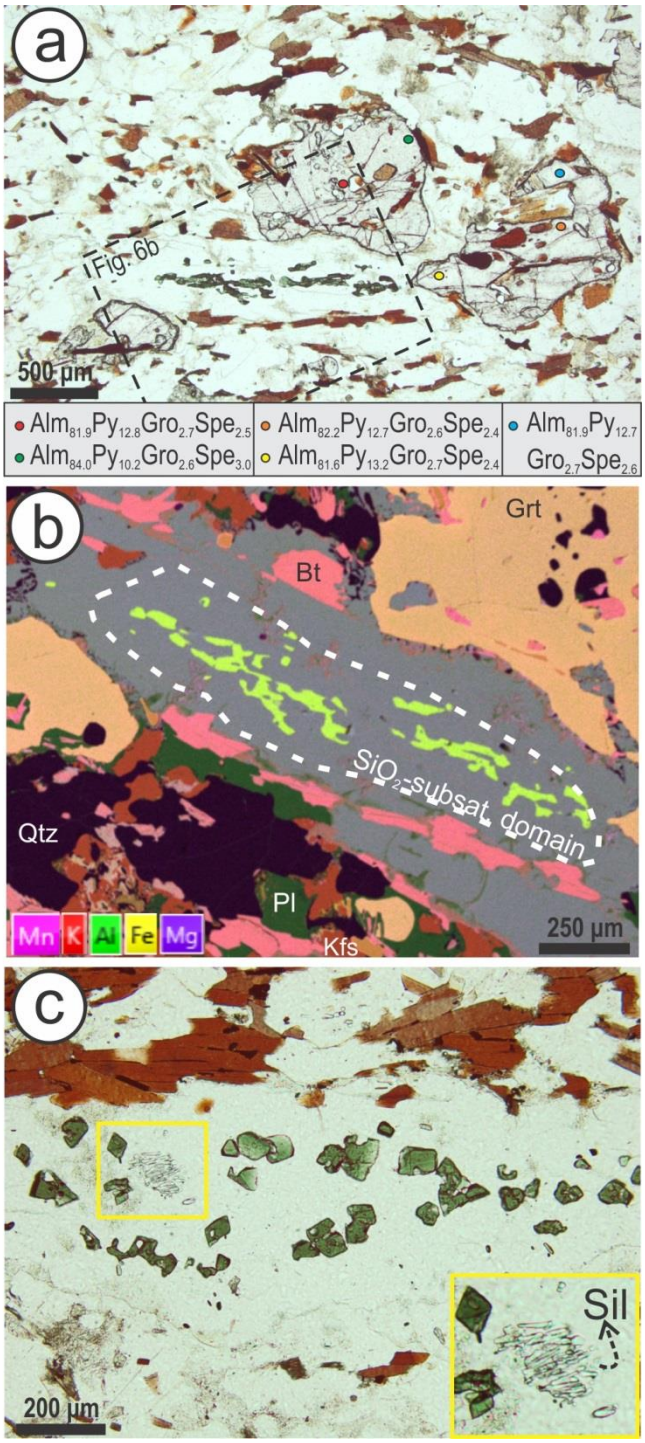

Figure 06 – VCC metapelite (MN12C) melanosome aspects. (a) Garnet and cordierite porphyroblasts with round inclusions of biotite and quartz, and subhedral, well-aligned green spinel, respectively. The dashed rectangle shows the area of the compositional map presented in figure 6b. The coloured dots mark the microprobe analysed points, with the respective composition indicated in the legend. Plan-polarized light. (b) SEM-EDS compositional map from a SiO2-subsaturated domain. The main minerals are represented by different colors and labelled. The white dashed line represents the area for which was estimated the system composition. Color code is indicated. (c) Cordierite porphyroblast including subhedral spinel and fine-grained sillimanite aggregate. Plan-polarized light.

4.2.2 VCC orthopyroxene-biotite tonalitic orthogneiss

Sample TM38C is dark-gray, fine-grained (≤ 0.5 mm) and well foliated tonalitic orthogneiss, as described in detail by Martil et al. (2011, 2017). The rock contains plagioclase with locally preserved igneous relicts of subhedral shape and mostly recrystallized granoblastic grains ≤ 0.1 mm (Fig. 7a); quartz, mostly as small, undeformed granoblastic grains; well-aligned biotite, sometimes in aggregates; and orthopyroxene, 0.2 – 0.5 mm skeletal or poikiloblastic (Fig. 7b). Ilmenite occurs as accessory phase.

The mineral chemistry results are summarized in Table 2. Plagioclase composition is anorthite 0.44 – 0.47, albite 0.50 – 0.53 and orthoclase 0.01 – 0.02, independent of grainsize or texture. Orthopyroxene shows even more regular composition, with enstatite 0.43 – 0.45 and ferrosilite 0.53 – 0.57. Biotite shows X_{Mg} values between 0.46 and 0.50.

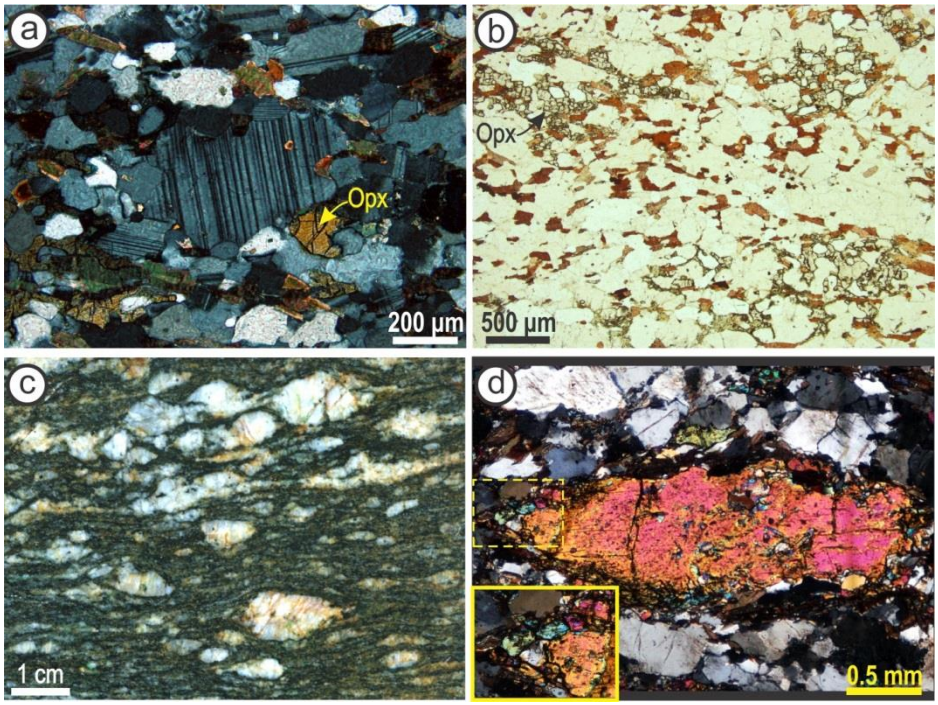

Figure 07 – VCC tonalithic orthogneiss (TM38C – a,b) and syntectonic syenite (GJ02B – c,d) petrographic features. (a) Typical aspect of a plagioclase porphyroclast partially recrystallized, surrounded by the polygonal metamorphic matrix containing orthopyroxene (indicated), biotite, quartz and plagioclase. Cross-polarized light. (b) Microscopic overview, with orthopyroxene (indicated) occurring as skeletal or poykiloblastic crystals overgrowing the matrix. Plan-polarized light. (c) Syntectonic syenite handsample aspect, with a well-defined mylonitic foliation characterized by stretched minerals and well-aligned biotite in the matrix, which surrounds assymetric K-feldspars porphyroclasts. (d) Clinopyroxene porphyroclast surrounded by mylonitic foliation. The dashed rectangle shows enlarged area of clinopyroxene recrystallization tail.

4.2.3 VCC clinopyroxene-biotite mylonitic syenite

The Arroio das Palmas Syenite shows strong mylonitic foliation parallel to the igneous fabric preserved in low-strain zones. The typical mylonite formed over the APS in dry high-strain zones (i.e. absent of late-magmatic fluids – see De Toni et al., 2016 for details) has variable amount of K-feldspar porphyroclasts in a mafic-rich matrix with biotite + clinopyroxene (Fig. 7c). Progressive recrystallization of K-feldspar porphyroclasts in dextral asymmetric tails leads to the formation of lens-like granoblastic aggregates which alternate with mafic-rich layers and define a discontinuous banding. The studied syenite sample (GJ02B, location as in Fig. 2a) presents up to 2 cm long K-feldspar porphyroclasts with relict igneous texture. Biotite forms mm-long, well-aligned grains containing apatite and zircon inclusions. Biotite X_{Mg} is 0.59 to 0.63. Clinopyroxene forms 0.5 – 2 mm long, elongate to equant crystals, and the larger grains behave as porphyroclasts in the groundmass (Fig. 7d) with local, discrete recrystallization tails. Recrystallized grains are 0.1 mm in size and developed polygonal granoblastic texture (Fig. 7d inset). Both recrystallized and relict grains show the same composition (Wo 0.45, En 0.38, Fs 0.17, with XMg 0.69 to 0.70 – microprobe data from De Toni et al., 2016).

4.2.4 CAC garnet-staurolite-quartz-muscovite schist

The garnet-staurolite-quartz-muscovite schist (sample MAB52A – Fig. 8a) is one of the metapelitic rocks from the Cerro da Árvore Complex. Muscovite-rich and quartz-rich layers alternate along the main schistosity, with the latter showing discontinuous, lens-like geometry and the former bearing staurolite (up to 2 mm – Fig. 8b) and garnet (3 to 5 mm – Fig. 8c and 8d) porphyroblasts. The compositional bands are interpreted either as a partially transposed, relict sedimentary layering or pre- to syn-kinematic veins. The regional schistosity dips 5° to 30°, mainly to NE, and sometimes contains a slightly oblique mineral lineation marked by muscovite trails or staurolite, and more rarely quartz stretching lineation.

Muscovite makes up to 50% of the rock volume. The crystals are about 0.5 mm long and strongly aligned in the schistosity plane.

Garnet porphyroblasts are in general up to 5 mm equant crystals (Fig. 8c and d). Garnet porphyroblasts commonly show quartz and ilmenite inclusion trails marking an internal foliation which curved shape and alignment marked the rotation of the garnet relative to the external matrix foliation during growth (Fig. 8d).

Staurolite porphyroblasts are numerous along certain foliation levels, as shown in figure 8b. They are strongly to completely replaced by fine-grained white mica pseudomorphs (*ca.* 2 mm), but many of them still preserve an unaltered core region (up to 1 mm), where staurolite is recognizable (Fig. 8b inset).

Quartz layers have irregular thickness and lens-like shape. Crystals are 0.05 to 0.3 mm long, many of them equant and polygonal.

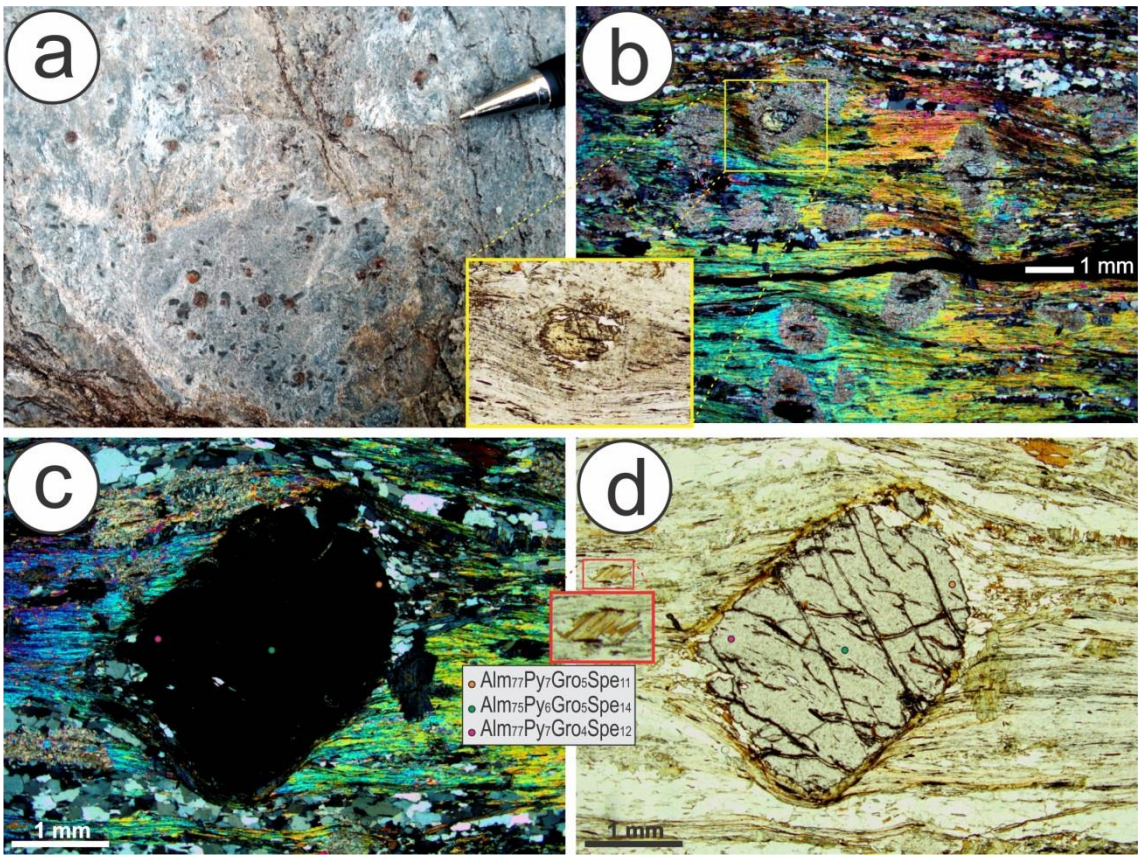

Figure 08 – CAC garnet-staurolite-mica schist (MAB52A) petrographic features. (a) Mesoscopic aspect in XY view at outcrop subhorizontal surface, with garnet (red) and staurolite (black) mm-size porphyroblasts in a muscovite-rich layer. (b) Microscopic overview of a staurolite-rich layer with cross-polarized light. Inset for partially replaced staurolite porphyroblast with characteristic golden yellow pleochroism, at plane-polarized light. (c) and (d) Garnet porphyroblast presenting synkinematic features at cross-polarized and plane-polarized light, respectively. Microprobe point analysis are marked by collored spots and the results are presented as calculated end-members.

Muscovite is commonly overgrown by biotite aggregates which crosscut the main schistosity (Fig. 8d inset). Chlorite is a late- to post-kinematic phase, and it overgrows the main schistosity as up to 1 mm-large, radial aggregates (as observed on the right-hand side of the garnet porphyroblast of figures 8c and 8d).

Kinematic indicators observed on XZ-parallel sections include discrete shear bands (Fig. 8b), rotated garnet porphyroblasts with internal foliation (Fig. 8d) and asymmetric pressure shadows containing mainly quartz (Fig. 8c), and sheared mica

aggregates (Fig. 08d inset). All kinematic indicators consistently point towards an oblique, tangential, dextral with top-to-the-SE sense of shear. On the other hand, observations from a sample collected in a neighbouring outcrop, presented opposite shear sense. Detailed structural mapping is still missing in this area.

MAB52A mineral chemistry is presented in Table 3. Garnet shows consistent zoning, with core composition almandine 0.73 to 0.75, spessartine 0.14 to 0.16, grossular 0.05 to 0.06, pyrope 0.06, and rims composed of almandine 0.76 to 0.77, spessartine 0.11 to 0.12, grossular 0.04 to 0.05, pyrope 0.06 to 0.07. Staurolite X_{Mg} is regularly between 0.11 and 0.13. Muscovite Si apfu is between 3.0 and 3.1, while biotite X_{Mg} is around 0.38.

4.3 PT estimates

Thermodynamic modelling of the samples described was performed using Perple_X 6.7.0 software (Connoly, 2005, version 6.7.0) in order to evaluate pressure and temperature conditions of observed metamorphic parageneses in each studied sample. The employed, internally consistent thermodynamic dataset is from Holland and Powell (1998; 2004 upgrade), with additional mixing models for feldspar (Fuhrman and Linsdley, 1988), pyroxene (Holland and Powell, 1996), muscovite (Coggon and Holland, 2002), biotite (Tajcmanová et al., 2009), chlorite (Holland et al., 1998) and melt (Holland and Powell, 2001; White et al., 2001).

4.3.1 Peak metamorphic conditions for VCC

Calculated P-T pseudosection using the whole-rock composition of sample MN12C (Fig. 9) indicates that the assemblage Bt + Crd + Grt + Qtz + Kfs + Pl + melt is stable approximately from 3.5 to 4.8 Kbar, and in the temperature range of 760 – 830°C. The presence of ilmenite is predicted at slightly higher temperature or lower pressure. Spinel was observed only as inclusions in cordierite grains in this sample, which is in agreement with the absence of this mineral in the calculated pseudosection, as it is apparently not in equilibrium with the matrix mineral assemblage. The same is valid for sillimanite, so the resulting matrix mineral assemblage is sillimanite-free. Isopleths for garnet end-members almandine (0.76 – 0.766 are the highest modelled values), pyrope (0.10 – 0.14), spessartine (0.025 – 0.03) and for XMg values of cordierite (0.52 – 0.54) and biotite (0.33 – 0.36) overlap in an interval around 790 – 820°C at 4.4 – 4.8 Kbar. The model does not predict

almandine content higher than 0.77, although the range 0.82 to 0.84 was measured in the sample.

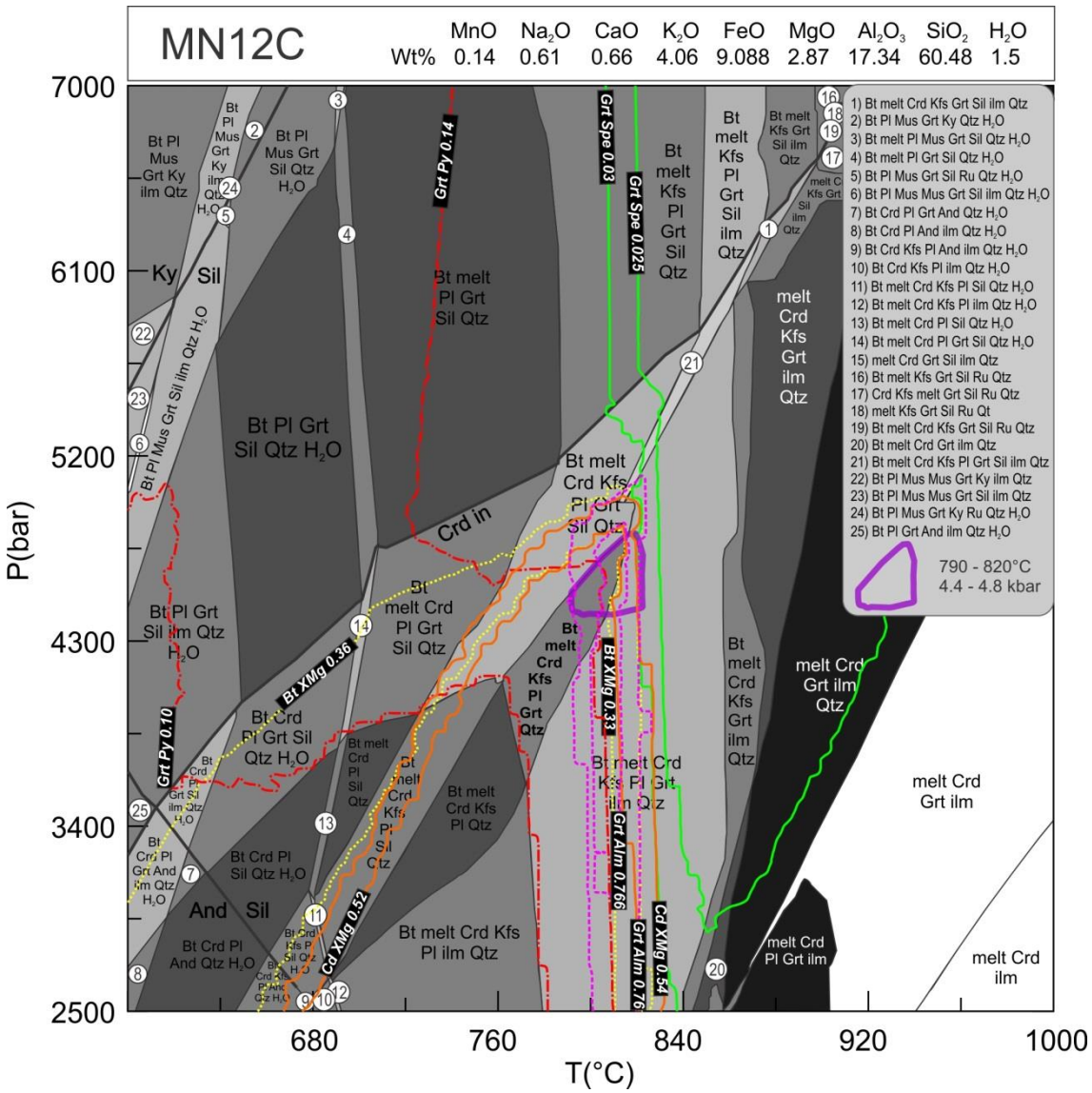

Figure 09 – VCC migmatitic metapelite (MN12C) pseudosection. The system chemical composition is shown in the upper bar. Main mineral stability fields are labeled and the observed assemblage (Bt+melt+Crd+Kfs+Pl+Grt+Qtz) is in bold letters. Smaller fields are labeled according to the numerical legend. Colored isopleths define an overlapping area correspondent to 790 – 820°C and 4.4 – 4.8 Kbar. Isopleths: red for garnet pyrope 0.10 – 0.14; pink for garnet almandine 0.76 – 0.766; orange for cordierite XMg 0.52 – 0.54; and yellow for biotite XMg 0.33 – 0.36. The curves for cordierite-in and the aluminum-silicate pseudomorph curves are also shown.

The P-T pseudosection calculated for sample TM38C (Fig. 10) predicts the stability of Opx-bearing assemblages at temperatures above ca. 780°C at variable pressures. Isopleths for anorthite content in plagioclase (0.45 – 0.47) and X_{Mg} for biotite (0.47 – 0.50) and orthopyroxene (0.43 – 0.46) overlap in the Opx+Bt+Kfs+Pl+Ilm+Grt+Qtz+melt stability field, which matches the assemblage

observed in the sample, except for the predicted stability of garnet. However, the modelled volume of garnet is small (ca. 2%) and its predicted stability probably represents some inaccuracy in the bulk composition determination. Stable mineral assemblage and composition of mineral phases indicate temperature conditions of equilibrium at ca. 810 – 865°C, whereas pressure conditions are uncertain.

Temperature conditions of solid-state deformation of the Arroio das Palmas Syenite were also established from a P-T pseudosection calculated for the whole rock composition of sample GJ02B (Fig. 11). The composition of biotite (X_{Mg} = 0.62 – 0.63) and clinopyroxene (X_{Mg} = 0.69 – 0.70) suggest temperatures of recrystallization of ca. 840 – 910°C, without pressure control.

4.3.2 VCC exhumation conditions

The crystallization of spinel in sample MN12C was modelled by using an estimated bulk composition of the cordierite + spinel domain (area shown in Fig. 6b). The observed cordierite + spinel intergrowth is a typical feature of rapid decompression in high-grade metasediments (e.g. Harris and Holland, 1984; Bindu, 1997; Johnson et al., 2004). Additionally, the embayed contact with garnet (Fig. 6b) and rare sillimanite aggregates included in corderite (Fig. 6c) point to the possibility of these minerals acting as reactants for the spinel-forming reaction, as proposed by Mezger et al. (2008):

$$Sil + Grt = Crd + Sp \quad (1)$$

The model (Fig. 12) predicts the stabilization of spinel below *ca.* 3.7 – 6.0 Kbar depending on the metamorphic temperature, in a wide PT field of the equilibrium assemblage Crd + Sp + Grt + Sil + Kfs. The isopleths for X_{Mg} of cordierite (0.56) and X_{Mg} spinel (0.87) and an additional curve corresponding to 1 vol.% of sillimanite suggest stabilization of spinel at *ca.* 660 to 680°C and 2.5 to – 3.4 Kbar (Fig. 12).

The evolution of modal composition of the domain was modelled systematically with decreasing pressure and temperature. Close to the estimated whole-rock peak metamorphic conditions (800°C/4.6 Kbar), the estimated volume % of the minerals are $Crd_{58.34}Sp_{2.67}Grt_{20.5}Sil_{17}Kfs_{1.4}$, whereas at the estimated equilibration conditions of 680°C and 3 Kbar the volume proportions change to $Crd_{88}Sp_{8.5}Grt_{1.5}Sil_{0.72}Kfs_{1.2}$. Decrease in volume of garnet and sillimanite and increase in volume of cordierite and spinel are in agreement with the proposed reaction (1). Small amounts of modelled K-feldspar are interpreted as an artificial effect caused by of small amounts of

potassium from biotite in the compositional mapped area together with modelling under anhydrous conditions.

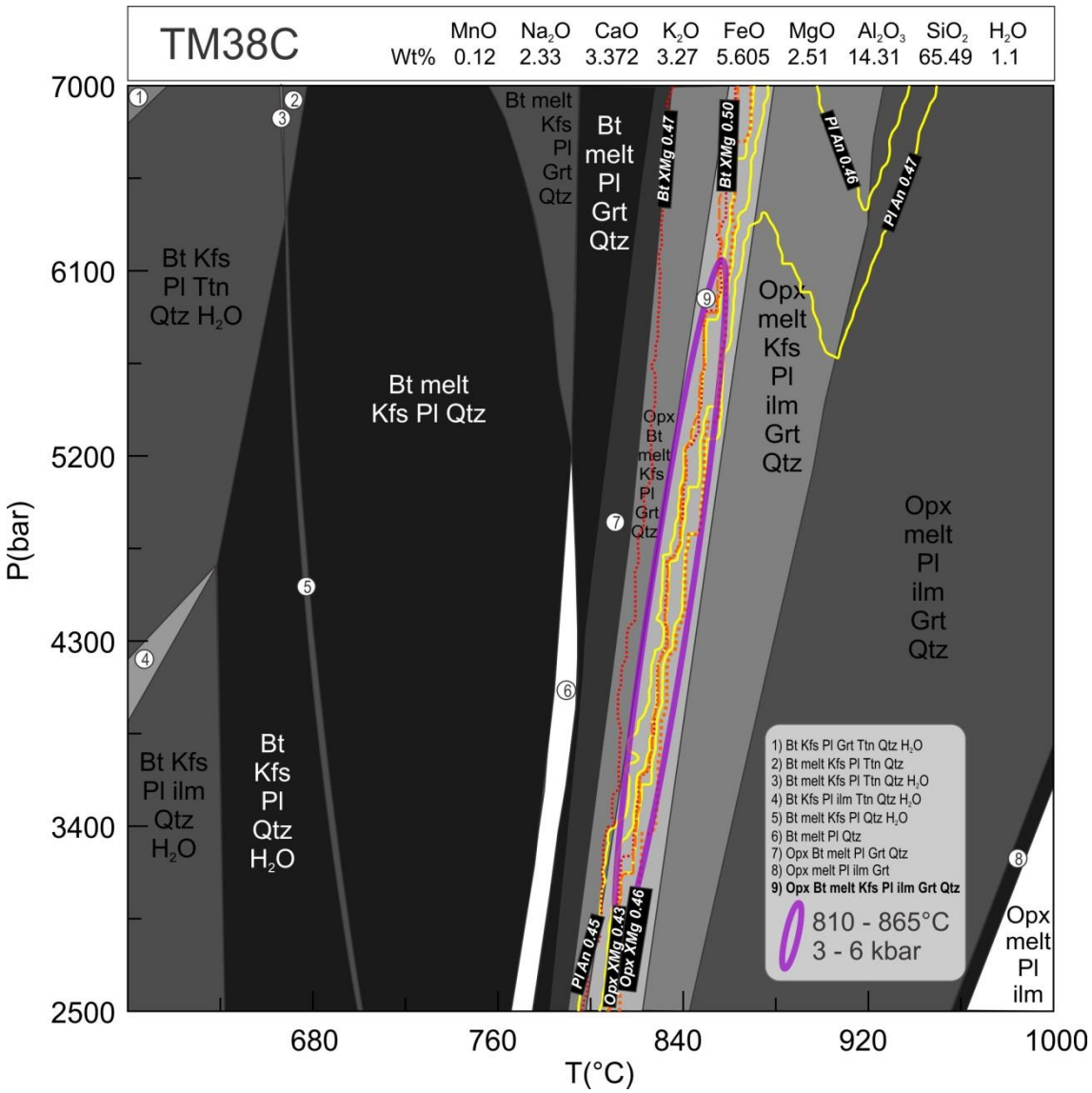

Figure 10 – VCC tonalithic orthogneiss (TM38C) pseudosection. The system chemical composition is shown in the upper bar. Mineral stability fields are labeled and smaller fields are labeled according to the displayed numerical legend, including the observed mineral assemblage (Opx+Bt+melt+Kfs+Pl+ilm+Grt+Qtz), in bold letters. Colored isopleths define a narrow, very inclined overlapping area correspondent to 810 – 865°C and 3 – 6 Kbar. Isopleths: yellow for plagioclase anorthite content 0.46 – 0.47; red for biotite XMg 0.47 – 0.50; orange for orthopyroxene XMg 0.43 – 0.46.

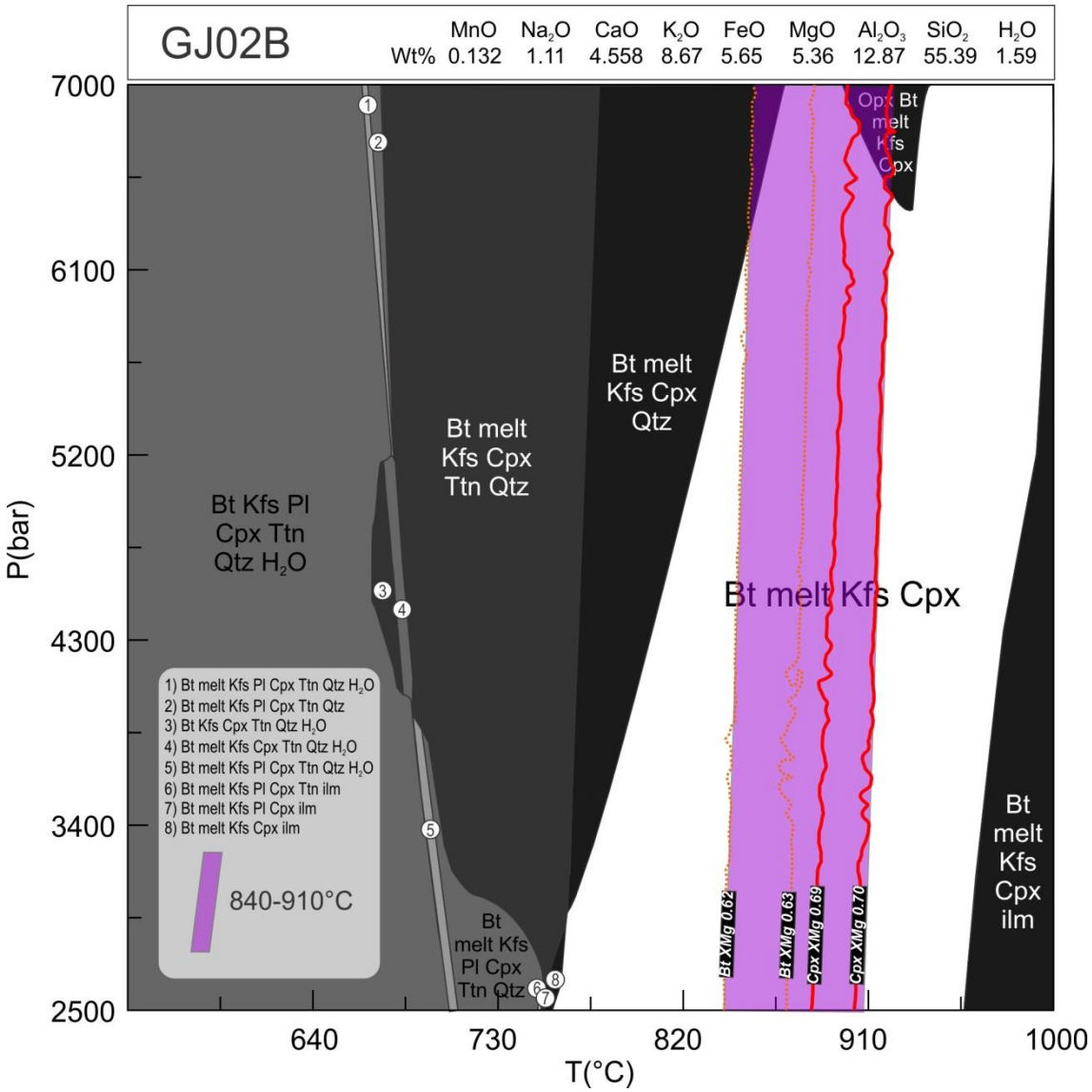

Figure 11 – Syntectonic syenite (GJ02B) pseudosection. The system (rock) chemical composition is shown in the upper bar. Mineral stability fields are labeled and smaller mineral stability fields are labeled according to the displayed numerical legend. The observed mineral assemblage (Bt+melt+Kfs+Cpx) define a wide field (in white). Colored isopleths define a partially overlapping area (purple stripe) which corresponds to deformation temperatures of 840 – 910°C. Isopleths: orange for biotite XMg 0.62 – 0.63; red for clinopyroxene XMg 0.69 – 0.70.

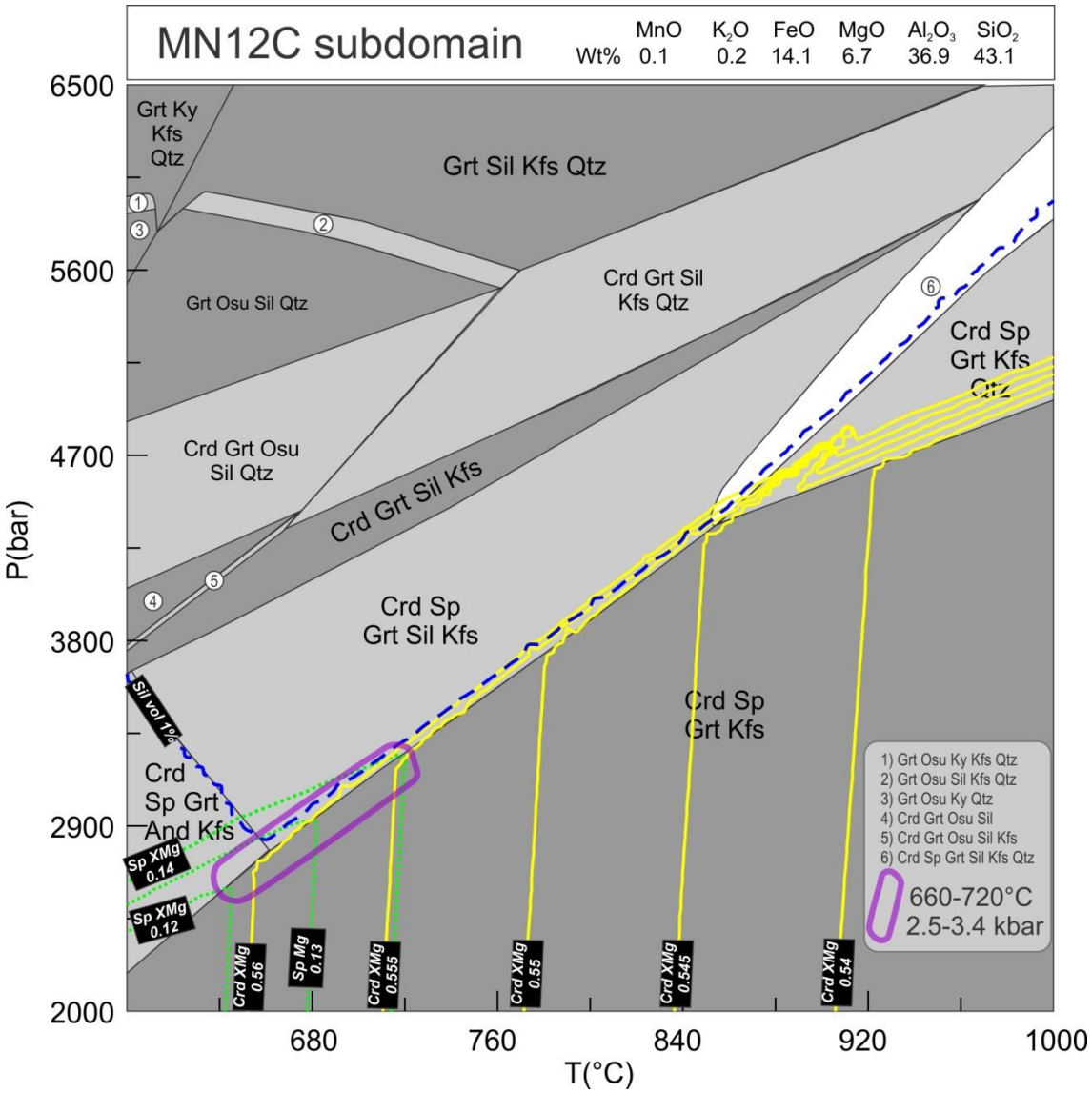

Figure 12 – VCC migmatitic metapelite (MN12C) SiO2-subsaturated domain pseudosection. The system chemical composition, taken from the compositional mapping from figure 05d, is shown in the upper bar. Main mineral stability fields are labeled and smaller fields are labeled according to the displayed numerical legend. The observed mineral assemblage (Crd+Sp+Grt+Sp+Kfs) define a wide field. Colored isopleths and the additional curve for sillimanite modal 1 % (blue dashed line) define a very small area, indicated by the purple ellipse and correspondent of 660 – 720°C and 2.5 – 3.4 Kbar. Isopleths: green for spinel XMg 0.12 – 0.14; yellow for cordierite XMg 0.54 – 0.56.

4.3.3 CAC progressive metamorphic conditions

The pseudosection for the garnet-staurolite-quartz-mica schist (MAB52A) presented in figure 13 was calculated using H_2O-saturated conditions. The composition of garnet cores with almandine 0.73 – 0.74 and spessartine 0.14 – 0.15 points to early growth of garnet at 555 – 565°C and 5.4 – 5.7 Kbar (Fig. 13). Further growth of garnet rims, with composition of almandine 0.76 – 0.77, spessartine 0.11 – 0.12 and grossular 0.04 – 0.05, occurred in stability with the metamorphic matrix, which contains staurolite of X_{Mg} 0.11 – 0.13, muscovite with Si apfu higher than 3.00, and

biotite with X_{Mg} about 0.38. The abovementioned isopleths partially overlap, constraining an area of the pseudosection which corresponds to 560 – 580°C and 5.8 – 6.3 Kbar (Fig. 13). The PT difference estimated from garnet core to rim is interpreted in terms of progressive metamorphic conditions.

4.3.4. Thermal effects of younger intrusions

Discrete roughly N-S fractures in the CAC metapelites contain up to 10 cm-long andalusite (Fig. 14a), as first described by Lenz (2006). These andalusite crystals present prismatic, subhedral shape, inclusions prefferentialy along central portion and diagonals of the transversal section, which presents a nearly square shape, two cleavage directions and low birefringence (Fig. 14b) as characteristic features of the andalusite mineral species (Deer et al., 1992). Staurolite inclusions are preserved from replacement by white mica.

CAC metapelite andalusites are interpreted to have formed during fluid-related contact metamorphism induced by the EG emplacement. According to the pseudosection (Fig. 13), andalusite stabilized in the schist composition (MAB52A) below 4.1 Kbar for *ca.* 580°C. The occurrence of andalusite as a later phase in CAC rocks points to the fact that this unit was brought to low pressures (andalusite stability field), during or before the emplacement of the Encruzilhada Granite, which occurred before retrogressive replacement of staurolite by white mica.

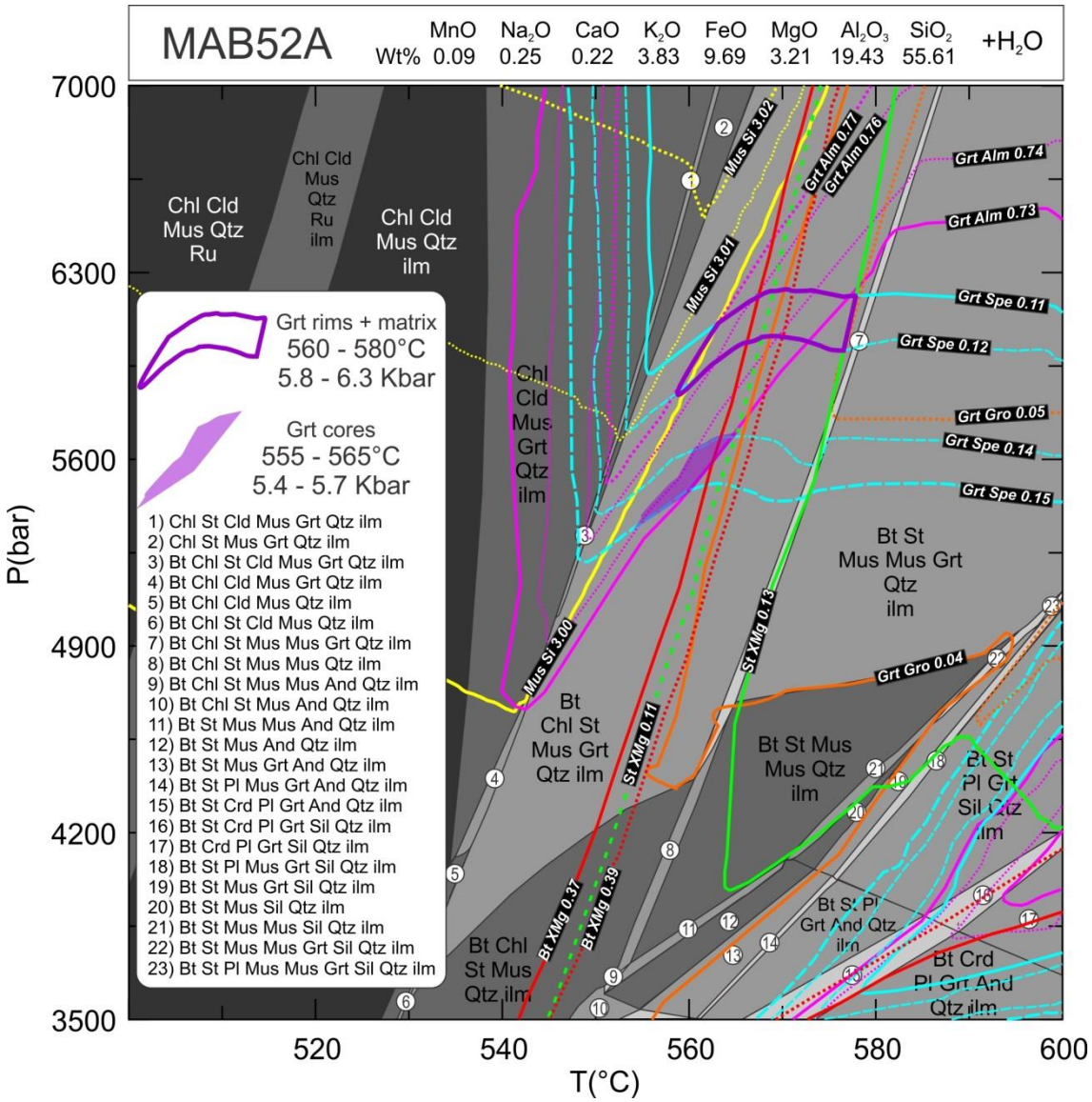

Figure 13 – CAC Staurolite-garnet-quartz-muscovite schist (MAB52A) pseudosection. The system is water-saturated and the composition is shown in the upper bar. Main mineral stability fields are labeled and smaller fields are labeled according to the numerical legend. Observed mineral assemblage (Bt+Chl+St+Mus+Grt+Qtz+ilm) defines the central polygon. Crossing colored isopleths defined two distinct metamorphic conditions. Garnet cores (smaller, purple area), with spessartine 0.14 – 0.15 and almandine 0.73 – 0.74 records 555 – 565°C and 5.4 – 5.7 Kbar early growth. Garnet rims with spessartine 0.11 – 0.12, almandine 0.73 – 0.77 and grossular 0.04 – 0.05, together with staurolite XMg 0.11 – 0.13, biotite XMg 0.37 – 0.39 and muscovite Si apfu 3.00 from the matrix, define an wider polygon (thicker purple contour) which points to 560 – 580°C and 5.8 – 6.3 Kbar as peak metamorphic conditions.

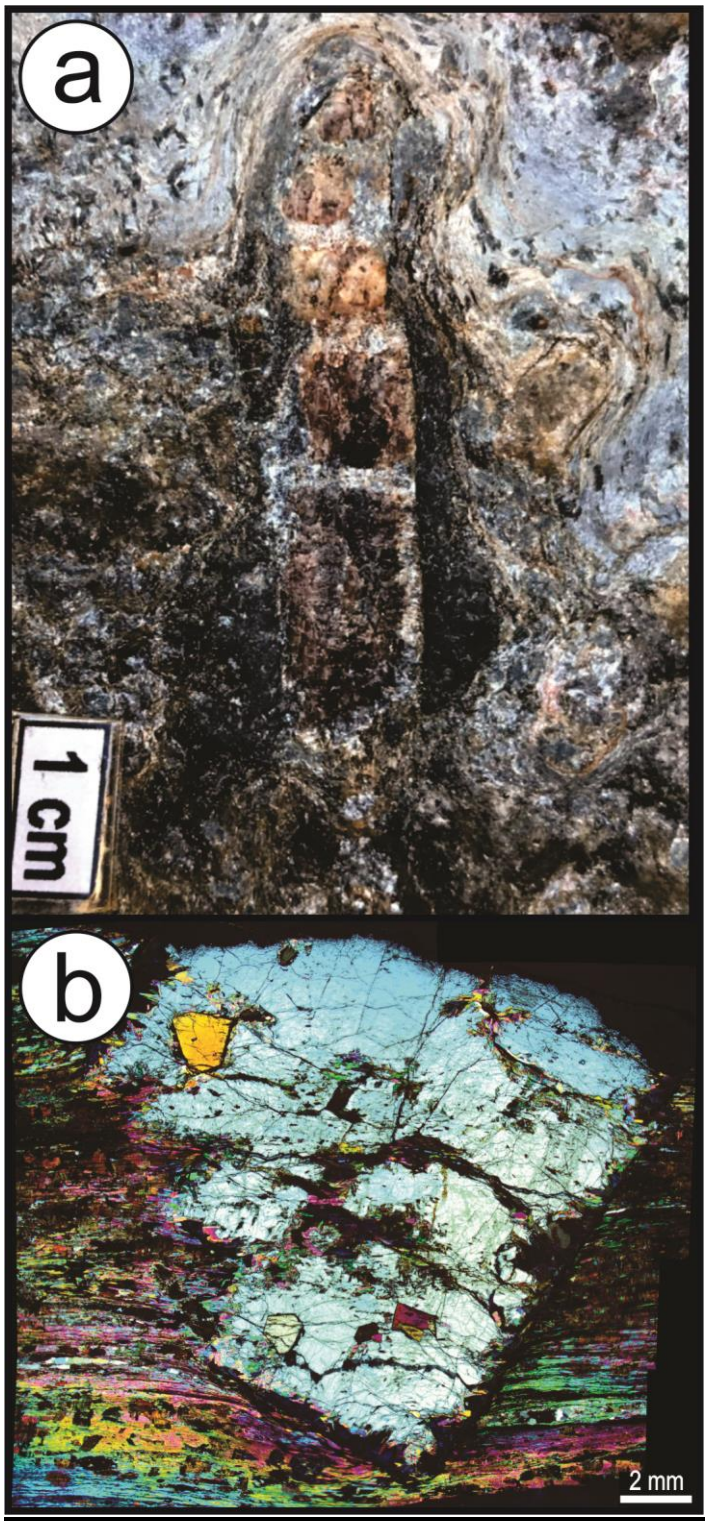

Figure 14 – Post-kynematic andalusite growth on CAC garnet-staurolite mica schist due to intrusion of the Encruzilhada Granite. (a) Cm-scale andalusite formed along fracture in Cerro do Facão metapelite. Note the basal partition. (b) Microscopic overview (photomicrographic mosaic) at cross-polarized light, respectively. The almost square basal section is well developed, as well as two cleavages, both characteristics of andalusite. Staurolite crystals included are preserved from replacement.

5. DISCUSSIONS

5.1 Correlation between Várzea do Capivarita and Cerro da Árvore complexes

The correlation between the VCC orthogneisses and CAC metavolcanics is Martil et al. (2017), who compared their geochemical composition and suggested that they shared similar protoliths. Both rock associations were classified as medium- to high-K calc-alkaline rocks and interpreted to have formed in *ca.* 800 – 780 Ma, mature continental arc conditions (Martil et al., 2011; 2017; Martil, 2016; Battisti et al., 2018).

The comparison was reinforced by Gruber et al. (2017a, b), who presented provenance data from metasedimentary rocks of both units with similar maximum depositional age, as well as identical Mesoproterozoic and Paleoproterozoic source areas. The metamorphic ages of both units are also similar (*ca.* 660–640 Ma – Lenz, 2006; Martil, 2016; Chemale Jr. et al., 2011). The younger VCC ages of ca. 620 Ma (Philipp et al., 2016b) and 626 - 604 Ma (Gross et al., 2006) are reinterpreted. The first one is a migmatization age, and therefore representative of the thermal relaxation period that follows the main collision (e.g. Weinberg, 2016). The second is thought to be a consequence of the later closure of the garnet Sm-Nd system due to prolonged high temperature conditions related to high-T metamorphism, migmatization and recurrent magmatic activity of the area. Therefore, both values possibly represent slightly younger ages than that of collisional peak metamorphism.

Recently, Battisti et al. (2018) presented a structural evolution of the CAC metavolcanic rocks near the EB NW margin and compared it with the evolution of the VCC orthogneisses. Both complexes show an original flat-lying metamorphic foliation (S_1) that dips to the east and bears a highly oblique stretching lineation (L_1). The foliation is asymmetrically folded with vergence towards the west. Along steeply-dipping short limbs, a strike-slip domain is established, and a subvertical mylonitic foliation (S_2), with subhorizontal lineation (L_2), is developed. Battisti et al. (2018) interpreted such evolution as progressive transpressional deformation (in the sense of Jones et al., 2004, and references therein) recorded in both complexes. The dextral character of the strike-slip movement is well documented in the VCC (Martil et al., 2011, Martil, 2016 and De Toni et al., 2016), but it is not that clear in the CAC metavolcanics so far (Battisti et al.., 2018).

A summary of the main geological features of the two units is presented in Table 4. These features show that the VCC and CAC are correlative in terms of igneous activity (geochemical affinity and age), sedimentation (source areas and timing of deposition), deformational pattern (transpressional D_1 top-to-W progressively

partitioned into D_2 strike-slip domains) and peak metamorphic age (*ca.* 660–640 Ma). The dataset suggests that VCC and CAC protoliths were deposited in a correlated environment which may be interpreted as a single basin or similar basins, as also argued by Battisti et al. (2018). In contrast, both complexes show very different metamorphic conditions, with high-T/low-P granulite-facies metamorphism and migmatization in the VCC, and amphibolite-facies metamorphism in the CAC.

5.2 Contrasting PTt paths of Várzea do Capivarita and Cerro da Árvore complexes

A summary of new PT data integrated with published information (Fig. 15) demonstrates the contrasting, yet convergent, metamorphic PTt path of the two studied complexes. The overlapping conditions for para- and orthogneiss (Figs. 9 and 10) suggest peak metamorphism in the range of 790 – 865 °C at ca. 4.4 – 4.8 kbar. Temperatures may have been locally even higher due to the syntectonic emplacement of syenite magmas which record deformation conditions at ca. 900°C (Fig. 11). The timing of granulite facies peak metamorphism in the gneisses (ca. 650 Ma according to Martil, 2016) and the crystallization age of the syntectonic syenite intrusions (642 ± 10, Bitencourt et al., 2016) constrain the VCC high-T/low-P metamorphism to the 650 – 640 Ma interval.

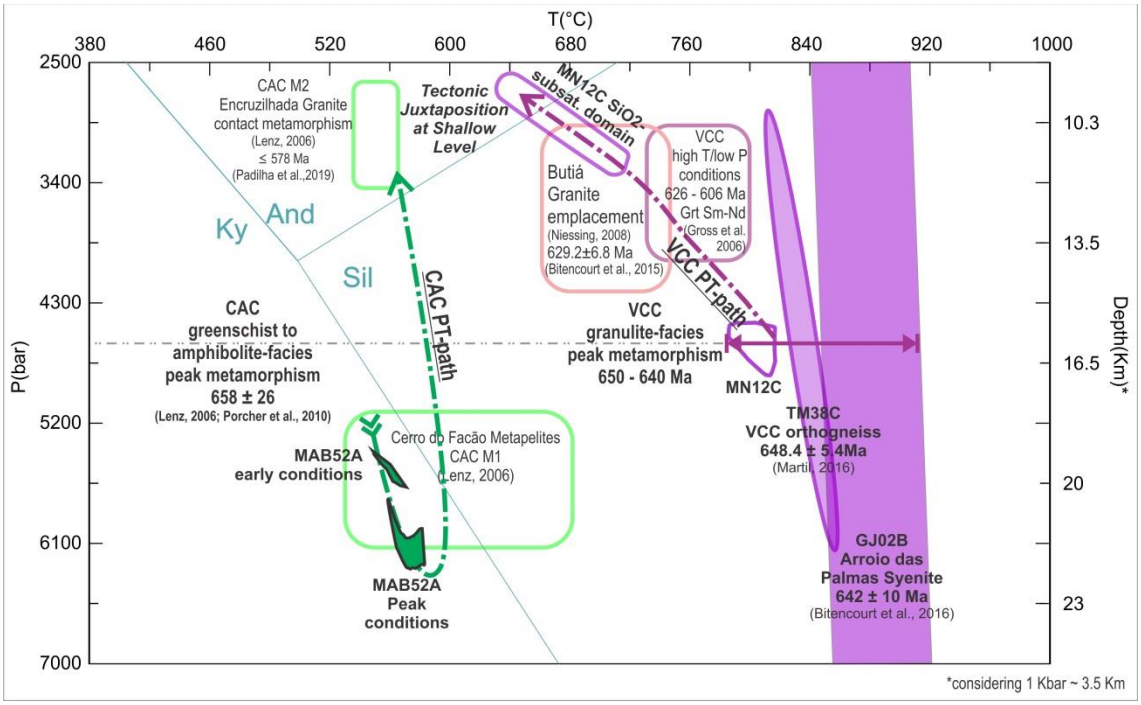

Figure 15 – Summarizing figure with all PT estimatives for VCC and CAC from this work integrated with previously published results from Gross et al. (2006), Lenz (2006) and Nieβing (2008), and ages from Martil (2016) and Bitencourt et al. (2015, 2016). PT-paths are traced with dashed lines.

Amphibolite-facies peak metamorphism is determined for the CAC rocks. Garnet cores record an early growth at 555 – 565°C and 5.4 – 5.7 kbar, with rims stable at 560 – 580°C and 5.8 – 6.3 kbar, together with the matrix assemblage. This interval is in agreement with peak metamorphic conditions estimated by Lenz (2006) for the same rocks (ca. 590°C at 5 – 6 kbar). Despite the high uncertainty of the metamorphic Rb-Sr age reported by Lenz (2006) (658 ± 26 Ma), synchronous metamorphism of the CAC and VCC at contrasting conditions would be implied.

Exhumation conditions for the VCC rocks were determined from the SiO_2-subsaturated association of cordierite + spinel ± sillimanite at 660 – 720°C and 2.5 – 3.4 kbar (Fig. 12). The results point to very shallow levels of a very hot crust during nearly isothermal decompression under high geothermal gradient. The emplacement conditions of 700 – 750 °C and 3 – 4.2 kbar determined for the associated sillimanite-bearing Butiá Granite (Niessing, 2008) are in agreement with the complex exhumation path and also plotted in figure 15. Considering the genetic link between this granite and VCC partial melting (Bom et al., 2014, Philipp et al., 2016b), and the age of the granite (629.8 ± 6.8 Ma, Bitencourt et al. 2015) we can infer that its syntectonic emplacement took place during exhumation of the VCC. If both complexes originated from two different portions of the same basin, which would be tectonically inverted, it is likely that during thrusting of the VCC rocks towards the west, its overweight affected the CAC rocks. This could be the cause of the higher pressures recorded by the underthrusted CAC peak metamorphic assemblage, with progressive burial of CAC simultaneous to VCC exhumation.

Considering the data from Martil (2007), Rivera (2019) and Padilha et al. (2019), the VCC exhumation led to the local development of metapelitic hornfelses with small andalusite crystals in xenoliths or roof pendants over the Piquiri Syenite Massif (Martil, 2007) and radial sillimanite in xenoliths in the Arroio do Silva Pluton (Padilha et al., 2019). The PSM is also responsible for obliteration of CAC metavolcanics foliation in its southwest roof pendant (Battisti et al., 2018). Overgrowth of cm-size, andalusite crystals observed along fractures of the CAC metapelites (Fig. 14) are interpreted as result from contact effect of the Encruzilhada Granite emplacement at less than 578 Ma. At this time that these late intrusives were emplaced the studied complexes were already side-by-side.

5.3 Proposed model for the origin of the Encruzilhada Block

Geothermal gradients as high as 50 to 60 °C/km registered in the VCC rocks point to a very hot collisional environment, suggestive of an attenuated pre-collisional lithosphere (Harris and Holland, 1984; Clark et al., 2011; Fowler et al., 2015; Hyndman et al., 2015). This is in sharp contrast with geothermal gradients of *ca.* 30 °C/km recorded by CAC metapelites.

Considering the similarities observed in table 04 and following the interpretation of Battisti et al. (2018), we propose that the protoliths of the VCC and CAC represent coeval and spatially close basins, if not a single one. This basin registered igneous activity at ca. 800 – 780 Ma (Martil et al., 2017; Battisti et al., 2018 and references therein) and sedimentation until at least ca. 730 Ma (Gruber et al., 2016a). In this scenario (Fig. 16a), VCC rocks represent the deeper part of this volcano-sedimentary basin in a highly-stretched continental crust under high geothermal gradient, while CAC was situated at the upper strata or at the shoulders of this rift-like, extensional environment.

At 660 – 640 Ma, the basin was inverted and the VCC was tectonically juxtaposed as a nappe (hereafter called Várzea do Capivarita Nappe – VCN) over its shallower and colder margin (CAC rocks) by west-verging transpression (Fig. 16b). The consequence of this deformation is the opposite PT-paths of both complexes, with exhumation of VCC rocks during thrusting, and tectonic burial of underthrusted CAC (Fig. 15).

Nearly isothermal decompression progressively followed Várzea do Capivarita Nappe peak-metamorphism during exhumation and thermal relaxation, with migmatization and the origin of peraluminous granites (Fig. 16c; 630 – 620 Ma), according to Philipp et al., 2016b; Bitencourt et al., 2015). This magmatism is found along the main shear zones of the SBSB (e.g. Philipp et al., 2013; Lyra et al., 2017). At this time the progressive deformation and strain partitioning activated transcurrent shear zones, and the Encruzilhada Block was limited by two of these regional discontinuities. The opposite shear sense recorded by synchronous and genetically related crustal magmatism points to the need to fit both structures in a coherent array (Lyra et al., 2017). Dextral shearing at *ca.* 630 Ma developed in the Butiá Granite and VCC rocks focused along Passo das Canas Shear Zone (Fig. 2a), and possibly also in the original western boundary of the Encruzilhada Block, affecting the CAC rocks (Fig. 16d), as interpreted from CAC dextral drag folds by Jost (1981). Movement along pervasive steeply-dipping, NNW-striking S_2 foliation, bearing sub-horizontal L_2,

possibly helped Várzea do Capivarita Nappe exhumation. The DCSZ has focused the sinistral shear southeast of the EB, starting with the *ca.* 635 Ma Quitéria Granite and followed by the 625 – 605 Ma Cordilheira Suite (Knijnik, 2018). A relative movement component of the EB to the south, at 630 – 610 Ma, is apparently necessary in order to keep strain compatibility, as pointed by Lyra et al. (2017).

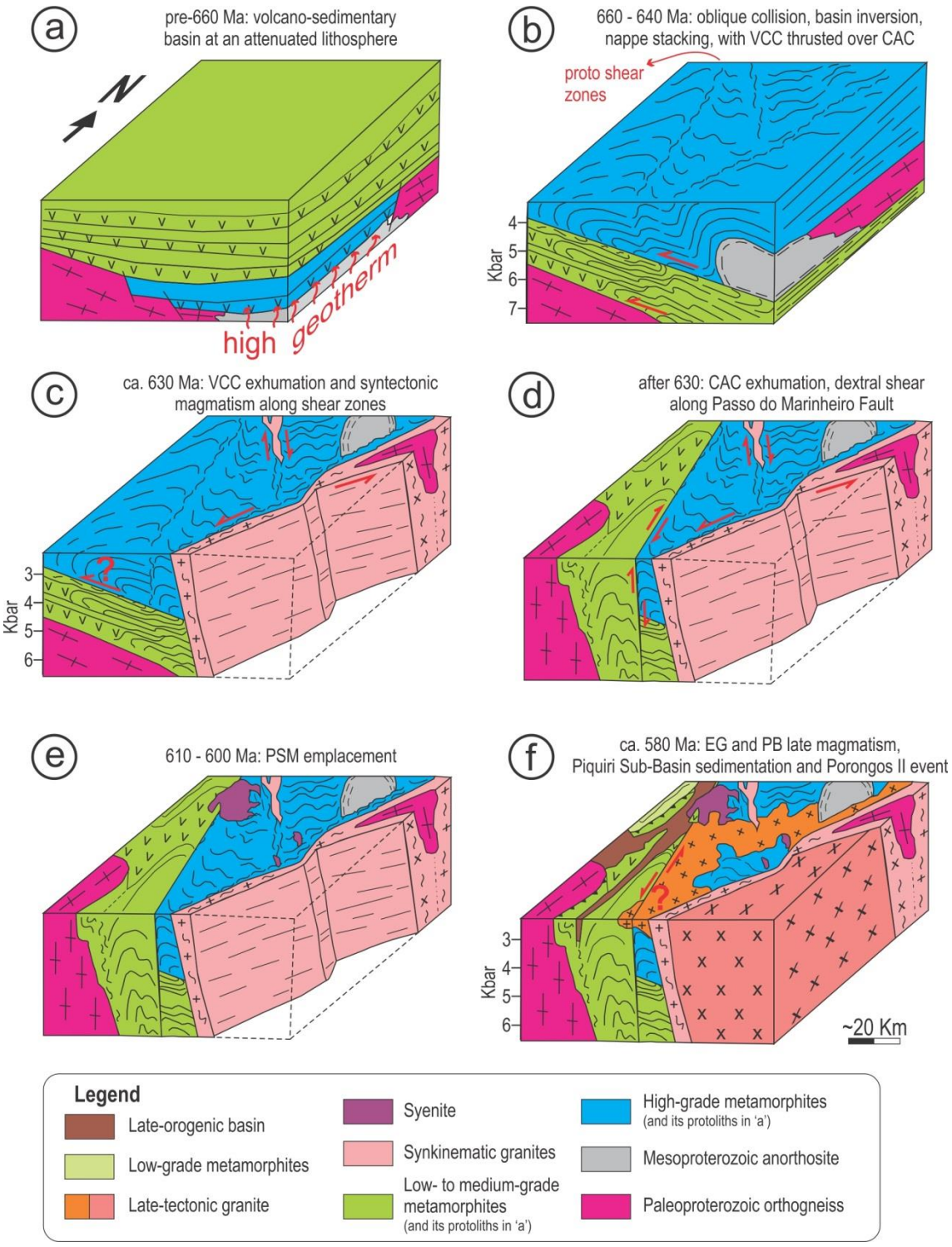

Figure 16 – A model for the origin of the Encruzilhada Block. (a) pre-660 Ma precursor volcano-sedimentary basin over an attenuated lithosphere, with high geothermal gradient. (b) 660-640 Ma basin inversion during oblique collision. (c) ca. 630 Ma exhumation of Várzea do Capivarita Nappe, active shear zones (cont.)

focused magmatism. (d) after 630 Ma exhumation of the Cerro da Árvore Complex along. (e) 610-600 Ma Piquiri Syenitic Massif (f) ca. 580 Ma Encruzilhada Granite emplacement blurred the western boundary of EB. It is followed by Porongos II event (soonly after 570 Ma), which gives the actual configuration (surface based on figure 02a and vertical sections loosely based on figure 04).

The hypothetical contact between VCC and CAC is considered to have facilitated the emplacement of these younger intrusive rocks. The modern expression of this structure is the Passo do Marinheiro Fault (Fig. 2, 3 and 4), which is considered to represent the reactivation of a former ductile shear zone. It is likely that the structure originally separating the two complexes accumulated displacement at least in two different moments: (i) during the main deformational episode of thrusting at 660 – 640 Ma and progressively afterwards (ca. 630 Ma), while the VCC was exhumed and the CAC was buried (Fig. 16b and c); and (ii) during exhumation of the CAC, before contact metamorphism at ca. 578 Ma (Fig 16d).

The original attitude of the presumed contact between the two complexes is in the realm of conjecture since there is no direct structural evidence of their original relation exposed. On the other hand, it is known that both VCC and CAC have original subhorizontal NNW-striking foliations with highly oblique lineations (nearly dip direction) related to thrusting, with progressive folding leading to NNW strike-slip tectonics. Therefore, it may have been an original subhorizontal plane, as reported for many Caledonian nappes (e.g. Fossen and Holst, 1995) further reworked by subvertical structures of the same orientation (S_2). It is also possible that the original structure was a subvertical, S_2-related one, since the S_2 was active during exhumation of the VCC (e.g. along Passo das Canas Shear Zone, during emplacement of the Butiá Granite). An additional argument comes from the aeromagnetometric image (Fig. 4a), where a very low signal in the area of the Encruzilhada Block suggests a thick sedimentary pile below surface. This may be interpreted as suggestive of the allochtonous origin of the block, favouring the hypothesis of an original subhorizontal contact surface between the complexes, which may be preserved in depth.

It is noteworthy the position difference between the southern portion of the DCSZ, marked by low-signal aerogammaspectrometric lineaments (Fig. 4b and 4c), and the southeastern limit of the EB, marked by aeromagnetometric lineaments (Fig. 4a). The apparent shift (Fig. 4d) may be due to the non-verticality of this structure, and suggests a steep dip towards the southeast, which is also suggested by Fernandes et al. (1995b).

It is outstanding that the shape revealed by radiometric data (Fig. 4b and 4c) for the PSM is very similar to the one observed on the geological map (Fig. 2a). In contrast, the magnetic data (Fig. 4a) show an elliptical shape for the massif, suggesting that the magmatic body continues in depth with an elliptic shape. The PSM horseshoe shape is thus interpreted as a possible effect of the Encruzilhada Granite intrusion in its southern portion close to surface, which in turn points to the shallow condition of the EG body.

Late-tectonic intrusions along the western EB boundary have partly obliterated the original contact between VCC and CAC after *ca.* 610 Ma, and the original boundary of the block itself. The PSM intrusion crosscuts the structure, and is not significantly affected by faulting, except for local reactivation. The crosscutting of the PMF trace by the PSM and its metavolcanic CAC roof pendants (studied by Battisti et al., 2018) (see Fig. 2), contradicts the concept of block at its stricto sensu (Sengör and Dewey, 1991), and suggests that there has been no significant activity along the fault after the PSM emplacement.

Recent work by Fambrini et al. (2018) about Ediacaran sedimentary basins west of the EB points out that the PSM must have been exposed to subaerial erosion at the time of basin deposition, which is indicated by many clasts of its rock types in the conglomerates.

This also points to the fact that erosion has played an important role in the Encruzilhada Block exhumation, and that no significant horizontal displacement has occurred along the main faults after sedimentation, since the local sedimentary source is found close to the basin (Fambrini et al., 2018).

The emplacement of the Encruzilhada Granite (after 578 Ma, according to Padilha et al., 2019) is interpreted by Jacobs et al. (2018) to have been controlled by previous discontinuities as the DCSZ and the PMF, which partly limit its map form to the EB (Fig. 16f, Fig. 2). At this time, both VCC and CAC are thought to have been side-by-side at very shallow crustal levels (less than 3 kbar or 10 km). This indirect evidence points to the epizonal character of the EG, with pressures lower than 3 kbar.

Observations recently made by the authors on the Encruzilhada Granite near the western margin of the EB have not shown any deformational feature over the EG in that area. What is rather seen is the apparent structural control of the intrusion by a pre-existent NS-striking subvertical structure, with aplo-pegmatitic veins parallel to it. Future detailed mapping, structural and petrological work is needed to improve these observations and support further conclusions regarding the later history of the

Encruzilhada Block and its relation with the Tijucas Fold Belt trough reactivation of the Passo do Marinheiro Fault and its effects on the southern portion of the EG and in CAC rocks.

6. Conclusions and implications for the Dom Feliciano Belt orogenic evolution

This integrated approach highlights the importance of the combination of petrological and structural work to unravell rock trajectory through the crust. Modelling of three samples from VCC and one from the CAC integrated with published data points to the contrastant PTt path of the correlated complexes. VCC was submitted to high-T/low-P granulite-facies conditions metamorphism and partial melting at 790 – 910 °C / 4.4 – 4.8 kbar at 650 – 640 Ma, which confirm and refine previous estimates. On the other hand, CAC was submitted to amphibolite facies progressive metamorphism, with early growth of garnet cores at 555 – 565°C and 5.4 – 5.7 kar, and peark metamorphism at 560 – 580°C and 5.8 – 6.3 kbar at *ca.* 660 Ma. All pointed silimarities are added up with the results to consider both complexes as being originally different parts of a correlated, if not the same, volcano-sedimentary basin inverted during oblique collision.

VCC exhumation is registered in SiO_2-subsaturated domains with cordierite + spinel ± sillimanite intergrowths that record metamorphic conditions of 660 – 720°C and 2.5 – 3.4 Kbar at *ca.* 630 Ma. The near-ITD exhumation process under high geothermal gradient (50 – 60°C) is probably related with a pre-collisional phase of ductile thinning of the lithosphere, followed by basin tectonic inversion, with VCC emplacement as a nappe verging west during progressive transpression, related to the main (oblique) collisional episode of the Dom Feliciano Belt. This process originated the Várzea do Capivarita Nappe, which original boundaries were later modified by deformation along subvertical planes (shear zones and faults) and post-collisional magmatism, with the resulted configuration of the so-called Encruzilhada Block.

Late-tectonic intrusions such as the PSM and EG are responsible for obliterating the original contact between the two complexes and the boundaries of the Encruzilhada Block. Their emplacement occurred taking advantage or crosscutting pre-existent structures during upward flow, which probably helped exhumation. Erosion was probably an additional factor during the Encruzilhada Block exhumation.

Contact metamorphism under andalusite stability field indirectly constrain emplacement of EG at 3 kbar or lower pressure conditions. It also point to the fact

that both VCC and CAC were side-by-side at the time of intrusions, which suggests later exhumation of the CAC rocks relative to the EB and prior to EG emplacement, before ca. 578 Ma.

Tectonic analysis of lineaments additionally confirms the structural similarity of the EB with the easternmost Tijucas Fold Belt, with predominantly NNW- to NNE-trending lineaments. Aerogamma and aeromagnetometric maps of the region confirm the ambiguous character of the EB in relation of both Tijucas Fold Belt and Pelotas Batolith previously reported by Hartmann et al. (2016). This is here explained in terms of the imprint of characteristics from both domains in the EB, due to: i) the common nature of rocks from the Várzea do Capivarita and Cerro da Árvore complexes, with similar aeromagnetometric low signal; and ii) the importance of the post-collisional magmatism in the Encruzilhada Block, transcending its limits, as well as in the whole Pelotas Batolith, which presents similar high aerogamma sign, mostly missing in the Tijucas Fold Belt.

The review of characteristics presented by the Encruzilhada Block discourage the use of term terrane since the neigbour blocks share many characteristics and can not be classified as exotic in relation to each other. It is also argumented against the understood of the Dorsal do Canguçú Shear Zone as a suture zone, as the occurrence of ca. 800 – 780 Ma correlated units in the TFB, EB and PB suggests a common pre-collisional environment for the whole area.

Late- to post-collisional magmatism in the Encruzilhada Block is markedly syenitic, shoshonitic to ultrapotassic (De Toni et al., 2016; Padilha et al., 2019; Rivera, 2019), pointing to mantle sources affected by previous subduction. This sums up with the high-T/low-P character of VCC metamorphism, suggestive of a pre-collisional attenuated lithosphere, towards the hypothesis of a back-arc rift as a plausible pre-collisional scenario (Konopásek et al., 2017; 2018).

One additional piece of evidence which may be considered to evaluate the intracontinental tectonic character of the area is given by the characteristic occurrence of the Capivarita Anorthosite. This unit may be correlated and spatially aligned to the Kunene Complex in southwest Angola (Mayer et al., 2004 and others), which suggests that these continents were not separated by an ocean in Mesoproterozoic times.

The unraveled history of the Encruzilhada Block as a former nappe is viewed as a key-piece towards understanding of the Dom Feliciano-Kaoko-Gariep orogenic system evolution.

7. Acknowledgements

GB De Toni thanks the Conselho Nacional de Pesquisa (CNPq) and the Coordenação de Aperfeiçoamento do Pessoal do Ensino Superior (CAPES) for the PhD scholarship. He also appreciatesfinancial support of his stay at the UiT - The Arctic University of Norway in Tromsø, organized within the framework of a CAPES (Brazil) – SIU (Norway) cooperation program. Prof. Jiří Konopásek is warmly acknowledged for his help with Perple_X and fruitful discussions. Diego Lyra is acknowledged for his help processing aerogeophysics. Prof. Rafael da Rocha Ribeiro and João VT Mello are acknowledged for their help with DEM. Kai Neufeld is acknowledged for his help with SEM compositional mapping at UiT. We are also grateful to Susan Drago for her kind help during microprobe analysis at UFRGS.

References

Arena, K.R., Hartmann, L.A., Lana, C., 2016. Evolution of Neoproterozoic ophiolites from the southern Brasiliano Orogen revealed by zircon U–Pb–Hf isotopes and geochemistry. Precambrian Research 285, 299–314

Babinski, M., Chemale Jr., F., Van Schmus, W.R., Hartmann, L.A.., and Silva, L.C. da, 1997. U-Pb and Sm-Nd geochronology of the Neoproterozoic granitic-gneissic Dom Feliciano Belt, southern Brazil. Journal of South American Earth Sciences, 10(3-4), 263–274.

Basei, M.A.S., Frimmel, H.E., Nutman, A.P., Preciozzi, F., Jacob, J. 2005. The connection between the Neoproterozoic Dom Feliciano (Brazil/Uruguay) and Gariep (Namibia/South Africa) orogenic belts. Precambrian Research, 139, 139–221.

Basei, M.A.S., Frimmel, H.E., Nutman, A.P., Preciozzi, F., 2008. West Gondwana amalgamation based on detrital zircon ages from Neoproterozoic Ribeira and Dom Feliciano belts of South America and comparison with coeval sequences from SW Africa. *in*: Pankhurst, R.J., Trouw, R.A.J., Brito Neves, B.B., De Wit, M.J. (eds) West Gondwana: Pre-Cenozoic Correlations Across the South Atlantic Region. Geological Society, London, Special Publications, 294, 239–256.

Battisti, M.A.B., Bitencourt, M.F., De Toni, G.B., Nardi, L.V.S., Konopásek, J., 2018. Metavolcanic rocks and orthogneisses from Porongos and Várzea do Capivarita complexes: A case for identification of tectonic interleaving at different crustal levels from structural and geochemical data in southernmost Brazil. Journal of South American Earth Sciences, 88, 253-274.

Bettucci, L.S., Burgueño, A.M., 1993. Análisis sedimentológico y faciológico de la Formación Rocha (ex Grupo Rocha). Revista Brasileira de Geociências, 23:323-329.

Bindu, R.S., 1997. Granulite Facies SpineLCordierite Assemblages from the Kerala Khondalite Belt, Southern India. Gondwana Research, 1(1), 121-128.

Bitencourt, M.F., Nardi, L.V.S., 2000. Tectonic setting and sources of magmatism related to the
Southern Brazilian Shear Belt. Revista Brasileira de Geociências 30, 186–189.

Bitencourt M.F., Nardi L.V.S., Florisbal L.M., Heaman L.M., 2015. Geology, geochronology and petrogenesis of a Neoproterozoic, syntectonic sillimanite-muscovite-biotite granite from southernmost Brazil. In: 8th Hutton Symposium on Granites and Related Rocks, Book of Abstracts.

Bitencourt, M.F., De Toni, G.B., Florisbal, L.M., Nardi, L.V.S., Martil, M.M.D., Heaman, L., DuFrane, A., Chemale Jr., F., 2016. Timing of syenitic syntectonic magmatism as a record of strain partitioning during Cryogenian collisional transpressive regime in southernmost Brazil. *in:* Primer Simposio de Tectonica Sudamericana – Acta. Santiago, Chile. 206 p.

Bom, F.M., Philipp, R.P., Zvirtes, G. 2014. Origem e evolução do Complexo Várzea do Capivarita, Encruzilhada do Sul, RS. Pesquisas em Geociências, 41(2), 131-153.

Borba, A.W., Maraschin, A.J., Noronha, F.L., Casagrande, J., Mizusaki, A.M.P., 2007. Provenance of the sedimentary rocks of the Bom Jardim Group (Neoproterozoic, Southern Brazil): evidence from petrography, geochemistry and neodymium isotopes. Latin American Journal of Sedimentology and Basin Analysis. 14(1), 25-42.

Brown, G.C., Hughes, D.J., Esson, J. 1973. New RFX data retrieval techniques and their application to U.S.G.S. standard rocks. Chemical Geology 11, 223-229.

Cenki , B., Kriegsman, L. M., Braun I., 2002. Melt-producing and melt-consuming reactions in the Achankovil cordierite gneisses, South India. Journal of Metamorphic Geology, 20, 543-561.

Chemale Jr., F., 2000. Evolução Geológica do Escudo Sul-rio-grandense. In: Geologia do Rio Grande do Sul. CIGO/UFRGS, Porto Alegre, 2002. 444 p.

Chemale Jr. F. Philipp R.P., Dussin I., Formoso M.L.L., Kawashita K., Berttotti A.L. 2011. Lu-Hf and U-Pb age determination of the Capivarita Anorthosite, Dom Feliciano Belt, Brazil, Precambriam Research, 186, 117-126.

Clark, C., Fitzsimons, I.C., Healy, D. and Harley, S.L., 2011. How does the continental crust get really hot? Elements, v. 7(4), 235-240.

CPRM. 2010. Projeto Aerogeofísico Escudo do Rio Grande do Sul. LASA PROSPECÇÕES S.A., Relatório Técnico, 260 pp.

Coggon, R., Holland, T.J.B. ,2002. Mixing properties of phengitic micas and revised garnet-phengite thermobarometers. Journal of Metamorphic Geology, 20, 683-696.

Connolly, J.,A.,D., 2005. Computation of phase equilibria by linear programming: a tool for geodynamic modeling and its application to subduction zone decarbonation. Earth and Planetary Science Letters, 236(1–2), 524–541.

De Yoreo, J.J., Lux, D.R., Guidotti, C.V., 1991. Thermal modelling in low-pressure/ high-temperature metamorphic belts. Tectonophysics 188, 209-238.

De Toni, G.B., Bitencourt, M.F., Nardi, L.V.S., 2016. Strain partitioning into dry and wet zones and the formation of Ca-rich myrmekite in syntectonic syenites: a case for melt-assisted dissolution replacement creep under granulite facies conditions. Journal of Structural Geology, 91:88-101.

De Toni, 2019. Correlação geológico-estrutural e modelo integrado de evolução para o Cinturão Dom Feliciano sob transpressão inclinada no Neoproterozoico do sul do Brasil. Unpublished Phd thesis. Universidade Federal do Rio Grande do Sul.

Deer, W.A., Howie, R.A., Zussman, J., 1992. An Introduction to the Rock-forming Minerals, second ed. In: Longman Scientific & Technical. Wiley, Harlow, Essex; New York.

ERDAS Imagine, 2014. https://www.hexagongeospatial.com/products/power-portfolio/erdas-imagine

Fernandes, L.A.D., Tommasi, A., Porcher, C.C., 1992. Deformation Patterns in the southern brazillan branch of the Dom Feliciano Belt: A reappraisal. Journal South American Earth Sciences 5, 77-96.

Fernandes, L.A.D., Menegat, R., Costa, A.F.U., Koester, E., Kramer, G., Tommasi, A., Porcher, C.C., Ramgrab, G.E., Camozzato, E., 1995a. Evolução tectônica do Cinturão Dom Feliciano no Escudo Sul-rio-grandense: Parte I – uma contribuição a partir do registro geológico. Revista Brasileira Geociências 25, 351-374.

Fernandes, L.A.D., Menegat, R., Costa, A.F.U., Koester, E., Kramer, G., Tommasi, A., Porcher, C.C., Ramgrab, G.E., Camozzato, E., 1995b. Evolução tectônica do Cinturão Dom Feliciano no Escudo Sul-rio-grandense: Parte II – uma contribuição a partir das assinaturas geofísicas. Revista Brasileira Geociências 25, 375-384.

Fernandes, L.A.D., Koester, E., 1999. The Neoproterozoic Dorsal de Canguçu strike-slip shear zone: its nature and role in the tectonic evolution of southern Brazil. J Afr Earth Sci 29: 3–24

Fossen, H., Cavalcante, G. C., de Almeida, R. P., 2017. Hot versus cold orogenic behavior: Comparing the Araçuaí-West Congo and the Caledonian orogens. Tectonics, 36. https://doi.org/10.1002/2017TC004743

Fossen, H., Holst, T.B., 1995. Nortwest-verging folds and the northwestward movement of the Caledonian Jotun Nappe, Norway. Journal of Structural Geology, 17:3-15.

Fowler, A., Hassen, I., Hassan, M., 2015. Tectonic evolution and setting of the Sa'al Complex, southern Sinai, Egypt: A Proterozoic continental back-arc rift model. Journal of African Earth Sciences, 104, 103-131.

Fuhrman, M.L.,Lindsley, D.H., 1988. Ternary-Feldspar Modeling and Thermometry. American Mineralogist 73, 201-15.

GEOSOFT. 2005. Sharpening using interactive reweighting inversion, Oasis Montaj best practice guide, www.geosoft.com.

Gregory, T.R.; Bitencourt, M.F.; Nardi, L.V.S.; Florisbal, L.M., Chemale Jr. 2015. Geochronological data from TTG-type rock associations of the Arroio dos Ratos Complex and implications for crustal evolution of southernmost Brazil in Paleoproterozoic times. Journal of South American Earth Sciences, 57:49-60.

Gross, A.O.M.S., Porcher, C.C., Fernandes, L.A.D., Koester, E., 2006. Neoproterozoic lowpressure/high-temperature collisional metamorphic evolution in the Varzea do Capivarita metamorphic suite, SE Brazil: thermobarometric and Sm/Nd evidence. Precambrian Research 147, 41–64.

Gruber, L., Porcher, C.C., Geller, H., Fernandes, L.A.D, Koester, E., 2016a. Geochronology (U-Pb) and isotope geochemistry (Sr/Sr and Pb/Pb) applied to the Várzea do Capivarita Metamorphic Suite, Dom Feliciano Belt, Southern Brazil: Insights and paleogeographical implications to West Gondwana evolution. Geochimica Brasiliensis 30(1): 55 – 71.

Gruber, L., Porcher, C.C., Koester, E., Bertotti, A.L., Lenz, C.,Fernandes, L.A.D, Remus, M.V.D, 2016b. Isotope Geochemistry and Geochronology of Syn-Depositional Volcanism in Porongos Metamorphic Complex, Santana Da Boa Vista Antiform, Dom Feliciano Belt, Brazil: Onset of an 800 Ma Continental Arc. Journal of Sedimentary Environments, 1(2):202-221.

Hand, M., Scrimgeour, I., Powell, R., Stuwe, K., Wilson, C.J.L., 1994. Metapelitic granulites from Jetty Peninsula, east Antarctica: formation during a single event or by polymetamorphism? Journal of Metamorphic Geology, 12, 557-573

Harley, S.L., 1986. A sapphirine-cordierite-garnet-sillimanite granulite from Enderby Land, Antarctica: implications for FMAS petrogenetic grids in the granulite facies. Contributions to Mineralogy and Petrology, 94, 452-460.

Harris, N.B.W., Holland, T.J.B., 1984. The significance of cordierite-hypersthene assemblages from the Beitbridge region of the Central Limpopo Belt: evidence for rapid decompression in the Archaen? American Mineralogist, 69:1037-1049.

Hartmann, L. A., Santos, J. O. S., Mcnaughton, N. J., Vasconcellos, M.A.Z., Silva, L.C. 2000. Ion microprobe (SHRIMP) dates complex granulite from Santa Catarina, southern Brazil. Anais da Academia Brasileira de Ciências, Rio de Janeiro, 72, 560-572.

Hartmann, L.A., Chemale Jr., F., Philipp, R.P., 2007. Evolução Geotectônica do Rio Grande do Sul no Pré-Cambriano. In: Ianuzzi, E.R., Frantz, J.C. (Eds.), 50 anos de Geologia: Instituto de Geociências. Contribuições. Comunicação e Identidade, Porto Alegre, 396p.

Hartmann, L.A., Lopes, W.R., Savian, J.,F., 2016. Integrated evaluation of the geology, aerogammaspectrometry and aeromagnetometry of the Sul-Riograndense Shield, southernmost Brazil. Anais da Academia Brasileira de Ciências, 188(1), 75-92.

Hasui, Y., Carneiro, C.D.R. And Coimbra, A.W., 1975. The Ribeira folded belt. Brazilian Journal of Geology, 5, 257-266.

Höfig, D.F., Marques, J.C., Basei, M.A.S., Giusti, R.O., Kohlrausch, C., Frantz, J.C., 2017. Detrital zircon geochronology (U-Pb LA-ICP-MS) of syn-orogenic basins in SW Gondwana: new insights into the cryogenian-ediacaran of Porongos complex, Dom Feliciano belt, southern Brazil. Precambrian Research, 306, 189-208.

Holland T.,Powell R. ,1996. Thermodynamics of order-disorder in minerals. 2. Symmetric formalism applied to solid solutions. American Mineralogist, 81, 1425-37.

Holland T., Baker J.,Powell R., 1998. Mixing properties and activity-composition relationships of chlorites in the system MgO-FeO-Al2O3-SiO2-H2O. European Journal of Mineralogy 10, 395-406.

Holland T.J.B., Powell R., 1998. An internally consistent thermodynamic data set for phases of petrological interest. Journal of Metamorphic Geology, 16, 309–343.

Holland T.,Powell R., 2001. Calculation of phase relations involving haplogranitic melts using an internally consistent thermodynamic dataset. Journal of Petrology, 42, 673-83.

Hyndman, R.D., Currie, C.A., Mazzotti, S.P., 2005. Subduction zone backarcs, mobile belts and orogenic heat. GSA Today, 15. http://dx.doi.org/10:1130/1052-5173(2005)0152.0.CO;2.

Jacobs, M. G., Philipp, R.P., Koester, E., Nardi, L.V.S., 2018. Magmatismo máfico associado ao Granito Encruzilhada do Sul, RS: implicações para a geração do magmatismo granítico pós-colisional do Cinturão Dom Feliciano. Pesquisas em Geociências, 46, e0669. DOI: https://doi.org/10.22456/1807-9806.88648

Johnson, T., Brown, M., Gibson, R., Wing, B., 2004. Spinel–cordierite symplectites replacing andalusite: evidence for melt-assisted diapirism in the Bushveld Complex, South Africa. Journal of Metamorphic Geology, 22:529–545.

Jones, R.R., Holdsworth, R.E., Clegg, P., McCaffrey, K., Tavarnelli, E., 2004. Inclined transpression. Journal of Structural Geology, 26, 1531–1548.

Jost, H., Bitencourt, M.F., 1980. Estratigrafia e tectônica de uma fração da Faixa de Dobramentos Tijucas no Rio Grande do Sul. Acta Geológica Leopoldensia, 4(7), 27-60. São Leopoldo, RS, Brazil.

Jost, H., 1981. Geology and Metallogeny of the Santana da Boa Vista Region, Southern Brazil. Unpublished PhD thesis. University of Georgia, USA. 220 p.

Jost, H., Hartmann, L.A., 1984. Província Mantiqueira – Setor Meridional. *in:* Pré-Cambriano do Brasil. Coord.: Almeida, F.F.M., Hasui, Y. p. 345-368.

Kelsey, D.E., Hand, M., 2011. On ultrahigh temperature crustal metamorphism: Phase equilibria, trace element thermometry, bulk composition, heat sources, timescales and tectonic settings. Geoscience Frontiers, 6, 311-356.

Knijnik, D.B., 2018. Geocronologia U-Pb E Geoquímica Isotópica Sr-Nd dos Granitoides Sintectônicos às Zonas de Cisalhamento Transcorentes Quitéria Serra do Erval e Dorsal de Canguçu, Rio Grande do Sul, Brasil. Unpublished PhD thesis. Universidade Federal do Rio Grande do Sul. 260 p. Avaliable at: https://lume.ufrgs.br/handle/10183/182067

Koester, E, Porcher, C.C., Pimentel, M.M., Fernandes, L.A.D., Vignol-Lelarge, M.L., Oliveira, L.D., Ramos, R.C., 2016. Further evidence of 777 Ma subduction-related continental arc magmatism in Eastern Dom Feliciano Belt, southern Brazil: The Chácara das Pedras Orthogneiss. Journal of South American Earth Sciences, 68, 155-166.

Konopásek, J., Sláma, J., Košler, J., 2016. Linking the basement geology along the Africa–South America coasts in the South Atlantic. Precambrian Research 280:221–230.

Konopásek, J., Hoffmann, K.H., Sláma, J., Košler, J., 2017. The onset of flysch sedimentation in the Kaoko Belt (NW Namibia)—implications for the pre-collisional evolution of the Kaoko–Dom Feliciano–Gariep Orogen. Precambrian Research 298, 220–234.

Konopásek, J., Janoušek, V., Oyhantçabal, P., Sláma J ., Ulrich, S., 2018. Did the circum-Rodinia subduction trigger the Neoproterozoic rifting along the Congo–Kalahari Craton margin? International Journal of Earth Sciences, 107(5), 1859-1894.

Lenz, C., 2006. Evolução metamórfica dos metapelitos da Antiforme Serra Dos Pedrosas: condições e idades do metamorfismo. Unpublished MSc thesis. Universidade Federal do Rio Grande do Sul, 128 p. Avaliable at: https://lume.ufrgs.br/handle/10183/8520

Lenz, C., Fernandes, L.A.D., McNaughton, N.J., Porcher, C.C., Masquelin, H., 2011. U–Pb SHRIMP ages for the Cerro Bori orthogneisses, Dom Feliciano Belt in Uruguay: evidences of a ~ 800 Ma magmatic and ~ 650 Ma metamorphic event. Precambrian Research 185, 149–163.

Lenz, C., Porcher, C.C., Fernandes, L.A.D., Masquelin, H., Koester, E., Conceição, R.V., 2013. Geochemistry of the Neoproterozoic (800–767 Ma) Cerro Bori orthogneisses, Dom Feliciano Belt in Uruguay: tectonic evolution of an ancient continental arc. Mineralogy and Petrology 107, 785–806.

Lister, G., Foster, M., 2009. Tectonic mode switches and the nature of orogenesis. Lithos, 113:274-291.

Lyra, D.S., Savian, J.F., Bitencourt, M.F., Trindade, R.I.F., Tomé, C.R., 2017. AMS fabrics and emplacement model of Butia Granite, an Ediacaran syntectonic peraluminous granite from southernmost Brazil. Journal of South American Earth Sciences, 87, 28-41.

Martil, M. M. D. 2007. Relações de intrusão do Maciço Sienítico Piquiri, RS com suas Encaixantes. Porto Alegre, 63 p. *Monografia de Conclusão de Curso*, Curso de Geologia, Instituto de Geociências, Universidade Federal do Rio Grande do Sul.

Martil, M.M.D., 2016. O magmatismo de arco continental pré-colisional (790 ma) e a reconstituição espaço-temporal do regime transpressivo (650 Ma) no Complexo Várzea do Capivarita, sul da Província Mantiqueira. Unpublished PhD thesis. Universidade Federal do Rio Grande do Sul. Avaliable at: https://www.lume.ufrgs.br/handle/10183/149194

Martil, M.M.D., Bitencourt, M.F., Nardi, L.V.S., 2011. Caracterização estrutural e petrológica do magmatismo pré-colisional do Escudo Sul-rio-grandense: os

ortognaisses do Complexo Metamórfico Várzea do Capivarita. Pesquisas em Geociências, 38, 181-201.

Martil, M.M.D., Bitencourt, M.F., Nardi, L.V.S., Koester, E., Pimentel, M.M., 2017. Pre-collisional, Neoproterozoic (ca. 790 Ma) continental arc magmatism in southern Mantiqueira Province, Brazil: geochemical and isotopic constraints from the Várzea do Capivarita Complex. Lithos 274–275:39–52

Masquelin H., Fernandes, L.A.D., Lenz, C., Porcher, C.C., McNaughton, N.J. 2012. The Cerro Olivo Complex: a pre-collisional Neoproterozoic magmatic arc in Eastern Uruguay. International Geology Review, 54, 1161–1183.

Mayer, A., Hoffmann, A.W., Sinigoi, S., Morais, E., 2004. Mesoproterozoic Sm–Nd and U–Pb ages for the Kunene Anorthosite Complex of SW Angola. Precambrian Research 133 (3–4), 187–206.

Mezger, J.E., Chacko, T., Erdmer, P., 2008. Metamorphism at a late Mesozoic accretionary margin: a study from the Coast Belt of the North American Cordillera. Journal of Metamorphic Geology, 19:121-137.

Nardi, L.V.S., Plá-Cid, J., Bitencourt, M.F., Stabel, L.Z., 2008. Geochemistry and petrogenesis of post-collisional ultrapotassic syenites and granites from southernmost Brazil: the Piquiri Syenite Massif. Anais da Academia Brasileira de Ciências 80(2): 353-371.

Niessing, M., 2008. Geology and stratigraphic definition of the Butiá Granite: a sillimanite-bearing syntectonic leucogranite from the Sul-rio-grandense Shield. Unpublished MSc thesis. Technischen Universität München.

Oliveira, C.H.E., Chemale Jr., F., Jelinek, A.R., Bicca, M.M., Philipp, R.P., 2014. U–Pb and Lu–Hf isotopes applied to the evolution of the late topost-orogenic transtensional basins of the dom feliciano belt, Brazil. Precambrian Research, 246:240–255.

Oriolo, S., Oyhantçabal, P., Wemmer, K., Heidelbach, F., Pfänder, J., Basei, M.A.S., Hueck, M., Hannich, F., Sperner, B., Siegesmund, S., 2016. Shear zone evolution and timing of deformation in the Neoproterozoic transpressional Dom Feliciano Belt, Uruguay. Journal of Structural Geology, 92:59-78.

Oyhantçabal, P., Siegesmund, S., Wemmer, K., Presnyakov, S., Layer, P., 2009. Geochronological constraints on the evolution of the southern Dom Feliciano Belt (Uruguay). Journal of the Geological Society of London 166, 1075-1084.

Oyhantçabal, P., Siegesmund, S., Wemmer, K., 2011. The Río de la Plata Craton: a review of units, boundaries, ages and isotopic signature. International Journal of Earth Sciences 100, 201-220.

Padilha, D.F., Bitencourt, M.F., Nardi, L.V.S., Forisbal, L.M., Reis, C. Geraldes, M., Almeida, B.S. 2019. Sources and settings of Ediacaran post-collisional syenite-monzonite-diorite shoshonitic magmatism from southernmost Brazil. Lithos, 344-345, 482-503.

Paim, P.S.G., Chemale Jr., F., Wildner, W., 2014. Estágios evolutivos da Bacia do Camaquã (RS). Ciência e Natura, Santa Maria, v. 36, p. 183–193.

Pertille J., Hartmann L.A., Philipp R.P., Petry T.S., Lana C.C. 2015. Origin of the Ediacaran Porongos Group, Dom Feliciano Belt, southern Brazilian Shield, with emphasis on whole rock and detrital zircon geochemistry and U-Pb, Lu-Hf isotopes. Journal of South American Earth Sciences, 64:69-93.

Picada, R.S., 1971. Ensaio sobre a tectônica do Escudo Sul-riograndense: caracterização dos sistemas de falhas. Anais do XXV Congresso Brasileiro de Geologia. Porto Alegre, Sociedade Brasileira de Geologia. p. 167-191.

Philipp, R.P., Machado, R., Nardi, L.V.S., Lafon, J.M., 2002. O Magmatismo Granítico Neoproterozóico do Batólito Pelotas no sul do Brasil: Novos dados e revisão da Geocronologia regional. Brazilian Journal of Geology 32, 277-290

Philipp, R.P., Machado, R., 2005. The late Neoproterozoic granitoid magmatism of the Pelotas Batolith, southern Brazil. Journal of South American Earth Sciences 19, 461-478.

Philipp, R.P., Massonne, H.J., Campos, R. 2013. Peraluminous leucogranites of the Cordilheira Suite: a record of Neoproterozoic collision and the generation of the Pelotas Batholith, Dom Feliciano Belt, Southern Brazil. Journal of South American Earth Sciences, 43, 8-24.

Philipp, R.P., Pimentel, M.M., Chemale, F. Jr., 2016a. Tectonic evolution of the Dom Feliciano Belt in Southern Brazil: Geological relationships and U-Pb geochronology. Brazilian Journal of Geology, 46(1), 83–104.

Philipp, R.P., Bom, F.M., Pimentel, M.M., Junges, S.L., Zvirtes, G., 2016b. SHRIMP U-Pb age and high temperature conditions of the collisional metamorphism in the Varzea do Capivarita Complex: implications for the origin of Pelotas Batholith, Dom Feliciano Belt, southern Brazil. Journal of South American Earth Sciences 66,196–207.

Philipp, R.P., Pimentel, M.M., Basei, M.A.S., 2018. The Tectonic Evolution of the São Gabriel Terrane, Dom Feliciano Belt, Southern Brazil: The Closure of the Charrua Ocean. *in:* S. Siegesmund et al. (eds.), Geology of Southwest Gondwana, Regional Geology Reviews, 243-265.

Plá-Cid J, Nardi LVS, Stabel LZ, Conceição RV, Balzaretti NM, 2003. High-pressure minerals in mafic microgranular enclaves: evidences for co-mingling between lamprophyric and syenitic magmas at mantle conditions. Contributions to Mineralogy and Petrology 145, 444–459.

Porcher, C.A., Lopes, R.D.C., 2000. Programa Levantamentos Geológicos Básicos do Brasil. Mapa Geologico da Folha Cachoeira do Sul, Folha SH.22-YA. Escala 1: 25.000. Serviço Geológico do Brasil (CPRM), Brasília.

Ramgrab, G.E., Wildner, W., Camozzato, E., 1996. Programa de Levantamentos Geológicos Básicos do Brasil, Mapa Geologico da Folha Porto Alegre SH. 22-YB. Escala 1:25.000. Serviço Geologico do Brasil (CPRM), Brasília, p. 144.

Ramos, R.C., Koester, E., Triboli, D.V., Porcher, C.C., Gezatt, J.N., Silveira, R.L., 2018. Insights on the evolution of the Arroio Grande Ophiolite (Dom Feliciano Belt, Brazil) from Rb-Sr and SHRIMP U-Pb isotopic geochemistry. Journal of South American Earth Sciences, 86:38-53.

Ring, U., Brandon, M.T., Willett, S.D., Lister, G.S., 1999. Exhumation processes. *in*: Ring, U., Brandon, M. T., Lister, G. S., Willett, S. D. (eds) Exhumation Processes: Normal Faulting, Ductile Flow and Erosion. Geological Society, London, Special Publications, 154, 1-27.

Rivera, C.B., 2019. Construção do Maciço Sienítico Piquiri (609 a 583 ma) por colocação sucessiva de pulsos de magma ultrapotássico e shoshonítico sob extensão no Escudo sul-rio-grandense. PhD thesis. Universidade Federal do Rio Grande do Sul. Porto Alegre, Brazil.

Saalmann, K., Remus, M.V.D., Hartmann, L.A., 2006. Structural evolution and tectonic setting of the Porongos Belt, southern Brazil. Geological Magazine, 143, 59-88.

Saalmann, K., Gerdes, A., Lahaye, Y., Hartmann, L.A., Remus, M.V.D., Läufer, A., 2011. Multiple accretion at the eastern margin of the Rio de la Plata craton: the prolonged Brasiliano orogeny in southernmost Brazil. International Journal of Earth Sciences, 100, 355-378.

Sbaraini, S., 2019. Dados de anisotropia de susceptibilidade magnética na modelagem tridimensional do Maciço Sienítico Piquiri. Unpublished Master Thesis. Universidade Federal do Rio Grande do Sul.

Sengör, A.M.C, Dewey, J.F., 1990. Terranology: Vice or Virtue? *in:* Dewey, J.F., Gass, I.G., Curry, G.B., Harris, N.B.W, Sengör, A.M.C., eds. Allochtonous terranes. Cambridge, Cambridge University Press. p. 23-29.

Shroder, J., 2014. Air and Space Technology in Resource Delineation: Peace and War. *in:* Natural Resources in Afghanistan, p.381-406. http://dx.doi.org/10.1016/B978-0-12-800135-6.00013-1

Silva, L.C., Hartmann, L.A., McNaughton, N.J., Fletcher, I.R., 1999. SHRIMP U/Pb Zircon dating of Neoproterozoic granitic magmatism and collision in the Pelotas Batholith, Southernmost Brazil. International Geology Review, 41, 531–551.

Stabel, L.S., Nardi, L.V.S., Plá Cid, J., 2001. Química mineral e evolução petrológica do Sienito Piquiri: magmatismo shoshonítico, neoproterozóico, pós-colisional no sul do Brasil. Revista Brasileira de Geociências, 31(2):211-222.

Stüwe, K., Barr, T.D., 1998. On uplift and exhumation during convergence. Tectonics, 17(1):80-88.

Tajcmanová, L., Konopásek J., Connoly, J.A.D., 2007. Diffusion-controlled development of silica-undersaturated domains in felsic granulites of the Bohemian Massif (Variscan belt of Central Europe). Contributions to Mineralogy and Petrology 153: 237-250.

Tajcmanová, L., Connolly, J.A.D.,Cesare, B., 2009. A thermodynamic model for titanium and ferric iron solution in biotite. Journal of Metamorphic Geology 27,153-64.

Tambara, GB, Koester, E, Ramos, RC, Porcher, CC, Vieira, DT, Fernandes, LAD, Lenz, C. Geoquímica e geocronologia dos Gnaisses Piratini: magmatismo cálcio-alcalino médio a alto-K de 784 Ma (U-Pb SHRIMP) no SE do Cinturão Dom Feliciano (RS, Brasil). Pesquisas em Geociências, v. 46 (2019), n. 2:e0769. doi.org/10.22456/1807-9806.95466

Thompson, A.B., Schulmann, K., Jezek, J., 1997. Thermal evolution and exhumation in obliquely convergent (transpressive) orogens. Tectonophysics, 280:171-184.

Tropper, P., Deibl, I., Finger, F., Kaindl, R., 2006. P–T–t evolution of spinel–cordierite–garnet gneisses from the Sauwald Zone (Southern Bohemian Massif, Upper Austria): is there evidence for two independent late-Variscan low-P /high-T events in the Moldanubian Unit? Int J Earth Sci (Geol Rundsch) (2006) 95: 1019–1037.

UFRGS, 2008. Mapeamento Geológico 1:25 000 de parte das folhas Passo das Canas SH-22-Y-A-III-4 (MI2984/4) e Capané SH 22-Y-A-III-3 (MI2984/3), RS. Instituto de Geociências, Universidade Federal do Rio Grande do Sul, Porto Alegre.
UFRGS, 2009. Mapeamento Geológico 1:25 000 de parte da Folha Passo das Canas SH-22-Y-A-III-4 (MI2984/4), RS. Instituto de Geociências, Universidade Federal do Rio Grande do Sul, Porto Alegre.
UFRGS, 2010. Mapeamento Geológico 1:25 000 de parte das folhas Encruzilhada SH-22-Y-A-VI-2 (MI2997/2) e Passo das Canas SH22-Y-A-III-4 (MI2984/4), RS. Instituto de Geociências, Universidade Federal do Rio Grande do Sul, Porto Alegre.
UFRGS, 2011. Mapeamento Geológico 1:25 000 de parte da folha Várzea do Capivarita SH-22-Y-B-I-4 (MI2985/2), RS. Instituto de Geociências, Universidade Federal do Rio Grande do Sul, Porto Alegre.
Weinberg, R.F., 2016. Himalayan leucogranites and migmatites: nature, timing and duration of anatexis. Journal of Metamorphic Geology, 34(8):821-843.
White, R.W., Powell, R.,Holland, T.J.B., 2001. Calculation of partial melting equilibria in the system Na2O-CaO-K2O-FeO-MgO-Al2O3-SiO2-H2O (NCKFMASH). Journal of Metamorphic Geology 19, 139-53.
Will, T.M., Gaucher, C., Ling, X.-H., Li, X.-H., Li, Q.-L., Frimmel, H.E. Neoproterozoic magmatic and metamorphic events in the Cuchilla Dionisio Terrane, Uruguay, and possible correlations across the South Atlantic. Precambrian Research, 320, 303-322.

TABLES

Table 1 – VCC metapelitic paragneiss (MN12C) mineral chemistry						
MINERAL	Cordierite					
SITE	01-2 center	01-2 center	01-2 center	01-2 margin	4 center	4 margin
DataSet/Point	1 / 1 .	4 / 1 .	5 / 1 .	6 / 1 .	7 / 1 .	8 / 1 .
Na2O	0.31	0.30	0.34	0.37	0.23	0.31
SiO2	47.72	48.07	48.03	47.78	48.11	48.12
MgO	7.17	7.09	6.87	6.94	7.29	7.04
Al2O3	32.52	32.37	32.55	32.58	32.50	32.48
K2O	0.00	0.01	0.00	0.01	0.01	0.00
CaO	0.03	0.02	0.02	0.03	0.02	0.03
TiO2	0.01	0.01	0.01	0.02	0.01	0.02
FeO	10.15	10.22	10.08	10.53	9.88	9.94
MnO	0.11	0.11	0.13	0.13	0.10	0.12
Cr2O3	0.00	0.00	0.00	0.01	0.00	0.00
ZnO	0.03	0.01	0.00	0.00	0.00	0.00
Total	98.05	98.20	98.03	98.38	98.17	98.06
No. Cations in Formula						
Na	0.062683	0.06054	0.068677	0.074691	0.04635	0.062552
Si	4.977304	5.003798	5.004402	4.97528	5.001022	5.008539
Mg	1.114628	1.099991	1.066875	1.07708	1.129453	1.092132
Al	3.998154	3.971766	3.99766	3.998874	3.982191	3.984894
K	0	0.001328	0	0.001328	0.001326	0
Ca	0.003352	0.00223	0.002233	0.003347	0.002227	0.003345
Ti	0.000784	0.000783	0.000783	0.001566	0.000782	0.001565
Fe	0.885244	0.889569	0.87822	0.91686	0.858783	0.865117
Mn	0.009717	0.009698	0.011472	0.011465	0.008804	0.010578
Cr	0	0	0	0.000823	0	0
Zn	0.00231	0.000768	0	0	0	0
TOTAL	11.05418	11.04047	11.03032	11.06131	11.03094	11.02872
XMg	55.73497	55.28814	54.8495	54.01768	56.80678	55.79934

Table 1 - (cont.)			
Spinel			
SITE	01-2	4	4
DataSet/Point	7 / 1 .	44 / 1 .	45 / 1 .
SiO2	0.01	0.03	0.01
MgO	2.68	2.67	2.57
Al2O3	55.9	55.41	56.35
CaO	0	0.01	0
TiO2	0.03	0.08	0.07
Cr2O3	0.1	0.1	0.14
FeO	32.18605	32.57935	33.04526
Fe2O3	2.638176	2.99012	2.027831
MnO	0.11	0.14	0.11
ZnO	4.12	3.59	3.52
Total	97.77422	97.59947	97.84309
No. Cations in Formula			
Si	0.002367	0.007128	0.002357
Mg	0.951473	0.951591	0.908696
Al	15.5655	15.48878	15.62677
Ca	0	0.002546	0
Ti	0.005325	0.014256	0.012375
Cr	0.018686	0.018758	0.026053
Fe(ii)	6.330698	6.426724	6.484164
Fe(iii)	0.466935	0.530768	0.358051
Mn	0.022002	0.028111	0.021912
Zn	0.722327	0.631842	0.614615
Total (S)	24.08532	24.1005	24.055
XFe	87.9	88.1	88.4
XMg	0.12	0.12	0.12

Table 1 - (cont.)										
Garnet										
SITE	01-2 center	01-2 margin	01-2 margin	01-2 center	01-2 margin	03 center	03 margin	03 small	03 small	03 small
DataSet/Point	1 / 1 .	2 / 1 .	18 / 1 .	19 / 1 .	20 / 1 .	24 / 1 .	25 / 1 .	32 / 1 .	33 / 1 .	34 / 1 .
SiO2	37.66	36.93	36.96	37.12	37.49	36.95	37.10	37.40	37.26	36.97
MgO	3.14	2.53	3.12	3.14	3.30	3.04	3.09	3.12	2.72	3.25
Al2O3	21.26	21.23	21.51	21.51	21.33	21.24	21.08	21.36	21.18	21.40
CaO	0.91	0.91	0.93	0.91	0.95	0.92	0.94	0.92	0.92	0.94
TiO2	0.03	0.04	0.03	0.06	0.03	0.04	0.03	0.03	0.04	0.05
FeO	35.76	36.90	35.81	36.09	36.27	36.13	36.31	36.51	36.90	35.77
MnO	1.09	1.33	1.14	1.03	1.06	1.46	1.14	1.22	1.18	1.06
Total	99.85	99.87	99.50	99.85	100.43	99.79	99.70	100.57	100.21	99.45
No. Cations in Formula										
Si	6.048	5.981	5.971	5.976	6.002	5.973	5.998	5.992	6.005	5.974
Mg	0.752	0.611	0.751	0.753	0.787	0.732	0.745	0.745	0.653	0.783
Al	4.025	4.053	4.096	4.082	4.025	4.047	4.017	4.034	4.023	4.076
Ca	0.157	0.158	0.161	0.157	0.163	0.159	0.163	0.158	0.159	0.163
Ti	0.004	0.005	0.004	0.007	0.004	0.005	0.004	0.004	0.005	0.006
Fe	4.802	4.997	4.838	4.859	4.856	4.883	4.908	4.891	4.973	4.834
Mn	0.148	0.182	0.156	0.140	0.144	0.200	0.156	0.166	0.161	0.145
TOTAL	15.936	15.987	15.977	15.975	15.981	15.999	15.990	15.988	15.979	15.981
End-member calculations										
PY	12.829	10.267	12.721	12.750	13.235	12.258	12.467	12.501	10.988	13.214
ALM	81.968	84.011	81.912	82.217	81.610	81.731	82.193	82.071	83.632	81.590
GRO	2.672	2.654	2.726	2.656	2.739	2.666	2.726	2.650	2.671	2.747
SP	2.531	3.067	2.641	2.377	2.416	3.345	2.614	2.778	2.709	2.449
XMg	0.135	0.109	0.134	0.134	0.140	0.130	0.132	0.132	0.116	0.139

Table 1 - (cont.)										
Micas										
SITE	01-2	01-2	01-2	01-2 included	1-1 (matrix)	01 aggregate	01 matrix	01 matrix	03 in leucosome	04 aggregate
DataSet/Point	3 / 1 .	4 / 1 .	5 / 1 .	15 / 1 .	17 / 1 .	23 / 1 .	29 / 1 .	35 / 1 .	42 / 1 .	50 / 1 .
Na2O	0.14	0.13	0.12	0.15	0.12	0.12	0.12	0.11	0.08	0.12
SiO2	35.25	35.99	35.89	35.40	35.64	35.95	35.76	35.43	36.01	35.76
MgO	6.30	6.20	6.26	6.57	6.31	6.12	6.67	6.86	6.87	6.74
Al2O3	17.78	17.46	18.04	17.33	17.93	17.64	17.52	18.03	17.27	18.03
K2O	9.23	9.38	9.37	9.25	9.14	9.30	9.36	9.35	9.54	9.41
CaO	0.00	0.00	0.00	0.00	0.00	0.00	0.00	0.00	0.00	0.00
TiO2	4.19	4.08	3.83	4.34	3.39	4.15	4.20	3.41	4.08	3.99
FeO	22.18	22.68	22.04	22.17	22.40	22.73	21.72	22.56	21.36	21.67
MnO	0.08	0.09	0.06	0.02	0.08	0.04	0.09	0.02	0.03	0.05
Total	95.16	96.00	95.61	95.24	95.01	96.06	95.45	95.78	95.24	95.75
No. Cations in Formula										
Na	0.042	0.039	0.036	0.045	0.036	0.036	0.036	0.033	0.024	0.036
Si	5.451	5.522	5.508	5.471	5.513	5.510	5.499	5.449	5.541	5.474
Mg	1.452	1.418	1.432	1.513	1.455	1.398	1.529	1.573	1.576	1.538
Al	3.241	3.158	3.264	3.157	3.269	3.187	3.175	3.269	3.132	3.253
K	1.821	1.836	1.834	1.823	1.803	1.818	1.836	1.834	1.872	1.837
Ca	0.000	0.000	0.000	0.000	0.000	0.000	0.000	0.000	0.000	0.000
Ti	0.487	0.471	0.442	0.504	0.394	0.478	0.486	0.394	0.472	0.459
Fe	2.868	2.910	2.829	2.865	2.897	2.913	2.793	2.901	2.748	2.774
Mn	0.010	0.012	0.008	0.003	0.010	0.005	0.012	0.003	0.004	0.006
Total	15.373	15.365	15.353	15.381	15.378	15.345	15.364	15.456	15.369	15.377
XMg	33.611	32.762	33.611	34.564	33.427	32.429	35.374	35.149	36.439	35.666

Table 2 - VCC orthogneiss (TM38C) mineral chemistry										
MINERAL	Plagioclase									
SITE	01-3 small	01-3 recryst.	01-3 relict	01-3 relict	01-2 bigger	01-2 center	01-2 recryst	02 bigger/relict?	02 bigger	02 smaller
DataSet/Point	6 / 1.	9 / 1.	10 / 1.	11 / 1.	19 / 1.	20 / 1.	21 / 1.	25 / 1.	31 / 1.	32 / 1.
Na2O	6.25	6.25	5.93	5.86	6.18	6.13	6.16	5.96	6.17	6.44
SiO2	56.95	56.89	56.20	55.46	56.59	56.58	56.11	56.20	56.64	56.94
MgO	0.00	0.00	0.00	0.01	0.01	0.01	0.01	0.01	0.02	0.02
Al2O3	27.07	27.12	27.70	27.51	27.21	27.34	27.16	27.27	27.11	26.92
K2O	0.22	0.25	0.27	0.29	0.24	0.29	0.21	0.28	0.28	0.30
CaO	9.29	9.14	9.86	9.93	9.36	9.53	9.45	9.68	9.38	8.82
TiO2	0.00	0.02	0.00	0.01	0.04	0.00	0.03	0.04	0.00	0.02
FeO	0.13	0.08	0.02	0.15	0.10	0.06	0.00	0.09	0.12	0.20
Total	99.90	99.74	99.99	99.22	99.73	99.95	99.12	99.52	99.73	99.66
No. Cations in Formula										
Na	2.178	2.180	2.068	2.063	2.158	2.138	2.165	2.088	2.156	2.250
Si	10.237	10.237	10.110	10.071	10.195	10.177	10.171	10.155	10.208	10.260
Mg	0.000	0.000	0.000	0.003	0.003	0.003	0.003	0.003	0.005	0.005
Al	5.736	5.752	5.874	5.888	5.778	5.797	5.803	5.808	5.759	5.718
K	0.050	0.057	0.062	0.067	0.055	0.067	0.049	0.065	0.064	0.069
Ca	1.789	1.762	1.900	1.932	1.807	1.836	1.835	1.874	1.811	1.703
Ti	0.000	0.003	0.000	0.001	0.005	0.000	0.004	0.005	0.000	0.003
Fe	0.020	0.012	0.003	0.023	0.015	0.009	0.000	0.014	0.018	0.030
TOTAL	20.009	20.003	20.018	20.048	20.017	20.026	20.030	20.011	20.022	20.038
End-member calculations										
Orthoclase	1.65832	1.89374	2.0283	2.1812	1.811	2.1721	1.5843	2.115	2.107	2.2614
Albite	53.95	54.216	51.015	50.473	53.41	52.578	53.22	51.54	53.16	55.592
Anorthite	44.3916	43.8902	46.956	47.346	44.78	45.249	45.196	46.34	44.74	42.147

Table 2 - (cont.)											
Biotite											
DataSet/Point	3 / 1 .	4 / 1 .	13 / 1 .	14 / 1 .	18 / 1 .	22 / 1 .	26 / 1 .	30 / 1 .	33 / 1 .	35 / 1 .	37 / 1 .
Na2O	0.11	0.07	0.13	0.13	0.11	0.12	0.11	0.11	0.12	0.13	0.08
SiO2	36.89	37.09	36.68	36.35	37.08	35.32	36.72	36.27	36.36	36.25	36.72
MgO	11.40	11.37	9.99	10.37	10.58	10.71	10.68	10.67	10.08	10.01	10.99
Al2O3	13.77	14.29	14.10	14.21	14.22	14.69	14.25	14.03	13.94	14.00	13.91
K2O	9.39	9.37	9.47	9.46	9.48	8.20	9.47	9.53	9.20	9.58	9.57
CaO	0.00	0.00	0.00	0.00	0.00	0.00	0.00	0.00	0.00	0.01	0.00
TiO2	3.29	3.59	6.02	5.40	4.42	4.91	3.77	5.17	4.62	5.81	4.45
FeO	20.86	20.18	19.90	19.71	20.55	20.80	20.98	20.09	20.73	19.75	19.71
MnO	0.19	0.14	0.14	0.16	0.26	0.14	0.19	0.13	0.16	0.12	0.18
Total	95.90	96.10	96.45	95.79	96.70	94.90	96.16	96.00	95.21	95.66	95.61
No. Cations in Formula											
Na	0.033	0.021	0.038	0.038	0.032	0.036	0.033	0.033	0.036	0.039	0.024
Si	5.645	5.634	5.559	5.547	5.615	5.441	5.607	5.537	5.602	5.547	5.613
Mg	2.600	2.574	2.257	2.358	2.388	2.459	2.431	2.428	2.315	2.283	2.504
Al	2.484	2.559	2.519	2.556	2.538	2.667	2.565	2.525	2.532	2.525	2.506
K	1.833	1.816	1.831	1.841	1.831	1.611	1.845	1.856	1.808	1.870	1.866
Ca	0.000	0.000	0.000	0.000	0.000	0.000	0.000	0.000	0.000	0.002	0.000
Ti	0.379	0.410	0.686	0.620	0.503	0.569	0.433	0.593	0.535	0.669	0.511
Fe	2.669	2.563	2.522	2.515	2.602	2.679	2.679	2.564	2.671	2.527	2.519
Mn	0.025	0.018	0.018	0.021	0.033	0.018	0.025	0.017	0.021	0.016	0.023
TOTAL	15.667	15.595	15.430	15.496	15.544	15.480	15.616	15.552	15.519	15.476	15.567
XMg	0.493	0.501	0.472	0.484	0.479	0.479	0.476	0.486	0.464	0.475	0.498

Table 2 - (cont.)											
Opx											
DataSet/Point	1 / 1.	2 / 1.	5 / 1.	12 / 1.	16 / 1.	17 / 1.	23 / 1.	27 / 1.	28 / 1.	29 / 1.	36 / 1.
SiO2	49.76	50.05	50.12	49.85	50.03	50.31	49.93	50.40	50.59	50.43	50.49
MgO	13.92	14.14	14.44	14.26	14.36	14.76	14.23	14.77	14.75	14.63	15.09
Na2O	0.02	0.01	0.00	0.02	0.00	0.00	0.01	0.00	0.00	0.00	0.01
Al2O3	0.70	0.79	0.74	0.76	0.69	0.68	0.71	0.64	0.64	0.66	0.78
CaO	0.80	0.72	0.74	0.67	0.64	0.66	0.64	0.67	0.74	0.67	0.63
K2O	0.00	0.01	0.00	0.01	0.00	0.01	0.00	0.00	0.00	0.00	0.01
TiO2	0.15	0.15	0.14	0.15	0.15	0.14	0.15	0.13	0.12	0.17	0.13
FeO	32.43	33.04	32.71	32.68	33.33	32.74	32.63	32.91	32.73	32.39	32.56
MnO	1.29	1.29	1.27	1.32	1.39	1.15	1.40	1.27	1.23	1.27	1.14
Cr2O3	0.00	0.03	0.03	0.03	0.00	0.02	0.04	0.01	0.04	0.02	0.02
Total	99.07	100.24	100.19	99.75	100.58	100.47	99.75	100.80	100.84	100.23	100.86
No. Cations in Formula											
Si	1.98	1.97	1.97	1.97	1.97	1.97	1.97	1.97	1.97	1.98	1.97
Mg	0.83	0.83	0.85	0.84	0.84	0.86	0.84	0.86	0.86	0.86	0.88
Na	0.00	0.00	0.00	0.00	0.00	0.00	0.00	0.00	0.00	0.00	0.00
Al	0.03	0.04	0.03	0.04	0.03	0.03	0.03	0.03	0.03	0.03	0.04
Ca	0.03	0.03	0.03	0.03	0.03	0.03	0.03	0.03	0.03	0.03	0.03
K	0.00	0.00	0.00	0.00	0.00	0.00	0.00	0.00	0.00	0.00	0.00
Ti	0.00	0.00	0.00	0.00	0.00	0.00	0.00	0.00	0.00	0.01	0.00
Fe	1.08	1.09	1.08	1.08	1.10	1.07	1.08	1.08	1.07	1.06	1.06
Mn	0.04	0.04	0.04	0.04	0.05	0.04	0.05	0.04	0.04	0.04	0.04
Cr	0.00	0.00	0.00	0.00	0.00	0.00	0.00	0.00	0.00	0.00	0.00
End-member calculation											
Enstatite (XMg)	0.43	0.43	0.44	0.44	0.43	0.45	0.44	0.44	0.45	0.45	0.45
Ferrosilite	0.55	0.55	0.55	0.55	0.55	0.55	0.55	0.55	0.55	0.55	0.55

Table 3 - Cerro da Árvore Complex grt-st-mica schist mineral chemistry											
Mineral	Staurolite										
DataSet/Point	1 / 1 .	2 / 1 .	4 / 1 .	26 / 1 .	27 / 1 .	32 / 1 .	33 / 1 .	34 / 1 .	36 / 1 .	37 / 1 .	39 / 1 .
SiO2	27.12	27.45	27.76	26.68	27.30	26.52	27.29	27.39	27.09	26.65	27.38
MgO	1.04	0.96	1.03	1.04	0.89	1.04	1	0.84	0.81	1.02	1.08
Al2O3	54.81	55.10	54.36	55.30	55.19	56.22	55.23	55.69	55.66	56.37	55.43
CaO	0.01	0.00	0.01	0.01	0.00	0	0	0.00	0.00	0.01	0
FeO	12.96	12.65	12.50	13.22	12.28	13.32	13.14	12.15	11.96	12.95	13.05
TiO2	0.70	0.59	0.71	0.37	0.43	0.38	0.88	0.45	0.38	0.33	0.48
MnO	0.27	0.21	0.26	0.22	0.27	0.21	0.25	0.24	0.28	0.27	0.25
ZnO	1.29	1.54	1.53	1.42	2.25	1.32	1.43	2.19	2.03	1.44	1.45
Total	98.20	98.51	98.15	98.25	98.62	99.02	99.23	98.97	98.2	99.05	99.12
No. Cations in Formula											
Si	7.53	7.58	7.69	7.41	7.55	7.31	7.50	7.54	7.50	7.34	7.53
Mg	0.43	0.40	0.43	0.43	0.37	0.43	0.41	0.34	0.33	0.42	0.44
Al	17.93	17.94	17.75	18.11	17.99	18.27	17.90	18.06	18.17	18.29	17.97
Ca	0.00	0.00	0.00	0.00	0.00	0.00	0.00	0.00	0.00	0.00	0.00
Fe	3.01	2.92	2.90	3.07	2.84	3.07	3.02	2.80	2.77	2.98	3.00
Ti	0.15	0.12	0.15	0.08	0.09	0.08	0.18	0.09	0.08	0.07	0.10
Mn	0.06	0.05	0.06	0.05	0.06	0.05	0.06	0.06	0.07	0.06	0.06
Zn	0.26	0.31	0.31	0.29	0.46	0.27	0.29	0.44	0.42	0.29	0.29
TOTAL	29.37	29.33	29.29	29.45	29.36	29.48	29.36	29.34	29.33	29.45	29.39
XMg	0.13	0.12	0.13	0.12	0.11	0.12	0.12	0.11	0.11	0.12	0.13
Xfe	0.87	0.88	0.87	0.88	0.89	0.88	0.88	0.89	0.89	0.88	0.87

Table 3 - (cont.)							
Garnets	core	core	rim	rim	core	core	rim
DataSet/Point	8 / 1 .	9 / 1 .	10 / 1 .	18 / 1 .	19 / 1 .	20 / 1 .	21 / 1 .
SiO2	37.25	37.11	37.27	37.15	37.18	37.35	37.32
MgO	1.46	1.53	1.56	1.66	1.54	1.49	1.61
Al2O3	20.89	20.65	20.91	21.16	21.05	21.24	21.06
CaO	1.87	2.02	1.69	1.53	1.75	1.7	1.47
TiO2	0.05	0.06	0.05	0.00	0.03	0.02	0.07
FeO	31.39	32.05	32.99	33.57	32.66	32.47	33.77
MnO	6.67	5.96	5.36	4.84	5.9	6.01	5.12
Total	99.58	99.38	99.83	99.91	100.11	100.28	100.42
No. Cations in Formula							
Si	6.057433	6.0541	6.050029	6.024477	6.025095	6.033615	6.030285
Mg	0.35	0.37	0.38	0.4	0.37	0.36	0.39
Al	4.004203	3.970946	4.000989	4.044748	4.020888	4.044425	4.011159
Ca	0.325781	0.353046	0.293905	0.265812	0.303819	0.29421	0.254469
Ti	0.006114	0.00736	0.006103	0	0.003656	0.002429	0.008505
Fe	4.268319	4.372097	4.477994	4.552134	4.425617	4.386038	4.562789
Mn	0.91864	0.823497	0.736919	0.664757	0.809774	0.822278	0.700686
sumX2+	5.87	5.92	5.89	5.88	5.91	5.86	5.91
Total (T)	15.93435	15.95307	15.94337	15.95315	15.96081	15.94174	15.95563
End-member calculations							
PY	6.0	6.3	6.4	6.8	6.3	6.1	6.6
ALM	72.8	73.8	76.1	77.4	74.9	74.8	77.3
GRO	5.6	6.0	5.0	4.5	5.1	5.0	4.3
SP	15.7	13.9	12.5	11.3	13.7	14.0	11.9
XMg	0.1	0.1	0.1	0.1	0.1	0.1	0.1
	core	core	rim	rim	core	core	rim

Table 3 - (cont.)										
Micas	Muscovite							Biotite		
DataSet/Point	3 / 1 .	5 / 1 .	22 / 1 .	28 / 1 .	31 / 1 .	35 / 1 .	38 / 1 .	6 / 1 .	11 / 1 .	14 / 1 .
Na2O	1.03	1.21	1.30	1.11	1.20	0.76	0.95	0.14	0.15	0.13
SiO2	46.29	46.21	45.95	46.10	46.93	46.19	45.62	34.15	35.19	34.70
MgO	0.37	0.31	0.36	0.25	0.43	0.35	0.42	8.10	7.77	7.81
Al2O3	36.48	37.10	37.29	37.51	36.31	37.06	37.11	19.68	19.65	19.05
K2O	9.49	9.24	9.38	9.52	9.26	9.05	9.33	7.29	7.98	7.45
TiO2	0.20	0.27	0.24	0.31	0.31	0.28	0.13	1.48	1.68	1.92
FeO	0.96	0.66	0.70	0.75	0.91	1.14	1.01	23.19	22.77	23.01
MnO	0.00	0.02	0.01	0.01	0.00	0.00	0.00	0.08	0.07	0.09
Total	94.83	95.01	95.23	95.56	95.34	94.83	94.58	94.10	95.25	94.16
No. Cations in Formula										
Na	0.265	0.310	0.333	0.283	0.306	0.195	0.245	0.042	0.045	0.039
Si	6.143	6.105	6.069	6.068	6.183	6.110	6.068	5.304	5.393	5.383
Mg	0.073	0.061	0.071	0.049	0.084	0.069	0.083	1.875	1.775	1.806
Al	5.706	5.778	5.806	5.820	5.638	5.779	5.819	3.603	3.549	3.484
K	1.606	1.557	1.580	1.598	1.556	1.527	1.583	1.444	1.560	1.474
Ti	0.020	0.027	0.024	0.031	0.031	0.028	0.013	0.173	0.194	0.224
Fe	0.107	0.073	0.077	0.083	0.100	0.126	0.112	3.012	2.918	2.985
Mn	0.000	0.002	0.001	0.001	0.000	0.000	0.000	0.011	0.009	0.012
TOTAL	13.920	13.913	13.961	13.932	13.899	13.834	13.923	15.464	15.441	15.407
XMg	0.407	0.456	0.478	0.373	0.457	0.354	0.426	0.384	0.378	0.377
Si apfu	3.07	3.05	3.03	3.03	3.09	3.06	3.03	2.65	2.70	2.69

TABLE 04 – Comparative table for main characteristics of Várzea do Capivarita Ccomplex and Cerro da Árvore Complex

Characteristic	VCC	Reference (method)	CAC (eastern PC)	Reference (method)
Igneous protolith geochemistry	Arc-like, medium- to high-K calc-alkaline	Martil et al., 2011, 2017;	Arc-like, medium- to high-K calc-alkaline	Battisti et al., 2018
Magmatic age	789.7 ± 8.7 Ma 770 ± 9.9 Ma 788 ± 5.3 Ma 790 ± 34 Ma	Martil, 2016 (U-Pb zircon, LA-ICP-MS and SHRIMP)	[1] 789 ± 7 Ma [2] 789 ± 39 Ma [3] 773±3.1; 801±4.7 [3'] 809 ± 4.1 Ma [4] 773 ± 8 Ma	[1] Saalmann et al., 2011 (U-Pb zircon LA-ICP-MS) [2] Soliani Jr., 1986 [3] Pertille et al., 2017 (U-Pb zircon [2,3]SHRIMP and [3']LA-ICP-MS) [4] Chemale Jr., 2000 (U-Pb zircon TIMS)
Metasedimentary provenance	MDA: 728 ± 11 Ma 1.4; 2 – 2.2 Ba	Gruber et al., 2016a (U-Pb zircon, SHRIMP)	800 – 780 Ma 1.4; 2 – 2.2 Ba	Gruber et al., 2016b (U-Pb zircon, LA-ICP-MS)
Metamorphic age	[5] 648.4 ± 5.4 Ma 648 ± 18 Ma [6] 618 ± 7.3 Ma [7] 614 ± 12 Ma ~~652 ± 26 Ma~~ 605.9 ± 2.4 Ma [8] 619 ±4.3 Ma	[5] Martil, 2016 (U-Pb zircon SHRIMP+LA-ICP-MS) [6] Gruber et al. 2016a (U-Pb zircon SHRIMP) [7] Gross et al., 2006 (Sm-Nd garnet-whole rock isochron) [8] Philipp et al., 2016b (U-Pb zircon SHRIMP)	[9] 658 ± 26 Ma	[9] Lenz, 2006 (Rb-Sr isochron muscovite-whole- rock composite of 5 samples)
Metamorphic conditions	[11] 730 – 800°C 3 – 4 Kbar [12] 790 – 865 (910)°C 4.4 - 4.8 Kbar – M_1 [12,] 665 - 725 °C 2.8 - 3.4 Kbar – M_2	[11] Gross et al., 2006 (THERMOCALC several samples) [12] This work (Perple_X 3 different samples) [12,] This work (Perple_X SiO_2-subsaturated domain from metapelite)	[14] 590 °C 6 Kbar – M_1 [14'] 550 °C 2.7 Kbar – M_2 [15] 560 – 580 °C 5.8 - 6.3 Kbar – M_1	[14/14,] Lenz, 2006 (THERMOCALC, Cerro do Facão metapelite) [15] This work (Perple_X, Cerro do Facão metapelite)
Structural pattern	NNW-striking progressive transpression from D_1 thrust-to-W to D_2 dextral strike-slip	Martil et al., 2011 Martil, 2016 De Toni et al., 2016	NNW-striking progressive transpression from D_1 thrust-to-W to D_2 (dextral?) strike-slip	Battisti et al., 2018

5. *Dom Feliciano Belt orogenic cycle tracked by its pre-collisional magmatism: the Tonian (ca. 800 Ma) Porto Belo Complex and its correlations in southern Brazil and Uruguay*

Assunto **Successfully received: submission Dom Feliciano Belt orogenic cycle tracked by its pre-collisional magmatism: the Tonian (ca. 800 Ma) Porto Belo Complex and its correlations in southern Brazil and Uruguay for Precambrian Research**

CHASQUE WEBMAIL
Universidade Federal do Rio Grande do Sul

Remetente Precambrian Research <EviseSupport@elsevier.com>
Para <gdetoni@ufrgs.br>
Responder para <precam-eo@elsevier.com>
Data 2019-10-15 19:25

This message was sent automatically.

Ref: PRECAM_2019_488
Title: Dom Feliciano Belt orogenic cycle tracked by its pre-collisional magmatism: the Tonian (ca. 800 Ma) Porto Belo Complex and its correlations in southern Brazil and Uruguay
Journal: Precambrian Research

Dear Dr. De Toni,

Thank you for submitting your manuscript for consideration for publication in Precambrian Research. Your submission was received in good order.

To track the status of your manuscript, please log into EVISE® at: http://www.evise.com/evise/faces/pages/navigation/NavController.jspx?JRNL_ACR=PRECAM and locate your submission under the header 'My Submissions with Journal' on your 'My Author Tasks' view.

Thank you for submitting your work to this journal.

Kind regards,

Precambrian Research

Have questions or need assistance?
For further assistance, please visit our Customer Support site. Here you can search for solutions on a range of topics, find answers to frequently asked questions, and learn more about EVISE® via interactive tutorials. You can also talk 24/5 to our customer support team by phone and 24/7 by live chat and email.

Dom Feliciano Belt orogenic cycle tracked by its pre-collisional magmatism: the Tonian (ca. 800 Ma) Porto Belo Complex and its correlations in southern Brazil and Uruguay

De Toni, G.B.[1]*; Bitencourt, M.F.[1]; Nardi, L.V.S. [1]; Florisbal, L.M.[2]; Almeida, B.S.[3]; Geraldes, M.[3]

[1] Programa de Pós-graduação em Geociências (PPGGEO), Universidade Federal do Rio Grande do Sul (UFRGS), Porto Alegre, RS, Brazil

[2] Programa de Pós-graduação em Geologia (PPGGeologia), Universidade Federal de Santa Catarina (UFSC), Florianópolis, SC, Brazil

[3] Departamento de Geologia Regional e Geotectônica, Universidade Estadual do Rio de Janeiro (UERJ), Rio de Janeiro, RJ, Brazil

* Corresponding author: gdetoni@ufrgs.br

ABSTRACT

Porto Belo Complex orthogneisses are dominantly intermediate, high-K calc-alkaline in composition and show Tonian age (ca. 800 Ma), representing the hinterland basement of northern Dom Feliciano Belt. These rocks are correlated to other pre-collisional Tonian orthometamorphic rocks of Dom Feliciano Belt. Their significance is discussed and integrated in an Occam's Razor model for the evolution of Kaoko-Dom Feliciano-Gariep Orogenic System. The model assume a single, eastward subduction, with variable subduction angle in time, which led to arc-magmatism migration prior to collision in the following stages: a) 925 – 880 Ma early subduction and fore-arc magmatism; b) 820 – 770 Ma flat-slab subduction and arc-magmatism migration towards the back-arc region, with genesis of arc-related Tonian magmatic protoliths; c) 765 – 700 Ma steepening subduction and arc-magmatism migration towards fore-arc, with genesis of São Gabriel Block rocks, while extension affected

the back-arc area and has triggers rifting; d) 700 – 660 Ma accretionary phase, after final consumption of the eastward subducting oceanic plate; e) 660 – 630 Ma oblique main collision leads to basin inversion and double-verging transpression, with hinterland high-T/low-P metamorphism and exhumation; f) 630 – 580 Ma post-collisional magmatism; g) 580 – 550 Ma secondary collision, with foreland deformation and later post-collisional magmatism recorded in Dom Feliciano Belt, while the main orogenic front migrated towards Kaoko and Gariep belts.

Keywords: Orogenic cycle; Pre-collisional; Dom Feliciano Belt; Arc magmatism; Back-arc rift; Occam's razor

1. Introduction

The Neoproterozoic history during west Gondwana assembly records diachronous collisions between cratonic nuclei building up a complex mosaic of tectonic environments in time and space (e.g. Almeida et al., 2000; Kroner and Stern, 2004; Bento dos Santos et al., 2015; Oriolo et al., 2017, among others). Orogenic belts along the Mantiqueira Province exhibit a fragmentary record of the pre-collisional period, strongly reworked and disrupted during collisional and post-collisional times (e.g. Martil et al., 2017; Peixoto et al., 2017). The exception is the juvenile São Gabriel Block, which exhibits the best preserved and complete record of a magmatic arc environment in the western portion of the Dom Feliciano Belt, Rio Grande do Sul state (Saalmann et al., 2005; 2006a; Lena et al., 2014; Gubert et al., 2016; Arena et al., 2016; 2017; Philipp et al., 2018 and references therein).

Deformed fragments of Tonian pre-collisional rocks are found along the whole orogenic system, usually correlated to the arc magmatism which preceded tectonic amalgamation in a regular Wilson Cycle. Examples of these rocks are the Serra da

Prata and Rio Negro arcs (Peixoto et al., 2017), and the Embú Complex (Cordani et al., 2002; Campanha et al., 2019), both in the Ribeira Belt. Similar register of orthogneissic, pre-collisional rocks is locally found eastwards, along the Dom Feliciano Belt, whose protoliths are usually interpreted as related to arc magmatism (e.g. Lenz et al., 2011, 2013; Koester et al., 2016; Martil et al., 2017 and references therein).

The fragmentary nature of such record has led to intense debate regarding the tectonic environment which it represents (e.g. Meira et al., 2015; Konopasek et al., 2018). In order to contribute to such discussion, the geology, age and geochemistry of the Porto Belo Complex gneissic rocks (first mentioned by Chemale Jr. et al., 2012; Florisbal et al., 2012a) is presented and correlated to other Tonian (800 – 770 Ma) orthometamorphic rocks exposed along the Dom Feliciano Belt in southernmost Brazil and Uruguay, bringing new insights into the early stages of this Orogenic Cycle. The proposed model attempts to stimulate further discussion among geoscientific community interested in the tectonic evolution of (southern) Brazil, Uruguay and its African counterparts.

2. Geological Setting

2.1 An overview of the Dom Feliciano Belt in southern Brazil and Uruguay

The Dom Feliciano Belt (DFB) is the south american portion of the Kaoko-Dom Feliciano-Gariep Orogenic System, formed during western Gondwana assembly (Konopásek et al., 2016, 2018). The DFB evolution has been subject of many distinct hypotheses proposed in the past decades (e.g. Fernandes et al., 1992; Chemale Jr., 2000; Hartmann et al., 2007; Philipp et al., 2016), which apart of their differences, are generally in agreement about its subdivisions.

The DFB western portion is the juvenile São Gabriel Block, exposed exclusively in the state of Rio Grande do Sul, southernmost Brazil (Fig.1a). The São Gabriel block records a long-lived history which started in the early Neoproterozoic with an oceanic domain (920 – 890 Ma ophiolites, magmatic ages by Arena et al., 2016), with subduction and an early (island?) arc development (ca. 880 Ma Passinho Metadiorite from Leite et al., 1998), evolving to a continental magmatic arc (770 – 690 Ma, according to Lena et al., 2014; Gubert et al., 2016; and others) and final accretion (690 – 650 Ma, Lena et al., 2014; or 650 – 600, Arena et al., 2017), with post-collisional magmatism (ca. 585 Ma, according to Arena et al., 2017). The structural framework of the São Gabriel Block is presented by Saalmann et al. (2006a), with NE-striking, low to medium angle, predominantly NW-dipping, oblique SE-verging plus dextral transpressional fabric. Many authors do not consider the São Gabriel Block as part of Dom Feliciano Belt, but as part of an independent orogeny (e.g. Chemale Jr., 2000; Philipp et al., 2016; 2018; among others).

Towards the east, two, over 2000 km long parallel domains of the Dom Feliciano Belt are well exposed side-by-side, from southernmost Uruguay, across Rio Grande do Sul, to the coast of Santa Catarina state, Brazil (Fig. 1a). The so called Tijucas Fold Belt (Hasui, 1975) represents a foreland fold and thrust belt formed by two distinct Tonian and Ediacaran sequences of low- to medium-grade schists (e.g. Jost and Bitencourt, 1980; Hofig et al., 2017; Battisti et al., 2018) containing gneiss domes of Paleoproterozoic basement (e.g. Encantadas in Rio Grande do Sul – Saalmann et al., 2006b; Camboriú Complex in Santa Catarina, see Fig. 1b – Basei et al., 2013; Martini et al., 2019).

To the east is a dominantly granitic region, considered to be the inner domain of the Dom Feliciano Belt, where Ediacaran, late- to post-collisional magmas were emplaced along a complex array of shear zones (the Southern Brazilian Shear Belt

of Bitencourt and Nardi, 2000). Paleoproterozoic basement is found locally (e.g. Gregory et al., 2015), while scattered register of Tonian (800 – 770 Ma) gneisses occurs along the belt (e.g. Silva et al., 1999; Koester et al., 2016) and in two main roof pendants (Fig. 1a). The structure of these domains was recently correlated across strike in Uruguay by Oriolo et al. (2016a), and in Brazil by Battisti et al. (2018) and De Toni (2019). Finally, a southeastern sector of low-grade schists is present exclusively in the easternmost coastal area of Uruguay, the Rocha Group, which is correlated to the Gariep Belt (Betucci and Burgueno, 1993).

2.2 800 – 770 Ma pre-collisional magmatism of the Dom Feliciano Belt

Amphibolite- to granulite-facies Tonian orthogneisses are widespread as xenoliths in the granitoids emplaced along the inner domain of the Dom Feliciano Belt (see locations in figure 1a). The occurrences are compared in table 1. All rock associations have 800 – 770 Ma magmatic protoliths (Silva et al., 1999; Lenz et al., 2011; Koester et al., 2016; Martil et al., 2017) and dominantly calc-alkaline affinity (Philipp and De Campos, 2004; Lenz et al., 2013; Martil et al., 2011, 2017). They show high-grade, collisional metamorphism at ca. 650 Ma (Koester et al., 2015; Tambara et al., 2019; Martil et al., 2017). It is noteworthy that Martil et al. (2017) points out that the easternmost metavolcanic rocks of the so called Porongos Complex, hereafter called Cerro da Árvore Complex (sensu Jost and Bitencourt, 1980), from the Tijucas Fold Belt, are correlated to the same Tonian magmatic event, which was later confirmed by the studies of Battisti et al. (2018).

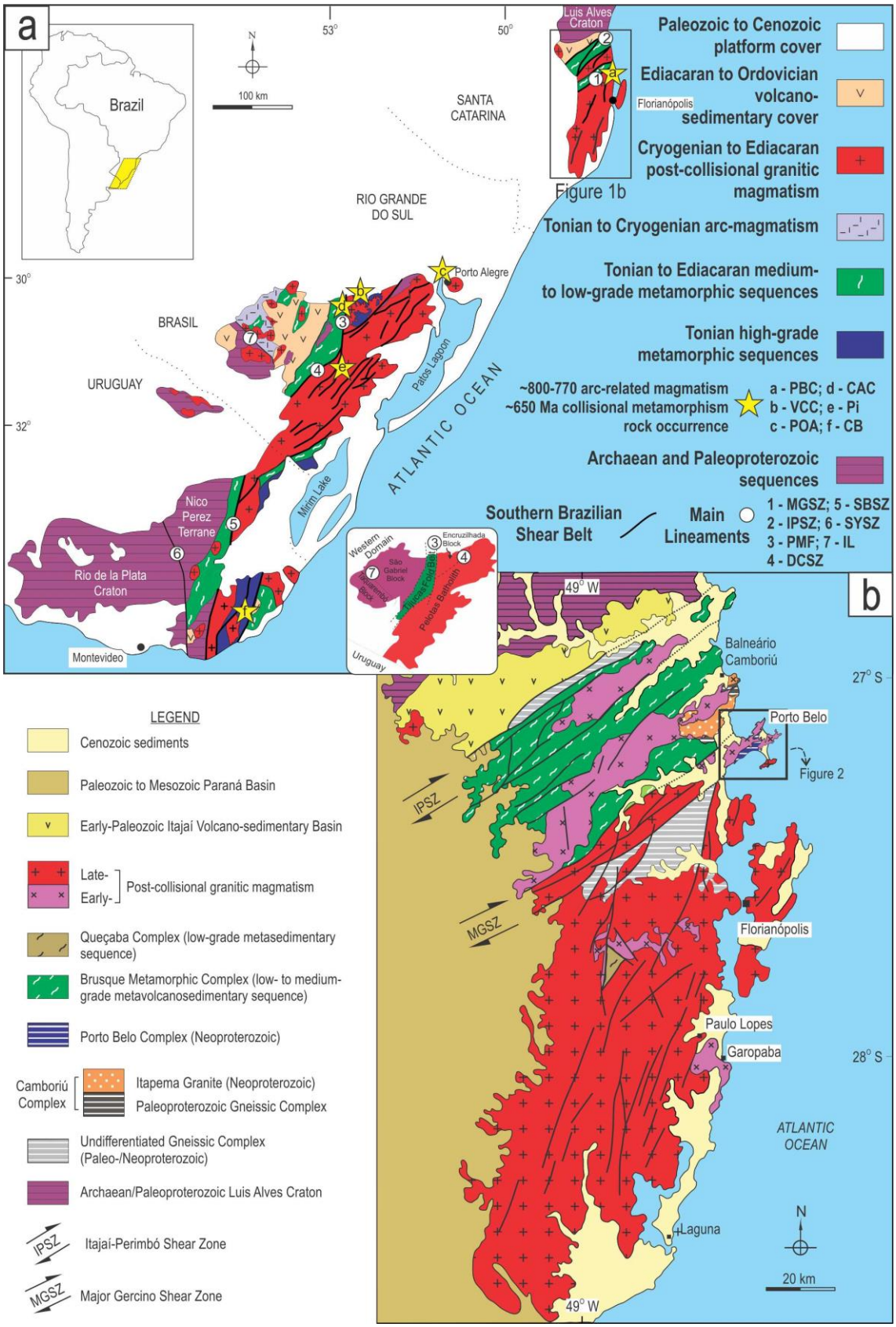

Figure 1 (a) Geotectonic sketch of Dom Feliciano Belt (modified from Bitencourt and Nardi, 2000; Ramos et al., 2018; Will et al., 2019) and cratonic adjacent areas. Tonian orthogneisses occurrences are indicated with yellow stars: Porto Belo Complex (PBC – this work), Várzea do Capivarita Complex (VCC – Gross et al., 2006; Martil et al., 2017), Porto Alegre orthogneiss (POA – Philipp and de Campos, 2004; Koester et al., 2016), (cont.)

Cerro da Árvore Complex metavolcanics (CAC – sensu Jost and Bitencourt, 1980; Battisti et al., 2018) Piratini orthogneiss (Pi – Silva et al., 1999; Tambara et al., 2019) and Cerro Bori orthogneiss (CB – Lenz et al., 2011; 2013). Main lineaments are shown with numbered white circles: Major Gercino Shear Zone (MGSZ - Bitencourt, 1996; Florisbal et al., 2012a; Chemale Jr. et al., 2012; Hueck et al., 2018), Itajaí-Perimbó Shear Zone (IPSZ), Passo do Marinheiro Fault (PMF), Dorsal de Canguçú Shear Zone (DCSZ – Fernandes and Koester, 1999), Sierra Balle Shear Zone (SBSZ – Oriolo et al., 2016 and references therein), Sarandi del Yi Shear Zone (SYSZ – Oriolo et al., 2016a,b) and Ibaré Lineament (IL). Rio Grande do Sul shield area subdivision is shown in the lower inset. (b) Geotectonic map of Santa Catarina State shield area (modified from Florisbal et al., 2012a), and location of study area (figure 2).

The Piratini and Porto Alegre orthogneisses are m- to dm-size xenoliths (e.g. Silva et al., 1999; Philipp and de Campos, 2004; Koester et al., 2016). Kilometer-size roof pendants are described in the Encruzilhada Block, northwest portion of the Pelotas Batolith, (Jost and Hartmann, 1984; De Toni, 2019) as the Várzea do Capivarita Complex ortho- and paragneisses (Martil et al., 2017. Another roof pendant is the Punta del Este Terrane in Uruguay, which includes the Cerro Bori orthogneisses, as part of the Cerro Olivo Complex (Masquelin et al., 2012; Lenz et al., 2011, 2013). In these two roof pendant areas it is possible to observe interleaved metasedimentary strata and a coherent flat-lying foliation recording a top-to-the-W/NW transpression (Masquelin et al., 2012; Martil, 2016; Martil et al., 2017) which, together with the high-grade metamorphism (Gross et al., 2006, 2009) points to an oblique collision event. The transpression led to strain partitioning and strike-slip tectonics during the post-collisional magmatic event (e.g. Florisbal et al., 2012a).

2.3 Major Gercino Shear Zone geology

A poorly-documented occurrence of Neoproterozoic orthogneisses, the Porto Belo Complex, is reported by Florisbal et al. (2012a) as the basement of the Major Gercino Shear Zone. This shear zone is the northern boundary between the batolithic

inner domain and the Tijucas Fold Belt exposed in Santa Catarina state, northern Dom Feliciano Belt (see Fig. 1b – Bitencourt, 1996; Florisbal et al., 2012a; Chemale Jr. et al., 2012; Hueck et al., 2018). The Porto Belo Complex rocks form m-size, structurally concordant xenoliths, or larger individual bodies (Fig. 2). The rocks are described as granitic to granodioritic orthogneisses with minor metatonalites and biotite gneisses, metamorphosed under amphibolite facies conditions, and no partial melt was described (Chemale Jr. et al., 2012).

The Major Gercino Shear Zone early deformation phase was controlled by a gently-dipping structure, dominantly dipping towards the SE/SSE (Bitencourt, 1996; Chemale Jr. et al., 2012). The flat-lying deformation phase affected basement rocks as well as the early-magmatism controlled by the shear zone. Chemale Jr et al. (2012) present an U-Pb zircon LA-ICP-MS concordant age of 649±10 Ma for a mafic tonalitic gneiss from the Porto Belo Complex, and a U-Pb zircon ID-TIMS age of 646 ± 15 for a fine-grained foliated mafic tonalite. The authors interpret these data as the crystallization age of the pre-transcurrence magmatic rocks.

The Quatro Ilhas Granitoids represent the progression from flat-lying towards steeply-dipping, strike-slip shearing, between 625 and 615 Ma (Chemale Jr. et al., 2012; Florisbal et al., 2012a,b). A series of granitic rocks were emplaced during dextral strike-slip shearing, between 610 and 590 Ma, as the peraluminous Mariscal Granite (ca. 610Ma), the shoshonitic Estaleiro Granitic Complex (610 – 600 Ma) and the A-type Zimbros Intrusive Suite (ca. 590 Ma), which includes the Morro dos Macacos Granite, emplaced outside (south) of the shear zone (see figure 2 –Bitencourt and Nardi, 1993; Bitencourt, 1996; Nardi and Bitencourt, 2009; Chemale Jr. et al., 2012; Florisbal et al., 2012a).

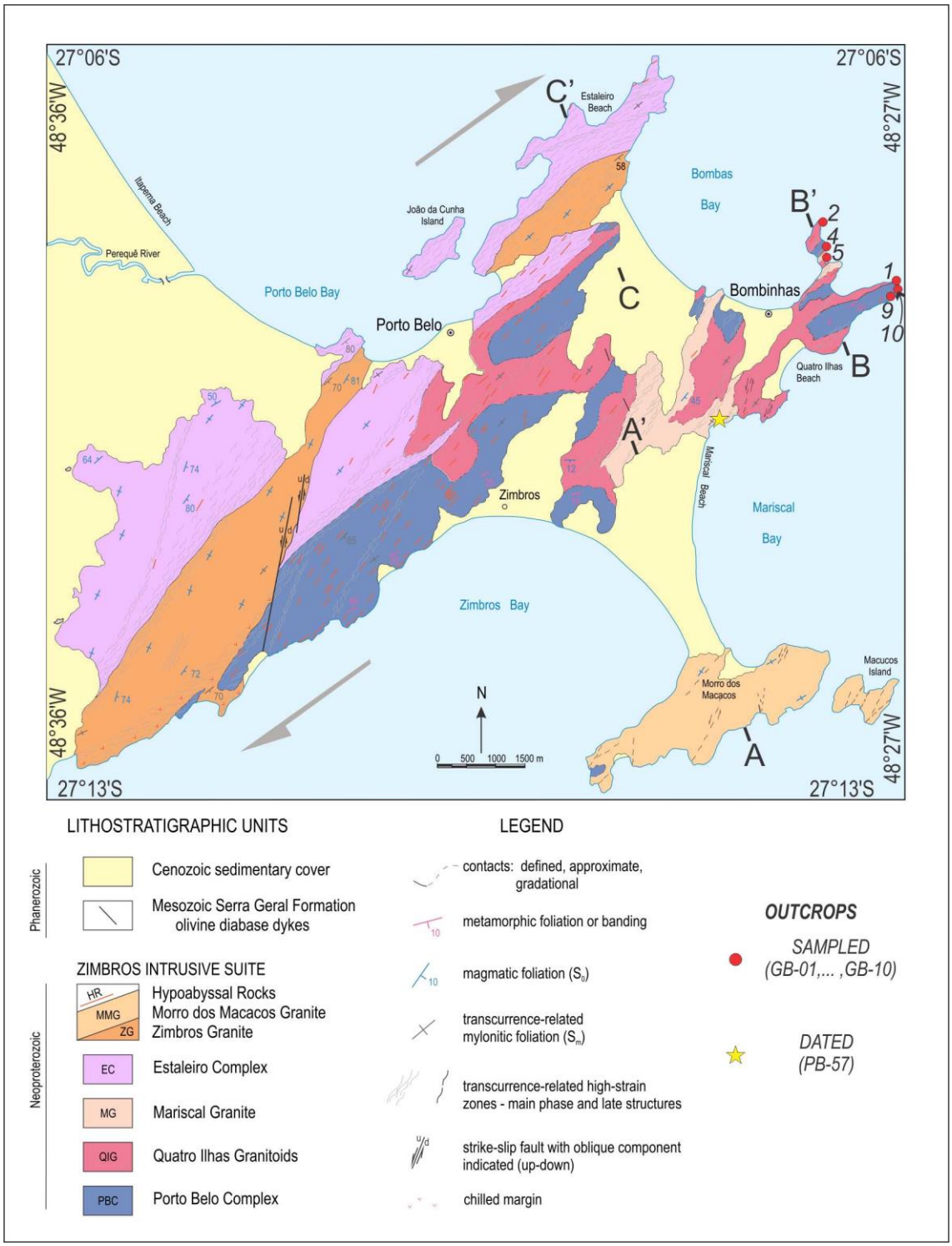

Figure 2 – Geological map of Porto Belo peninsula (modified from Bitencourt, 1996; Florisbal et al., 2012a). Studied outcrops are shown, as well as references for the composite cross-section (figure 3).

3. Materials and methods

This paper presents the results of integrated fieldwork, structural and petrographic observations with geochronology and whole-rock geochemistry. Geochemical data

were obtained from 17 samples of the Porto Belo Complex through ion coupled plasma mass spectrometer (ICP-MS) for major and trace elements at ActLab (Canada), from which 15 are considered as representative of the pre-collisional magmatism, and 2 show interference of partial melting processes in their chemical composition.

One of the representative samples was selected for U-Pb zircon LA-MC-ICP-MS geochronological determinations. About 110 zircon crystals were separated from the least magnetic mineral fraction of sample PB-57G (see location in Fig. 02a), mounted and polished in a standard epoxy mount. The sample was conventionally prepared at LGI/UFRGS (Laboratório de Geologia Isotópica/Universidade Federal do Rio Grande do Sul), as described by Florisbal et al. (2012a). All zircons were imaged by back-scattered electron (BSE) and cathodoluminescence (CL) before LA-MC-ICP-MS analyses, using a Neptune MC-ICP-MS at LM/UERJ(Laboratório Multiusuário/Universidade Estadual do Rio de Janeiro). Analytical protocols and collector configurations were according Jackson et al. (2004) and Chemale et al. (2012), and correction of laser-induced elemental fractional and instrumental mass discrimination was made by zircon standard (GJ-1) as suggested by Wiedenbecket al. (1995). 72 spots were analysed from 49 zircon crystals, with 42 spots (20 μm) presenting less than 5% of discordance.

4. The Porto Belo Complex Orthogneisses

4.1 Fieldwork and Petrography

Fieldwork was carried out along the coastal outcrops at the eastern portion of the Porto Belo peninsula, which represents the easternmost tip and also the inner portion of the Major Gercino Shear Zone (Fig. 2). The area was selected due to good exposure of the early magmatism along the shear zone, as well as of the earlier

deformational increments over both basement and early intrusive rocks (Fig. 3). In the study area, the Porto Belo Complex is exposed as (i) orthogneiss xenoliths of 1 m to tens of meters in size found in the Quatro Ilhas Granitoids and Mariscal Granite concordant with their foliation and usually associated with either concordant or discordant leucogranitic injections (Fig. 4); ii) roof pendant of hundreds of meters, as for example in the Ponta das Bombas outcrop (Fig. 5a and 5b; see Fig. 2 and 3 for location), formed by orthogneisses m-thick tabular bodies (Fig. 5c) or lenses, with evidence of partial melting (Fig. 5d), immerse in a granitoid which grades from a banded (Fig. 5b) to a foliated, enclave-rich rock (Fig. 5e). These rocks are interpreted as intimately linked in a migmatitic system.

Orthogneisses within the migmatites show variable degrees of partial melting, from mafic-rich restites to slightly migmatitic orthogneisses. In the later, discrete mm-lenses of in source leucosome (Fig. 5d) and evidence of in situ leucosome (Fig. 6d), suggest low melt mobility from the source.

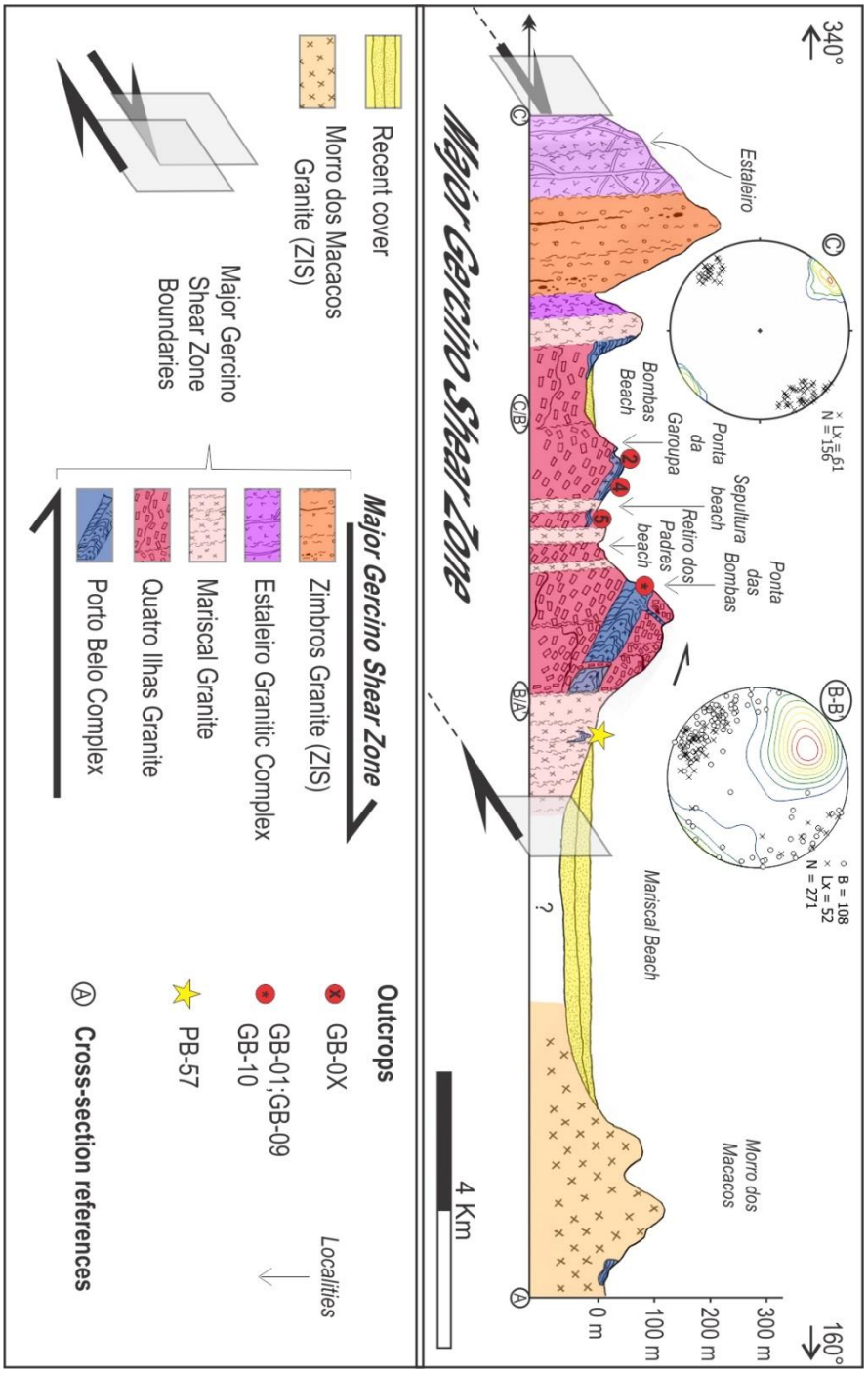

Figure 3 – Major Gercino Shear Zone composite cross-section (see figure 2 for location). Representative stereonets of the gently-dipping, inner portion of the shear zone (B-B' section – data from De Toni, 2019) and of the strike-slip controlled Estaleiro Granitic Complex (from its type-section: C' – data from Bitencourt, 1996) are shown to illustrate the progressive/partitioned transpressional deformation. Studied outcrops are shown.

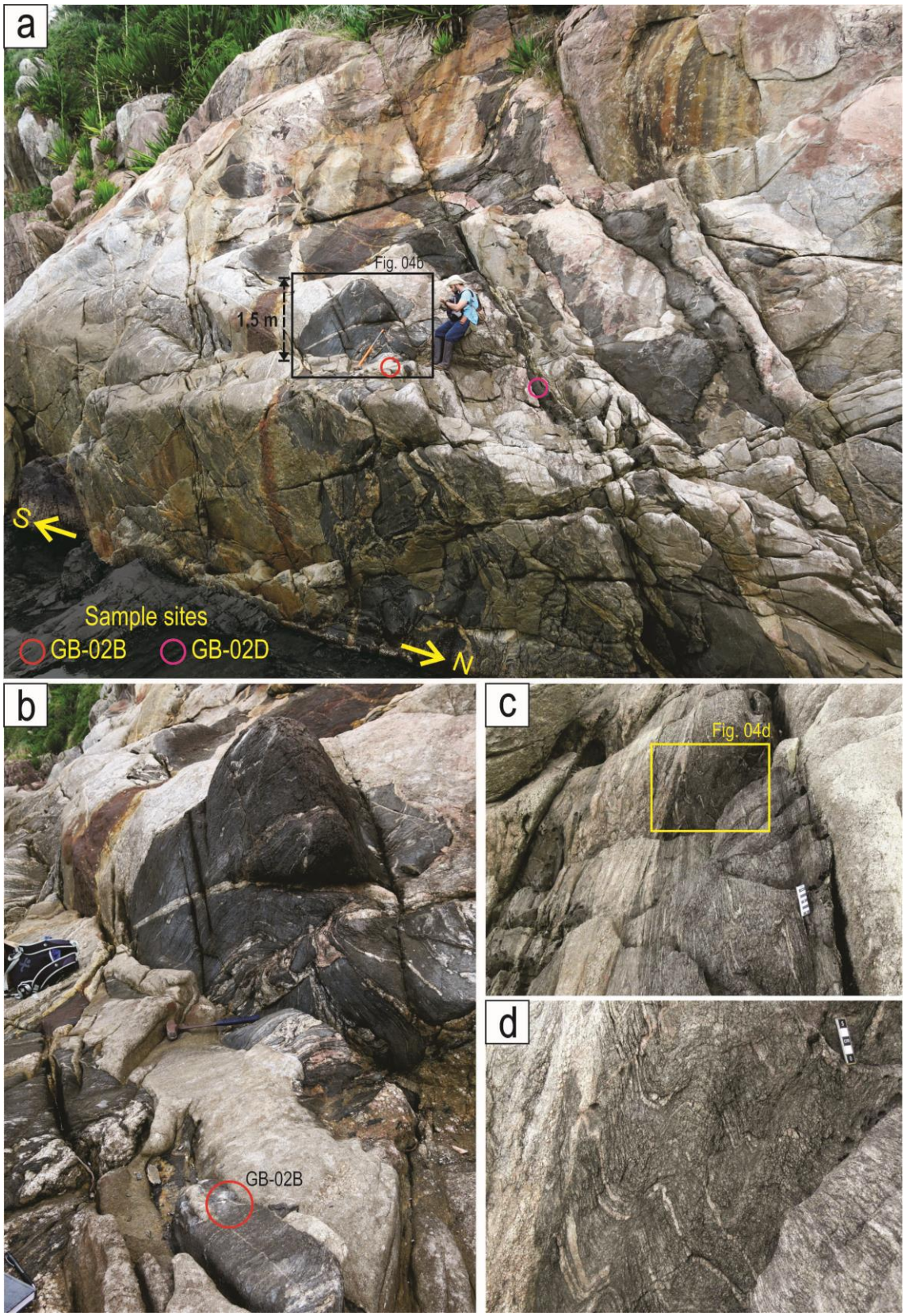

Figure 4 – (a) Outcrop aspect of Porto Belo Complex orthogneiss (749925 mE/6996087 mN; 22J; datum SAD-69) as fragments on Quatro Ilhas Granitoids. Orthogneisses are moderate to tightly folded and stretched according to the NE-striking main foliation of the shear zone, being also cutted by irregular leucogranitic injections. Sample locations are shown as well a detail for figure 4b. (b) Detail of one orthogneiss fragment showing an (cont.)

antiform cutted by a major leucogranitic injection. (c) Outcrop aspect of an occurrence of Porto Belo Complex orthogneiss along a strike-slip high-strain zone within the Mariscal Granite (748294 mE/6992911 mN; 22J; datum SAD-69). Figure 4d presents a detail. (d) Folded banding of the orthogneiss, highlighted by concordant veinlets. A discrete, subvertical, axial plane transposition foliation can be observed (see figure 7 for details).

Along the section between Ponta das Bombas and Ponta da Garoupa (B-B' in figures 02 and 03), the flat-lying foliation dips to the SE, with a variation from highly oblique to a strike-parallel mineral and stretching lineation (stereonet in Fig. 3), which is considered typical of oblique transpression (e.g. Jones et al., 2004; Fernandez and Díaz-Azpiroz, 2009). The foliation is asymmetrically folded, verging towards NNW (Fig. 4d and Fig. 5a to c). This vergence is confirmed in kinematic indicators at several scales, as asymmetric porphyroclasts (Fig. 6d). Progressive deformation during folding has rotated the original gently-dipping foliation (S_1) towards the vertical, which is considered as the process responsible for the local development of a subvertical discrete mylonitic foliation (S_2) in the orthogneisses (Fig. 7a) and in the Quatro Ilhas Granitoids (as argued by Florisbal et al., 2012b). S_2 is controlled by dextral strike-slip tectonics (Fig. 7b) which conditioned the emplacement of mostly granitoids along the Major Gercino Shear Zone.

The orthogneiss protoliths are tonalitic (Fig. 6a to b) to quartz-dioritic (Fig. 6c), more rarely granodioritic. The common rock type is dark gray, fine to very fine grained, usually showing regular or discontinuous, mm-thick banding commonly enhanced by deformed leucocratic veins (Fig. 4d and 5d). Mm-size porphyroclasts are common (Fig. 6d), and rarely reach cm-size (Fig. 6e).

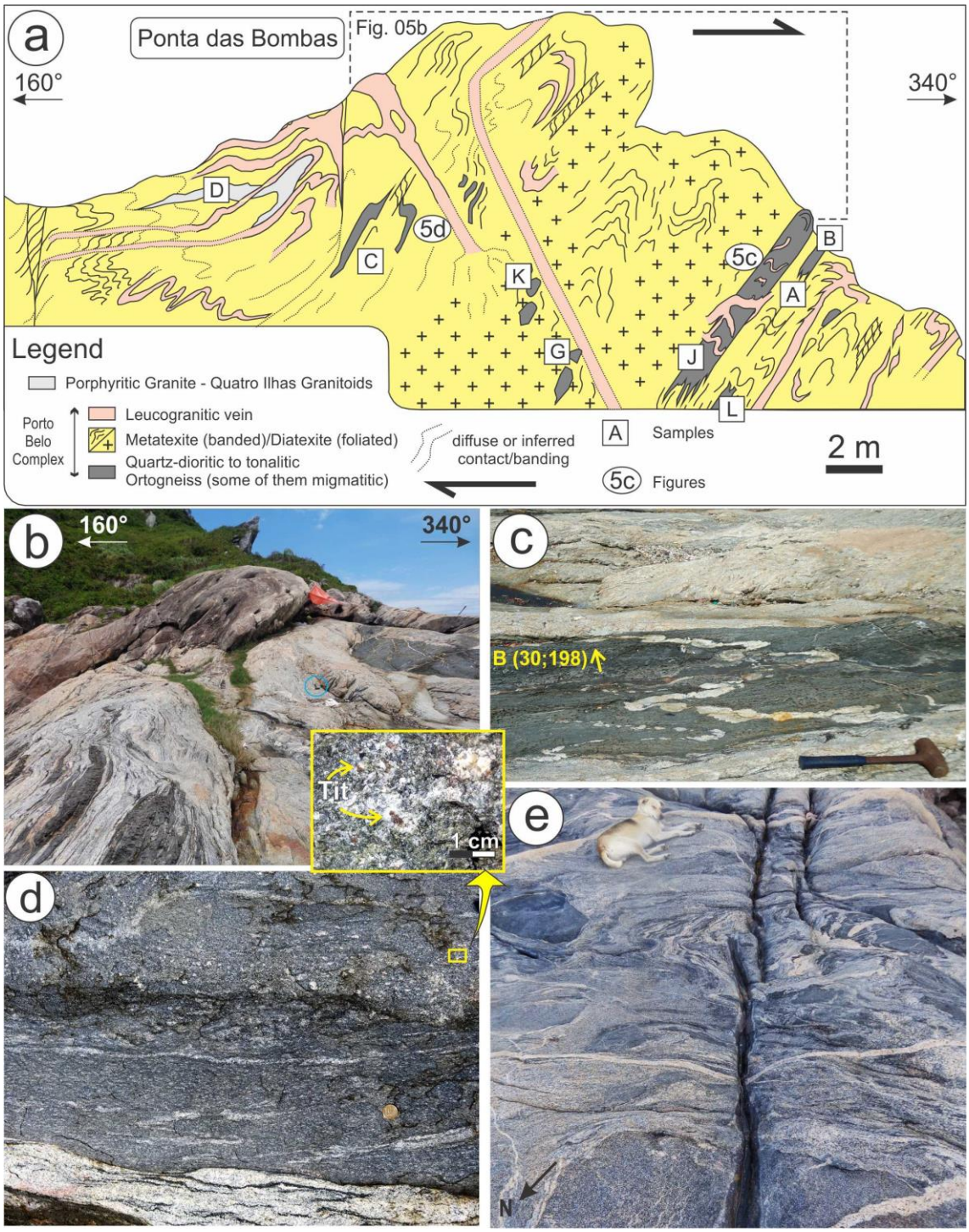

Figure 5 – Porto Belo Complex general features at Ponta das Bombas area. (a) Ponta das Bombas, 340° - 160° cross-section (751180 mE / 6995180 mN; 22J; datum SAD-69), presenting the lithology distribution and its main structural features. Sample sites and references to pictures are indicated. (b) Outcrop overview. The antiform structure is expressed in the outcrop morphology, with both limbs and the axial plane dipping towards SSE. In the first plan, the banded granite with disrupted orthogneiss fragments along the banding is crossed by a leucogranitic vein. (c) Orthogneiss tabular body along the main foliation of the leucocratic granite. Cm-size veins are folded and boudinaged. Fold axis is indicated. (d) Migmatitic orthogneiss heterogeneous deformation. Small patches with titanite-bearing, leucogranitic material, are interpreted as in situ pocket melts (see inset). The lower (cont.)

portion presents the surrounding leucogranite with schlieren. (e) Typical aspect of a diatexite in horizontal exposition. The dog for scale is 75 cm long. Outcrop located ca. 100 m south of the portion represented in figure 5a (not shown).

Plagioclase in the orthogneisses can present prismatic shape, up to 5 mm-size, as igneous relicts (Fig. 6a and 7c), is part of the gneiss granoblastic groundmass (ca. 0.1 mm – Fig. 6b and 6c), or occurs as porphyroclasts (Fig. 6d and 6e). Corroded, either irregular or rounded porphyroclast boundaries are common (Fig. 6d), usually facing fine-grained white mica aggregates (Fig. 7c). Another very common characteristic of plagioclase, observed in all samples, is the presence of rounded inclusions of quartz (Fig. 6a and 7c). Plagioclase from a few samples also present more abundant and irregularly shaped quartz intergrowths, as observed in the terminal portions of the porphyroclast of figure 6e. The difference in extinction angle of that crystal terminal sectors, together with the local presence of quartz intergrowth and heterogeneous fine-grained replacement by white mica, suggests a (strain+fluid)-driven calcification reaction, leading to grain-size reduction and strain softening along recrystallization tails (similarly to the case discussed by De Toni et al., 2016).

Quartz usually occurs as granoblastic grains of up to 0.1 mm and also as within a very fine-grained (≤0.01 mm) granoblastic matrix (Fig. 7c). More rarely, anhedral or elongated crystals, sometimes exhibiting cusp shapes (Fig. 6d inset) are observed and interpreted as crystallized from melt patches in a migmatitic system. Quartz crystals are usually strain-free, possibly due to annealing processes (as in Fig. 6e and 7c).

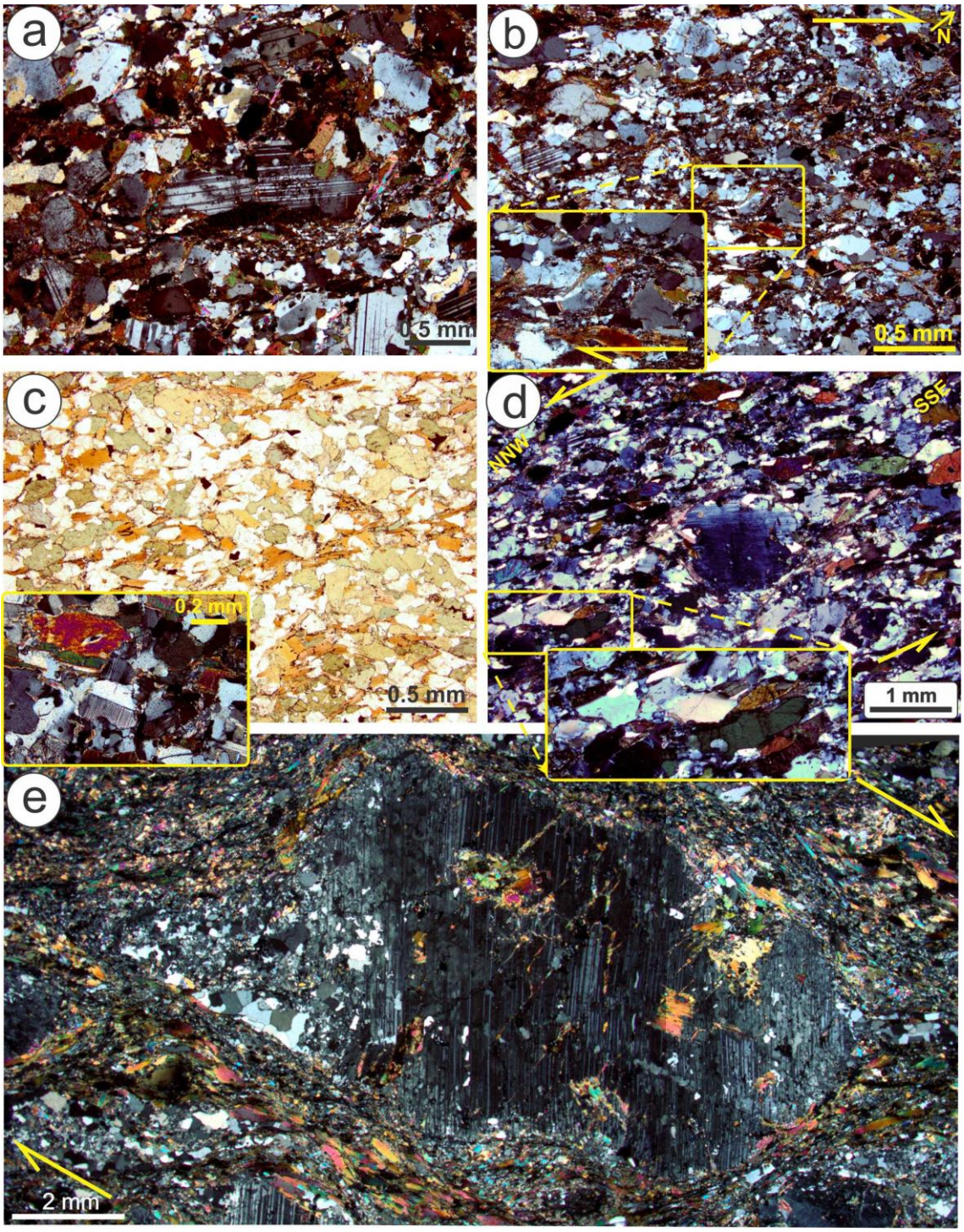

Figure 6 – Petrographic and microstructural aspects of Porto Belo Complex orthogneisses. Pictures are under crossed-polarizers, except when indicated. (a) Intermediate orthogneiss (GB-02C) with an igneous relict, kinked subhedral plagioclase. S-C, dextral fabric is marked by biotite and muscovite, and by fine-grained lens of polygonal texture. (b) Acidic orthogneiss (GB-05B) witha conspicuous S-C, dextral fabric, defined by biotite and stretched quartz-feldspathic aggregates (see inset). (c) Intermediate orthogneiss with biotite and hornblend (GB-09DA) and characteristic polygonal granoblastic texture under plane-polarized light (see inset; crossed-polarizers). (d) Slightly migmatitic intermediate orthogneiss with biotite and hornblend (GB-01J). A plagioclase porphyroclast in the center indicate a top-to-the-NNW shear sense. The inset shows interstitial, cuspide quartz.

(e) Porphyroclastic, intermediate orthogneiss (GB-04D) with a ca. 1 cm long plagioclase porphyroclast, with asymmetric recrystallization tail indicative of dextral shear sense.

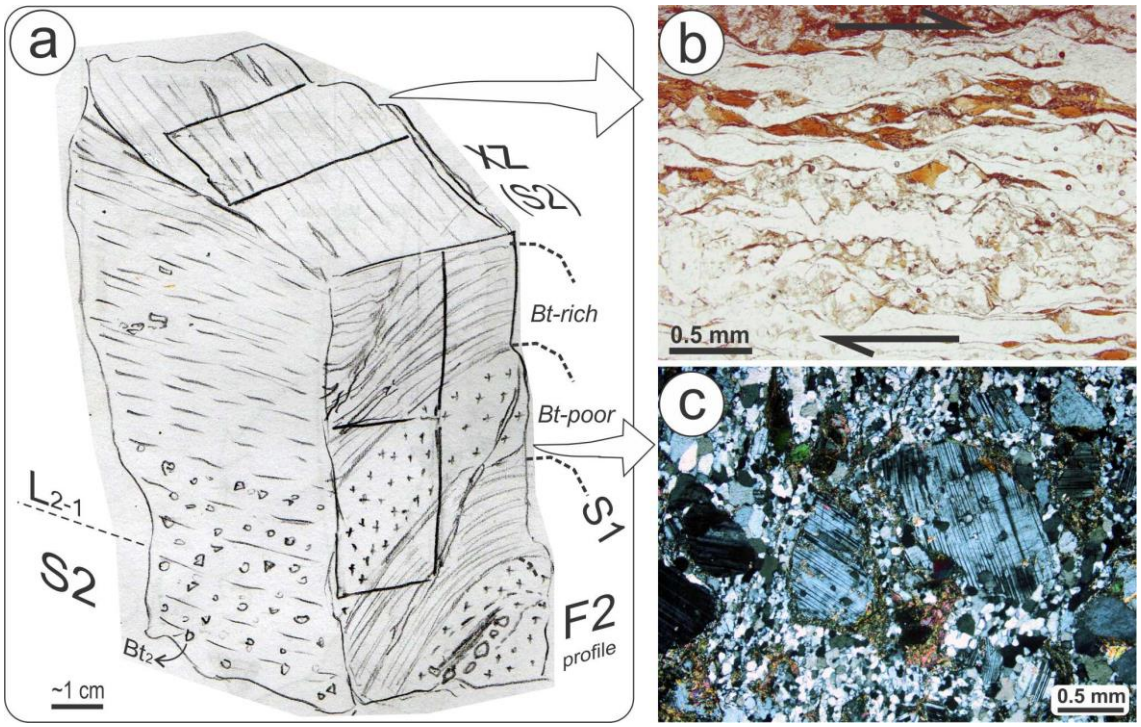

Figure 7 – Petrographic and microstructural aspects of the dated sample (PB-57G, acidic orthogneiss). (a) Hand sample block diagram. The frontal face is the fold profile (F_2) and shows the main compositional banding (S_1). The left-side plane is the transposition foliation S_2, with intersection lineation, sub-parallel to the stretching lineation, which is discrete in the sample. S_2 planes are marked by biotite neocrystallization (Bt_2). The top-view is the horizontal XZ plane, perpendicular to S_2 and parallel to the strike-slip stretching lineation, as shown in figure 7b. (b) XZ, top-view showing mylonitic microstructure of the orthogneiss, defined by a compositional banding with biotite-rich and biotite-poor sub-mm bands. Biotite fish indicate dextral kinematics, and locally developed S-C-C' fabric (upper-right portion). The half-bottom portion is a biotite-poor band with abundant plagioclase porphyroclasts showing dextral asymmetry. Plane-polarized light. (c) General aspect of a biotite-poor band in F_2 fold profile, with rounded plagioclase porphyroclasts presenting characteristic rounded quartz inclusions immersed in a quartz-feldspathic, polygonal granoblastic matrix. Fine grained white mica overgrowth is noteworthy in the left-hand porphyroclast. Cross-pozarized light.

Biotite is the main mafic phase in orthogneisses (10 – 20% estimated proportion). It is the mineral which most of times define the main foliation of these rocks, and which differences of modal proportion, also define a compositional banding (Fig. 7a). Biotite is reddish to dark brown, and locally replaces amphibole (Fig. 6c). Mica fishes are

common, being specially developed along S_2 XZ sections (Fig. 7b). Two grain-size populations are usually observed, with the larger (0.1 – 0.5 mm) locally recrystallized to the finer-grained (≤ 0.01 mm – Fig. 6b inset).

Amphibole occurs as a subordinated mafic phase in three representative samples (GB-01J, GB-01L and GB-10), and is the main mafic phase of sample GB-09DA (Fig. 6c). It occurs as elongated (prismatic) to equant crystals, with dark- to light-green pleochroism, classified as hornblende.

A very fine-grained, (quartz+mica)-rich granoblastic matrix, is observed along discrete shear bands (Fig. 6a), which in high-strain zones developed S-C(-C') structures (figures 6b, 6e and 7b). Epidote and titanite are occasionally observed as accessory phases. The epidote is interpreted as a subproduct of the amphibole replacement by biotite, and titanite as a peritetic phase after partial melt reactions (as in figure 5d inset).

4.2 Geochronology

The difficulty of distinguish between early-Neoproterozoic and Paleoproterozoic basement xenoliths or roof pendants in the post-collisional, late-Neoproterozoic granitoids of Dom Feliciano Belt is discussed and illustrated by several works (e.g. Leite et al., 1998; Martil et al., 2011; Martini et al., 2019). Therefore, one representative sample was selected for geochronological studies to guide further correlation. PB-57G is a fine-grained, mm-banded tonalitic orthogneiss which occurs as a m-scale elongated xenolith along the mylonitic foliation of the Mariscal Granite (Fig. 4c and 4d – see location in Fig. 2). The banding is defined by different proportions of biotite and quartz-feldspathic material, and is folded according to a axial plane which define a discrete S_2 cleavage, marked by secondary biotite (Fig. 7a and b).

The representative results (< 5% discordance) of 42 spots are presented in table 2. Most zircons are prismatic, bi-pyramidal, and present concentric, oscillatory zoning (see Fig. 8a). These characteristics are taken as evidence of its igneous nature. Inherited cores present Archean (ca. 2.6 – 2.8 Ba), Paleoproterozoic (1.8 – 2.15 Ba) and Mesoproterozoic (1.0 – 1.2 Ba) concordant populations (Fig. 8b). Additionally, one early Tonian age (ca. 980 Ma) was also observed.

Thirty isotopic measurements taken from regularly zoned portions of igneous-looking zircons were used to calculate the concordia age of 798.9 ±3.9 Ma (2σ). This value is interpreted as the crystallization age of the ortogneiss Tonian protolith (Fig. 8c). This new data allow the correlation of the pre-collisional magmatism recorded in the Major Gercino Shear Zone basement with other Tonian rocks preserved in the southern part of Dom Feliciano Belt (Silva et al., 1999; Lenz et al., 2011; Koester et al., 2015; Martil et al., 2017).

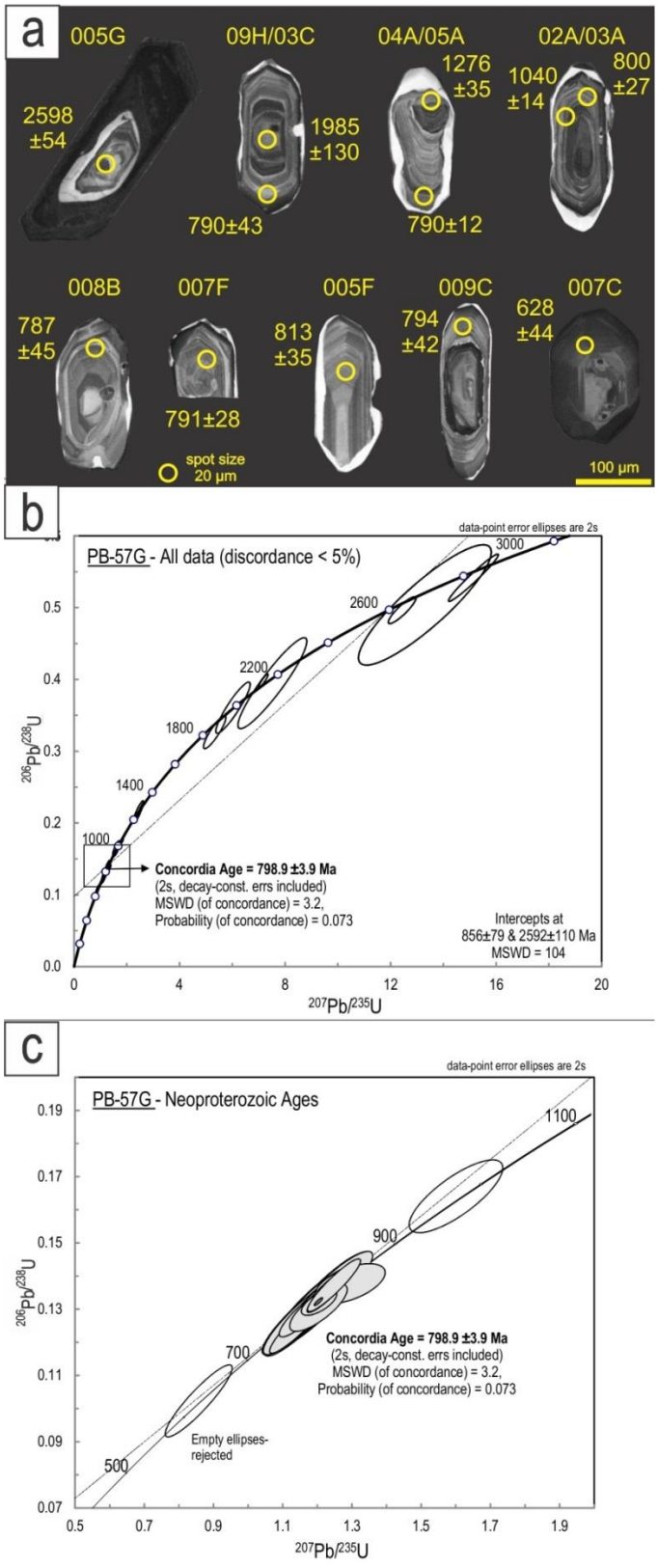

Figure 8 – Geochronology results of Porto Belo Complex acidic orthogneiss (sample PB-57G). (a) Cathodoluminescence images of zircon grains from sample PB-57G. $^{206}Pb/^{238}U$ for all ages are shown in the figure (b) .LA-ICP-MS concordia diagram for Porto Belo Complex showing Archean, Paleoproterozoic and Mesoproterozoic heritage. (c) LA-ICP-MS concordia diagram for Porto Belo Complex Tonian crystallization age. Full ellipses were considered in age calculation. Ellipses present error of 2σ.

A very fine, lighter/brighter, and more rarely darker , irregular overgrowth is observed (see Fig. 8a), but no reliable age determination was possible. One single, shorter, dark grain with complex internal pattern was dated as 628 ±44 Ma, which is considered as a reference age for tectonic reworking and metamorphism of the orthogneiss during collisional and/or post-collisional times. The reference age is in agreement with the early post-collisional magmatism dated by Florisbal et al. (2012a). The reference age also partially overlaps the determinations by Chemale Jr et al. (2012) for the Porto Belo Complex, which they interpreted as crystallization ages of pre-transcurrent tonalites. However, their concordia diagram for twelve dated zircons (figure 05 from Chemale Jr et al., 2012) shows a majority of ca. 650 Ma zircon with a tonian heritage (770 – 800 Ma approximately), which is correlated to the age hereby determined for the orthogneiss protolith. The ca. 650 Ma, pre-transcurrent event dated by Chemale Jr. et al. (2012) is reinterpreted as the record of a collisional tectono-metamorphic event, possibly with partial melting, which affected a Tonian (770 – 800, approximately) pre-collisional magmatic association.

4.3 Geochemistry

The role of mantellic and crustal contributions in the genesis of granitoids is greatly emphasized by Barbarin (1999). The importance in recognize acidic rocks in the context of the magmatic series is also highlighted by Nardi (2016) as a tool to unravel ancient tectonic environments and the evolution of mantle and crust as an integrated system.

Seventeen Porto Belo Complex samples collected along a cross-section were analysed for major and trace elements (locations in Fig. 2 and 3). Among them, fifteen orthogneiss samples are considered compositionally representative of the

magmatic protolith. Major and trace elements results are shown in table 3. Porto Belo Complex orthogneisses have dominant intermediate composition, with two slightly migmatitic samples, and three with acidic character, which were discriminated in the diagrams. Two restites are additionally shown for comparison.

Porto Belo Complex data are compared with data of correlated orthometamorphic associations, including the Porto Alegre Orthogneiss (Philipp and de Campos, 2004) Cerro Bori Orthogneiss (Masquelin et al., 2012; Lenz et al., 2013), Várzea do Capivarita Complex orthogneiss (Martil et al., 2011; 2017), Piratini Orthogneiss (Tambara et al., 2019) and Cerro da Árvore Complex metavolcanics (Battisti et al., 2018). Additionally, the geochemistry of juvenile associations of São Gabriel Block (from Saalmann et al., 2005), younger than 770 Ma, is also presented for comparison.

Figure 9 shows the dataset plotted on TAS classification diagram (Cox et a., 1979), with all representative samples along a subalkaline trend. Twelve Porto Belo Complex samples are intermediate (SiO_2 54.79 – 61.81 wt%), mostly representative of andesitic compositions, characteristic of continental arc magmatism (Murphy, 2007 and references therein). When compared to the intermediate rocks of correlated associations, the Porto Belo Complex rocks are relatively richer in alkali elements. On the other hand, the Porto Belo Complex acidic rocks are alkali impoverished compared to the intermediate ones, which may indicate crustal contamination.

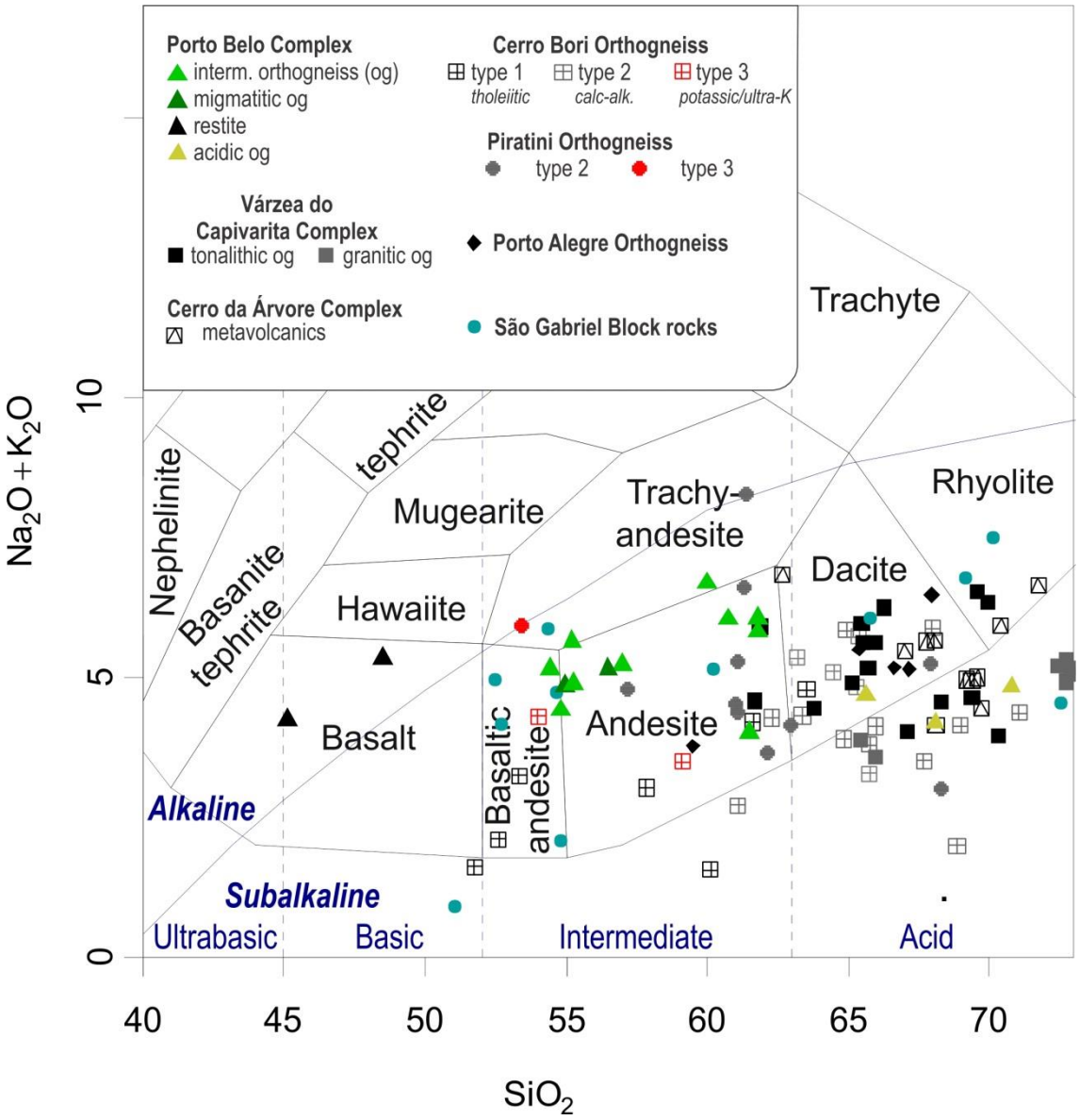

Figure 9 – TAS diagram (Cox et al., 1979) for Porto Belo Complex (green, yellow and black triangles) and correlated Tonian arc-related magmatism of Dom Feliciano Belt, with data from Várzea do Capivarita Complex (gray and black squares – Martil et al., 2017), Porto Alegre orthogneiss (black diamond – Philipp and de Campos, 2004), Cerro da Árvore Complex metavolcanics (triangle inside square – Battisti et al., 2018) Piratini orthogneiss (gray and red circles – Tambara et al., 2019) and Cerro Bori orthogneiss (black, gray and red cross inside square – Lenz et al., 2013). São Gabriel Block rocks are also plotted for comparison (blue circle – Saalmann et al., 2005).

When plotted in the AFM diagram (Fig. 10 – Irvine and Baragar, 1971), the calc-alkaline character of Porto Belo Complex rocks is clear, as well as of most Tonian orthometamorphic association. Such features are consistent with magmatic series generated in continental magmatic arcs (e.g. Murphy, 2007). Exception are some of

the Cerro Bori Orthogneisses, classified by Lenz et al. (2013) as “type1”, tholeiitic rocks, interpreted by those authors as produced in the early stages of an oceanic-arc magmatism.

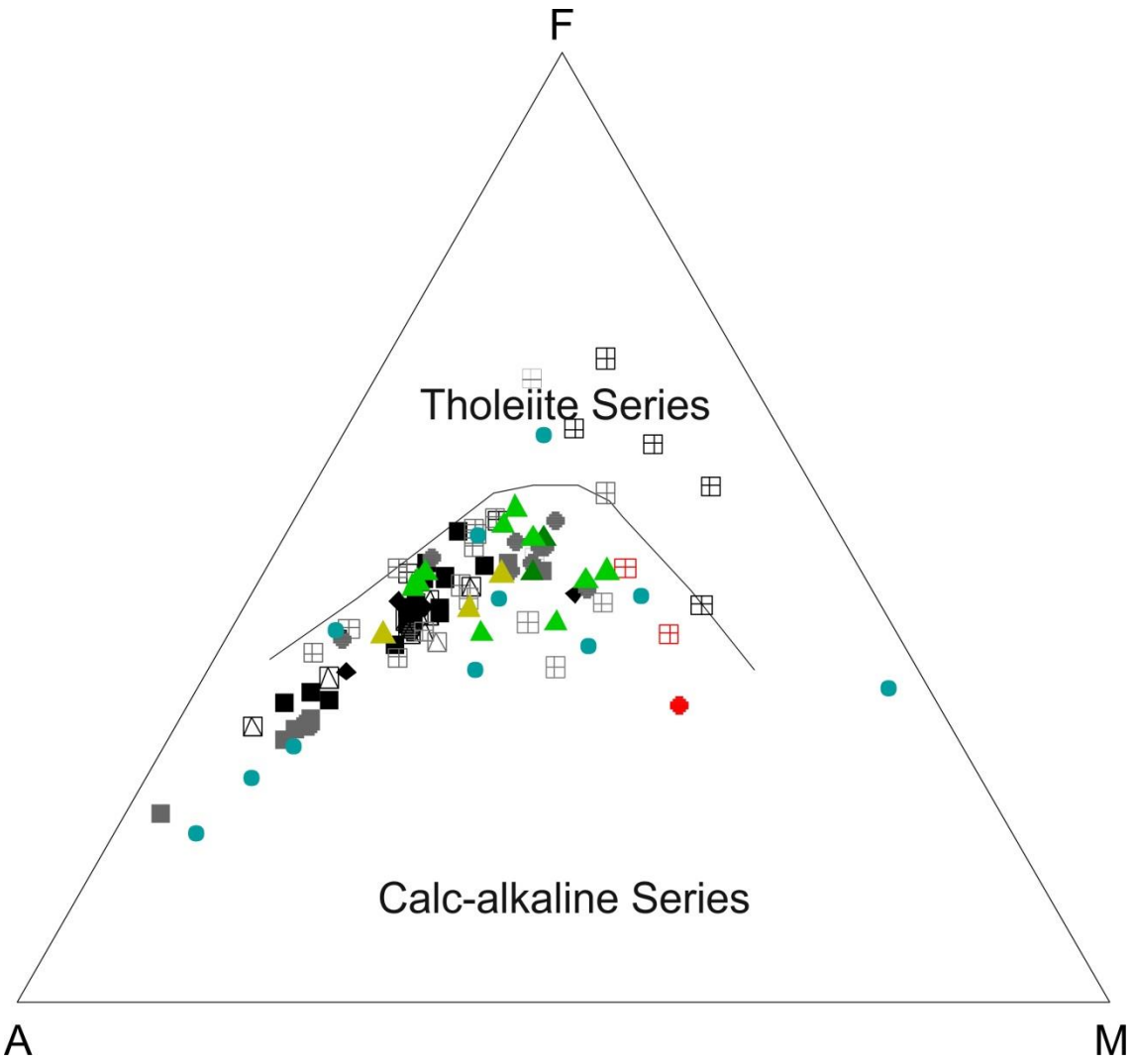

Figure 10 – AFM diagram (Irvine and Baragar, 1971) for Porto Belo Complex and Tonian correlated units, with São Gabriel Blocks also plotted for comparison. Legend is the same as in figure 9, but Porto Belo Complex restites are not plotted.

The high-K character of the Porto Belo Complex calc-alkaline series is evident in the K_2O vs. SiO_2 diagram (first diagram of Fig. 11 – Le Maitre, 2002). PBC intermediate rocks grouped with considerably higher K_2O values when compared to correlated rocks with similar differentiation index. High K_2O content is indicative of the mature continental arc character of the magmatism. The decrease of K_2O with increase of

SiO_2 towards the acidic orthogneisses is confirmed and suggests that the compositional evolution is not merely result of fractional crystallization, but also, involved crustal contamination processes.

Multiple plots of major elements versus SiO_2 as a differentiation index (Harker diagrams – Fig. 11) show that both samples of migmatitic orthogneisses preserved their original composition. Most of Porto Belo Complex samples representing intermediate rocks, fill a previous gap defined by the full dataset. This is very clear in MgO, CaO, Na_2O and $FeO_{(t)}$ diagrams. On the other hand, São Gabriel Block rocks constitute a distinct association, as exemplified by a parallel trend in the $FeO_{(t)}$ diagram, below the main negative trend of the full dataset. Similar behavior, yet not so evident, is observed in MgO diagram. A distinct behavior can be seen in TiO_2 diagram, with São Gabriel Block rocks featuring a constant, near horizontal trend, while the main group presents a strong negative correlation. Na_2O also clearly separate the ca. 800 Ma association from São Gabriel Block rocks, as the later grouped with near-constant 3 to 4% weight, independent of SiO_2 content, while the main group present a positive correlation between sodium and silica, with intermediate samples containing Na_2O between 0.5 and 2 wt%.

Trace element spidergrams normalized by values typical of magmas from different sources pointed out that the OIB magmas, melts from mantle previously metasomatized by subduction, show higher similarity with the magmas of Porto Belo Complex (Fig. 12a – Sun and McDonough, 1989), when compared to NMORB and EMORB normalization (not shown). The relationship with a mantle wedge affected by subduction is also pointed out by pronounced Nb negative anomalies, since high-field-strength elements are concentrated in residual phases in the oxidized mantle wedge (e.g. Saunders et al., 1991).

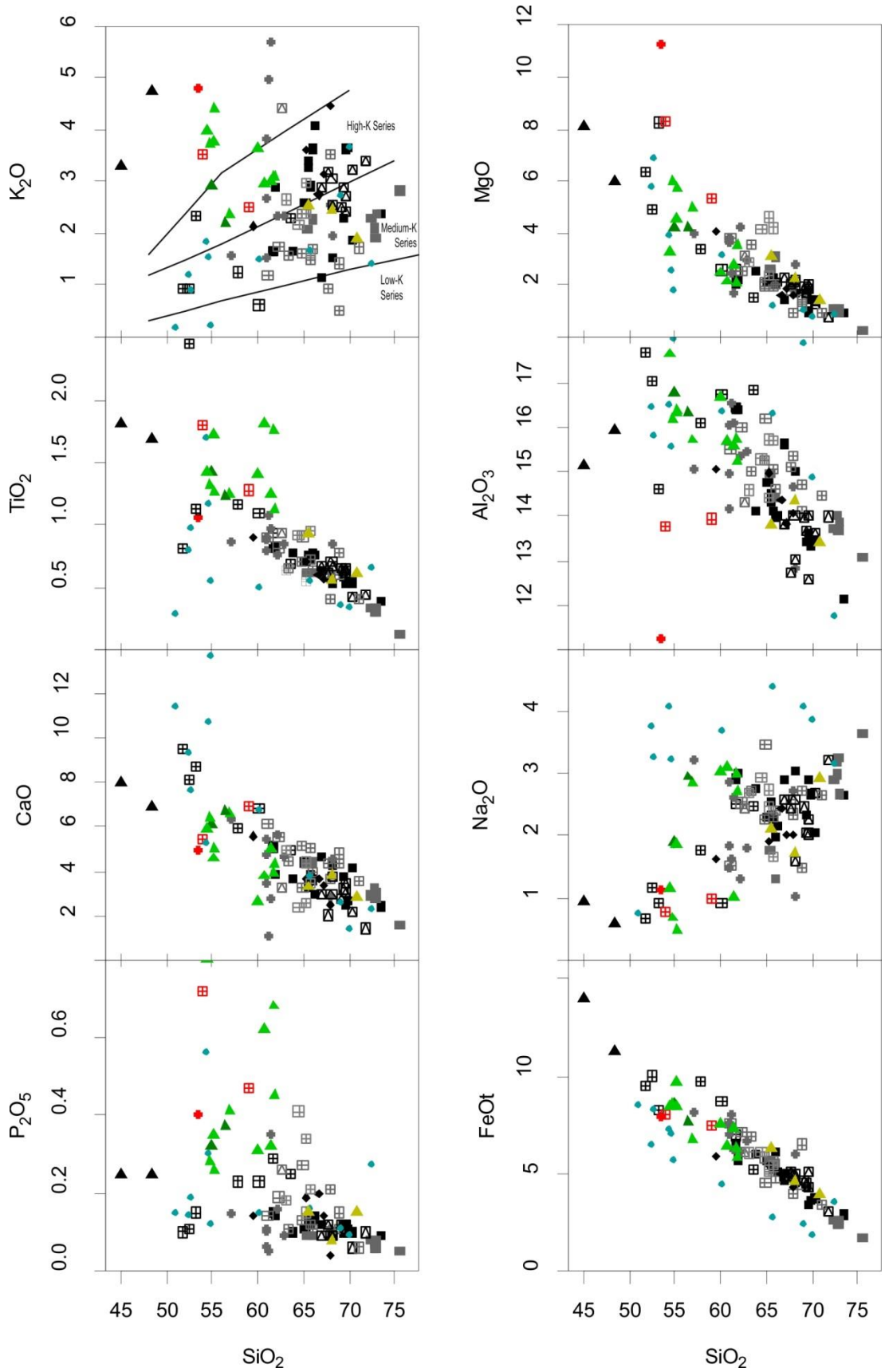

Figure 11 – Major element diagrams plotted against SiO_2 differentiation index (Harker diagrams). K_2O diagram is according to Le Maitre (2002). Legend is the same as in figure 9. Sample BR126-3 (Cambaí Complex metadiorite

of Saalmann et al., 2005) is not show on MgO and Al2O3 diagrams due to very discrepant values (which resulted in scale distortion) in order to better display the full dataset.

The comparison with other ca. 800 Ma calc-alkaline magmatic associations (Várzea do Capivarita Complex and Cerro Bori orthogneisses, and Cerro da Árvore Complex metavolcanics) shows very similar normalized patterns (Fig. 12a), with Porto Belo Complex samples mostly plotting within the compositional fields of other units. It is noteworthy that Cs, Rb and K are characteristically highly concentrated in Porto Belo Complex rocks in comparison to other units, which points to a greater contribution of fluids derived from the subducted slab to the mantle wedge (Jones et al. 2016). Ti and P relative enrichment may be attributed to a lower degree of mantle partial melting in the origin of these rocks when compared to other units. On the other hand, PBC acidic orthogneisses are relatively P and Ti impoverished compared to intermediate ones, which suggests contamination as an additional differentiation process.

Rare earth element patterns of Porto Belo Complex samples, chondrite-normalized composition (Boynton, 1984), are very similar to each other and also to correlated units, mostly overlapping their compositional fields (Fig. 12b). LaN/LuN around 20 and Eu negative anomalies are characteristic features of the full dataset, being recognized as typical of calc-alkaline magmatic series (e.g. Murphy, 2007).

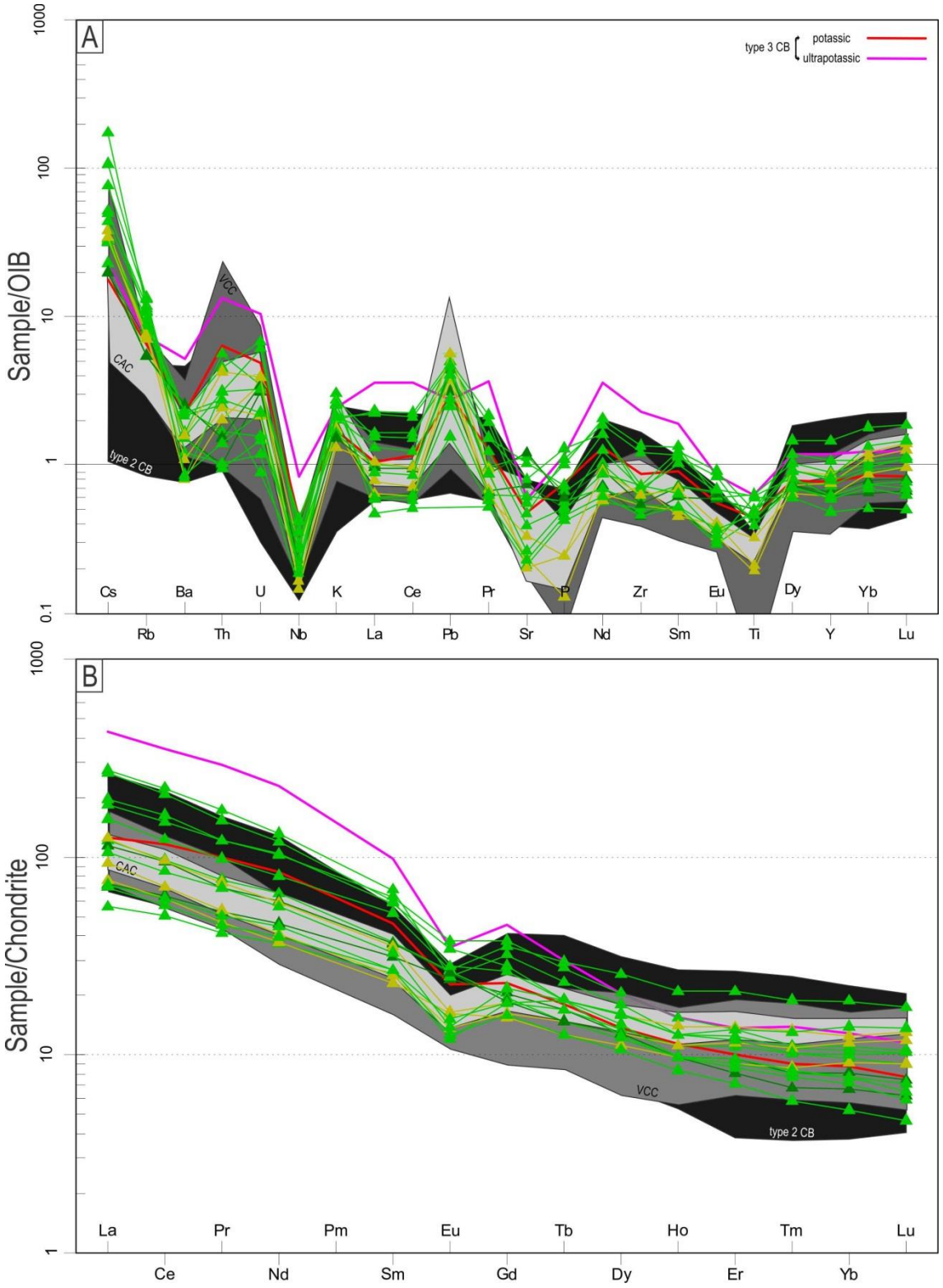

Figure 12 – Spidergrams for Porto Belo Complex in comparison to Várzea do Capivarita Complex (dark gray field), Cerro Bori orthogneiss (black field) and Cerro da Árvore Complex metavolcanics (light gray field). Cerro Bori orthogneiss "type 3", potassic and ultrapotassic samples of Lenz et al. (2013) is also plotted in red and pink, respectively. (a) Multi-elementar diagram normalized by OIB composition (Sun and McDonough, 1989). (b) Rare Earth Element diagram normalized by chondrite composition (Boynton, 1984).

The acidic orthogneisses tend to be relatively LREE-impoverished in relation to the average intermediate orthogneisses. Intermediate rocks present increasing LaN/YbN (from 10 to 50) with increasing SiO_2 or decreasing $MgO+FeO_{(t)}$, which points to the more incompatible character of LREE in relation to HREE during magmatic differentiation. On the other hand, acidic rocks show much less fractionated pattern (LaN/YbN up to 10). This may be explained by contamination by crustal melts or by the highly differentiated character of these rocks (e.g. Miller and Mittlefehldt, 1982). Acidic orthogneisses from Porto Belo Complex are interpreted as originated from andesitic magma differentiation, possibly contaminated by crustal melts. Its origin solely by crustal melt is not coherent with the compositional similarities observed for all set of trace elements contents.

The close relationship between Porto Belo Complex magmatic source and arc magmatism is also confirmed by Pearce (2008) diagram based on Nb, Th and Yb behavior (Fig. 13). Most samples from the full dataset are aligned along the volcanic arc array, including the São Gabriel Block rocks.

Plotting on tectonic setting discrimination diagrams developed by Pearce et al. (1984) also confirms the magmatic arc as the most plausible environment for the studied magmatism (Fig. 14). Although these diagrams were developed for granitic rocks, Pearce (1996) considers that its use can be extended to intermediate rocks, since differentiation will affect mainly Rb, in a predictable way. It is noteworthy that Porto Belo Complex rocks are Rb-enriched, reason why their samples are displaced in the diagrams which consider this element, together with a few other samples from the correlated units, towards the syn-collisional granite field. The diagram of Nb vs. Y shows a few samples over the boundary of within-plate granites, including type 3, potassic to ultra-K orthogneisses from Lenz et al. (2013). This occurs possibly due to Y enrichment, which may reflect magmatism maturity, thicker continental margins

and/or deeper subduction. Rb enrichment may be attributed to the same causes. The Ta vs. Yb diagram illustrates the best grouping, with virtually the full dataset plotting on the volcanic arc granite field, suggestive of the continental-arc character of the Tonian magmatism of Dom Feliciano Belt.

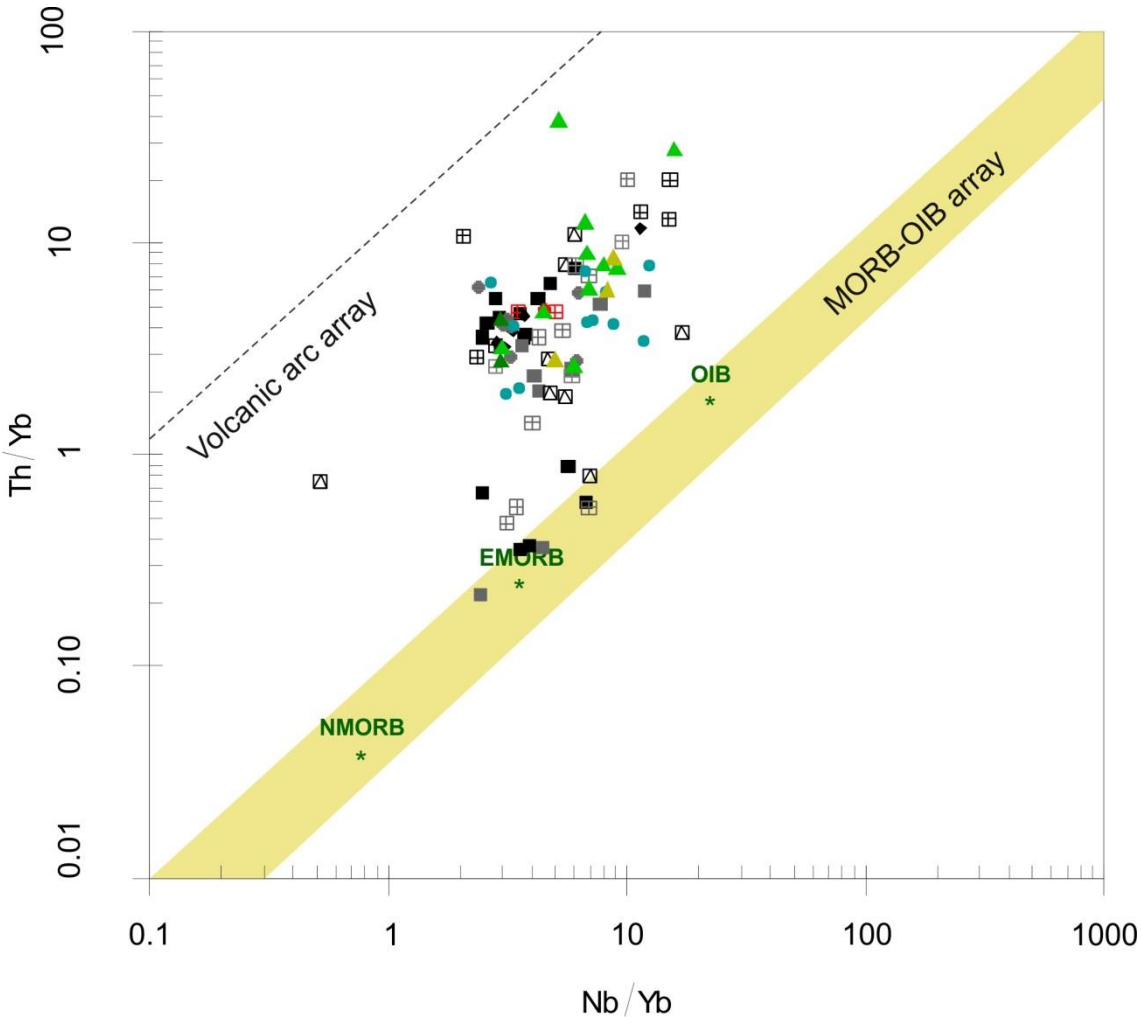

Figure 13 – Porto Belo Complex and Tonian correlated units plotted in the diagram for basalt tectonic setting discrimination of Pearce (2008). São Gabriel Block rocks are also plotted for comparison. Legends as in figure 9.

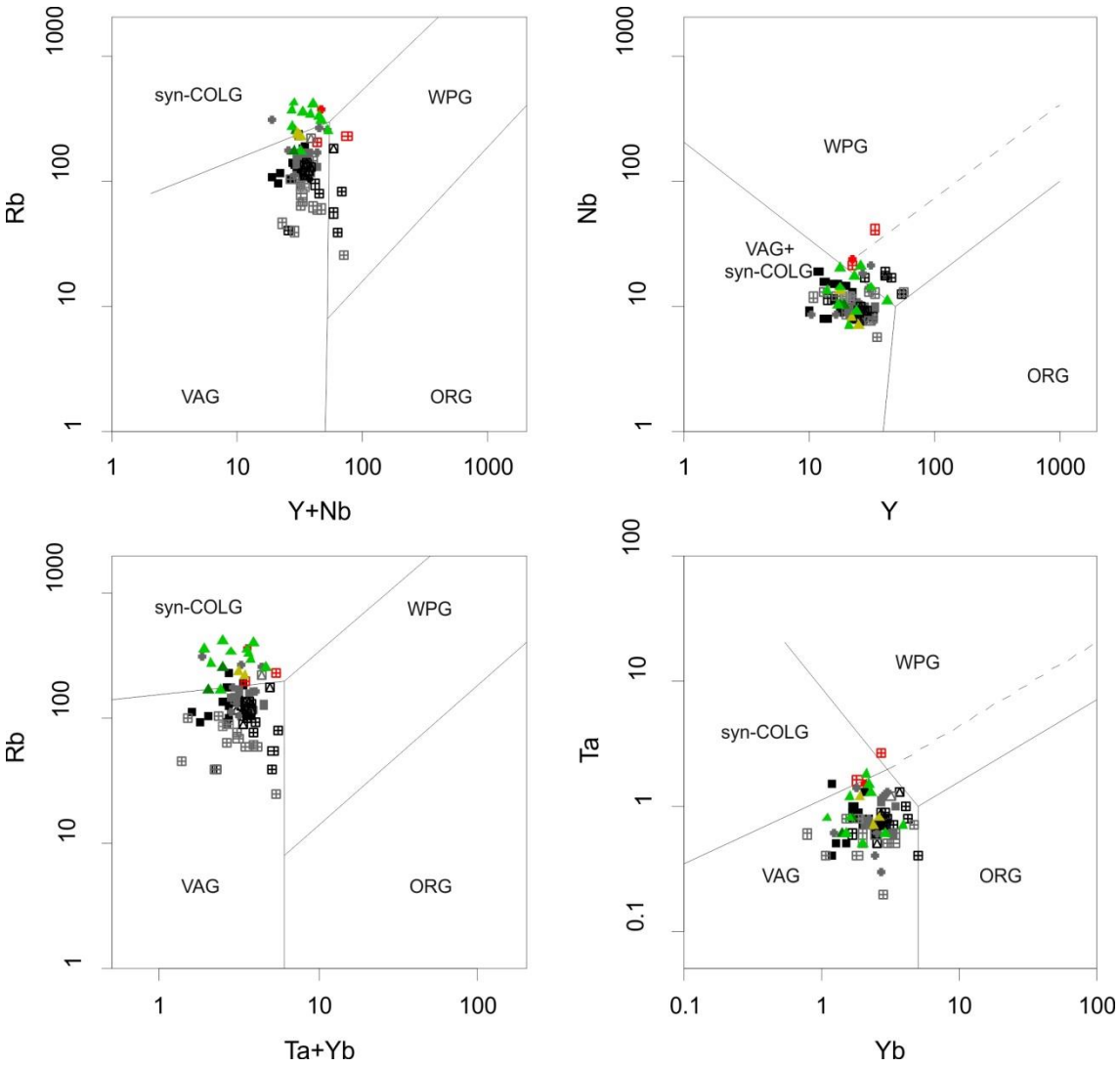

Fig 14 – Porto Belo Complex and Tonian correlated units plotted in the diagrams for granite tectonic setting discrimination of of Pearce et al. (1984). São Gabriel Block rocks are not shown due to insufficient trace element dataset.

5. Discussion

5.1 Tectonic correlations along the Dom Feliciano Belt

The Dom Feliciano Belt collisional period (660 – 630 Ma, approx.) was marked by intense transpressional deformation which affected both hinterland and foreland, progressively evolving from oblique thrust to strike-slip (e.g. Florisbal et al., 2012b; Oriolo et al., 2016a; Martil et al., 2017; Battisti et al., 2018; De Toni, 2019). Oblique, transpressive top-to-the-W/NNW thrusting plus dextral or sinistral shearing affected the hinterland under hight-T/low-P, upper-amphibolite to granulite facies conditions,

as recorded in paragneisses of the Cerro Olivo Complex (Punta del Este Terrane – Gross et al., 2006; Masquelin et al., 2012) and Várzea do Capivarita Complex (Encruzilhada Block – Gross et al., 2009; Martil, 2016; De Toni, 2019). Thrusting under high-T/low-P metamorphic conditions points to a very hot geothermal gradient (up to 50°C/Km, according to De Toni, 2019) prior to continental collision. The same event is recorded in the Porto Belo Complex, which correlation with other Tonian orthogneisses of Dom Feliciano Belt extends the occurrence area of this pre-collisional rock association for the whole length of the belt hinterland (De Toni, 2019).

On the other hand, foreland deformation occurred at medium-P, greenschist to amphibolite facies conditions, as recorded in pelitic schists from the Cerro da Árvore Complex (De Toni, 2019), and pelitic and mafic schists of the Brusque Complex (Philipp et al., 2004; Campos et al., 2012; De Toni, 2019). Tectonic juxtaposition of distinct crustal levels is interpreted as a consequence of progressive oblique transpression during collision (De Toni, 2019).

Apart from differences between segments of the Dom Feliciano Belt, the deformation and tectonic vergence is relatively coherent along and perpendicular to its strike. The coherent ca. 650 Ma collisional deformation through the belt suggests a possible integrated correlation of its pre-collisional scenario.

Philipp et al. (2016) proposed criteria for recognizing the Dom Feliciano Belt basement inliers as related to the Nico Perez Terrane (NPT – Uruguay). The authors correlated the Paleoproterozoic Encantadas Complex, a basement inlier in the foreland Tijucas Fold Belt of Rio Grande do Sul state (Saalmann et al., 2006b), with the NPT. Oriolo et al. (2016b) established the correlation between the NPT and Congo Craton. These authors suggested that the NPT was separated from Congo Craton by a Cryogenian rifting, and afterwards was accreted to the Rio de La Plata during the Ediacaran. The correlation criteria include: Archean protolith,

Paleoproterozoic reworking, Mesoproterozoic anorogenic magmatism and Neoproterozoic reworking related to Gondwana assembly. In this sense, the Camboriú Complex, with respect to all criteria (see geochronological summary by Basei et al., 2013) is correlated with the NPT and the Congo Craton, and therefore is possibly allochtonous in relation to the Luis Alves Craton (see figure 1b). According to these criteria, the Dom Feliciano belt foreland basement inliers are correlated to the Nico Perez Terrane and Congo.

5.2 Discussion of previous tectonic models

Previous tectonic models for the Dom Feliciano Belt evolution disagree about subduction vergence and also about the number of subductions and plates involved (e.g. Chemale Jr., 2000; Saalman et al., 2006; Hartmann et al., 2007; Philipp et al., 2018). It is also noteworthy that recently published models do not consider the São Gabriel Block as part of the Dom Feliciano Belt evolution (e.g. Philipp et al., 2016, 2018; Vieira et al., 2019).

Many authors have argued for the allochtonous character of the granitic domain of Dom Feliciano Belt in relation to the foreland domain, and interpreted the Sierra Ballena and Dorsal de Canguçu Shear Zones to be continuous with the Major Gercino Shear Zone, as a single suture (e.g. Basei et al., 2005, 2011; Passarelli et al., 2011; Hueck et al., 2019). This has been recently challenged by structural and petrological correlations of pre- and post-collisional units of both domains, pointing to a close origin and contiguity of these domains since pre-collisional times (e.g. Florisbal et al., 2012a; Martil et al., 2017; Battisti et al., 2018; De Toni, 2019).

Konopásek et al. (2018) presents a distinct interpretation for the pre-collisional history of the Kaoko-Dom Feliciano-Gariep Orogenic System. The authors attribute the 820-785 Ma age interval to a bi-modal magmatism within the Coastal Terrane

metamorphic sequences from the Kaoko Belt, which is correlated with Tonian rocks of the Dom Feliciano Belt. These are mostly interpreted as products of partial melting of pre-Neoproterozoic basement rocks, assuming that the arc-like geochemical signature is inherited from its crustal sources. On the other hand, basic members shown dominantly a tholeiitic signature. Such observations have led those authors to reinterpret the Dom Feliciano Belt Tonian orthogneisses as originated in a rift environment, located in a back-arc position relative to the São Gabriel Block. Campos et al. (2012) had previously assumed a rift origin for the metabasic rocks at the bottom of the Brusque Complex metavolcano-sedimentary succession. Additionally, Konopásek et al. (2017), argue that the time difference between the last increments of crustal stretching (during Sturtian glaciation at 680 – 660 Ma) and the first flysch sedimentation over the Congo Craton (before 635 Ma) is too short (ca. 25 Ma) for a hypothetical oceanic spread in the back-arc domain before collision built up the orogen as a source for flysch sediments.

On the other hand, Ramos et al. (2018, 2019) reported rocks found in the northeastern portion of the Punta del Este Terrane which were interpreted as supra-subduction ophiolitic remnants. The rock association includes high-T/low-P amphibolites and serpentinites/talc-schists of the Arroio Grande Complex and its Uruguayan correlated Paso del Dragón Complex (Peel et al., 2018). Fieldwork and geochronological data of Peel et al. (2018) point out that the Cerro Olivo Complex is the basement of Arroio Grande and Paso del Dragón complexes. The intimate relation of these rocks were addressed by recent PT estimatives on the Arroio Grande Complex amphibolites (Ramos et al., 2019) and geochronology of associated rocks (Ramos et al., 2018), which suggest that the sequence was submitted to synchronous (650 – 640 Ma) and similar metamorphic conditions of Cerro Olivo and Várzea do Capivarita complexes during the collisional event.

A tectonic model which aims at integrating the pre-collisional history of the Dom Feliciano Belt should take into account such heterogeneities of the geological record in a tectonic scale. It includes the apparent contradiction of magmatic arc and rift pre-collisional environments between Dom Feliciano and Kaoko belts (respectively), and the short time period between crustal stretching and collision in the Kaokoan side (Konopásek et al., 2017, 2018) when compared to the southern local development of an oceanic domain followed by obduction in southernmost Brazil and Uruguay (Peel et al., 2018; Ramos et al., 2018, 2019). The evidence seems to be indicative of diachronous and distinct evolution of the different segments of the belt.

5.3 The Occam's Razor model for the Dom Feliciano Belt orogenic cycle

Based on several regional cross-sections along different latitudes of the Andean Orogen, Ramos (2009) proposed the Andean Orogenic Cycle. His model tells that the magmatic front of a continental magmatic arc may migrate towards the back arc region due to flat-slab subduction, and creates a compressive stress field in that region. This may occur after a more buoyant portion of the subducting slab arrives at the trench, or after slab break-off. At the opposite end, the magmatic front may migrate towards the forearc region, followed by extension behind the arc due to steepening of the slab during subduction, which may occur when a denser portion of the subducting plate arrives at the trench after subduction of a highly buoyant portion of the slab, or even due to increasing slab pull after eclogitization of oceanic crust (van Hunen et al., 2002; Klemd et al., 2011). Zhang et al. (2018) show the successive migration of arc magmatism towards fore-arc and back-arc positions in the Indo-Myanmar Orogenic Belt due to alternating steep and gently-dipping subduction in a long-lived system (189 Ma ago to the present). Another example is given by Bachman et al. (1983), who describe the superposition of fore-, intra- and

back-arc settings in the Luzon Central Valley, Philippines, due to changes in subduction angle and polarity (from Eocene to the present).

The model here proposed take as assumptions: i) that during subduction, arc magmatism should occur on the upper plate margin (Miyashiro, 1982); and ii) based upon the available evidence, the best scenario is the less complicate one, as pointed out by the Occam's Razor Principle (1960). The model correlates the arc magmatism which occurred in the São Gabriel Block around 880 Ma (Leite et al., 1998) and between 770 and 690 Ma (Lena et al., 2014; Gubert et al., 2016) with the 800 – 770 Ma pre-collisional magmatism recorded by orthogneisses and metavolcanics of the Dom Feliciano Belt, assuming that both were produced during the same subduction, while their spatial and temporal distribution was controlled by variation of the subduction angle (Fig. 15).

The model assumes an eastward single subduction of an oceanic domain (the Charrua Ocean, as in Philipp et al., 2018) which separated the Rio de la Plata Craton from the Nico Perez Terrane/Congo Craton and its correlated basement inliers along the Dom Feliciano Belt (as drawn by Oriolo et al., 2017; Konopásek et al., 2018). This is in agreement with the proposition of Oriolo et al. (2017) to extend the Western Gondwana Orogen from Sahara to Uruguay. According to the author, this long orogen is characterized by Paleoproterozoic cratons to the west of locally preserved records of eastward subduction zones, which were responsible for accretion of long-lived, metacratonic domains (as the Nico Perez Terrane in Uruguay), with records of back-arc extension prior to collision.

The early-phase of the Dom Feliciano Belt tectonic evolution is constrained in São Gabriel Block by reported 925 – 890 Ma ophiolite ages (Arena et al., 2016) and by the ca. 880 Ma Passinho metadiorite (Leite et al., 1998), interpreted as the first magmatic arc activity related to subduction (Fig. 15a). The record of this early-phase

is only locally preserved and still poorly documented. It is considered that it may represent either an oceanic island arc (Leite et al., 1998; Philipp et al., 2018 and others) or early manifestations of the continental arc magmatism.

In the present model, subduction angle variations are thought to have led to magmatic arc migration from fore-arc towards back-arc position, as proposed by Ramos (2009) and Zhang et al. (2018) amongst others (see fig. 15b), creating a magmatic gap in the São Gabriel Block (between the so-called Passinho and São Gabriel orogenies of Philipp et al., 2018), while arc-related magmatism was active along the inner portion of the Dom Feliciano Belt. The arc-related character of the Tonian magmatism is now defined by the correlation of distinct orthometamorphic rock units through the whole Dom Feliciano Belt, represented by a full range from basic to intermediate and acidic protoliths. Distinct mantle sources were active to generate juvenile magmatism of basic and intermediate compositions, with different degrees of subduction-related effects (e.g. LILE-enrichment, high-K calc-alkaline affinity of Porto Belo Complex and tholeiitic “type 1” Cerro Bori orthogneiss), which may have evolved by fractionation, contamination and assimilation processes. Acidic melts derived from re-melted old crustal sources possibly mixed with juvenile magma (Martil et al., 2017; Konopásek et al., 2018).

The steepening of subduction after 770 Ma (re-) stablished the arc magmatism westwards in the São Gabriel Block, leading to extension in the back-arc region (Fig. 15c). As discussed by many authors (e.g. Harris and Holland, 1984; Clark et al., 2011; Fowler et al., 2015; Hyndman et al., 2015) back-arc extension leads to high geothermal gradients, which favours high-T/low-P conditions reached by collision-related metamorphism, as recorded by Tonian orthogneisses and coeval metasedimentary rocks (Gross et al., 2006; 2009; Ramos et al. 2019; De Toni, 2019). The presence of late- to post-collisional potassic to ultrapotassic rocks, and

especially of many syenites (e.g. Nardi et al., 2008; De Toni et al., 2016; Padilha et al., 2019) that outcrop in the Encruzilhada Block is an additional argument to the presence of an underlying mantle enriched by previous subduction. Their spatial correlation with high-T/low-P metamorphic rocks of VCC has led De Toni (2019) to conclude that the mantle affected by subduction became shallow, providing heat to collisional metamorphism and source for late- to post-collisional magmatism.

The proposed model, assuming a pre-collisional scenario for the Dom Feliciano Belt and, as consequence, for the Kaoko-Dom Feliciano-Gariep Orogenic System, does not conflict with the arguments and conclusions of Konopásek et al. (2017, 2018) neither with previous interpretations of Tonian orthogneisses of Dom Feliciano Belt (Lenz et al., 2011, 2013; Koester et al., 2015; Martil et al., 2017; Battisti et al., 2018). In fact, these are complementary interpretations of different parts of the same orogeny, nowadays separated by an ocean. A discussion regarding limitations on correlations across the ocean is made by Konopásek et al. (2016).

Considering a back-arc rifting, it is logical that the rift system will be naturally asymmetric, with one shoulder facing the magmatic arc (future Dom Feliciano Belt facing the São Gabriel Block magmatic arc), while the opposite one will be sitting on the craton margin, distant from the influence of arc magmatism (future Kaoko Belt facing Congo Craton). This explains why the record of arc magmatism is restrict or absent in the Kaoko Belt, but conspicuous along the Dom Feliciano Belt. The same spatial argument is valid for equivalence in time, when considering that the arc-like signature is observed in the 820 – 785 Ma magmatism of the Coastal Terrane, while within-plate signature is clearly demonstrated for the 740 – 710 Ma Congo Craton cover volcanism (Konopásek et al., 2018).

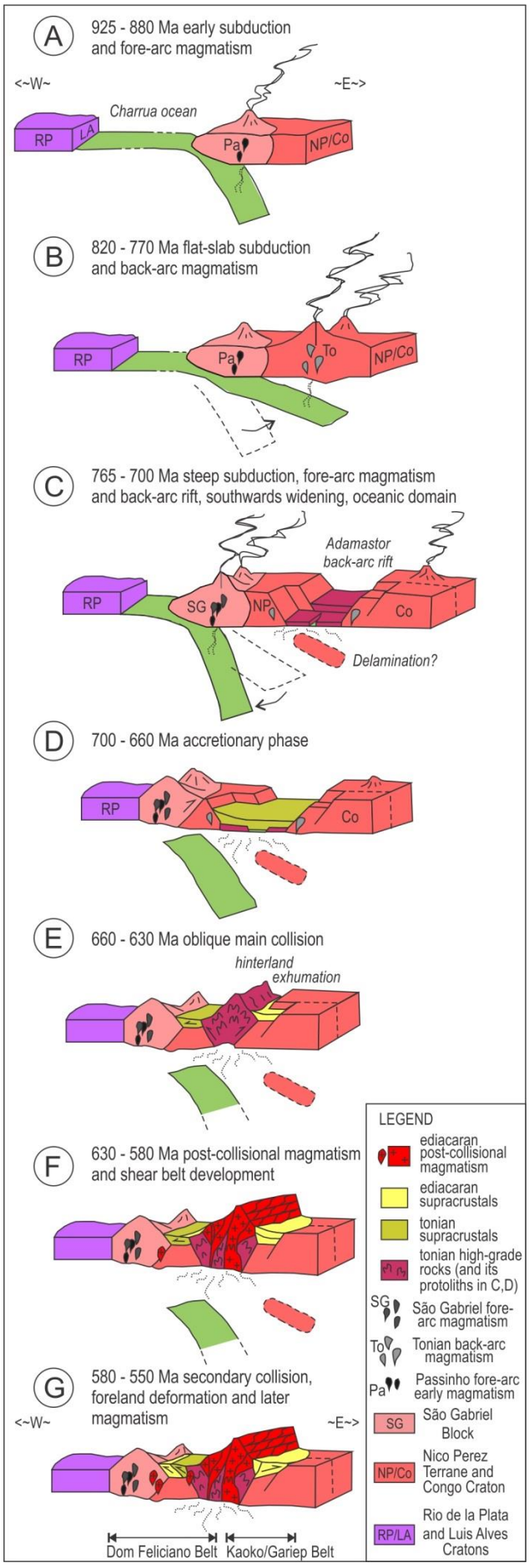
A
925 - 880 Ma early subduction and fore-arc magmatism
<~W~
~E~>
Charrua ocean
RP
LA
Pa
NP/Co
B
820 - 770 Ma flat-slab subduction and back-arc magmatism
RP
Pa
To
NP/Co
C
765 - 700 Ma steep subduction, fore-arc magmatism and back-arc rift, southwards widening, oceanic domain
Adamastor back-arc rift
RP
SG
NP
Co
Delamination?
D
700 - 660 Ma accretionary phase
RP
Co
E
660 - 630 Ma oblique main collision
hinterland exhumation
F
630 - 580 Ma post-collisional magmatism and shear belt development
G
580 - 550 Ma secondary collision, foreland deformation and later magmatism
<~W~
~E~>
Dom Feliciano Belt
Kaoko/Gariep Belt
LEGEND
ediacaran post-collisional magmatism
ediacaran supracrustals
tonian supracrustals
tonian high-grade rocks (and its protoliths in C,D)
SG São Gabriel fore-arc magmatism
To Tonian back-arc magmatism
Pa Passinho fore-arc early magmatism
SG São Gabriel Block
NP/Co Nico Perez Terrane and Congo Craton
RP/LA Rio de la Plata and Luis Alves Cratons

Figure 15 (previous page) – Cartoon for an eastwards single-subduction tectonic evolution model of Kaoko-Dom Feliciano-Gariep Orogenic System: (a) 925 – 880 Ma early subduction stage; (b) 820 – 770 Ma flat-slab subduction and back-arc magmatism; (c) 765 – 700 Ma steep subduction and fore-arc magmatism towards São Gabriel Block, while extension in the back-arc led to rifting, possibly with lithospheric delamination; (d) 700 – 660 Ma accretion between São Gabriel Block and Rio de la Plata Craton; (e) 660 – 630 Ma oblique main collision and tectonic inversion of the back-arc rift, with hight-T/low-P metamorphism and hinterland thrusting over the foreland supracrustals; (f) 630 – 580 Ma post-collisional magmatism is abundant in the hinterland, along the Southern Brazilian Shear Belt, and locally occurs along the foreland; (g) 580 – 550 Ma secondary collision, foreland deformation and later magmatism in Dom Feliciano Belt, while the orogenic front migrated towards Kaoko and Gariep belts.

Gruber et al. (2016a) pointed out that sedimentation of the Várzea do Capivarita Complex parametamorphic protoliths associated with Tonian orthogneisses of the Encruzilhada Block occurred at a maximum age of 728 ± 11 Ma based on metapelite provenance data, while $^{87}Sr/^{86}Sr$ isotope data in marble sequences are indicative of deposition between 750 – 717 Ma. Those authors (Gruber et al., 2016a) also discuss $^{206}Pb/^{204}Pb$ and $^{207}Pb/^{204}Pb$ ratios which correlated VCC marbles with Gariep Belt stromatolitic dolomites (Frimmel and Fölling, 2004).

It is likely that small oceanic domains may have opened during back-arc rifting of the southern portion (present day coordinates) of the system, as exemplified by Arroio Grande and Paso del Dragón complexes (Peel et al., 2018; Ramos et al., 2018, 2019). The short time interval between spreading and closure (as argumented by Konopásek et al., 2017) should favour its obduction instead of subduction, since the latter promoted by incremented density of the oceanic slab with time (e.g. Stern, 2004).

The combination of narrow rifting northwards (Adamastor Rift of Konopásek et al., 2017, 2018) with a small ocean domain to the south (Adamastor Ocean of Hartnady et al., 1985; Ramos et al., 2018, 2019 and references therein) resembles the model of confined orogen (also called “nutcracker”) proposed for the Araçuaí-West Congo

Orogen (e.g. Pedrosa-Soares et al., 2001; Cavalcante et al., 2019). Since the orginal proposition of Adamastor Ocean by Hartnady et al. (1985), southward ocean widening is admitted, and now apparently confirmed.

Final accretion of the São Gabriel Block to the Rio de la Plata Craton (Fig. 15d) occurred between 700 and 660 Ma (Lena et al., 2014) or shortly after (Arena et al., 2017). The structural record of this event is interpreted by Saalmann et al. (2006a) as a top-to-the-SE dextral transpression. Oriolo et al. (2016a, 2016b) pointed out the structural coherence of the transpressional structures in the Nico Perez Terrane when compared to eastern sectors of the Uruguayan segment of the Dom Feliciano Belt, and suggest its accretion to the Rio de la Plata Craton after Cryogenian rifting of the Nico Perez-Congo blocks.

Oblique continental collision has affected the entire Dom Feliciano Belt (Fig. 15e), which records widespread dextral transpression at 660-630 Ma (e.g. Lenz et al., 2011; Lena et al., 2014; Oriolo et al., 2016; Martil et al., 2017; De Toni, 2019). In the Uruguayan portion of the belt, W-verging transpression is recorded in the Cerro Olivo Complex (Punta del Este Terrane – Masquelin et al., 2012), while NW-verging transpression is described in the reworked Nico Perez Terrane (Oriolo et al., 2016a,b). High-T/low-P, W-verging transpression is also recorded in the Várzea do Capivarita Complex (e.g. Gross et al., 2009), accompanied by syntectonic syenitic magmatism (De Toni et al., 2016). NW-transpression is registered in the supracrustal rocks of the Tijucas Fold Belt (Jost and Bitencourt, 1980; Saalmann et al., 2006b), which are, in part, correlated to the VCC (Battisti et al., 2018; De Toni, 2019). It is possible that high-T/low-P metamorphism, and syn- to post-collisional, potassic to ultra-potassic magmatism (e.g. De Toni et al., 2016; Nardi et al., 2008; Padilha et al., 2019) has been caused by delamination of the lithosphere, with strong exhumation plus heating due to proximity of the asthenospheric mantle.

Recent work reported by Vieira et al. (2019) correlates the ca. 680 Ma shoshonitic magmatism registered as a fragmentary record in southernmost Brazil, with the Tonian arc magmatism of the Piratini Gneisses (Tambara et al., 2019). The compatibility of the 680 Ma magmatic age with the accretionary phase of the São Gabriel Block, in contrast with the 800 – 770 Ma ages of the migration of arc-magmatism towards the back-arc, suggests a distinct interpretation. Additionally, the similarities of this plutonism with other (ultra-) potassic intrusive rocks of similar age, composition and setting (e.g. De Toni et al., 2016) should be considered. They may thus represent an early record of the syncollisional magmatism produced from a metasomatized mantle wedge related to the Tonian subduction.

The northern portion of the Dom Feliciano Belt also records NW/NNW-verging transpression, both in the granitic domain northern boundary, along the Major Gercino Shear Zone (Fig. 1b), and in the foreland, affecting supra- and infra-structural domains. The oblique transpression culminates with tectonic juxtaposition of infra- and suprastructural domains of the Dom Feliciano Belt (De Toni, 2019).

The dominantly NW-verging transpression of the Dom Feliciano Belt and the SE-vergence of the São Gabriel Block documented by Saalmann et al. (2006a) may be interpreted as resulting from the same collisional event. The opposite vergence of the São Gabriel Block may be due to local effects of deformation against uplifted basement blocks related to the Nico Perez Terrane (Oriolo et al., 2016b), as for example, the Encantadas Gneiss, as pointed out by Saalmann et al., (2006b). An alternative interpretation should consider it as a consequence of the high obliquity between convergence vector and the Ibaré Lineament, which is the boundary between the São Gabriel and Taquarembó blocks (see Fig. 1a - related to Nico Perez Terrane – Girelli et al., 2018).

Late- to post-collisional magmatism related to distinct magmatic series is mostly controlled by the Southern Brazilian Shear Belt (Fig. 15f), which has focused magmatism in the hinterland along dominantly NE-trend (340° to 060°), subvertical, regional-scale, anastomosing shear zones after ca. 630 Ma, with local preservation of sub-horizontal syn-collisional structures suggestive of progressive transpressional deformation (e.g. Bitencourt and Nardi, 1993, 2000; Florisbal et al., 2012a). Most regional-scale shear zones are marked by peraluminous granites (e.g. Butiá Granite of Lyra et al., 2018; Cordilheira Suite of Fernandes and Koester, 1999; Philipp et al., 2013; Mariscal Granite of Florisbal et al., 2012a).

The opposite shear sense which is dominant in the dextral Major Gercino Shear Zone (Bitencourt and Nardi, 1993; 2000) and in the sinistral Dorsal de Canguçu Shear Zone (Fernandes et al., 1992; Fernandes and Koester, 1999) does not allow their direct correlation (as proposed by Basei et al., 2005, 2011; Passarelli et al., 2011; Hueck et al., 2019). Passarelli et al. (2011) interpret this apparent incompatibility as caused by their difference in orientation in relation to a N65W-trending principal compression axis. An alternative explanation to this apparent incoherence should consider that the boundary between hinterland and foreland in the northern Rio Grande do Sul state shield area is not the sinistral Dorsal de Canguçu Shear Zone, but the Passo do Marinheiro Fault (see fig 1a). This structure separates the Várzea do Capivarita Complex granulitic rocks and abundant later intrusives to the east from supracrustal rocks to the west, and is interpreted as a reactivated NNW-strike, top-to-W, dextral transpressional shear zone (De Toni, 2019). It is not possible to affirm if any of these structures is continuous with the Major Gercino Shear Zone. However, the shear zone which bounded the western Encruzilhada Block is kinematically compatible with the Major Gercino Shear Zone. It is also noteworthy that the inclined transpression model (Jones et al., 2004;

Fernandez and Díaz-Azpiroz, 2009), considering the oblique extrusion of material from the inner portion of the shear zone, predicts an opposite shear sense in both walls, leading to extrusion. In the case of the Encruzilhada Block, the synchronous movement of both dextral and sinistral shear zones supports its exhumation, with a southward-directed resultant vector.

While late post-collisional magmatism is widespread in the hinterland, it locally intruded the foreland of the Dom Feliciano Belt after ca. 600 Ma (e.g. Bitencourt and Nardi, 2000; Florisbal et al., 2012a). This is the timing of foreland sedimentation along narrow, lineament bounded basins distributed along the belt (Camaquã Basin - Paim et al., 2014; Oliveira et al., 2014; Itajaí Basin - Guadagnin et al., 2014; and chrono-correlated units from Uruguay - Albet et al., 2014).

Both Tonian magmatism and Cryogenian collision are locally preserved in the Coastal Terrane of the Kaoko Belt (Konopásek et al., 2008, 2018). Exhumation and erosion of the inner portions of the orogen is recorded by ca. 650 Ma provenance of flysch sediments reported by Konopásek et al. (2017) covering the Congo Craton. In contrast, most of the Kaoko Belt records late (ca. 550 Ma) peak metamorphism and transpressional deformation verging east (fig. 15g), which indicates a migration of the orogenic front towards the foreland (Goscombe et al., 2003a,b; Konopásek et al., 2008).

A similar migration is suggested in Dom Feliciano Belt by data of Höfig et al. (2018) and Battisti et al. (2018), which describe the interleaving of Tonian (830-780 Ma – Porongos I) and Ediacaran (615-580 Ma – Porongos II) foreland sequences deformed in the Capané Antiform of Tijucas Belt after 580 Ma (fig. 15g). The younger deformed sequence is recognized by Pertille et al. (2017) as correlated to the foreland sedimentary rocks (e.g. Camaquã Basin of Paim et al., 2014), indicating that tectonic mode continued to switch during post-collisional times.

Oriolo et al. (2016a, 2017) consider that kinematic inversion of shear zones in Uruguay are related to diachronic collision, first between Rio de la Plata and Congo (ca. 650 – 630 Ma), and later with Kalahari (600 – 584 Ma). The latter may be the cause of diachronic deformation increments during Ediacaran to Cambrian times, first in the Dom Feliciano Belt (ca. 580 Ma or soon after) and later in the Kaoko Belt (ca. 550 Ma), when the whole orogenic system can be understood as a crustal-scale, double-verging, positive flower. It is likely that the Dom Feliciano Belt hinterland, together with the Coastal Terrane of western Kaoko Belt, represent the hinterland roots of an ancient, high-T/low-P, exhumed orogenic plateau.

6. Final Remarks

Porto Belo Complex orthogneisses from the inner portion of Major Gercino Shear Zone are Tonian (crystallization age at 798.9±3.9 Ma) and show, dominantly, intermediate, high-K calc-alkaline compositions. Acidic rocks are subordinate, and major and trace element data indicate its origin through fractionation plus crustal contamination. Porto Belo Complex is correlated to other Tonian (800 – 770 Ma), arc-related orthogneisses and metavolcanic rocks from Dom Feliciano Belt: Várzea do Capivarita Complex orthogneiss, Cerro Bori orthogneiss, Porto Alegre orthogneiss, Piratini orthogneiss and Cerro da Árvore Complex easternmost metavolcanics. Their relationship with chronologically related rift-sequences of Kaoko Belt and ophiolites of southern Dom Feliciano Belt were discussed and an integrated tectonic model for the evolution of the orogenic system is proposed. It is assumed that São Gabriel Block is an integrated part of Dom Feliciano Belt, as well as, of Kaoko-Dom Feliciano-Gariep Orogenic System. This hypothesis takes into account the whole evolution of the system, as result of a single eastward subduction (present day coordinates) between Rio de la Plata Craton and Nico Perez Terrane/Congo Craton. Apart of diachronism

and other differences between northern and southern portions of the belt, the proposed tectonic evolution (Fig. 15) can be summarized as follows:

a) 925 – 880 Ma early subduction and fore-arc magmatism;

b) 820 – 770 Ma flat-slab subduction and arc-magmatism migration towards the back-arc region, with genesis of arc-related Tonian magmatic protoliths;

c) 765 – 700 Ma steepening subduction and arc-magmatism migration towards fore-arc, with genesis of São Gabriel Block rocks, while extension affected the back-arc area and triggers rifting, perhaps with lithospheric delamination. The back-arc rift widens southwards, with local development of oceanic domains;

d) 700 – 660 Ma accretionary phase, after final consumption of the eastward subducting oceanic plate, and subsequent collision of Rio de la Plata Craton with São Gabriel Block and Nico Perez Terrane;

e) 660 – 630 Ma oblique main collision leads to basin inversion and double-verging transpression, with hinterland high-T/low-P metamorphism and exhumation, and strain propagation towards Dom Feliciano Belt foreland under lower temperature and higher pressure metamorphic conditions;

f) 630 – 580 Ma post-collisional magmatism both syntectonic to shear belt development in the hinterland, with major strike-slip displacement, and locally intruding the foreland, at relatively low-strain zones;

g) 580 – 550 Ma secondary collision, with foreland deformation and later post-collisional magmatism recorded in Dom Feliciano Belt, while the main orogenic front migrated towards Kaoko and Gariep belts.

Arc magmatism migration from fore-arc towards back-arc and vice-versa due to cyclic changes in subduction angle and its effects in the tectonic mode switches of orogenic belts are recognized in Dom Feliciano Belt and linked to the Kaoko-Dom Feliciano-

Gariep Orogenic System. Such evidences suggest that modern-style plate tectonics operated at the Tonian.

7. Acknowledgements

GB De Toni thanks the Conselho Nacional de Pesquisa (CNPq) and the Coordenação de Aperfeiçoamento do Pessoal do Ensino Superior (CAPES) for the PhD scholarship. He also is grateful to J. Konopásek and A. Martini by friendly and fruitful discussion on collisional and pre-collisional settings.

References

Albet, N.R., Pecoits, E., Heaman, L.M., Veroslavsky, G., Gingras, M.K., Konhauser, K.O., 2014. Ediacaran in Uruguay: Facts and controversies. Journal of South American Earth Sciences, 55, 43-57.

Almeida, F.F.M., de Brito Neves, B.B., Carneiro, C.D.R., 2000. The origin and evolution of south american platform. Earth-Science Reviews, 50, 77-111.

Arena, K.R., Hartmann, L.A., Lana, C., 2016. Evolution of Neoproterozoic ophiolites from the southern Brasiliano Orogen revealed by zircon U–Pb–Hf isotopes and geochemistry. Precambrian Research, 285, 299–314

Arena, K.R., Hartmann, L.A., Lana, C., 2017. Tonian emplacement of ophiolites in the southern Brasiliano Orogen delimited by U-Pb-Hf isotopes of zircon from metasomatites. Gondwana Research, 49, 296–332

Bachman, S.B., Lewis, S.D., Schweller, W.J., 1983. Evolution of a forearc basin, Luzon Central Valley, Philippines. The American Association Petroleum Geologists Bulletin, 67(7), 1143-1162.

Barbarin, B. 1999. A review of the relationships between granitoid types, their origins and their geodynamic environments. Lithos, 46, 605-626.

Basei, M.A.S., Frimmel, H.E., Nutman, A.P., Preciozzi, F., Jacob, J., 2005. The connection between the Neoproterozoic Dom Feliciano (Brazil/Uruguay) and Gariep (Namibia/South Africa) orogenic belts. Precambrian Research, 139, 139–221.

Basei, M.A.S., Campos Neto, M.C., Castro, N.A., Nutman, A.P., Wemmer, K., Yamamoto, M.T., Hueck, M., Osako, L., Siga, O., Passarelli, C.R., 2011. Tectonic evolution of the Brusque group, Dom Feliciano belt, Santa Catarina, Southern Brazil. Journal of South American Earth Sciences, 32(4), 324–350.

Basei, M.A.S., Campos Neto, M.C., Lopes, A.P., Nutman, A.P., Liu, D., Sato, K., 2013. Polycyclic evolution of Camboriú Complex migmatites, Santa Catarina, Southern Brazil: integrated Hf isotopic and U-Pb age zircon evidence of episodic reworking of a Mesoarchean juvenile crust. Brazilian Journal of Geology, 43, 427–443.

Battisti M.A., Bitencourt, M.F., De Toni, G.B., Nardi, L.V.S., Konopásek, J., 2018. Metavolcanic rocks and orthogneisses from Porongos and Várzea do Capivarita complexes: A case for identification of tectonic interleaving at different crustal levels from structural and geochemical data in southernmost Brazil. Journal of South American Earth Sciences, 88, 253-274.

Bento dos Santos, T.M., Tassinari, C.C.G, Fonseca, P.E., 2015. Diachronic collision, slab break-off and long-term high thermal flux inthe Brasiliano–Pan-African orogeny: Implications for the geodynamicevolution of the Mantiqueira Province. Precambrian Research, 260, 1-22.

Bettucci, L.S., Burgueño, A.M., 1993. Análisis sedimentológico y faciológico de la Formación Rocha (ex Grupo Rocha). Revista Brasileira de Geociências, 23, 323-329.

Bitencourt, M.F., 1996. Granitóides sintectônicos da região de Porto Belo, SC: uma aboradagem petrológica e estrutural do magmatismo em zonas de cisalhamento.

Tese de Doutorado, Instituto de Geociências, Universidade Federal do Rio Grande do Sul, 310 pp.

Bitencourt, M.F., Nardi, L.V.S. 1993. Late- to Post-collisional Brasiliano Magmatism in Southernmost Brazil. Anais da Academia Brasileira de Ciências, 65, 3-16.

Bitencourt, M.F., Nardi, L.V.S., 2000. Tectonic setting and sources of magmatism related to the Southern Brazilian Shear Belt. Revista Brasileira de Geociências 30, 186–189.

Boynton, W.V., 1984. Cosmochemistry of the Rare Earth Elements: Meteorite Studies. Developments in Geochemistry, 63–114.

Campanha, G.A.C., Faleiros, F.M., Cawood, P.A., Cabrita, D.I.G., Ribeiro, B.V., Basei, M.A.S., 2019. The Tonian Embu Complex in the Ribeira Belt (Brazil): revision, depositional age and setting in Rodinia and West Gondwana. Precambrian, 320:31-45.

Campos, R.S., Philipp, R.P., Massonne, H.J., Chemale Jr., F., Theye, T., 2012. Petrology and isotope geology of mafic to ultramafic metavolcanic rocks of the Brusque Metamorphic Complex, southern Brazil. International Geology Reviews, 54(6), 686–713

Cavalcante, C., Fossen, H., Almeida, R.P., Hollanda, M.H.B.M., Egydio-Silva, M., 2019. Reviewing the puzzling intracontinental termination of the Araçuaí-West Congo orogenic belt and its implications for orogenic development. Precambrian Research, 322, 85-98.

Chemale Jr., F., 2000. Evolução Geológica do Escudo Sul-rio-grandense. In: Geologia do Rio Grande do Sul. CIGO/UFRGS, Porto Alegre, 2002. 444 p.

Chemale Jr., F., Mallmann G., Bitencourt M.F., Kawashita K. 2012. Time constraints on magmatism along the Major Gercino Shear Zone, southern Brazil: implications for West Gondwana reconstruction. Gondwana Research, 22, 184-199.

Clark, C., Fitzsimons, I.C., Healy, D. and Harley, S.L., 2011. How does the continental crust get really hot? Elements, v. 7(4), 235-240.

Cordani, U.G., Coutinho, M.V., Nutman, A.P., 2002. Geochronological constrains on the evolution of the Embu Complex, São Paulo, Brazil. Journal of South American Earth Sciences, 14, 903–910.

Cox, K.G., Bell, J.S., and Pankhurst, R.J., 1979, The Interpretation of Igneous Rocks: Allen and Unwin, London, 450 p.

De Toni, 2019. Correlação geológico-estrutural e modelo integrado de evolução para o Cinturão Dom Feliciano sob transpressão inclinada no Neoproterozoico do sul do Brasil. Universidade Federal do Rio Grande do Sul, Brazil. Unpublished PhD thesis. Xx p.

De Toni, G.B., Bitencourt, M.F., Nardi, L.V.S., 2016. Strain partitioning into dry and wet zones and the formation of Ca-rich myrmekite in syntectonic syenites: a case for melt-assisted dissolution replacement creep under granulite facies conditions. Journal of Structural Geology, 91, 88-101

Fernandes, L.A.D., Koester, E., 1999. The Neoproterozoic Dorsal de Canguçu strike-slip shear zone: its nature and role in the tectonic evolution of southern Brazil. Journal of African Earth Sciences 29, 3–24.

Fernandes, L.A.D., Tommasi, A., Porcher, C.C., 1992. Deformation Patterns in the southern brazillan branch of the Dom Feliciano Belt: A reappraisal. Journal South American Earth Sciences 5, 77-96.

Fernández, C., Díaz-Azpiroz, M., 2009. Triclinic transpression zones with inclined extrusion. Journal of Structural Geology 31, 1255-1269.

Florisbal, L.M., Janasi, V.A., Bitencourt, M.F., Heaman, L.M., 2012a. Space–time relation of post-collisional granitic magmatism in Santa Catarina, southern Brazil: U–

Pb LA-MC-ICP-MS zircon geochronology of coeval mafic-felsic magmatism related to the Major Gercino Shear Zone. Precambrian Research, 216, 132–151.

Florisbal, L.M., Bitencourt, M.F., Janasi, V.A., Nardi, L.V.S., Heaman, L.M., 2012b. Petrogenesis of syntectonic granites emplaced at the transition from thrusting to transcurrent tectonics in post-collisional setting: whole-rock and Sr–Nd–Pb isotope geochemistry in the Neoproterozoic Quatro Ilhas and Mariscal granites, southern Brazil. Lithos 153, 53–71.

Fowler, A., Hassen, I., Hassan, M., 2015. Tectonic evolution and setting of the Sa'al Complex, southern Sinai, Egypt: A Proterozoic continental back-arc rift model. Journal of African Earth Sciences, 104, 103-131.

Frimmel, H.E. and Föelling, P.G. 2004. Late Vendian Closure of the Adamastor Ocean: Timing of Tectonic Inversion and Syn-orogenic Sedimentation in the Gariep Basin Gondwana Research, 7, pp. 685-699.

Girelli, TJ, Chemale Jr, F, Lavina, ELC, Laux, JH, Bongiolo, EM, Lana, C, 2019. Granulite accretion to Rio de la Plata Craton, based on zircon U-Pb-Hf isotopes: Tectonic implications for Columbia Supercontinent reconstruction. Gondwana Research, 56:105-118.

Goscombe B, Hand M, Mawby J, Gray D, 2003a. The metamorphic architecture of a transpressional orogen: the Kaoko Belt, Namibia. J Petrol 44:679–711

Goscombe B, Hand M, Gray D, 2003b. Structure of the Kaoko Belt, Namibia: progressive evolution of a classic transpressional orogeny. Journal of Structural Geology, 25:1049-1081.

Gross, A.O.M.S., Porcher, C.C., Fernandes, L.A.D., Koester, E., 2006. Neoproterozoic lowpressure/high-temperature collisional metamorphic evolution in the Varzea do Capivarita metamorphic suite, SE Brazil: thermobarometric and Sm/Nd evidence. Precambrian Research 147, 41–64.

Gross, A.O.M.S., Droop, G.T.R., Porcher, C.C., Fernandes, L.A.D. 2009. Petrology and thermobarometry of mafic granulites and migmatites from the Chafalote Metamorphic Suite: new insights into the Neoproterozoic P–T evolution of the Uruguayan-Sul- Rio-Grandense shield. Precambrian Research, 170, 157–174.

Gruber, L., Porcher, C.C., Geller, H., Fernandes, L.A.D, Koester, E., 2016a. Geochronology (U-Pb) and isotope geochemistry (Sr/Sr and Pb/Pb) applied to the Várzea do Capivarita Metamorphic Suite, Dom Feliciano Belt, Southern Brazil: Insights and paleogeographical implications to West Gondwana evolution. Geochimica Brasiliensis 30(1), 55 – 71.

Gruber, L., Porcher, C.C., Koester, E., Bertotti, A.L., Lenz, C.,Fernandes, L.A.D, Remus, M.V.D, 2016b. Isotope Geochemistry and Geochronology of Syn-Depositional Volcanism in Porongos Metamorphic Complex, Santana Da Boa Vista Antiform, Dom Feliciano Belt, Brazil: Onset of an 800 Ma Continental Arc. Journal of Sedimentary Environments, 1(2), 202-221.

Guadagnin, F., Chemale, F. Jr., Dussin, I.A., Jelinek, A.R., Santos, M.N., Borba, M.L., Justino, D., Bertotti, A.L., Alessandretti, L., 2010. Depositional age and provenance of the Itajaí Basin, Santa Catarina State, Brazil: implications for SW Gondwana correlation. Precambrian Research 180, 156–182.

Gubert, M., Philipp, R.P., Basei, M.A.S., 2016. Geochronology of the Bossoroca Complex, São Gabriel Terrane, Dom Feliciano Belt, southernmost Brazil: tectonic implications for a Neoproterozoic São Gabriel Arc. Journal of South American Earth Sciences, 70, 1–17.

Harris, N.B.W., Holland, T.J.B., 1984. The significance of cordierite-hypersthene assemblages from the Beitbridge region of the Central Limpopo Belt: evidence for rapid decompression in the Archaen? American Mineralogist, 69, 1037-1049.

Hartmann, L.A., Chemale Jr., F., Philipp, R.P., 2007. Evolução Geotectônica do Rio Grande do Sul no Pré-Cambriano. In: Ianuzzi, E.R., Frantz, J.C. (Eds.), 50 anos de Geologia: Instituto de Geociências. Contribuições. Comunicação e Identidade, Porto Alegre, 396p.

Hartnady, C.J.H., Joubert, P., Stowe, C., 1985. Proterozoic crustal evolution in southwestern Africa. Episodes, 8(4), 236–244.

Hasui, Y., Carneiro, C.D.R. and Coimbra, A.W., 1975. The Ribeira folded belt. Revista Brasileira de Geociências, 5, 257–266.

Höfig, D.F., Marques, J.C., Basei, M.A.S., Giusti, R.O., Kohlrausch, C., Frantz, J.C., 2017. Detrital zircon geochronology (U-Pb LA-ICP-MS) of syn-orogenic basins in SW Gondwana: new insights into the cryogenian-ediacaran of Porongos complex, Dom Feliciano belt, southern Brazil. Precambrianian Research, 306, 189-208. https://doi.org/10.1016/j.precamres.2017.12.031.

Hueck, M., Basei, M.A.S., Wemmer, K., Oriolo, S., Heidelbach, F., Siegesmund, S., 2019. Evolution of the Major Gercino Shear Zone in the Dom Feliciano Belt, South Brazil, and implications for the assembly of southwestern Gondwana. International Journal of Earth Sciences 108(2), 403–425.

Hyndman, R.D., Currie, C.A., Mazzotti, S.P., 2005. Subduction zone backarcs, mobile belts and orogenic heat. GSA Today 15. http://dx.doi.org/10:1130/1052-5173(2005)0152.0.CO;2.

Irvine, T.N. & Baragar, R.W.A. 1971. A guide to the chemical classification of the common volcanic rocks. Canadian Journal of Earth Sciences, 8, 523-548.

Jackson, S.E., Pearsona, N.J., Griffina, W.L., Belousova, E.A., 2004. The application of laser ablation-inductively coupled plasma-mass spectrometry to in situ U–Pb zircon geochronology. Chemical Geology, 211, 47–69.

Jones, R.R., Holdsworth, R.E., Clegg, P., McCaffrey, K., Tavarnelli, E., 2004. Inclined transpression. Journal of Structural Geology 26, 1531–1548.

Jones, R.E., Kirstein, L. A., Kasemann, S.A., Litvak, V.D., Poma, S., Alonso, R.N., Hintin, R. 2016.The role of changing geodynamics in the progressive contamination of Late Cretaceous to Late Miocene arc magmas in the Southern Central Andes. Lithos, 262, 169–191. DOI: 10.1016/j.lithos.2016.07.002

Jost, H., Bitencourt, M.F., 1980. Estratigrafia e tectônica de uma fração da Faixa de Dobramentos Tijucas no Rio Grande do Sul. Acta Geológica Leopoldensia, 4(7):27-60. São Leopoldo, RS, Brazil.

Jost, H., Hartmann, L.A., 1984. Província Mantiqueira – Setor Meridional. in: Pré-Cambriano do Brasil. Coord.: Almeida, F.F.M., Hasui, Y. p. 345-368.

Klemd, R., John, T., Scherer, E.E., Rondenay, S., Gao, J., 2011. Changes in dip of subducted slabs at depth: petrological and geochronological evidence from HP-UHP rocks (Tianshan, NW China). Earth and Planetary Science Letters, 310, 9–20.

Koester, E, Porcher, C.C., Pimentel, M.M., Fernandes, L.A.D., Vignol-Lelarge, M.L., Oliveira, L.D., Ramos, R.C., 2016. Further evidence of 777 Ma subduction-related continental arc magmatism in Eastern Dom Feliciano Belt, southern Brazil: The Chácara das Pedras Orthogneiss. Journal of South American Earth Sciences, 68, 155-166.

Konopásek, J., Košler, J., Tajc˘manová, L., Ulrich, S., Kitt, S.L., 2008. Neoproterozoic igneous complex emplaced along major tectonic boundary in the Kaoko Belt (NW Namibia): ion probe and LA-ICP-MS dating of magmatic and metamorphic zircons. Journal of the Geological Society of London, 165, 153–165.

Konopásek, J., Sláma, J., Košler, J., 2016. Linking the basement geology along the Africa–South America coasts in the South Atlantic. Precambrian Research, 280, 221–230.

Konopásek, J., Hoffmann, K.H., Sláma, J., Košler, J., 2017. The onset of flysch sedimentation in the Kaoko Belt (NW Namibia)—implications for the pre-collisional evolution of the Kaoko–Dom Feliciano–Gariep Orogen. Precambrian Research, 298, 220–234.

Konopásek, J., Janoušek, V., Oyhantçabal, P., Sláma J ., Ulrich, S., 2018. Did the circum-Rodinia subduction trigger the Neoproterozoic rifting along the Congo–Kalahari Craton margin? International Journal of Earth Sciences. https://doi.org/10.1007/s00531-017-1576-4

Kroner, A., Stern, R.J., 2004. Pan-african orogeny. in: Encyclopedia of Geology, vol.1, 01-12. Elsevier.

Le Maitre, R.W., 2002. Igneous Rocks - A classification and Glossary of Terms. Cambridge University Press, Cambridge, 236pp.

Leite, J. A. D., Hartman, L. A., Mcnaughton, N. J., Chemale Jr., F., 1998. SHRIMP U/Pb Zircon Geochronology of Neoproterozoic Juvenile and Crustal-Reworked Terranes in Southernmost Brazil, International Geology Review, 40, 8, 688-705.

Lena, L.O.F., Pimentel, M.M., Philipp, R.P., Armstrong, R., Sato, K., 2014. The evolution of the Neoproterozoic São Gabriel juvenile terrane, southern Brazil based on high spatial resolution U-Pb ages and 18O data from detrital zircons. Precambrian Research, 247, 126–138

Lenz, C., 2006. Evolução metamórfica dos metapelitos da Antiforme Serra Dos Pedrosas: condições e idades do metamorfismo. Unpublished MSc thesis. Universidade Federal do Rio Grande do Sul, 128 p. Avaliable at: https://lume.ufrgs.br/handle/10183/8520

Lenz, C., Fernandes, L.A.D., McNaughton, N.J., Porcher, C.C., Masquelin, H., 2011. U–Pb SHRIMP ages for the Cerro Bori orthogneisses, Dom Feliciano Belt in

Uruguay: evidences of a ~ 800 Ma magmatic and ~ 650 Ma metamorphic event. Precambrian Research, 185, 149–163.

Lenz, C., Porcher, C.C., Fernandes, L.A.D., Masquelin, H., Koester, E., Conceição, R.V., 2013. Geochemistry of the Neoproterozoic (800–767 Ma) Cerro Bori orthogneisses, Dom Feliciano Belt in Uruguay: tectonic evolution of an ancient continental arc. Mineralogy and Petrology 107, 785–806.

Martil, M.M.D., Bitencourt, M.F., Nardi, L.V.S., 2011. Caracterização estrutural e petrológica do magmatismo pré-colisional do Escudo Sul-rio-grandense: os ortognaisses do Complexo Metamórfico Várzea do Capivarita. Pesquisas em Geociências, 38, 181-201. ISSN 1518-2398.

Lyra, D.S., Savian, J.F., Bitencourt, M.F., Trindade, R.I.F., Tomé, C.R., 2017. AMS fabrics and emplacement model of Butia Granite, an Ediacaran syntectonic peraluminous granite from southernmost Brazil. Journal of South American Earth Sciences, 87, 25-41.

Martil, M.M.D., 2016. O magmatismo de arco continental pré-colisional (790 ma) e a reconstituição espaço-temporal do regime transpressivo (650 Ma) no Complexo Várzea do Capivarita, sul da Província Mantiqueira. Unpublished PhD thesis. Universidade Federal do Rio Grande do Sul. Avaliable at: https://www.lume.ufrgs.br/handle/10183/149194

Martil, M.M.D., Bitencourt, M.F., Nardi, L.V.S., 2011. Caracterização estrutural e petrológica do magmatismo pré-colisional do Escudo Sul-rio-grandense: os ortognaisses do Complexo Metamórfico Várzea do Capivarita. Pesquisas em Geociências, 38, 181-201. ISSN 1518-2398.

Martil MMD, Bitencourt MF, Nardi LVS, Koester E, Pimentel MM, 2017. Pre-collisional, Neoproterozoic (ca. 790 Ma) continental arc magmatism in southern

Mantiqueira Province, Brazil: geochemical and isotopic constraints from the Várzea do Capivarita Complex. Lithos 274–275:39–52

Martini, A., Bitencourt, M.F., Weinberg, R., De Toni, G.B., Nardi, L.V.S., 2019. From migmatite to magma - crustal melting and generation of granite in the Camboriú complex, South Brazil. Lithos, 340-341, 270-286.

Masquelin, H., Fernandes, L.A.D., Lenz, C., Porcher, C.C., McNaughton, N.J., 2012. The Cerro Olivo Complex: a pre-collisional Neoproterozoic magmatic arc in Eastern Uruguay. International Geology Reviews, 54, 1161–1183.

Meira, V.T., García-Casco, A., Juliano, C., Almeida, R.P., Schorscher, J.H.D., 2015. The role of intracontinental deformation in supercontinent assembly: insights from the Ribeira Belt, Southeastern Brazil (Neoproterozoic West Gondwana). Terra Nova, 27, 206-217.

Miller, C.F., and Mittlefehldt, D.W., 1982. Depletion of light rare-earth elements in felsic magmas. Geology, 10, 129-133.

Miyashiro, A., 1982. Theory of orogeny based on plate tectonics. In: Miyashiro, A., Aki, K., Sengör, A.M., (Eds.) Orogeny. John Wiley and Sons, Chichester, pp. 49-119.

Murphy, J.B., 2007. Arc Magmatism II: Geochemical and Isotopic Characteristics. Geoscience Canada, 34(1):7-35.

Nardi, L.V.S., Plá-Cid, J., Bitencourt, M.F., Stabel, L.Z., 2008. Geochemistry and petrogenesis of post-collisional ultrapotassic syenites and granites from southernmost Brazil: the Piquiri Syenite Massif. Anais da Academia Brasileira de Ciências 80(2), 353-371.

Nardi, L.V.S, Bitencourt, M.F., 2009. A-type granitic rocks in post-collisional settings in southernmost Brazil: their classification and relationship with tectonics and magmatic series. The Canadian Mineralogist, 47, 1287-1297.

Nardi, L.V.S., 2016. Granitoides e séries magmáticas: o estudo contextualizado dos granitoides. Pesquisas em Geociências, 43 (1), 85-99.

Occam's Razor (1960). Unidentified author. The Lancet, 276(7145), 302.

De Oliveira, C.H.E., Chemale Jr., F., Jelinek, A.R., Bicca, M.M., Philipp, R.P., 2014. U–Pb and Lu–Hf isotopes applied to the evolution of the late topost-orogenic transtensional basins of the Dom Feliciano Belt, Brazil. Precambrian Research, 246, 240-255.

Oriolo, S., Oyhantçabal, P., Wemmer, K., Heidelbach, F., Pfänder, J., Basei, M.A.S., Hueck, M., Hannich, F., Sperner, B., Siegesmund, S., 2016a. Shear zone evolution and timing of deformation in the Neoproterozoic transpressional Dom Feliciano Belt, Uruguay. J Struct Geol 92, 59–78.

Oriolo, S., Oyhantçabal, P., Basei, M.A.S., Wemmer, K., Siegesmund, S., 2016b. The Nico Pérez Terrane (Uruguay): from Archean crustal growth and connections with the Congo Craton to late Neoproterozoic accretion to the Río de la Plata Craton. Precambrian Research, 280, 147–160.

Oriolo S., Oyhantçabal P., Wemmer K., Siegesmund S., 2017. Contemporaneous assembly of Western Gondwana and final Rodinia break-up: Implications for the supercontinent cycle. Geoscience Frontiers 8, 1431-1445.

Padilha, D.F., Bitencourt, M.F., Nardi, L.V.S., Florisbal, L.M., Reis, C., Geraldes, M., Almeida, B.S., 2019. Sources and settings of Ediacaran post-collisional syenitemonzonite-diorite shoshonitic magmatism from southernmost Brazil. Lithos, 344-345, 482-503.

Paim, P.S.G., Chemale Jr., F., Wildner, W., 2014. Estágios evolutivos da Bacia do Camaquã (RS). Ciência e Natura, Santa Maria, 36, 183–193.

Passarelli, C.R., Basei, M.A.S., Wemmer, K., Siga Jr., O., Oyhantçabal, P., 2011. Major shear zones of southern Brazil and Uruguay: escape tectonics in the eastern

border of Rio de La plata and Paranapanema cratons during the Western Gondwana amalgamation. International Journal of Earth Sciences, 100, 391–414.

Pearce, J.A., 1996. A user's guide to basalt discrimination diagrams. In: Wyman DA (eds) Trace element geochemistry of volcanic rocks: applications for massive sulphide exploration. Geological Association of Canada, Short Course Notes, 12, 79–113

Pearce, J.A., 2008. Geochemical fingerprinting of oceanic basalts with applications to ophiolite classification and the search for Archean oceanic crust. Lithos, 100, 14–48.

Pearce, J.A., Harris, N.B.W., Tindle, A.G., 1984. Trace element discrimination diagrams for the tectonic interpretation of granitic rocks. Journal of Petrology, 25, 956–983.

Pedrosa-Soares, A.C., Noce, C.M., Wiedemann, C.M., Pinto, C.P., 2001. The Araçuaí-West-Congo Orogen in Brazil: an overview of a confined orogen formed during Gondwanaland assembly. Precambrian Research, 110(1–4), 307–323. https://doi.org/10.1016/S0301-9268(01)00174-7.

Peel, E., Sánchez-Bettucci, L., Basei, M.A.S., 2018. Geology and geochronology of Paso del Dragón Complex (northeastern Uruguay): implications on the evolution of the Dom Feliciano Belt (Western Gondwana). Journal of South American Earth Sciences, 85, 250–262.

Peixoto, C.A., Heilbron, M., Ragatky, D., Armstrong, R., Dantas, E., Valeriano, C.M., Simonetti, A., 2017. Tectonic evolution of the Juvenile Tonian Serra da Prata magmatic arc in the Ribeira belt, SE Brazil: Implications for early west Gondwana amalgamation. Precambrian Research, 302:221-254

Pertille J., Hartmann L.A., Santos, O.S., McNaughton, N.J., Armstrong, R., 2017. Reconstructing the Cryogenian–Ediacaran evolution of the Porongos fold and thrust

belt, Southern Brasiliano Orogen, based on Zircon U–Pb–Hf–O isotopes. International Geology Review, DOI: 10.1080/00206814.2017.1285257

Philipp, R.P., Campos, R.S., 2004. Geologia, Petrografia e Litogeoquímica dos Gnaisses Porto Alegre, RS, Brasil: Implicações Geotectônicas. Pesquisas em Geociências 31 (2), 79-94.

Philipp, R.P., Mallmann, G., Bitencourt, M.F., Souza, E.R., Liz, J.D., Wild, F., Arend, S., Oliveira, A.S., Duarte, L.C., Rivera, C.B., and Prado, M., 2004. Caracterização Litológica e Evolução Metamórfica da Porção Leste do Complexo Metamórfico Brusque, Santa Catarina: Revista Brasileira de Geociências, v. 34, no. 1, p. 21–34.

Philipp, R.P., Massonne, H.J., Campos, R. 2013. Peraluminous leucogranites of the Cordilheira Suite: a record of Neoproterozoic collision and the generation of the Pelotas Batholith, Dom Feliciano Belt, Southern Brazil. Journal of South American Earth Sciences, 43, 8-24.

Philipp RP, Pimentel MM, Chemale Jr., F, 2016. Tectonic evolution of the Dom Feliciano Belt in Southern Brazil: Geological relationships and U-Pb geochronology. Brazilian Journal of Geology, 46(1), 83–104.

Philipp, R.P., Pimentel, M.M., Basei, M.A.S., 2018. The Tectonic Evolution of the São Gabriel Terrane, Dom Feliciano Belt, Southern Brazil: The Closure of the Charrua Ocean. in: S. Siegesmund et al. (eds.), Geology of Southwest Gondwana, Regional Geology Reviews, https://doi.org/10.1007/978-3-319-68920-3_10

Ramos, R.C., Koester, E., Vieira, D.T., Porcher, C.C., Gezatt, J.N., Silveira, R.L., 2018. Insights on the evolution of the Arroio Grande ophiolite (Dom Feliciano belt, Brazil) from Rb-Sr and SHRIMP U-Pb isotopic geochemistry. Journal of South American Earth Sciences, 86, 38–53.

Ramos, R.C., Koester, E., Vieira, D.T., 2019. Plagioclase-hornblende geothermobarometry of metamafites from the Arroio Grande Ophiolite, Dom Feliciano

Belt, southernmost Brazil. Journal of South American Earth Sciences, 95:102262. https://doi.org/10.1016/j.jsames.2019.102262

Ramos, V.A., 2009, Anatomy and global context of the Andes: Main geologic features and the Andean orogenic cycle, in Kay, S.M., Ramos, V.A., and Dickinson, W.R., eds., Backbone of the Americas: Shallow Subduction, Plateau Uplift, and Ridge and Terrane Collision: Geological Society of America Memoir 204, 31–65. DOI: 10.1130/2009.1204(02).

Saalmann K., Remus, M.V.D., Hartmann, L.A., 2005. Geochemistry and crustal evolution of volcano-sedimentary successions and orthogneisses in the São Gabriel belt, southernmost Brazil—relics of Neoproterozoic magmatic arcs. Gondwana Research, 8, 143–162.

Saalmann, K., Remus, M.V.D., Hartmann, L.A., 2006a. Tectonic evolution of the Neoproterozoic juvenile São Gabriel Block, southern Brazil – constraints on Brasiliano orogenic evolution of the Rio de la Plata cratonic margin. Journal of South American Earth Sciences, 21, 204-227.

Saalmann, K., Remus, M.V.D., Hartmann, L.A., 2006b. Structural evolution and tectonic setting of the Porongos Belt, southern Brazil. Geological Magazine, 143(1), 59-88.

Saalmann, K., Gerdes, A., Lahaye, Y., Hartmann, L.A., Remus, M.V.D., Läufer, A., 2011. Multiple accretion at the eastern margin of the Rio de la Plata craton: the prolonged Brasiliano orogeny in southernmost Brazil. International Journal of Earth Sciences, 100, 355-378.

Saunders, A.D., Norry, M.J., and Tarney, J., 1991. Fluid influence on the trace element composition of subduction zone magmas. Philosophical Transactions of the Royal Society of London, 335, 377-392.

Silva, L.C., Hartmann, L.A., Mcnaughton, N.J., Fletcher, I.R. 1999. SHRIMP U/Pb zircon timing of Neoproterozoic granitic magmatism and collision in the Pelotas Batholith in southernmost Brazil. International Geology Review, 41, 531-551.

Sun, S-S, and McDonough W.F., 1989. Chemical and isotopic systematics of oceanic basalts: implications for mantle composition and processes, in: Saunders A.D., and Norry, M.J. (eds.) Magmatism in the Oceanic Basins. Geological Society of London Special Publication 42, 313-345.

Tambara, G.B., Koester, E., Ramos, R.C., Porcher, C.C., Vieira, D.T., Fernandes, L.A.D., Lenz, C., 2019. Geoquímica e geocronologia dos Gnaisses Piratini: magmatismo cálcio-alcalino médio a alto-K de 784 Ma (U-Pb SHRIMP) no SE do Cinturão Dom Feliciano (RS, Brasil). Pesquisas em Geociências, 46(2), e0769. DOI: https://doi.org/10.22456/1807-9806.95466

van Hunen, J., van den Berg, A.P., Vlaar, N.J., 2002. On the role of subducting oceanic plateaus in the development of shallow flat subduction. Tectonophysics, 352, 317–333.

Vieira, DT, Koester, E, Ramos, RC, Porcher, CC, 2019. Sr-Nd-Hf isotopic constraints and U-Pb geochronology of the Arroio Pedrado Gneisses, Dom Feliciano Belt, Brazil: A 680 Ma shoshonitic event in the final stages of The Piratini Arc evolution. Journal of South American Earth Sciences, 95, 102294. DOI: https://doi.org/10.1016/j.jsames.2019.102294

Wiedenbeck, M., Alle, P., Corfu, F., Griffin, W.L., Meier, M., Oberli, F., Von Quadt, A., Roddick, J.C., Spiegel, W., 1995. Three natural zircon standards for U-Th-Pb, Lu-Hf, trace element and REE analyses. Geostandards Newsletter, 191, 1–23.

TABLE 01 – Comparative table for main characteristics of 800 - 770 Ma pre-collisional orthometamorphic associations of Dom Feliciano Belt

Characteristic	Porto Belo Complex	Cerro Bori orthogneiss	Piratini Gneiss	Porto Alegre orthogneiss	Varzea do Capivarita Complex	Cerro da Árvore Complex	References (method):	
Igneous protolith geochemistry	high-K calc-alkaline	type 1 - tholeiitic type 2 - calc-alkaine type 3 - potassic to ultra-K (14)	medium-K calc-alkaline, (type 2); one sample ultra-K (type 3) (7)	medium to high-K, slightly peraluminous granodiorites of calc-alkaline affinity (18)	medium- to high-K calc-alkaline (1)	medium- to high-K calc-alkaline (8)	1 2	Martil et al., 2017; Martil, 2016
Magmatic age	798.9 ± 3.9	802 ± 12 Ma 771 ± 6 Ma 780 ± 5 Ma 793 ± 4 Ma (15)	781 ± 5 Ma (22) 784±4 Ma (7)	777 ± 4 Ma (23)	789.7 ± 8.7 Ma (2) 770 ± 9.9 Ma 788 ± 5.3 Ma 790 ± 34 Ma	789 ± 7 Ma (9) 773±3.1; 801±4.7 809 ± 4.1 Ma (10) 773 ± 8 Ma (11)	3 4 5 6	Gruber et al., 2016 (U-Pb zircon, SHRIMP) Gross et al., 2006 Philipp et al., 2016 (U-Pb zircon SHRIMP) De Toni, 2019
Isotope signature	ƐNd(646 Ma) -5 (16) ƐNd(646 Ma) -5.6 and -4.73 (17) TDM 1.24 Ga; (16) and TDM 1.89 and 1.48 Ga; 17) 87Sr/86Sr(i) 0.705 (16); 0.73109 and 0.71934 (17)	Ɛnd(t=750) -6.67 to -2.12 TDM 1290 to 2092 (16)	not known	ƐNd(t=777)-6 TDM 1.8 to 2.0 Ga Sr(i) ~0.712 (23)	Ɛnd(t=790) -7.10 to -10.06 TDM 1834 to 2287 Ma 87Sr/86Sr(i) 0.71628 to 72509 (1)	Ɛnd(t=790) -8.54 TDM 1796 Ma (1) 87Sr/86Sr(i) 0.72248	7 8 9	Tambara et al., 2019 (SHRIMP) Battisti et al., 2018 Saalmann et al., 2011 (U-Pb zircon LA-ICP-MS)
Metasedimentary provenance	not known	not known	not existent	not existent	MDA: 728 ± 11 Ma 1.4; 2 – 2.2 Ba (3)	800 – 780 Ma 1.4; 2 – 2.2 Ba (12)	10 11	Pertille et al., 2017 Chemale Jr., 2000 (U-Pb zircon TIMS)
Intrusive heritage	700, 850, 950 Ma; 2.0-2.2 Ga Mariscal Granite (19)	not known	not known	Older ages, with discordance <10%, are of 745, 777, 836 and 1022 Ma.(23)	not known	not known	12 13	Gruber et al., 2016b (U-Pb zircon, LA-ICP-MS) Lenz, 2006
Metamorphic age	650 - 645 (16)	654±3 (15) 671±7 (20)	ca. 660 (7)	ca. 650 Ma (23)	648.4 ± 5.4 Ma 648 ± 18 Ma (2) 618 ± 7.3 Ma (3) 614 ± 12 Ma (4) 605.9 ± 2.4 Ma 619 ±4.3 Ma (5)	658 ± 26 Ma (13)	14 15 16 17 18 19	Lenz et al., 2013 Lenz et al., 2011 (U-Pb zircon, SHRIMP) Chemale Jr. et al., 2012 Florisbal et al., 2012b Philipp and De Campos (2004) Florisbal et al., 2012a
Metamorphic conditions	upper amphibolite, water-fluxed melting ~4.5 Kbar, ~700°C (6)	7-10Kbar/830-950°C (peak M2) (21) 4.8-5.5Kbar/788-830°C (exhum. M3) 3-6Kbar/600-750°C (M4)	not known	upper amphibolite (23)	730 – 800°C/ 3 – 4 Kbar (4) 760 – 865 (900)°C/ 4.6 Kbar – M1 (6) 680 °C/ 3 Kbar – M2 (6)	590 °C/6 Kbar - M1 (13) 550 °C/2.7 Kbar - M2 (13) 560 – 580 °C/ 5.8 - 6.3 Kbar (6)	20 21 22	Masquelin et al., 2012 Gross et al. 2009 Silva et al., 1999
Structural pattern	ENE-striking progressive transpression, from thrust-to-NNW to dextral strike-slip (6)	"gneissic layering predominantly trends E–W to NW–SE" (20)	xenoliths (7)	ENE-strike, dipping to NNW (18)	NNW-striking progressive transpression from thrust-to-W to dextral strike-slip (1,2)	NNW-striking progressive transpression from D_1 thrust-to-W to D_2 (dextral?) strike-slip (8)	23	Koester et al., 2016 (SHRIMP)

Table 2 - PB-57G zircon LA-MC-ICP-MS U–Pb data used for U–Pb age calculation (discordance < 5%)

spot	spot size µm	ƒ 206a	Pb ppm	Th ppm	U ppm	Th/Ub	207Pb/ 235U	1σ [%]	206Pb/ 238U	1σ [%]	Rho	207Pb/ 206Pbe	1σ [%]	206Pb/ 238U (Ma)	1σ (Ma)	207Pb/ 235U (Ma)	1σ (Ma)	207Pb/ 206Pb (Ma)	1σ (Ma)	% Concf
Magmatic age - Neoproterozoic																				
003A	20	0.001004094	22.80761341	88.46686513	146.279621	0.604779152	1.191355571	3.592915243	0.132123695	3.419622228	0.951768132	0.065397239	1.102371878	799.9693488	27.35592967	796.5886527	28.62075513	787.1420811	8.677232946	101.6296
005A	20	0.000705232	28.89702815	131.6981339	202.4419246	0.650547727	1.173644652	1.844913851	0.130320826	1.56319953	0.847302181	0.065316293	0.979854247	789.6954647	12.3445158	788.3488062	14.54435632	784.5411053	7.687359338	100.6569904
006A	20	0.001013898	17.94349723	55.67000305	115.1326306	0.483529324	1.193489501	3.535432452	0.132222004	3.311287905	0.936600529	0.065465666	1.238811945	800.5291046	26.50782342	797.5769458	28.19779417	789.3374343	9.778406419	101.4178563
005B	20	0.001008155	21.57116742	90.73331571	147.1259306	0.616705127	1.236953643	6.309872227	0.135985757	5.600370255	0.88755684	0.065971859	2.906946943	821.9228541	46.03072304	817.5000857	51.58321086	805.4829832	23.41496295	102.0409954
007B	20	0.000666242	17.07525142	55.95569761	118.8803204	0.470689324	1.194564661	6.364059555	0.131952812	5.565100762	0.874457681	0.065658316	3.087216794	798.9962509	44.46494644	798.074524	50.789938	795.5017825	24.55886462	100.4392785
008B	20	0.001585932	19.86394583	62.13394088	139.8619309	0.444251988	1.182466466	6.447034134	0.129856215	5.746721923	0.891374515	0.0660427	2.922231383	787.045165	45.22929704	792.4614344	51.09025917	807.7298165	23.60371958	97.43922239
001C	20	0.000612304	41.83098598	49.64990096	308.2980327	0.161045144	1.174697919	7.41418618	0.12954033	6.90244778	0.93097848	0.065768801	2.706727057	785.2426241	54.20096208	788.8407039	58.48611845	799.0261772	21.62745773	98.27495601
002C	20	0.000571747	41.61619911	58.66181057	307.7418215	0.19062021	1.178163286	6.88290134	0.130046555	6.320459301	0.918284164	0.06570605	2.725091755	788.1310638	49.81350313	790.4574224	54.40640451	797.0254221	21.71967407	98.88405589
004C	20	0.001339752	27.1302747	31.09720311	198.6179691	0.156567924	1.181546796	6.191574353	0.130358393	5.555772507	0.897311764	0.065737117	2.732944351	789.9097116	43.88558658	792.0334717	49.0393413	798.016292	21.80934117	98.98415854
006C	20	0.000969978	21.9331827	53.94142448	155.651394	0.346552788	1.14566201	6.37143411	0.127295443	5.701211727	0.894808238	0.065274323	2.844531148	772.4180562	44.03718881	775.1922973	49.39086645	783.1908496	22.27810767	98.62449959
009C	20	0.001625281	28.72671841	104.3359259	209.1069346	0.498959665	1.193694941	6.073521845	0.131142432	5.398560565	0.888868222	0.066015945	2.782662651	794.3795263	42.88505984	797.6720411	48.44678567	806.8813055	22.45278473	98.45060493
002D	20	0.002222099	12.42375177	41.54474619	78.54826695	0.528907229	1.204948196	5.299519151	0.132082445	4.650853413	0.877599133	0.066164038	2.540564065	799.734462	37.19447752	802.8674565	42.54811461	811.569459	20.61844204	98.54171483
003D	20	0.003160126	11.33277319	34.87755657	72.54137038	0.480795391	1.236459858	3.871355331	0.134722867	3.207754402	0.828586923	0.066563696	2.167418694	814.7523013	26.13525281	817.2759256	31.63965512	824.1518725	17.86282175	98.85948554
004D	20	0.001893427	13.85990876	37.79614805	94.93786682	0.39811457	1.145888558	5.325656507	0.126233654	4.95731572	0.930836548	0.065836382	1.946185521	766.3433778	37.99006074	775.2995004	41.28978829	801.178033	15.59241087	95.65207062
005D	20	0.002598306	11.61934722	32.11622405	79.11657892	0.40593545	1.163918434	3.295721976	0.128885704	3.040990037	0.922708305	0.065496263	1.270497122	781.5055205	23.76550502	783.795165	25.8317095	790.3180855	10.04096853	98.88493442
009D	20	0.002971576	10.23930696	25.70986159	62.21295357	0.413255763	1.190008071	4.24600534	0.132911978	4.053699348	0.954708961	0.064935847	1.263361764	804.4563418	32.61024148	795.964085	33.79667756	772.2585755	9.756419558	104.1692986
001E	20	0.001585704	17.72269355	68.9179897	125.5419923	0.548963645	1.152967415	4.091345068	0.128659532	3.579434357	0.874879605	0.064994079	1.981603933	780.2138521	27.92724268	778.6435331	31.85699379	774.144791	15.34048363	100.7839698
002E	20	0.003431204	9.443303873	31.60803502	67.24530339	0.470040782	1.184974418	3.645690127	0.130729227	3.114565024	0.854314249	0.065740803	1.894872347	792.0242295	24.66810964	793.6275784	28.93320227	798.1338059	15.12361678	99.23451729
004E	20	0.001408885	23.98953964	99.14015728	156.5683981	0.633206691	1.208220659	3.853682969	0.133417566	3.483404557	0.903915705	0.065679823	1.648261241	807.3325564	28.12265906	804.3733154	30.99799746	796.1884489	13.12326561	101.3996821
005E	20	0.002270462	16.63256611	82.87046434	112.127652	0.739072502	1.221412899	3.471837005	0.135404713	2.919496011	0.840908144	0.065422547	1.878881378	818.6247393	23.89971661	810.4213174	28.13650719	787.9543879	14.80472826	103.8924019
006E	20	0.002568958	22.72861102	71.12863123	165.4369975	0.42994392	1.206277027	4.147526397	0.131870506	3.057267593	0.737130352	0.066343459	2.80269336	798.5275031	24.41312258	803.4792015	33.32451198	817.2306533	22.90446926	97.71139884
007E	20	0.001585167	26.06113657	80.30492772	186.8060885	0.429883888	1.22841631	3.580632878	0.135899426	3.145471356	0.878467987	0.065558148	1.710830721	821.4329264	25.83793741	813.6174627	29.13265437	792.299667	13.5549061	103.6770506
008E	20	0.001655707	17.27537219	58.13352561	118.1797055	0.491907856	1.206320661	3.608153044	0.133847827	3.026235168	0.838721399	0.065365738	1.964858544	809.779241	24.50582417	803.4992831	28.99148384	786.1303907	15.44635015	103.0082605
009E	20	0.003167064	45.30203764	186.9952355	305.7496123	0.611595986	1.288921387	5.258780435	0.137773669	2.879555991	0.547571063	0.067851418	4.400332824	832.0607984	23.95965657	840.8191062	44.21683065	864.0188657	38.01970575	96.30123038
004F	20	0.003537136	10.1513617	31.14258152	61.36707655	0.507480285	1.210462202	3.060542781	0.133489716	2.604202866	0.850895757	0.065766109	1.607808926	807.7429072	21.03526394	805.4034976	24.6497186	798.9403852	12.84543483	101.1017746
005F	20	0.002183328	12.21144196	33.44299662	75.68946032	0.441844829	1.212195213	4.624618516	0.134436534	4.330229209	0.936343007	0.065396421	1.623641408	813.1254258	35.21019469	806.1992503	37.28363981	787.1158283	12.77993852	103.3044181
007F	20	0.003802675	12.42610465	35.02829928	80.43175547	0.435503354	1.196251032	4.646172019	0.130478893	3.605405698	0.77599488	0.066493744	2.930522853	790.5968861	28.50422518	798.8544757	37.11615313	821.9568482	24.08763328	96.18471916
009F	20	0.001753343	11.81449748	34.02290219	70.69948627	0.481232665	1.197827624	2.859414769	0.13202612	1.913185509	0.669082894	0.065801105	2.125082124	799.4137214	15.29426747	799.583113	22.86339763	800.0551579	17.00182914	99.91982597
001G	20	0.002658069	10.1833643	31.98976661	70.664716	0.452697873	1.217215556	2.939973383	0.134411468	2.633336431	0.895700773	0.065679509	1.307280662	812.982987	21.40857718	808.500944	23.76971255	796.178433	10.40828669	102.1106517
002G	20	0.002728604	13.45194467	38.38078292	89.49924174	0.428839197	1.241936141	4.133581394	0.13728189	3.831646497	0.926955618	0.065612221	1.550799878	829.2738642	31.77484296	819.7591929	33.88541347	794.0290687	12.31380183	104.4387286
Neoproterozoic inheritance																				
008G	20	0.005701448	35.74909523	154.4772161	203.0413854	0.760816401	1.603733798	5.644166999	0.164145755	4.411152646	0.781541837	0.070860033	3.521129569	979.774767	43.21936056	971.66725	54.84252226	953.3784915	33.56969197	102.7687089
Neoproterozoic rework (metamorphic/migmatitic)																				
007C	20	0.001170829	14.97739609	92.80284404	136.5300425	0.679724714	0.849210844	7.642876714	0.102465202	6.99554628	0.915302777	0.060108772	3.078294449	628.8397398	43.99077502	624.2158473	47.70804764	607.4924199	18.70040544	103.514006
Mesoproterozoic inheritance																				
002A	20	0.00033297	50.28309791	118.8071838	279.774437	0.424653464	1.822072005	1.670329635	0.175087733	1.327363568	0.794671627	0.075475942	1.013956136	1040.082584	13.8056773	1053.430846	17.5957676	1081.203896	10.96293326	96.19671069
004A	20	0.000490899	45.12406663	72.33714663	182.8499496	0.395609333	2.519083003	2.91919331	0.218847926	2.752363478	0.942850708	0.083483138	0.972720341	1275.784624	35.11423004	1277.55541	37.29431204	1280.535475	12.45602904	99.62899498
009B	20	0.000924967	32.73594267	43.04028523	148.0431325	0.290728009	2.436337879	5.344301616	0.215166576	4.796946444	0.897581534	0.082122363	2.356027286	1256.284716	60.26330503	1253.395273	66.98522381	1248.436287	29.41349956	100.6286608
Paleoproterozoic inheritance																				
001D	20	0.000856501	45.42245039	84.0785838	93.13820945	0.902729227	7.177880022	1.653647856	0.398004547	1.53488958	0.928184059	0.130799742	0.615357791	2159.844617	33.15122997	2133.759406	35.28486668	2108.729613	12.97623197	102.4239715
001H	20	0.001265215	26.77685281	47.11668879	60.8008371	0.77493487	5.333400024	5.237633983	0.326522998	4.640152326	0.885925275	0.118464741	2.42936126	1821.506734	84.52068709	1874.231833	98.1654034	1933.195987	46.96431439	94.22255921
004H	20	0.00252843	22.91741664	24.72360986	40.86027156	0.605076984	7.521738128	11.46545923	0.394707987	10.59609636	0.924175486	0.138210494	4.3794403	2144.625723	227.2466081	2175.580368	249.4402801	2204.903751	96.56244344	97.26618327
009H	20	0.001193973	27.03205869	26.76895839	58.07545825	0.460934088	6.027399639	7.141293694	0.360585478	6.531642312	0.91463012	0.121232896	2.887165451	1984.948304	129.6497233	1979.810877	141.3841093	1974.448979	57.00560876	100.5317598
Archean inheritance																				
008D	20	0.000694118	78.75524648	116.0483822	113.4553354	1.022855221	15.14242482	4.116605457	0.54166629	4.004545346	0.972778516	0.202750691	0.953969106	2790.419583	111.7436175	2824.238095	116.2627395	2848.468035	27.17350504	97.96211676
005G	20	0.000745417	121.7622968	109.4187348	233.2633992	0.469078026	12.43743183	2.775858264	0.496389701	2.48539347	0.895360365	0.181721652	1.236207266	2598.261664	64.57702572	2638.010086	73.22742097	2668.645771	32.98999291	97.36255342
006H	20	0.013653879	14.77717729	14.20102362	28.19992062	0.503583815	13.30142817	12.4998853	0.503768118	10.98213084	0.878578529	0.191498916	5.969919153	2629.969615	288.8267043	2701.283855	337.6573835	2755.077621	164.4759066	95.45900251

Table 03 - Porto Belo Complex whole-rock geochemistry results.

qz-dio og = quartz-dioritic orthogneiss; ton og = tonalithic orthogneiss; gdio og = granodioritic orthogneiss; Pl+Qtz = plagioclase+quartz abundant interogrowth

Sample n	GB 01B	GB 01G	GB 01J	GB 01K	GB 01L	GB02B	GB 02C	GB 02D	GB 04D	GB 05B	GB 09B	GB 09C	GB 09DA	GB 09E	GB 10B	GB 10D	PB 57G
Rock	*restite*	*qz-dio og*	*qz-dio og*	*ton og*	*gdio og*	*ton og*	*ton og*	*ton og*	*qz-dio og*	*ton og*	*ton og*	*qz-dio og*	*qz-dio og*	*ton og*	*ton pg*	*restite*	*ton og*
Obs	*Bt-rich*	*migmatitic*		*Pl+Qtz*	*migmatitic*					*acidic*	*sericitic Pl*				*acidic*	*Hb-rich*	*acidic*
SiO2	48.49	54.97	56.97	55.22	56.49	60.74	61.77	61.81	54.45	70.78	61.47	55.27	54.79	60.01	65.61	45.12	68.07
TiO2	1.694	1.432	1.243	1.729	1.231	1.812	1.767	1.131	1.418	0.606	1.251	1.26	1.319	1.411	0.924	1.811	0.553
Al2O3	15.92	16.78	15.71	16.3	16.33	15.67	15.74	15.26	17.64	13.4	15.57	16.37	16.2	16.67	13.82	15.12	14.35
Fe2O3T	12.56	9.59	7.52	10.76	8.55	7.19	7.02	6.56	9.43	4.39	8.16	9.41	9.55	8.4	7.05	15.6	5.07
MnO	0.241	0.148	0.121	0.127	0.133	0.103	0.109	0.094	0.125	0.072	0.123	0.12	0.177	0.12	0.127	0.258	0.092
MgO	6.02	4.21	5.01	4.55	4.19	2.13	2.1	3.54	3.3	1.45	2.79	5.72	5.97	2.47	3.09	8.15	2.28
CaO	6.88	6.13	6.62	4.57	6.68	3.78	3.92	4.32	5.89	2.87	5.01	5.01	6.43	2.66	3.29	8.03	3.79
Na2O	0.6	1.91	2.86	1.87	2.94	3.1	2.99	2.72	1.17	2.92	1.01	0.49	0.68	3.04	2.11	0.94	1.72
K2O	4.74	2.93	2.36	3.76	2.2	2.94	3.07	3.08	3.97	1.9	2.99	4.39	3.73	3.65	2.55	3.29	2.45
P2O5	0.25	0.32	0.41	0.35	0.37	0.62	0.68	0.45	0.8	0.15	0.32	0.26	0.28	0.31	0.15	0.25	0.08
LOI	1.94	1.25	0.93	1.07	0.76	1.09	0.86	1.35	2.16	0.83	1.25	1.73	1.36	1.43	0.9	1.71	1.2
Total	99.33	99.68	99.74	100.3	99.87	99.17	100	100.3	100.3	99.37	99.95	100	100.5	100.2	99.63	100.3	99.65
Sc	21	15	17	17	17	9	8	13	17	13	21	28	29	16	13	22	15
Be	5	3	2	4	2	5	5	3	6	3	2	2	3	5	3	3	3
V	175	214	148	260	175	129	116	127	217	67	156	194	209	123	98	257	85
Ba	200	535	842	532	894	580	548	792	793	555	751	424	300	286	280	240	381
Sr	302	483	747	406	796	369	311	675	527	134	257	140	151	173	218	158	156
Y	32	19	18	14	18	26	18	17	31	25	42	21	24	23	18	18	22
Zr	135	127	168	149	152	379	339	182	203	177	196	142	128	203	204	113	151
La	21.8	22.6	37.5	22.3	35.4	85.6	82.1	61	57.3	38.5	48.4	17.4	21.8	32.8	23.7	10.9	28.9
Ce	47	51.6	78.2	49.8	76.2	180	169	132	121	77.3	98.8	41	46.2	68.2	49.7	24.2	57
Pr	6.38	6.45	9.4	6.12	8.52	21	18.7	14.8	14.8	9.1	12	5.05	5.55	8.53	5.7	3.23	6.56
Nd	27.5	27.7	39.2	26.6	35.9	78.7	71.3	62.1	61.8	35.2	48.2	21.8	23.7	33.6	22.3	13.4	24.5
Sm	6.7	6.1	7.2	5.2	7.1	13.3	11.6	11.4	12.3	6.9	10.2	5	5.2	6.4	4.5	3.8	4.9
Eu	1.79	1.76	1.95	0.93	1.91	1.83	2.06	2.53	2.75	1.21	1.98	0.88	1.11	1.01	1.18	1.4	1
Gd	6.8	5.3	5	4.1	4.8	8.3	6.8	7.3	9.8	4.7	9.2	4.7	4.7	5.6	4	3.6	4.2
Tb	1.1	0.8	0.7	0.6	0.7	1.1	0.9	0.9	1.3	0.9	1.4	0.8	0.9	0.9	0.6	0.6	0.7
Dy	6.3	4.1	3.9	3.4	4.1	5.8	4.6	4	6.6	5.1	8.2	4.3	5.1	5.2	3.6	3.7	4.1

Table 03 - Porto Belo Complex whole-rock geochemistry results.

qz-dio og = quartz-dioritic orthogneiss; ton og = tonalithic orthogneiss; gdio og = granodioritic orthogneiss; Pl+Qtz = plagioclase+quartz abundant interogrowth

Sample n.	GB 01B	GB 01G	GB 01J	GB 01K	GB 01L	GB02B	GB 02C	GB02D	GB 04D	GB 05B	GB 09B	GB 09C	GB 09DA	GB09E	GB 10B	GB 10D	PB57G
Rock	*restite*	*qz-dio og*	*qz-dio og*	*ton og*	*gdio og*	*ton og*	*ton og*	*ton og*	*qz-dio og*	*ton og*	*ton og*	*qz-dio og*	*qz-dio og*	*ton og*	*ton pg*	*restite*	*ton og*
Obs	*Bt-rich*	*migmatitic*		*Pl+Qtz*	*migmatitic*					*acidic*	*sericitic Pl*				*acidic*	*Hb-rich*	*acidic*
Ho	1.2	0.7	0.7	0.6	0.7	0.9	0.7	0.7	1.1	1	1.5	0.8	0.9	0.9	0.7	0.8	0.8
Er	3.4	2	1.9	1.5	1.7	2.6	2	1.8	2.8	2.9	4.4	2.3	2.8	2.5	1.9	2.2	2.4
Tm	0.49	0.26	0.26	0.19	0.22	0.35	0.27	0.25	0.36	0.43	0.61	0.33	0.42	0.33	0.28	0.31	0.35
Yb	3.2	1.7	1.6	1.1	1.4	2.2	1.6	1.5	2.3	2.6	3.9	2	2.9	2.1	1.9	2.2	2.4
Lu	0.46	0.24	0.23	0.15	0.2	0.33	0.21	0.19	0.34	0.42	0.56	0.29	0.44	0.33	0.29	0.36	0.38
Hf	3.3	3.2	3.9	3.6	3.5	8.9	8.4	4.5	4.8	4.4	5.1	3.5	3.4	5	4.8	2.7	3.9
Ta	0.9	0.8	0.8	0.8	0.6	1.5	1.2	0.6	1.3	0.8	0.7	0.5	0.6	1.8	1.2	0.4	0.7
W	3	< 1	3	2	2	< 1	3	2	< 1	3	< 1	< 1	2	3	< 1	3	2
Pb	14	10	13	8	14	16	15	13	16	18	9	< 5	5	15	12	7	13
Th	2.2	4	6.7	3.8	6.1	22.4	12.5	11	18.1	17	10.2	4.1	5.6	12.5	8.1	2.3	9.7
U	2.1	3.2	1.6	1.5	3.5	3.5	3.3	2.3	6.9	4	0.9	1.2	2.3	6.2	3.6	0.5	2.2
Co	41	30	24	37	28	14	16	19	21	8	22	30	32	16	21	60	13
Ni	80	30	70	60	30	30	20	30	20	< 20	30	50	40	30	50	110	20
Cu	< 10	60	< 10	40	< 10	20	20	10	30	20	40	70	30	< 10	< 10	10	40
Zn	120	120	90	150	110	170	140	120	110	70	90	110	110	180	80	140	60
Ga	21	21	22	26	22	28	26	23	25	17	20	18	20	26	18	21	17
Rb	432	253	169	365	169	299	340	272	330	220	254	417	353	409	234	265	238
Nb	11	10	14	13	10	21	20	10	14	7	11	7	9	17	13	7	8
Cs	26.4	12.4	8.9	19.2	7.7	13.1	16.9	12.6	19.9	13.2	12.4	41.5	66.9	29.5	14.9	13.9	12.8
Cr	60	30	150	30	40	30	40	110	< 20	40	20	150	150	30	70	230	50
Ge	2	1	1	1	1	1	1	1	2	2	1	1	2	2	2	3	1
As	< 5	< 5	< 5	< 5	< 5	< 5	< 5	< 5	< 5	< 5	< 5	< 5	< 5	< 5	< 5	< 5	< 5
Mo	< 2	< 2	< 2	< 2	< 2	< 2	< 2	< 2	< 2	< 2	< 2	< 2	< 2	< 2	< 2	< 2	< 2
Ag	0.5	< 0.5	0.6	< 0.5	< 0.5	1.8	1.4	0.5	0.9	0.5	0.9	0.6	< 0.5	0.5	0.8	< 0.5	0.6
In	< 0.2	< 0.2	< 0.2	0.2	< 0.2	< 0.2	< 0.2	< 0.2	< 0.2	< 0.2	< 0.2	< 0.2	< 0.2	< 0.2	< 0.2	< 0.2	< 0.2
Sn	8	5	2	12	3	7	6	4	7	5	4	3	5	18	3	3	4
Sb	< 0.5	< 0.5	< 0.5	< 0.5	< 0.5	< 0.5	< 0.5	< 0.5	< 0.5	< 0.5	< 0.5	< 0.5	< 0.5	< 0.5	< 0.5	< 0.5	< 0.5
Tl	1.9	1.2	1	2	1.1	1.6	2	1.7	1.7	1.5	1.4	2.3	2	2.6	1.4	1.8	1.4
Bi	0.5	< 0.4	< 0.4	< 0.4	< 0.4	< 0.4	< 0.4	< 0.4	< 0.4	< 0.4	< 0.4	< 0.4	< 0.4	< 0.4	< 0.4	< 0.4	< 0.4

6. SÍNTESE

Esta tese apresenta novos dados e interpretações sobre duas áreas-chave para o entendimento da evolução tectônica do Cinturão Dom Feliciano, a partir de uma abordagem integrada, com a obtenção de dados através de diferentes técnicas de análise. Estes dados, confrontados com a bibliografia, servem de base para uma correlação regional e elaboração de um novo modelo para o ciclo orogênico do Cinturão Dom Feliciano.

6.1 Partição da deformação transpressiva em Santa Catarina

Uma seção geológica permitiu a correlação cinemática entre o norte do Batólito Florianópolis e o Cinturão de Dobramento Tijucas, no setor norte do Cinturão Dom Feliciano (Escudo Catarinense). Uma colisão oblíqua afetou a área como um todo em 650-645 Ma, e está especialmente preservada no interior da Zona de Cisalhamento Major Gercino, nas rochas do Complexo Porto Belo, que sofreram migmatização (~700°C/4.3 Kbar) e recordam um empurrão de topo-para-NNW destral. A partição da deformação transpressiva levou a uma progressão para movimentos tangenciais destrais ao longo de planos de baixo ângulo, com componente de topo-para-NNW (625-615 Ma), que progrediram para franca transcorrência destral (pós-615 Ma).

Enquanto isso, o componente contracional da transpressão foi absorvido pelo Cinturão de Dobramentos Tijucas, causando a exumação da sua infra-estrutura, composta pelos migmatitos do Complexo Camboriú (de mais de 5 para 3.4 Kbar), concomitante ao abatimento da sua supra-estrutura, em torno de 635 Ma. A justaposição destes níveis crustais distintos se deu ao longo de uma zona de descolamento entre os complexos. Como consequências na supra-estrutura observa-se o aquecimento do Complexo Brusque, localmente atingindo fácies anfibolito, e a inversão de empurrões para movimento extensional, localmente registrado em estruturas discretas.

As idades e a sequência de eventos proposta aponta para o fato de que o Complexo Porto Belo e a Faixa de Dobramentos Tijucas já estivessem lado-a-lado, se comportando como uma massa continental relativamente coerente, a 650-645 Ma. Esta hipótese contraria outras que consideram a colisão principal de blocos supostamente alóctones em idade igual ou posterior a 615 Ma, quando o sistema transpressivo já estava em franca partição da deformação.

6.2 Origem do Bloco Encruzilhada e seu significado tectônico

A análise da assinatura aeromagnética do Bloco Encruzilhada, juntamente com a análise de lineamentos, e a correlação dos protólitos ígneos e sedimentares tonianos dos complexos Várzea do Capivarita e Cerro da Árvore permite considerar este bloco como parte integrante da Faixa de Dobramentos Tijucas. Ao mesmo tempo, o magmatismo pós-colisional presente no bloco geralmente o leva a ser incluso no Batólito Pelotas, com o qual compartilha forte assinatura aerogamaespetrométrica. O Bloco Encruzilhada é, portanto, um “terreno suspeito”.

Tanto o Complexo Várzea do Capivarita quanto o Complexo Cerro da Árvore Ambos registram uma transpressão com componentes destral e de topo-para-oeste/noroeste e idade metamórfica entre 660 e 640 Ma. A geotermobarometria das rochas do Complexo Várzea do Capivarita indica pico metamórfico entre 800 e 900°C e pressões entre 4,4 e 4,8 Kbar, o que caracteriza fácies granulito de baixa pressão. Subdomínios subsaturados em sílica em paragnaisses pelíticos contém a assembleia cordierita+espinélio±silimanita, e apontam uma exumação para 660-720°C e 2,5-3,4 Kbar a cerca de 630 Ma. Gradientes geotérmicos estimados para estas rochas variam de 50 a 60°C/Km. Pelo outro lado, metapelitos do Complexo Cerro da Árvore registram um metamorfismo progressivo de ca. 560 °C/5,4-5,7 Kbar para 560-580°C/5,8-6,3 Kbar, o qual aponta o seu soterramento tectônico (*underthrusting*). Os novos dados, juntamente com os dados da literatura, sugerem que ambos complexos se originaram em bacias semelhantes, se não numa mesma bacia, sobre uma litosfera atenuada, com alto gradiente geotérmico. A colisão oblíqua causou a inversão da bacia, empurrando suas porções mais profundas e quentes sobre suas margens. A progressão da deformação transpressiva, assim como reativações posteriores, juntamente com o magmatismo pós-colisional, obliteraram os contatos originais destes complexos, criando e modificando os limites do Bloco Encruzilhada.

6.3 O ciclo orogênico do Cinturão Dom Feliciano

A caracterização de campo, petrográfica e geoquímica das rochas ortognáissicas do Complexo Perto Belo permite classifica-las como rochas predominantemente inermediárias, de composição cálcio-alcalina alto-K. Estas rochas tem idade Toniana, de ca. 800 Ma, e representam o embasamento do *hinterland* do Cinturão Dom Feliciano, sendo correlatas a tantas outras unidades

ortognáissicas aflorantes no *hinterland* deste cinturão, assim como ao Complexo Cerro da Árvore.

O seu significado é discutido frente a diversas outras evidências registradas ao longo de todo Cinturão Dom Feliciano, assim como das suas contra-partes africanas, e integrado em um modelo. Este modelo é uma proposta (que como tal vêm para ser discutida) baseada no princípio filosófico da Navalha de Occam (1960), e busca a um só tempo conciliar hipóteses anteriormente entendidas como contraditórias e dar resposta a todas as observações até então documentadas, erguendo neste interím o menor número de pressupostos possíveis.

O modelo assume uma única subducção, no sentido leste (coordenadas atuais), de um oceano que separaria o Cráton Rio de la Plata do Terreno Nico Perez, com ângulo de subducção variável no tempo, tal que: a) 925-880 Ma espalhamento oceânico e subducção precoce, com primeiros registros de magmatismo no ante-arco; b) 820-770 Ma subducção em baixo ângulo e migração do magmatismo de arco em direção ao retro-arco; c) 765-700 Ma verticalização da subducção e migração do magmatismo de arco em direção ao ante-arco, com gênese do Bloco São Gabriel, enquanto extensão afeta o retro-arco e causa rifteamento; d) 700-660 Ma acresção/colisão entre o Bloco São Gabriel e o Cráton Rio de la Plata, após término da subducção; e) 660-630 Ma colisão oblíqua principal, causando inversão da bacia de retro-arco e transpressão bi-vergente, com metamorfismo de alta-T/baixa-P e exumação do além país; f) 630-580 Ma magmatismo pós-colisional; g) 580-550 Ma colisão secundária, com deformação do ante-país e magmatismo pós-colisional tardio no Cinturão Dom Feliciano, enquanto o fronte orogênico principal migrava para os cinturões Kaoko e Gariep.

6.4 Considerações finais e perspectivas futuras

Existe uma coerência estrutural e uma correlação entre associações petro-tectônicas dispostas longitudinalmente nos segmentos norte (Santa Catarina), central (Rio Grande do Sul) e sul (Uruguai) do Cinturão Dom Feliciano, marcando uma espécie de zonação deste cinturão.

A faixa a leste (além-país ou *hinterland*) é dominantemente formada por granitos (tardi- a) pós-colisionais, sin- a pós-cinemáticos. Pendentes de teto e xenólitos gnáissicos de alto grau têm protólitos sedimentares e magmáticos Tonianos do período pré-colisional (800 – 770 Ma), enquanto a deformação e o

metamorfismo marcam o evento de colisão oblíqua (660 – 630 Ma, aprox.), com vergência em direção ao cráton.

A faixa a oeste (ante-país ou *foreland*) é dominantemente formada por xistos e metamórficas de baixo a médio-grau, marcando pelo menos duas sequências vulcanossedimentares, uma Toniana, pré-colisional, e outra Ediacarana, pós-colisional (conforme antevisto por Jost e Bitencourt, 1980; e recentemente resgatado por Höfig et al., 2017; Battisti et al., 2018 – vide apêndice). O embasamento Arqueano a Paleoproterozoico (localmente Mesoproterozoico) da região aflora em núcleos de antiformes com diferentes graus de retrabalhamento.

A estruturação do domínio de além-país pelo Cinturão de Cisalhamento Sul-Brasileiro é bem reconhecida (Bitencourt e Nardi, 2000). A correlação cinemática, especialmente das fases deformacionais iniciais, deste domínio com o cinturão de xistos do ante-país aponta a necessidade de se revisar o conceito deste cinturão de cisalhamento. Como argumentado por Bitencourt (1996), o magmatismo granítico transcende e é transcendido pelo Cinturão de Cisalhamento Sul-Brasileiro, visto a ocorrência de corpos graníticos de idade similar fora das principais zonas de deformação, bem como corpos tardi- a pós-tectônicos cortando estruturas miloníticas dentro dele. Porém, zonas de cisalhamento contemporâneas e correlatas estiveram ativas dentro e fora deste cinturão granítico. Estas zonas, ao nuclearem-se, condicionaram o surgimento deste orógeno, através do posicionamento de nappes de alto grau e de lascas do embasamento pré-brasiliano, e posteriormente a intrusão de granitoides, e foram elemento estruturante também do *foreland*.

A simples correlação entre as unidades Tonianas de *hinterland* com o Complexo Cerro da Árvore argumenta contra a suposta sutura que separaria estes domínios tectônicos do Cinturão Dom Feliciano. No entanto, não há registro dessas rochas vulcânicas preservadas em outra porção do *foreland* até o momento. Pelo contrário, a diversidade de rochas no *foreland* aponta para o fato de que múltiplas bacias e ambientes tectônicos tenham coexistido e se sucedido ao longo do ante-país do orógeno Dom Feliciano, incluindo magmatismo de retro-arco (Complexo Cerro da Árvore, conforme discutido, e Complexo Lavalleja – Bettucci et al., 2001) e de rift (segmento norte – Complexo Brusque). Possivelmente domínios oceânicos restritos tenham existido à sul (Complexo Arroio Grande e Paso del Dragón – *foreland* ou *hinterland*?), onde o rift alargou-se.

Crosta quente e profunda foi tectonicamente disposta sobre crosta fria e rasa, na forma de nappes, com gradientes geotérmicos de ca. 50°C/km interpretados nas

rochas metapelíticas do Complexo Várzea do Capivarita, na região de Encruzilhada do Sul. Gradientes geotérmicos semelhantes são descritos para os paragnaisses do Complexo Cerro Olivo, no Uruguai (Gross et al., 2009). Tudo leva a crer que o chamado Terreno Punta del Este tenha uma origem semelhante à descrita aqui para o Bloco Encruzilhada. Ambos complexos são correlatos ao Complexo Porto Belo, cuja principal diferença é as condições mais brandas, de fácies anfibolito, também de baixa pressão, com abundantes evidências de fusão, petrográficas e de campo, sugestivas da presença de água.

A presença de água fica evidente quando observamos a fusão parcial do Complexo Camboriú (Martini et al., 2019a,b). A proximidade espacial e temporal com o Complexo Porto Belo, assim como as semelhanças nas evidências petrográficas e de campo, sugerem processos semelhantes de fusão parcial assistida por água em ambos os complexos. Qual o significado da presença da água como catalizadora do processo de fusão parcial durante o período sin- a tardi-colisional no segmento catarinense do Cinturão Dom Feliciano? Por quê esta água não aparece nos demais setores? Um estudo mais aprofundado das condições de fusão, assim como novas tentativas de datação da idade da fusão (frustradas durante o desenvolvimento desta tese), são possibilidades de continuidade de estudo no Complexo Porto Belo.

Outra diferença marcante entre os setores estudados é a variação cinemática entre zonas de cisalhamento componentes do Cinturão de Cisalhamento Sul-brasileiro. Enquanto a partição da deformação entre domínios tectônicos agora é evidente em Santa Catarina, ela aparentemente não foi tão efetiva, ou ainda carece de mais estudos no Rio Grande do Sul (e Uruguai?). Uma hipótese é a de que a presença de fusão parcial abundante no embasamento do *foreland* catarinense tenha favorecido a absorção do componente de cisalhamento puro pelo Complexo Camboriú, e portanto concentrado o cisalhamento simples destral ao longo da Zona de Cisalhamento Major Gercino. O caso do Bloco Encruzilhada, limitado por zonas de cisalhamento transcorrentes de cinemática oposta sugere que um componente de cisalhamento puro mais amplo se decompôs, com uma resultante global de extrusão para sul. A relação entre estes movimentos e sua compatibilidade é outra questão por ser investigada. Análises de vorticidade poderiam ser empregadas no estudo de amostras-chave representativas do estado de deformação finita de cada zona de cisalhamento ou domínio estrutural.

A comparação petrológica do magmatismo pré-colisional Toniano preservado no hinterland é também uma linha de pesquisa que emerge das correlações

propostas. Salienta-se a importância da aparição de rochas de composição intermediária no setor norte, enquanto estas até então são raras nos setores central e sul do hinterland. Para tanto, a obtenção de dados de geoquímica isotópica das rochas menos e mais diferenciadas do Complexo Porto Belo está em andamento.

O entendimento do período pré-colisional depende de uma caracterização dos efeitos desta colisão. A colisão em si, para ser corretamente compreendida, depende de uma boa documentação também da situação pós-colisional, para que se possa de fato “olhar para trás”, abstraindo estruturas e rochas que “não estavam lá”, quando as coisas que estamos tentando entender de fato aconteceram. Tenho a impressão de que este é um trabalho que está só começando.

REFERÊNCIAS

Bachman, S.B., Lewis, S.D., Schweller, W.J., 1983. Evolution of a forearc basin, Luzon Central Valley, Philippines. The American Association Petroleum Geologists Bulletin, 67(7), 1143-1162.

Basei, M.A.S., Frimmel, H.E., Nutman, A.P., Preciozzi, F., Jacob, J., 2005. The connection between the Neoproterozoic Dom Feliciano (Brazil/Uruguay) and Gariep (Namibia/South Africa) orogenic belts. Precambrian Research, 139, 139–221.

Basei, M.A.S., Frimmel, H.E., Nutman, A.P., Preciozzi, F., 2008. West Gondwana amalgamation based on detrital zircon ages from Neoproterozoic Ribeira and Dom Feliciano belts of South America and comparison with coeval sequences from SW Africa. In: Pankhurst, R.J., Trouw, R.A.J., de Brito Neves, B.B., de Wit, M.J. (eds) West Gondwana: Pre-Cenozoic Correlations Across the South Atlantic Region, London. Geological Society London, Special Publication 294, pp 239–256.

Basei, M.A.S., Campos Neto, M.C., Castro, N.A., Nutman, A.P., Wemmer, K., Yamamoto, M.T., Hueck, M., Osako, L., Siga, O., Passarelli, C.R., 2011. Tectonic evolution of the Brusque group, Dom Feliciano belt, Santa Catarina, Southern Brazil. Journal of South American Earth Sciences, 32(4), 324–350.

Battisti M.A., Bitencourt, M.F., De Toni, G.B., Nardi, L.V.S., Konopásek, J., 2018. Metavolcanic rocks and orthogneisses from Porongos and Várzea do Capivarita complexes: A case for identification of tectonic interleaving at different crustal levels from structural and geochemical data in southernmost Brazil. Journal of South American Earth Sciences, 88, 253-274.

Bettucci, L.S., Cosarinsky, M., Ramos, V.A., 2001. Tectonic setting of the late Proterozoic Lavalleja Group (Dom Feliciano Belt), Uruguay. Gondwana Research, 4(3), 395-407.

Bitencourt, M.F., 1996. Granitóides sintectônicos da região de Porto Belo, SC: uma aboradagem petrológica e estrutural do magmatismo em zonas de cisalhamento. Tese de Doutorado, Instituto de Geociências, Universidade Federal do Rio Grande do Sul, 310 pp.

Bitencourt, M.F., Nardi, L.V.S., 2000. Tectonic setting and sources of magmatism related to the Southern Brazilian Shear Belt. Revista Brasileira de Geociências 30, 186–189.

Brown, M. 1994 The generation, segregation, ascent and emplacement of granite magma: the migmatite-to-crustally-derived granite connection in thickened orogens. Earth Sci. Rev. 36, 83-130.

Brown, M. & Solar, G. S. 1998 Shear zone systems and melts: feedback relations and self-organization in orogenic belts. J. Struct. Geol 20, 211-227.

Brown, M. & Solar, G. S. 1999 The mechanism of ascent and emplacement of granite magma during transpression: a syntectonic granite paradigm. Tectonophysics 312, 1-33.

Bruno, H., Almeida, J., Heilbron, M., Salomão, M., Cury, L., 2018. Architecture of major precambrian tectonic boundaries in the northern part of the Dom Feliciano Orogen, southern Brazil: Implications for the West Gondwana amalgamation. Journal of South American Earth Sciences, 86, 301-317.

Burchfield, B.C, Zhiliang, C., Hodges, K.V., Yuping, L., Royden, L.H., Changrong, D., Jiene, X., 1992. The South Tibetan Detatchment System, Himalayan Orogen: extension contemporaneous with and parallel to shortening in a collisional mountain belt. Geological Society of America, Special paper, 269.

Carosi, R., Palmeri, R., 2002. Orogen-parallel tectonic transport in the Variscan belt of northeastern Sardinia (Italy): implications for the exhumation of medium-pressure metamorphic rocks. Geological Magazine, 139, 497-511.

Cawood, P.A., Kröner, A., Collins, W.J., Kusky, T.M., Mooney, W.D., Windley, B.F. 2013. Accretionary orogens through Earth history. Special Publications, Geological Society of London, 319, 1-36.

Chatzaras, V., Xypolias, P., Kokkalas, S., Koukouvelas, I., 2013. Tectonic evolution of a crustal-scale oblique ramp, Hellenides thrust belt, Greece. Journal of Structural Geology, 57, 16-37.

Chemale Jr., F., 2000. Evolução Geológica do Escudo Sul-rio-grandense. In: Holz, M., De Ros, L.F. Geologia do Rio Grande do Sul. CIGO/UFRGS, Porto Alegre, 2002. 444 p.

Chetty, T.R.K., Bhaskar Rao, Y.J., 2006. The Cauvery Shear Zone, Southern Granulite Terrain, India: A crustal-scale flower structure. Gondwana Research, 10, 77-85.

Dewey, J.F., Holdsworth, R.E., Strachan, R.A., 1998. Transpression and transtension zones. In: Holdsworth, R.E., Strachan, R.A., Dewey, J.F. (Eds.), Continental Transpressional and Transtensional Tectonics. Special Publication of the Geological Society, London 135, pp. 1–14.

Dias, R., Ribeiro, A. 1994. Constriction in a transpressive regime: an example in the Iberian branch of the Ibero-Armorican arc. Journal of Structural Geology, 16, 1543-1554.

Egydio-Silva, M., Vauchez, A., Raposo, M.I.B., Bascouc, J., Uhleind, A., 2005. Deformation regime variations in an arcuate transpressional orogeny (Ribeira belt, SE Brazil) imaged by anisotropy of magnetic susceptibility in granulites. Journal of Structural Geology, 27, 1750-1764.

Fernandes, L.A.D., Tommasi, A., Porcher, C.C., 1992. Deformation Patterns in the southern brazillan branch of the Dom Feliciano Belt: A reappraisal. Journal South American Earth Sciences 5, 77-96.

Fernandes, L.A.D., Menegat, R., Costa, A.F.U., Koester, E., Kramer, G., Tommasi, A., Porcher, C.C., Ramgrab, G.E., Camozzato, E., 1995a. Evolução tectônica do Cinturão Dom Feliciano no Escudo Sul-rio-grandense: Parte I – uma contribuição a partir do registro geológico. Revista Brasileira Geociências 25, 351-374.

Fernandes, L.A.D., Menegat, R., Costa, A.F.U., Koester, E., Kramer, G., Tommasi, A., Porcher, C.C., Ramgrab, G.E., Camozzato, E., 1995b. Evolução tectônica do Cinturão Dom Feliciano no Escudo Sul-rio-grandense: Parte II – uma contribuição a partir das assinaturas geofísicas. Revista Brasileira Geociências 25, 375-384.

Fernández, C., Díaz-Azpiroz, M., 2009. Triclinic transpression zones with inclined extrusion. Journal of Structural Geology 31, 1255-1269.

Fernandez, C., Czeck, D.M., Díaz-Azpíroz, M., 2013. Testing the modelo f oblique transpression with oblique extrusion in two natural cases: Steps and consequences. Journal of Structural Geology, 54, 85-102.

Florisbal, L.M., Bitencourt, M.F., Janasi, V.A., Nardi, L.V.S., Heaman, L.M., 2012a. Petrogenesis of syntectonic granites emplaced at the transition from thrusting to transcurrent tectonics in post-collisional setting: whole-rock and Sr–Nd–Pb isotope geochemistry in the Neoproterozoic Quatro Ilhas and Mariscal granites, southern Brazil. Lithos 153, 53–71.

Florisbal, L.M., Janasi, V.A., Bitencourt, M.F., Heaman, L.M., 2012b. Space–time relation of post-collisional granitic magmatism in Santa Catarina, southern Brazil: U–Pb LA-MC-ICP-MS zircon geochronology of coeval mafic-felsic magmatism related to the Major Gercino Shear Zone. Precambrian Research, 216, 132–151.

Fossen, H., 2010. Structural Geology. Cambridge University Press. 584p.

Fossen, H., Tikoff, B., 1993. The deformation matrix for simultaneous simple shearing, pure shearing and volume change, and its application to transpression–transtension tectonics. Journal of Structural Geology 15, 413–422.

Foster, D.A., Goscombe, B.D., Gray, D.R., 2009. Rapid exhumation of deep crust in an obliquely convergent orogen: The Kaoko Belt of the Damara Orogen. Tectonics, 28, TC4002.

Fragoso-Cesar, A.R.S., 1980. O Cráton Rio de La Plata e o Cinturão Dom Feliciano no Escudo Sul-riograndense. IN: Congresso Brasileiro de Geologia, 31. SBG, V.5, Balneário Camboriú, 2979-2892.

Fragoso Cesar, A.R.S., 1991. Tectônica de placas no Ciclo Brasiliano: as orogenias dos cinturões Dom Feliciano e Ribeira no Rio Grande do Sul. Tese de doutorado. USP, São Paulo, 367p. Disponível em: https://teses.usp.br/teses/disponiveis/44/44134/tde-23042013-162133/pt-br.php

Fragoso Cesar, A.R.S., Figueiredo, M.C.H., Soliani Jr., E., Faccini, U.F., 1986. O Batólito Pelotas (Proterozoico/Eo-Paleozoico) no Escudo do Rio Grande do Sul. Anais do Congresso Brasileiro de Geologia, 34, Goiânia, vol. 3, 1322-1343.

Fragoso Cesar, A.R.S, Machado, R., Monteiro, R.L., Sallet, R., 1990. Nappes e estruturas correlatas do Cinturão Dom Feliciano no Escudo Uruguaio Sul-Riograndense: uma introdução ao problema. Acta Geológica Leopoldensia, 30(13):75-92.

Girard, R., 1993. Orogen-scale strain partitioning and an analogy to shearbands in the Torngat Orogen, northeastern Canadian Shield. Tectonophysics 224, 363–370.

Goodwin, L.B., Tikoff, B., 2002. Competency contrast, kinematics, and the development of foliations and lineations in the crust. Journal of Structural Geology 24, 1065–1085

Goscombe, B., Gray, D.R., 2009. Metamorphic response in orogens of different obliquity, scale and geometry. Gondwana Research, 15, 151-167.

Gross, A.O.M.S., Droop, G.T.R., Porcher, C.C., Fernandes, L.A.D. 2009. Petrology and thermobarometry of mafic granulites and migmatites from the Chafalote Metamorphic Suite: new insights into the Neoproterozoic P–T evolution of the Uruguayan-Sul- Rio-Grandense shield. Precambrian Research, 170, 157–174.

Harland, W.B., 1971. Tectonic transpression in Caledonian Spitzbergen. Geological Magazine 108, 27–42.

Hartmann, L.A., Chemale Jr., F., Philipp, R.P., 2007a. Evolução Geotectônica do Rio Grande do Sul no Pré-Cambriano. In: Ianuzzi, E.R., Frantz, J.C. (Eds.), 50 ano de

Geologia: Instituto de Geociências. Contribuições. Comunicação e Identidade, Porto Alegre, 396p.

Hasui, Y., Carneiro, C.D.R. And Coimbra, A.W., 1975. The Ribeira folded belt. Revista Brasileira de Geociências, 5, 257–266.

Höfig, D.F., Marques, J.C., Basei, M.A.S., Giusti, R.O., Kohlrausch, C., Frantz, J.C., 2017. Detrital zircon geochronology (U-Pb LA-ICP-MS) of syn-orogenic basins in SW Gondwana: new insights into the cryogenian-ediacaran of Porongos complex, Dom Feliciano belt, southern Brazil. Precambrianian Research, 306, 189-208.

Holdsworth, R.E., Tavarnelli, E., Clegg, P., Pinheiro, R.V.L., Jones, R.R., McCaffrey, K.J.W., 2002. Domainal deformation patterns and strain partitioning during transpression: an example from the Southern Uplands terrane, Scotland. Journal of the Geological Society of London 159, 401–415.

Hueck, M., Basei, M.A.S., Wemmer, K., Oriolo, S., Heidelbach, F., Siegesmund, S., 2018. Evolution of the Major Gercino Shear Zone in the Dom Feliciano Belt, South Brazil, and implications for the assembly of southwestern Gondwana. International Journal of Earth Sciences, 108(2), 403-425.

Jones, R.R., Tanner, P.W.G., 1995. Strain partitioning in transpression zones. Journal of Structural Geology 17, 793–802

Jones, R.R., Holdsworth, R.E., 1998. Oblique simple shear in transpression zones. In: Holdsworth, R.E., Strachan, R.A., Dewey, J.F. (Eds.), Continental Transpressional and Transtensional Tectonics. Special Publication of the Geological Society, London 135, pp. 35–40.

Jones, R.R., Holdsworth, R.E., Bailey, W., 1997. Lateral extrusion in transpression zones: the importance of boundary conditions. Journal of Structural Geology 19, 1201–1217.

Jones, R.R., Holdsworth, R.E., Clegg, P., McCaffrey, K., Tavarnelli, E., 2004. Inclined transpression. J. Struct. Geol. 26, 1531–1548.

Jost, H., Bitencourt, M.F., 1980. Estratigrafia e tectônica de uma fração da Faixa de Dobramentos Tijucas no Rio Grande do Sul. Acta Geológica Leopoldensia, 4(7):27-60. São Leopoldo, RS, Brazil.

Klerey, P., Klepeis, K.A., Vine, F.J., 2009. Global Tectonics. Wiley-Blackwell, UK.

Kober, L., 1921. Der bau der Ende. Berlim: Borntraeger.

Konopásek, J., Sláma, J., Košler, J., 2016. Linking the basement geology along the Africa–South America coasts in the South Atlantic. Precambrian Research, 280, 221–230.

Konopásek, J., Hoffmann, K.H., Sláma, J., Košler, J., 2017. The onset of flysch sedimentation in the Kaoko Belt (NW Namibia)—implications for the pre-collisional evolution of the Kaoko–Dom Feliciano–Gariep Orogen. Precambrian Research, 298, 220–234.

Konopásek, J., Janoušek, V., Oyhantçabal, P., Sláma J ., Ulrich, S., 2018. Did the circum-Rodinia subduction trigger the Neoproterozoic rifting along the Congo–Kalahari Craton margin? International Journal of Earth Sciences. https://doi.org/10.1007/s00531-017-1576-4

Liégeois, J.P., 1998. Some words on the post-collisional magmatism. Preface to Special Edition on Post-Collisional Magmatism. Lithos 45, xv–xvii.

Lister, G.S., Williams, P.F., 1983. The partitioning of deformation in flowing rock masses. Tectonophysics 92, 1–33.

Martil, M.M.D., 2016. O magmatismo de arco continental pré-colisional (790 ma) e a reconstituição espaço-temporal do regime transpressivo (650 Ma) no Complexo Várzea do Capivarita, sul da Província Mantiqueira. Unpublished PhD thesis. Universidade Federal do Rio Grande do Sul. Avaliable at: https://www.lume.ufrgs.br/handle/10183/149194

Martini, A., Bitencourt, M.F., Weinberg, R., De Toni, G.B. Nardi, L.V.S., 2019a. From migmatite to magmas - crustal melting and generation of granite in the Camboriu Complex, south Brazil. Lithos, 340–341:270–286.

Martini, A., Bitencourt, M.F., Weinberg, R., De Toni, G.B, 2019b. Melt-collecting structures and the formation of extraction dykes during syntectonic anatexis of the Camboriú Complex, south Brazil. Journal of Structural Geology, 127:103866.

Mattauer, M., 1986. Intracontinental subduction, crust–mantle decollement and crustal-stacking wedge in the Himalayas and other collision belts. Geological Society of London Special Publications 19 (1), 37–50

Miyashiro, A., 1982. Theory of orogeny based on plate tectonics. In: Miyashiro, A., Aki, K., Sengör, A.M., (Eds.) Orogeny. John Wiley and Sons, Chichester, pp. 49-119.

Molnar, P., 1992. Brace–Goetze strength profiles, the partitioning of strikeslip and thrust faulting at zones of oblique convergence, and the stressheat flow paradox of the San Andreas Fault. In: Evans, B., Wong, T.-F. (Eds.), Fault Mechanics and Transport Properties of Rocks, Academic Press, London, pp. 435–459.

Navalha de Occam - *Occam's Razor* (1960). Unidentified author. The Lancet, 276(7145), 302.

Neves, S. P., Vauchez, A. and Archanjo, C. J. (1996) Shear zone-controlled magma emplacement or magma-assisted nucleation of shear zones? Insights from northeast Brazil. Tectonophysics 262, 349-364.

Oriolo, S., Oyhantçabal, P., Wemmer, K., Heidelbach, F., Pfänder, J., Basei, M.,A.,S., Hueck, M., Hannich, F., Sperner, B., Siegesmund, S., 2016. Shear zone evolution and timing of deformation in the Neoproterozoic transpressional Dom Feliciano Belt, Uruguay. Journal of Structural Geology, 92, 59–78.

Oyhantçabal, P., Siegesmund, S., Wemmer, K., Frei, R., Layer, P., 2007. Post-collisional transition from calk-alkaline to alkaline magmatism during transcurrent deformation in the southernmost Dom Feliciano Belt (Braziliano – Pan-African, Uruguay). Lithos,98, 141-159.

Oyhantçabal, P., Siegesmund, S., Wemmer, K., 2011. The Río de la Plata Craton: a review of units, boundaries, ages and isotopic signature. International Journal of Earth Sciences. 100, 201–220.

Passarelli, C.R., Basei, M.A.S., Wemmer, K., Siga Jr., O., Oyhantçabal, P., 2011. Major shear zones of southern Brazil and Uruguay: escape tectonics in the eastern border of Rio de la Plata and Paranapanema cratons during the western Gondwana amalgamation. International Journal of Earth Sciences, 100, 391-414.

Paterson, S.R., Vernon, R.H., Tobisch, O.T., 1989. A review of criteria for the identification of magmatic and tectonic foliations in granitoids. Journal of Structural Geology, 11(3), 349-363.

Peel, E., Sánchez-Bettucci, L., Basei, M.A.S., 2018. Geology and geochronology of Paso del Dragón Complex (northeastern Uruguay): implications on the evolution of the Dom Feliciano Belt (Western Gondwana). Journal of South American Earth Sciences, 85, 250–262.

Picada, R.S., 1971. Ensaio sobre a tectônica do Escudo Sul-riograndense: caracterização dos sistemas de falhas. Anais do XXV Congresso Brasileiro de Geologia. São Paulo.

Pinet, N. & Cobbol d, P. R. 1992. Experimental insights into the partitioning of motion within zones of oblique subduction. Tectonophysics, 206, 371-388.

Philipp, R.P., Machado, R., 2005. The Neoproterozoic to Cambrian granitic magmatism of Pelotas Batholith, southern Brazil. Journal of South American Earth Sciences 19, 461-478.

Philipp RP, Pimentel MM, Chemale Jr., F, 2016. Tectonic evolution of the Dom Feliciano Belt in Southern Brazil: Geological relationships and U-Pb geochronology. Brazilian Journal of Geology, 46(1), 83–104.

Ramberg, H. 1975. Particle paths, displacement and progressive strain applicable to rocks. Tectonophysics 28, 1-37.

Ramsay, J.G., 1967. Folding and Fracturing of Rocks. McGraw-Hill, New York.

Ramos, R.C., Koester, E., Vieira, D.T., Porcher, C.C., Gezatt, J.N., Silveira, R.L., 2018. Insights on the evolution of the Arroio Grande ophiolite (Dom Feliciano belt, Brazil) from Rb-Sr and SHRIMP U-Pb isotopic geochemistry. Journal of South American Earth Sciences, 86, 38–53.

Ramos, R.C., Koester, E., Vieira, D.T., 2019. Plagioclase-hornblende geothermobarometry of metamafites from the Arroio Grande Ophiolite, Dom Feliciano Belt, southernmost Brazil. Journal of South American Earth Sciences, 95:102262. https://doi.org/10.1016/j.jsames.2019.102262

Ramos, V.A., 2009, Anatomy and global context of the Andes: Main geologic features and the Andean orogenic cycle, in Kay, S.M., Ramos, V.A., and Dickinson, W.R., eds., Backbone of the Americas: Shallow Subduction, Plateau Uplift, and Ridge and Terrane Collision: Geological Society of America Memoir 204, 31–65. DOI: 10.1130/2009.1204(02).

Robin, P.-Y.F., Cruden, A.R., 1994. Strain and vorticity patterns in ideally ductile transpression zones. Journal of Structural Geology 16, 447–466.

Romeo, I., Capote, R., Tejero, R., Lunar, R., Quesada, C., 2006. Magma emplacement in transpression: The Santa Olalla Igneous Complex (Ossa-Morena Zone, SW Iberia). Journal of Structural Geology, 28, 1821 – 1834.

De Saint Blanquat, M., Horsman, E., Habert, G., Morgan, S., Vanderhaeghe, O., Law, R., Tikoff, B., 2011. Magmatic pulsing, duration of pluton construction, and the paradoxical relationship between tectonism and plutonism. Tectonophysics 500, 20–33.

Sanderson, D.J., Marchini, W.R.D., 1984. Transpression. Journal of Structural Geology 6, 449–458.

Schwerdtner, W. M. 1989. The solid-body tilt of deformed paleohorizontal planes: application to an Archean transpression zone, southern Canadian Shield. J. Struct. Geol. 11, 1021-1027

Sengör, A.M.C., 1990. Plate tectonics and erogenic research after 25 years: synopsis of a Tethyan perspective. Tectonophysics, 187, 315-344.

Stern, R.J., 2002. When and how did plate tectonics begin? Theoretical and empirical considerations. Chinese Science Bulletin, 52, 578-591.

Thompson, A.B., Schulmann, K., Jezek, J., 1997. Thermal evolution and exhumation in obliquely convergent (transpressive) orogens. Tectonophysics, 280, 171-184.

Tikoff, B., Tessier, C., 1994. Strain modeling of displacementfield partitioning in transpressional orogens. J. Struct. Geol. 11, 1575-1588.

Tikoff, B., Teyssier, C., Waters, C., 2002. Clutch tectonics and the partial attachment of lithospheric layers. EGU Stephan Mueller Special Publication Series, 1, 57–73.

Tommasi, A., Vauchez, A., Fernandes, L.A.D., Percher, C.C., 1994. Magma-assisted strain localization in an orogen parallel transcurrent shear zone of southern Brazil. Tectonics, 13, 421-437.

Van der Pluijm, B.A., Marsak, S., 2004. Earth Structure. 2nd ed. Norton, US.

Vanderhaegue, O., 2012. The thermal–mechanical evolution of crustal orogenic belts at convergent plate boundaries: A reappraisal of the orogenic cycle. Journal of Geodynamics, 56-57, 124-145.

Vauchez, A. & Nicolas, A. 1991. Mountain building: strike-parallel displacements and mantle anisotropy. Tectonophysics 185, 183-201.

Xypolias, P., Kokkalas, S., Skourlis, K., 2003. Upward extrusion and subsequent transpression as a possible mechanism for the exhumation of HP/LT rocks in Evia Island (Aegean Sea, Greece). Journal of Geodynamics, 35, 303-332.

Zhang, J., Xiao, W., Windley, B.F., Wakabayashi, J., Cai F., Sein K., Wu, H., Naing, S., 2018. Multiple alternating forearc- and backarc-ward migration of magmatism in the Indo-Myanmar Orogenic Belt since the Jurassic: Documentation of the orogenic architecture of eastern Neotethys in SE Asia. Earth-Science Reviews, 185, 704-731.

Zibra, I., Kruhl, J.H., Montanini, A., Tribuzio, R., 2012. Shearing of magma along a highgrade shear zone: evolution of microstructures during the transition from magmatic to solid-state flow. J. Struct. Geol. 37, 150–160.

Zibra, I., Smithies, R.H., Wingate, M.T.D, Kirkland, C.L., 2014. Incremental pluton emplacement during inclined transpression. Tectonophysics, 623, 100-122.

Zoback, M. D. & Healy, J. H. 1992. In situ stress measurements to 3.5 km depth in the Cajon Pass scientific research borehole: implications for the mechanics of crustal faulting. J. geophys. Res. 97, 5039-5057.

APÊNDICE – *Why Cerro da Árvore Complex?*

About the adopted Porongos (Super?) Complex subdivision

Since the seminal work of Jost and Bitencourt (1980) it is noticed that the so called Porongos Complex (also called Porongos Metamorphic Complex or Porongos Group in the regional literature) is composed of two different metavolcanosedimentary subunits with a distinct stratigraphic record. The mentioned authors named the Cerro da Árvore Complex (CAC) the eastern unit, which makes contact with the EB, with stratigraphic record of an active margin, and the Cerro dos Madeiras Complex the western unit, registering a passive margin. The (sub)units are separated by a major thrust. The same authors noticed the increasing of metamorphic conditions towards the east, with maximum amphibolite-facies conditions nearby the Passo dos Marinheiros Fault, which is the eastern limit of the Porongos Complex.

Porcher and Fernandes (1990) demonstrated that the Cerro dos Madeiras Group (sensu Jost and Bitencourt, 1980) metaarkosean rocks (originally called Arroio dos Neves Formation by Jost and Bitencourt, 1980) are actually mylonitized granites related to the Paleoproterozoic basement (Encantadas Complex). Later works were focused in smaller areas (e.g. Capané Antiform – Marques et al, 1998a, 1998b; Gollmann et al. 2008; Santana da Boa Vista Dome – Salmann et al., 2006 and references therein). More recently a lot of effort was given to dating (e.g. Kohlrausch, 2013 Pertille et al., 2015; Gruber et al., 2016 and others), which resulted in many new provenance and crystallization ages with lack of field and structural data to explain it (see discussion about this problem in Höfig et al., 2017).

Among these relatively new geochronological data, several authors dated acidic to intermediate (meta) volcanic rocks of 780 – 800 Ma (Tonian age) from easternmost PC (a summary of ages and locations is given by Höfig et al., 2017 and the main results are listed in table 01 below). These (meta) volcanic strata are good time markers for the depositional environment recorded in the easternmost PC. Salmaan et al. (2011) reported 789 ± 7 Ma as magmatic age (U-Pb zircon LA-ICP-MS) of acidic metavolcanic rocks from Serra dos Pedrosas antiform, in the Cerro da Árvore region. Similar ages are reported for a metandesite (789 ± 39 Ma U-Pb zircon SHRIMP – Soliani Jr., 1986) from the same area, for metarhyolites from the eastern limb of Santana da Boa Vista antiform (773 ± 3.1 and 801 ± 4.7 U-Pb zircon SHRIMP – Pertille et al., 2017) and for metarhyolite (809 ± 4.1 U-Pb zircon LA-ICP-MS – Pertille et al., 2017) and metandesite (773 ± 8 U-Pb zircon TIMS – Chemale Jr., 2000) from Godinho antiform.

Regarding metamorphic ages, Lenz (2006) and Porcher et al. (2010) presents the so far unique metamorphic dating from the Porongos Complex: 658 ± 26 (Rb-Sr composed isochron of five whole-rock and five white mica analysis). Porcher et al. (2010) presents additionally single muscovite-whole-rock isochrones from two samples, dated as 654 ± 15 and 601 ± 41. The ages comes from PC easternmost region rocks, the so called Cerro Cambará metapelites. Lenz (2006) also presents the so far unique attempt in determine metamorphic conditions for Porongos Complex rocks. The data was obtained from the very easternmost portion of the complex, called Cerro do Facão metapelites. Her results point to two-stage of metamorphism: M1 is estimated in 590 °C and 6 Kbar and interpreted as peak regional (collisional) metamorphism, while M_2 is estimated as 550 °C and 2.7 Kbar, related with the intrusion of the Encruzilhada Granite. So it is very likely that the younger age presented by Porcher et al. (2010) is related to M_2 effects.

Contrastantly, it is well known that relatively younger volcanics (600 – 580 Ma – Kohlraulsch, 2013), alkaline intrusive (ca. 600 Ma – Zvirtes et al., 2015) and (volcano-)sedimentary rocks (615 – 580 Ma – Höfig et al., 2017) are described and dated in the PC. Mostly of them are describeded at the Capané antiform, in the northern portion of PC.

Pertille et al. (2017) recognized maximum depositional ages of 570 Ma and correlated this second volcano-sedimentary cycle of Porongos Complex to the Camaquã Basin evolution in a foreland fold and thrust belt.

This second depositional cycle is followed by a second collisional stage, since the rocks were deformed after deposition/crystallization. It is outstanding that these younger volcanic and depositional ages are much younger than the collisional metamorphism which affected the easternmost portion. As suggested by Battisti et al. (2018) it seems that during the second pulse of collision recorded by the PC, the collisional front migrated towards the west, since there is no obvious vestige of it in the CAC neither in the EB.

Höfig et al. (2017) named these different sequences as Porongos I and Porongos II. In this work we choosed to keep the original tectono-stratrigraphic name proposed originally by Jost and Bitencourt (1980) and Jost (1981), as recommended by the International Subcommission on Stratigraphic Classification of IUGS and the International Commission on Stratigraphy (Murphy and Salvador, 1999), and we consider the Cerro da Árvore Complex the correspondent of the Porongos I of Höfig et al. (2017). It is possible that in future works it will arise the discussion of the nomenclature of the PC, considering the joint of the CAC with the originally called Cerro dos Madeiras Group (regarding the corrections made by Porcher and Fernandes, 1990 in the interpretations of Jost and Bitencourt, 1980, this unit is probably equivalent to the Porongos II from Höfig et al., 2017). These considerations lead to the promotion of the PC to Porongos Super Complex. This subject is, however, out of the objectives of this paper, and needs further discussion and effort among the geological community interested in the tectono-stratigraphy of the Dom Feliciano Belt and correlated units.

~~~~~~

Este texto foi escrito originalmente como um apêndice para o manuscrito ***Origin and tectonic meaning of the Encruzilhada Block, Dom Feliciano Belt, south Brazil, based on aerogeophysics, image analysis and PT-paths***. Por tratar-se de uma discussão de “interesse local”, o apêndice acabou sendo cortado e a própria discussão excessivamente resumida na versão submetida. A maior parte das referências citadas neste texto estão no manuscrito apresentado nesta tese, ou constam como referências dos artigos publicados por Höfig et al. (2017) e Battisti et al. (2018).
~~~~~~

ANEXO I

Título da Dissertação/Tese:

"CORRELAÇÃO GEOLÓGICO-ESTRUTURAL E MODELO INTEGRADO DE EVOLUÇÃO PARA O CINTURÃO DOM FELICIANO SOB TRANSPRESSÃO INCLINADA NO NEOPROTEROZOICO DO SUL DO BRASIL"

Área de Concentração: Geoquímica

Autor: **Giuseppe Betino de Toni**

Orientadora: Profa. Dra. Maria de Fátima Bitencourt

Examinador: Prof. Dr. Léo Afraneo Hartmann

Data: 08/11/2019

Conceito: A - Excelente

PARECER:

Avaliação geral

1. Tema muito adequado para uma tese de doutorado, com conexão entre estudos detalhados de vários tipos (geologia de campo, estrutural, petrografia, microssonda eletrônica, geoquímica de rocha total, geocronologia U-Pb de zircão por LA, interpretação de dados aerogeofísicos e Landsat), integração dos dados novos com o conhecimento existente e com aspectos de escala orogênica, incluindo acresção juvenil, colisão continental, refusão de rochas, graus de metamorfismo, napes, estratigrafia. A capacidade do doutorando em identificar problemas científicos, utilizar metodologia específica e integrar o conhecimento em várias escalas fica demonstrada.
2. Os objetivos propostos foram alcançados na tese.
3. A estrutura da tese está boa, com 3 artigos internacionais submetidos a revistas de alto impacto, uma introdução e uma síntese.
4. A formatação da tese está boa, com boa redação de português e de inglês, boa apresentação de figuras, figuras todas pertinentes nas várias escalas e todas necessárias.
5. A ciência é de boa qualidade, pois interpretações estão baseadas nos dados obtidos ou compilados.

A tese do doutorando Giuseppe aborda a evolução geotectônica de terrenos Neoproterozóicos de SC e RS, de forma integrada. O tema é meritório de tese e de grande significado para o entendimento da evolução do Orógeno Brasiliano em amplas regiões. Uma seção geológica entre Porto Belo e Camboriú, e região de Encruzilhada do Sul leva a um modelo de evolução para o Sistema Orogênico Kaoko-Dom Feliciano-Gariep.

A estrutura da tese consiste de introdução conceitual a vários aspectos orogênicos, muito bem feita. Ao final, há uma síntese integradora. No centro da tese, 3 artigos submetidos a revistas científicas internacionais de alto impacto.

Problemas da tese são de pequena proporção, conforme listado a seguir.

A declaração de objetivo é feita de forma difusa e não específica na introdução dos artigos 1 e 2 submetidos. Consta do artigo 3.

1. As referências bibliográficas são muito extensas nos artigos, da ordem de 10-16 páginas. É melhor reduzir para 3 páginas.
2. Os anexos aos artigos estão mal apresentados; tabelas não são legíveis, tem linhas no corpo da tabela.
3. Os artigos 1 e 2 estão muito bem elaborados, o artigo 3 vai encontrar dificuldade para ser publicado, pois apresenta poucos dados (17 análises químicas RT e poucos cristais de zircão datados U-Pb de uma amostra). A generalização é extensa e ampla, a partir desses dados. Pode ser recomendável a divisão em dois artigos, um local com os dados novos em revista regional, e outro de revisão para uma revista de alto impacto.
4. Os *abstract* deviam seguir a regra de 4: declaração do problema a ser estudado, métodos usados, resultados obtidos, interpretação. Da forma como estão, os abstract consistem essencialmente de apresentação de resultados e interpretação.
5. O doutorando esclarece que o Complexo Cerro da Árvore tem sinal aeromagnetométrico baixo, ou seja, é um resultado de sua natureza metassedimentar, mas o doutorando não declara essa interpretação. Essa origem metassedimentar reforça a correlação geológica entre o Complexo Várzea do Capivarita e o Complexo Cerro da Árvore, conforme feita pelo doutorando.
6. A geoquímica de RT do Complexo Porto Belo tem um componente alto de refusão de crosta continental. Isso é visto no número elevado de cristais de zircão com herança antiga. Qual é o processo de refusão de crosta continental que escolhe cristais de zircão para inclusão no magma neoformado e que exclui todos os demais componentes mineralógicos e químicos?
7. Onde estão as associações de rochas oceânicas que estavam entre o Cráton Rio de la Plata e o Terreno Nico Pérez antes da colisão toniana? Ofiolitos, sedimentos pelágicos? Somente granitos formados? Parece mais um modelo do tipo Rift de Oslo do que o fechamento do Mar Vermelho.
8. Excesso de extrapolação. A ocorrência de um anortosito em Capivarita e outro na África mostra que não havia um grande oceano entre os dois no Mesoproterozóico?
9. Uso excessivo de siglas: VCC, CAC, PSM, VCN, EB, DCSZ, EG, TFB, PB. A redação científica deve ser feita sem uso de siglas.

Assinatura: Leo Hartmann Data: 08/11/2019

Ciente do Orientador:

Ciente do Aluno: Giuseppe Bolino De Toni

ANEXO I

Título da Tese:

"CORRELAÇÃO GEOLÓGICO-ESTRUTURAL E MODELO INTEGRADO DE EVOLUÇÃO PARA O CINTURÃO DOM FELICIANO SOB TRANSPRESSÃO INCLINADA NO NEOPROTEROZOICO DO SUL DO BRASIL"

Área de Concentração: Geoquímica

Autor: **Giuseppe Betino de Toni**

Orientadora: Profa. Dra. Maria de Fátima Bitencourt

Examinadora: Profa. Dra. Renata da Silva Schmitt

Data:
08/11/2019

Conceito:
A (EXCELENTE)

PARECER:

A robusta tese de doutorado de Giuseppe B. de Toni reflete o alto nível da pesquisa acadêmica. A proposta é ambiciosa, mas justificável levando-se em conta uma abordagem filosófica com a integração do conhecimento consolidado dos terrenos tectônicos do Cinturão Dom Feliciano correlacionáveis ao longo da sua direção principal. Este principio serve como base para os modelos e hipóteses levantadas por esta tese, em adição é apresentado detalhamento geológico em duas áreas-chave: (a) domínio da zona de cisalhamento Major Gercino e uma parte da Faixa Tijucas (Santa Catarina); e (b) domínio do Bloco Encruzilhada e seus contatos com áreas adjacentes (Rio Grande do Sul). A tese está bem estruturada em três artigos que abordam essas duas áreas, além de apresentar uma parte introdutória e de revisão conceitual (capítulos 1 e 2) muito bem elaborada, de alta qualidade científica e excelência, relevante para a argumentação, e bem redigida.

A evolução tectônica do Cinturão Dom Feliciano retrata uma complexa sequencia de eventos geológicos de 900 até 450 milhões de anos que consolidaram os escudos uruguaio, sul-rio-grandense e catarinense. Todavia sua área é restrita e truncada por coberturas fanerozóicas e ainda parte de sua evolução esta preservada no lado africano. A tentativa de integrar e simplificar partindo dos consensos é fundamental, mérito desta tese. Por outro lado, em alguns momentos o autor extrapola suas interpretações para além dos dados inéditos e da compilação. Outro ponto a ressaltar é o excesso de nomes de unidades e siglas nos três artigos, que por vezes parecem escritos para o restrito grupo de pesquisadores que trabalha neste cinturão. A fim de avançarmos nas interpretações tectônicas precisamos trazer novas visões de pesquisadores de distintas escolas de pensamentos. Para tal faz-se necessário saber apresentar e os problemas locais para uma audiência maior. Abaixo comento cada um dos artigos, suas questões cientificas e contribuições e a parte final da tese (síntese).

O artigo do capitulo 3 é, na minha opinião, a contribuição de maior profundidade e ineditismo. O autor apresenta uma excelente secção geológica a partir de secções detalhadas com densa matriz de dados estruturais e petrográficos. O resultado final (fig. 16) exibe um modelo 3D bastante realístico desde a porção ao norte do batólito de Florianópolis até os ortognaisses do embasamento em Camboriú. Fica clara a relação entre os protólitos da infra- e da supra-estrutura deste domínio tectônico, mesmo com a penetrante tectônica transpressiva-transcorrente que segmenta e em parte oblitera as relações estratigráficas. O artigo faz a análise geométrica e cinemática propondo um modelo para evolução tectônica tardia da relação embasamento (Complexo Camboriu) e cobertura (Complexo Brusque). A

principal intenção é mostrar evidências de que a zona de cisalhamento Major Gercino é uma estrutura intra-continental e não uma sutura de placas. Para tal os autores fazem uma comparação entre os ortognaisses Camboriu e Porto Belo, destacando similaridades na origem e ainda evolução tectono-metamórfica. A introdução está bastante confusa e sem elaboração, falta definir claramente essas questões cientificas controversas. Também poderia reduzir o volume do artigo, existem muitos detalhes descritivos que podem ser transportados para anexos, tornando a leitura mais fluida e destacando o enfoque do trabalho.

Prefiro comentar antes o artigo 3 (cap. 5), por ser mais uma sequencia do primeiro. Este apresenta dados geoquímicos e geocronológicos de uma amostra dos ortognaisses do Complexo Porto Belo (cristalização toniana). A partir de uma revisão, os autores ainda provam que os dados obtidos são semelhantes aos diversos "*inliers*" tonianos no Cinturão Dom Feliciano ao longo de mais de 700 km. Praticamente todas as faixas móveis brasilianas-pan-africanas possuem lentes de ortoderivadas tonianas (800-700 Ma) em meio às unidades orogênicas ediacaranas-cambrianas. A origem/paleogeografia destes cinturões mais antigos ainda é pouco compreendida e antecede a amalgamação do Gondwana em mais de 300 milhões de anos, estando, portanto, vinculada a outro contexto geodinâmico. Esse artigo ainda discute visões antagônicas entre uma origem ligada a arcos magmáticos ou a riftes, propondo que não é preciso escolher uma ou outra, ambas podem ocorrem concomitantes lateralmente ou em tempos diferentes ao longo do *strike* do orógeno. O principal mecanismo responsável seria as variações no angulo de subducção das placas convergentes tonianas. Apesar desta boa sugestão, os autores extrapolam muito temporalmente a discussão no modelo, além dos seus dados e da compilação. A proposta inicial já é de excelente relevância e poderia ser melhor explicada e exemplificada, ficando o modelo neste contexto geodinâmico do Toniano e inicio do Criogeniano. O modelo (fig.15) não se sustenta com os dados e argumentos, apresentando especificidades locais desconhecidas e tirando o foco da contribuição para a comunidade cientifica.

O artigo sobre o Bloco Encruzilhada (cap. 4) fornece dados de geotermobarometria (muito bem analisados e interpretados) que sustentam a hipótese de que este domínio é contiguo a faixa Tijucas e suas unidades metassedimentares compartilhariam da mesma bacia. Contudo mostram trajetórias PT distintas resultado das *nappes* cristalinas geradas na inversão da bacia num ambiente colisional intracontinental. Os dados geofísicos ficaram desconectados na introdução; só na discussão são contextualizados na hipótese principal. Ainda fica em aberto a existência de uma sutura na borda leste do bloco, zona de cisalhamento Dorsal de Canguçu. De qualquer maneira esse artigo é primoroso na integração de dados quantitativos de PT e a trajetória cinemática de corpos rochosos, analisando distintos níveis crustais na evolução dos orógenos.

Concluindo o parecer, considero a tese excelente por ser uma abordagem ambiciosa, mas necessária para o estudo da evolução tectônica do Cinturão Dom Feliciano. Exibe a maturidade e conhecimento profundo do autor, reforçando que o levantamento detalhado de dados de campo é fundamental para o sucesso nos dados analíticos e ratificação de modelos tectônicos mais fidedignos.

Assinatura: Data: 8/11/19

Ciente do Orientador:

Ciente do Aluno: Giuseppe Betino De Toni

ANEXO I

Título da Dissertação/Tese:

"CORRELAÇÃO GEOLÓGICO-ESTRUTURAL E MODELO INTEGRADO DE EVOLUÇÃO PARA O CINTURÃO DOM FELICIANO SOB TRANSPRESSÃO INCLINADA NO NEOPROTEROZOICO DO SUL DO BRASIL"

Área de Concentração: Geoquímica

Autor: **Giuseppe Betino de Toni**

Orientadora: Profa. Dra. Maria de Fátima Bitencourt

Examinador: Prof. Dr. Sebastian Oriolo

Data: 08/11/2019

Conceito: **A (EXCELENTE)**

PARECER:

La tesis doctoral de Giuseppe Betino de Toni presenta una vasta y novedosa base de datos estructurales, microestructurales, termobarométricos, geoquímicos y geocronológicos. Estos datos se analizan e integran críticamente, incluyendo también una revisión exhaustiva de antecedentes. Como resultado, se presenta um modelo de evolución estructural, tectonometamórfico y magmático para el Neoproterozoico de la región de estudio, el cual no sólo ajusta la información disponible sino que también permite reconciliar modelos pre-existentes, aparentemente contrapuestos.

El trabajo se destaca por la calidad y abundancia de nuevos datos presentados, desarrollado en el marco de um enfoque multidisciplinario, donde herramientas de diferentes disciplinas se integran de manera muy adecuada. Asimismo, cabe destacar la crítica evaluación de los resultados y la presentación de un modelo tectónico novedoso, clave para la evolución del Gondwana Occidental. En su conjunto, la tesis cumple con los más altos estándares de investigación científica y demuestra de manera clara la capacidad del tesista para desarrollar un trabajo de investigación de forma autónoma.

Por los motivos expuestos anteriormente, se adjudica la máxima calificación, A (Excelente), a este excelente trabajo doctoral.

Assinatura: Data: 08/11/2019

Ciente do Orientador:

Ciente do Aluno: Giuseppe Betino De Toni